



Peer Reviewed

Title:

Transient Seepage Through Levees and the Influence of Roots and Animal Burrows

Author:

[Cobos Roa, Diego](#)

Acceptance Date:

2015

Series:

[UC Berkeley Electronic Theses and Dissertations](#)

Degree:

Ph.D., [Civil and Environmental Engineering](#) [UC Berkeley](#)

Advisor(s):

[Cobos Roa, Diego](#)

Committee:

[Sitar, Nicholas](#), [Seed, Raymond](#), [Dietrich, William](#)

Permalink:

<http://escholarship.org/uc/item/56w38938>

Abstract:

Copyright Information:

All rights reserved unless otherwise indicated. Contact the author or original publisher for any necessary permissions. eScholarship is not the copyright owner for deposited works. Learn more at http://www.escholarship.org/help_copyright.html#reuse

Transient Seepage Through Levees and the Influence of Roots and
Animal Burrows

By

Diego Andres Cobos-Roa

A dissertation submitted in partial satisfaction of the requirements for
the degree of

Doctor of Philosophy

in

Engineering - Civil and Environmental Engineering

in the

Graduate Division

of the

University of California, Berkeley

Committee in charge:

Professor Nicholas Sitar, Chair

Professor Raymond Seed

Professor William Dietrich

Summer 2015

Abstract

Transient Seepage Through Levees and the Influence of Roots and Animal Burrows

by

Diego Andres Cobos-Roa

Doctor of Philosophy in Civil and Environmental Engineering

University of California, Berkeley

Professor Nicholas Sitar, Chair

Current levee analysis and design standards require the assumption of fully developed steady-state flow conditions for estimation of susceptibility of a levee to underseepage and/or piping via calculation of average uplift gradients. The use of steady state analysis conditions is generally considered the most critical scenario in terms of the development of pore pressure through and under the embankment; however, steady state seepage is not necessarily representative of real flooding conditions. Therefore, the objective of this research was to explore the transient development of pore pressure within and underneath a levee embankment, and to evaluate the influence of roots and animal burrows on the potential for development of preferential seepage and/or piping.

The first part of this dissertation focused on an assessment of the importance of transient seepage analysis in the estimation of heave or uplift gradients in levees for cases where a fine-grained blanket overlays a coarse aquifer layer. A series of analyses was performed to compare steady state and transient uplift gradients as a function of site geometry, aquifer and blanket hydraulic conductivity and flood duration. The results show that for high conductivity aquifers the transient seepage gradients exceed 90% of the steady state values within a few days during a flood event. However, for other geometries and flood durations, steady state seepage is overly conservative. Therefore, transient seepage analyses should be considered for newly designed levees or levees that are being re-constructed, assuming the sites are well characterized with respect to the geometry and properties of the foundation deposits.

The second part of the research focused on the assessment of the effects of woody vegetation and animal burrowing on levee performance, particularly seepage through the embankments. The results of two field seepage tests and the mapping of burrows at two test sites were used to provide prototype conditions for the transient seepage analyses. In general, the seepage tests showed that tree roots/root balls" tended to inhibit seepage front propagation and live roots did not serve as conduits for water as has been postulated in previous studies. The animal burrows, on the other hand, clearly presented readily available seepage paths when open to the waterside of the levee. The density of the burrows and their linear extent was found to be a function of the available food source, vegetation cover, and the frequency with which the burrows were eliminated. However, animal burrows that are not open to the water side do not

fill with water until full saturation is reached at the burrow/tunnel wall. This outcome can be shown analytically or through numerical simulations as shown herein. Consequently, the results show that the continuity, the length of the burrows, location of the burrows, and degree of saturation all play a role in the development of through seepage with the through going burrows/pipes clearly providing a direct seepage path and an opportunity for piping to occur. On the other hand, burrows from the land side of the levees that do not penetrate completely do not start to flow with a significant velocity until after the adjacent soil mass is completely saturated.

TABLE OF CONTENTS

CHAPTER 1 - INTRODUCTION	1
1.1. OBJECTIVES	2
CHAPTER 2 – INFLUENCE OF SEEPAGE ON LEVEE PERFORMANCE: STATE OF PRACTICE	3
2.1. INTRODUCTION	3
2.2. UNDERSEEPAGE BASICS, SAND BOILS, AND BLANKET HEAVE	3
2.3. CURRENT USACE AND CALIFORNIA DWR SEEPAGE GUIDELINES	14
CHAPTER 3 – TRANSIENT ANALYSIS OF LEVEE UNDERSEEPAGE	19
3.1. INTRODUCTION	19
3.2. CROSS SECTION AND MODEL PARAMETERS	20
3.3. MATERIAL PROPERTIES	23
3.3.1. Volumetric Water Content	23
3.3.2. Hydraulic Conductivity	24
3.4. RESULTS	26
3.4.1. Isochrones for Hydraulic Conductivity Ratio = 1,000	29
3.4.2. Isochrones for Hydraulic Conductivity Ratio = 100	30
3.4.2. Isochrones for Hydraulic Conductivity Ratio = 10	31
3.5. SUMMARY	32
CHAPTER 4 – INFLUENCE OF WOODY VEGETATION AND ANIMAL BURROWING ON LEVEE SEEPAGE	33
4.1. INTRODUCTION	33
4.2. REPORTED DETRIMENTAL EFFECTS OF WOODY VEGETATION IN LEVEES	33
4.2.1. URS (2011) Literature Review	34
4.2.2. Instances Reported by the USACE	37
4.3. EVALUATIONS OF LEVEE DISTRESS AND LEVEE BREACHES BY OTHERS	50
4.3.1. East Saint Louis Levee System, June 2008 Flood	50
4.3.2. Cap Au Gris Levee Breaches, Mississippi River, Winfield, MO	51
4.3.3. 1993 Missouri River Flood	53
4.4. BURROWING ANIMAL ACTIVITY	54
4.4.1. Pin Oak Levee Breach	58
4.4.2. Truckee Canal Breach, Fernley, NV	59

4.4.3. Medford Island Levee, CA	62
4.4.4. American River Flood Control District, Sacramento, CA	63
4.5. SUMMARY	71
CHAPTER 5 – FIELD EVALUATION OF BURROWING ANIMAL IMPACTS AND EFFECTIVENESS OF REMEDIAL MEASURES	73
5.1. INTRODUCTION	73
5.2. METHODS OF INVESTIGATION	74
5.2.1. Site Selection	74
5.2.2. Site Survey	74
5.2.3. Grouting Program	75
5.3. SITE 1: SANDY LEVEE	80
5.3.1. SITE 2: CLAYEY LEVEE SITE	85
5.4. EXCAVATION AND SURVEYING OF GROUTED BURROW GEOMETRY	92
5.4.1. SITE 1: Sandy Levee Site, Sacramento River	92
5.4.2. SITE 2: Clayey Levee Site, Cache Creek	100
5.5. SIGNIFICANCE OF THE COMPLETELY PENETRATING BURROW	103
5.6. SUMMARY OF RESULTS AND OBSERVATIONS	104
5.7. EFFECTIVENESS OF CEMENT-BENTONITE GROUT	108
5.8. CONCLUDING REMARKS	109
CHAPTER 6 – ANALYSIS OF THE INFLUENCE OF ROOTS AND BURROWS ON SEEPAGE THROUGH LEVEES	110
6.1. INTRODUCTION	110
6.2. CAL EXPO FIELD TEST	110
6.2.1. Summary of Recorded Data	113
6.2.2. Excavation	119
6.2.3. Modeling the Tree Root System	124
6.2.4. Soil Layers	125
6.2.5. Soil Properties	127
6.2.6. 3D Flow Model	131
6.3. TWITCHELL ISLAND SEEPAGE MODELING	136
6.3.1. Hydraulic Properties and Calibration	137
6.4. MODELING ANIMAL BURROWS AND OTHER DISCONTINUITIES	146

6.4.1. Idealized Simulations	146
6.4.2. Animal Burrow Field Test Modeling	152
6.5. PIPING POTENTIAL OF COMPLETELY PENETRATING BURROWS	158
6.5.1. Clayey Levee Site Modeling	160
6.6. CONCLUSIONS	162
CHAPTER 7 – FINDINGS AND CONCLUSIONS	164
CHAPTER 8 – REFERENCES	166

LIST OF FIGURES

Figure 2-1. Sand boil. Image from USACE (2011a)	4
Figure 2- 2. Schematic diagram showing heave mechanism	7
Figure 2-3. Piping mechanism	8
Figure 2-4. Calculation of heave potential (TAW, 1999)	9
Figure 2-5. Estimation of heave gradient (USACE, 2003)	11
Figure 2-6. Critical gradient i_c in relation to unit weight	11
Figure 2-7. Sellmeijer (1989) piping model (TAW, 1999)	13
Figure 2-8. Equilibrium hydraulic head in Sellmeijer's model (TAW, 1999)	14
Figure 2-9. Historical review of underseepage history, USACE (1956)	16
Figure 2-10. Flow chart for heave susceptibility on Dutch levees (TAW, 1999)	17
Figure 2-11. Flowchart for piping susceptibility on Dutch levees (TAW, 1999)	18
Figure 3-1. Definition of residual head used in underseepage analyses (USACE, 2003)	20
Figure 3-2. Cross section used for transient models	21
Figure 3-3. SEEP/W input section. All dimensions in meters	22
Figure 3-4. Base hydrograph used in transient analyses	22
Figure 3-5. Soil Water Characteristic Curves for clayey and sandy materials in transient models	24
Figure 3-6. Hydraulic conductivity functions used in the transient models	26
Figure 3-7. Example of evolution of total heads beneath clay blanket, $X_e/L=0$, $K_{aq}/K_{bl}=1,000$, peak duration= 5 days	28
Figure 3-8. Steady-state base case $X_e/L=0$, $K_{aq}/K_{bl}=1,000$	28
Figure 3-9. Transient head contours, $X_e/L=0$, $K_{aq}/K_{bl}=0$, time= 10 days	29
Figure 3-10. Example of time series of heave gradients, $X_e/L=0$, $K_{aq}/K_{bl}=1,000$, peak duration= 5 days	29
Figure 3-11. Isochrones for $K_{aq}/K_{bl}=1,000$	30
Figure 3-12. Isochrones for $K_{aq}/K_{bl}=100$	31
Figure 3-13. Isochrones for $K_{aq}/K_{bl}=10$	31
Figure 4-1. Performance records related to vegetation in California levees (URS, 2011)	37
Figure 4-2. 1993 Des Moines River breach (USACE, 1993). Red oval highlights root system	39
Figure 4-3. Downstream view of Des Moines River levee break (USACE, 1993). Red oval highlights root system	39
Figure 4-4. Erosion on waterside slope after tree toppling (USACE, 2007)	40
Figure 4-5. Cottonwood toppled on Puyallup River (WA). Image courtesy USACE	41
Figure 4-6. Damage on waterside toe, Touchet River (USACE, 2008)	41
Figure 4-7. View of landside toe area, St. Genevieve levee distress (USACE, 2008)	42
Figure 4-8. Active sand boils around trees, St. Genevieve levee distress (USACE, 2008)	43
Figure 4-9. Trees along landside toe. Grand Tower Levee (USACE, 2008)	44
Figure 4-10. Dense vegetation inhibiting visual inspection along Aniak levee in Alaska (USACE, 2008)	45
Figure 4-11. Vegetation covered slopes, Klutina River levee, Alaska (USACE, 2008)	45
Figure 4-12. Vegetation covered slopes, Tanana River levee, Alaska (USACE, 2008)	46
Figure 4-13. Tree growing inside landside subdrain system. Rio Grande, New Mexico (USACE, 2008).....	47
Figure 4-14. Trees at waterside toe and channel dug by beaver, Alamosa levee, Colorado (USACE, 2008)	47
Figure4-15. Beaver tunnel on waterside slope, just below tree line. Alamosa levee, Colorado (USACE, 2008)	48

Figure 4-16. Levee distress, Coffeyville levee, Kansas (USACE, 2007)	49
Figure 4-17. View of exposed roots on Coffeyville levee distress, Kansas (USACE, 2007)	49
Figure 4-18. Uprooted trees and root balls at the East St. Louis site. (Harder et al., 2009)	50
Figure 4-19. Sand boil at East St. Louis site (Harder et al., 2009)	51
Figure 4-20. Cap Au Gris - Site 1 (Harder et al., 2009)	52
Figure 4-21. View of eroded levee at Cap Au Gris - Site 1 (Harder et al., 2009)	52
Figure 4-22. Number of breaches as a function of woody corridor length (modified from Allen et al., 2003) [1 ft: 0.3048 m]	54
Figure 4-23. Effects of animal burrows in embankments	55
Figure 4-24. Pin Oak Levee breach (Harder et al., 2009)	58
Figure 4-25. Animal burrows on Pin Oak Levee breached section (Harder et al., 2009)	59
Figure 4-26. Truckee Canal cross sections (URS, 2008)	60
Figure 4-27. Developed breach looking downstream (URS, 2008)	61
Figure 4-28. Exposed grouted burrows 250 ft downstream of breached site (URS, 2008)	61
Figure 4-29. Collapse feature at the landside edge of burrow complex (URS, 2008)	62
Figure 4-30. Schematic of beaver den cave-in (MBK, 2009)	62
Figure 4-31. Beaver den cave-in, Medford Island, CA. Photo Courtesy Dustin Sanoski (DWR)	63
Figure 4-32. Internal view of the den showing access tunnels from the waterside (MBK, 2009)	64
Figure 4-33. View of the landside cave-in from the levee crown (MBK, 2009)	64
Figure 4-34. Waterside berm collapse at Arcade Creek levee. Images courtesy of Richard Marck (ARFCD)	65
Figure 4-35. Beaver den at Arcade Creek levee in 2006. Images courtesy of Richard Marck (ARFCD)	66
Figure 4-36. Beaver hole at waterside toe in 2004. Image courtesy of Richard Marck (ARFCD)	67
Figure 4-37. Beaver den at Arcade Creek. Images courtesy of Richard Marck (ARFCD)	67
Figure 4-38. Reoccurrence of beaver intrusion in Arcade Creek	68
Figure 4-39. Beaver den at the southern end of Arcade Creek in 2004. Images courtesy of Richard Marck (ARFCD)	68
Figure 4-40. Beaver burrow collapse at waterside toe near Arcade Creek in 2004. Images courtesy of Richard Marck (ARFCD)	69
Figure 4-41. Beaver burrow below paved bike path along north levee of American River in 2006. Images courtesy of Richard Marck (ARFCD)	70
Figure 4-42. Waterside slope collapse from beaver burrow along NEMDC in 2006. Images courtesy of Richard Marck (ARFCD)	70
Figure 4-43. Beaver den collapse at PGCC levee near Sacramento, CA. Photo courtesy Ray Costa (2012)	71
Figure 4-44. Remediation activities on beaver den at PGCC near Sacramento, CA. Photo courtesy Ray costa (2012)	71
Figure 5-1. Reference targets used for aligning T-LiDAR scans	75
Figure 5-2. DWR portable grout mixer for field tests	76
Figure 5-3. Typical DWR grouting procedure	77
Figure 5-4. Experiment setup: (a) injection tubing prior to installation, (b) installation of tubing using jackhammer	78
Figure 5-5. Experiment setup: example of triangular grid of chemical injection points	78
Figure 5-6. Experiment setup: (a) double-stroke pump system, (b) 'F assembly' injection device	79
Figure 5-7. Flow chart of polyurethane grout injection process	79
Figure 5-8. View of chemical grout injection procedure	80
Figure 5-9. Cross section at Sandy Levee Site [1 m: 3.28 ft]	81
Figure 5-10. Typical active squirrel burrows on landside slope at Sandy Levee Site	81

Figure 5-11. Largest active squirrel burrows on waterside slope at Sandy Levee Site	82
Figure 5-12. Plan view of surveyed burrows at Sandy Levee Site	83
Figure 5-13. Plan view of cement-bentonite and polyurethane injection points at Sandy Levee Site.	84
Figure 5-14. Simplified cross section at Sandy Levee Site	85
Figure 5-15. Cross section at Clayey Levee Site	86
Figure 5-16. High water on Clayey Levee Site during 1998. Images courtesy Al Romero, DWR	87
Figure 5-17. Volume of grout used on the Clayey Levee Site from 1995 to 2004 (data provided by Al Romero, DWR)	88
Figure 5-18. Location of burrows on landside slope at Clayey Levee site. Pink flagging indicates location of undifferentiated burrows, green flagging indicates burrows historically grouted with cement-bentonite by DWR.	89
Figure 5-19. Typical squirrel burrows on waterside slope at Clayey Levee Site	90
Figure 5-20. Plan view of identified burrows at the Clayey Levee Site	90
Figure 5-21. Map of grout injection points at the Clay Levee Site	91
Figure 5-22. Embankment cross section at Clayey Levee Site.	91
Figure 5-23. Exposed burrow system near waterside toe, Sandy Levee Site	93
Figure 5-24. Continuation of waterside burrow into the levee, Sandy Levee Site	94
Figure 5-25. Close up of den (grout mass) near waterside toe, Sandy Levee Site. The wooden stake points to a short burrow below the den	95
Figure 5-26. New hole after cement-bentonite grout on waterside toe, Sandy Levee Site. (a) shows the location of the new burrow and (b) shows the partially excavated open burrow below the cement-grouted main tunnel	95
Figure 5-27. Aerial view of east edge of main complex near landside edge of crown	97
Figure 5-28. Oblique view looking upstream of main complex near landside edge of crown	97
Figure 5-29. Lateral view of landside levee slope burrow system	98
Figure 5-30. Cross section showing LiDAR data on Sandy Levee Site	99
Figure 5-31. Close-up of landside burrow system (a) shows a cross section view, (b) a front view [1 m: 3.28 ft]	99
Figure 5-32. Views of the waterside burrow system [1 m: 3.28 ft]	100
Figure 5-33. View of excavated landside slope at Clayey Site	101
Figure 5-34. View of completely penetrating burrow	102
Figure 5-35. View looking north of completely penetrating burrow	102
Figure 5-36. Oblique view of waterside burrow system	104
Figure 5-37. Cross section view of completely penetrating burrow at Clayey Levee Site	104
Figure 5-38. Plan view of burrow system at Clayey Levee Site	105
Figure 5-39. Layer interface facilitating burrowing at Sandy Levee Site	106
Figure 5-40. New burrows on landside slope of reconstructed Sandy Levee Site	107
Figure 5-41. Ungrouted burrows on Sandy Levee Site. (a) shows a burrow near Level 1 of the large landside burrow complex, and (b) is an ungrouted burrow to the west of the same complex	107
Figure 6-1. Generalized cross section of wetting front test (Shriro et al., 2011)	112
Figure 6-2. Plan view of wetting front test (Cobos et al., 2012) [1 ft: 0.31 m]	112
Figure 6-3. Instrument layout of wetting front test. T: tensiometer, P: piezometer, EX: hand augered boring [1 ft: 0.3 m]	113
Figure 6-4. Calibration for 18" long tensiometers	114
Figure 6-5. Dry run data for control trench	115
Figure 6-6. Dry run data for stump trench	116
Figure 6-7. Test data for control section (Line C)	116
Figure 6-8. Test data for section away from stump (Line B)	117

Figure 6-9. Test data for stump section (Line A)	117
Figure 6-10. Saturation times of Line B	118
Figure 6-11. Saturation times for Line C	118
Figure 6-12. Saturation times for Line A	119
Figure 6-13. Reflective targets around mammal holes and decomposed roots, and metallic paint along stratigraphic contacts. Image modified from Cobos et al (2012)	121
Figure 6-14. Excavated stump	121
Figure 6-15. Baseline scan	122
Figure 6-16. Scans of excavation progression	123
Figure 6-17. Soil horizons highlighted from LiDAR scans	123
Figure 6-18. 3D views of stump	124
Figure 6-19. Root system point cloud	125
Figure 6-20. Isolated soil horizons	125
Figure 6-21. Generated stratigraphic contacts	126
Figure 6-22. Simplified analysis section	126
Figure 6-23. Gradation analyses for Cal Expo site	129
Figure 6-24. Initial moisture contents	130
Figure 6-25. Soil Water Characteristic curves	131
Figure 6-26. Model results for instrument Line A (stump). Solid lines: instrument data, Dots: model data	133
Figure 6-27. Model results for instrument Line B (gopher burrow). Solid lines: instrument data, Dots: model data	133
Figure 6-28. Saturation front after 1 hour of test simulation	134
Figure 6-29. Saturation front after 10 hours of test simulation	135
Figure 6-30. Saturation front after 50 hours of test simulation	135
Figure 6-31. Simulation results changing conductivity of roots	136
Figure 6-32. Location of instruments and analysis sections at the Twitchell Island centerline test site (Shriro, 2014)	139
Figure 6-33. Instrument line C showing instrument location and boundary conditions	139
Figure 6-34. Instrument line C devices TC2-36 and TC4-24	140
Figure 6-35. Instrument line C devices TC4-60 and TC4-36	141
Figure 6-36. Instrument line B section and boundary conditions	142
Figure 6-37. Instrument line B devices TB2-36 and TB4-36	142
Figure 6-38. Instrument line B devices TB4-60 and TB5-36	143
Figure 6-39. Instrument line A section and boundary conditions	144
Figure 6-40. Instrument line A devices TA2-36 and TA4-24	144
Figure 6-41. Instrument line A devices TA4-36 and TA4-60	145
Figure 6-42. Instrument line A devices TA5-24 and TA5-36	145
Figure 6-43. Idealized model section	147
Figure 6-44. Results of idealized model	148
Figure 6-45. Idealized model for flow into a single cavity	148
Figure 6-46. Material properties for single-cavity idealized model	149
Figure 6-47. Results of the single-cavity idealized model using sand	150
Figure 6-48. Results of the single-cavity idealized model using fine-grained soil	150
Figure 6-49. Multiple cavity idealized simulation	151
Figure 6-50. Multiple cavity simulation results	151
Figure 6-51. No cavity simulation results	152
Figure 6-52. Simplified representation of animal burrow networks	153

Figure 6-53. Steady state simulation of Sandy Levee Site burrows. Total head contour interval 0.25 m	153
Figure 6-54. Geometry of the model section with completely penetrating burrows	154
Figure 6-55. Results from transient analysis after one day of simulation with burrow at C. contour interval: 0.25 m	154
Figure 6-56. Evolution of pore pressures on a vertical section across the levee crown for Hole C.....	155
Figure 6-57. Results from transient analysis after one day of simulation. No holes present. Total head contour interval: 0.25 m	155
Figure 6-58. Evolution of pore pressures on a vertical section across the levee crown for the case of no hole	156
Figure 6-59. Results from transient analysis after one day of simulation with burrow at A. Total head contour interval: 0.25 m	156
Figure 6-60. Evolution of pore pressures on a vertical section across the levee crown at burrow A..	157
Figure 6-61. Results from transient analysis after one day of simulation with burrow at B. Total head contour interval: 0.25 m	157
Figure 6-62. Evolution of pore pressures on a vertical section across the levee crown for Hole B	158
Figure 6-63. Piping potential evaluation using the Ohja (2003) formula	159
Figure 6-64. Piping potential evaluation using the Sellmeijer (1988) formula	159
Figure 6-65. High water on Clayey Levee Site in 1998. Images courtesy Al Romero, DWR	160
Figure 6-66. Clayey levee site 3D model	161
Figure 6-67. Critical flow velocities for different particle sizes compared to range of velocities along burrow	162

LIST OF TABLES

Table 2-1. Seepage factors for piping (Rijkswaterstaat, 1999)	12
Table 3-1. Summary of material properties for transient models	26
Table 3-2. Summary of transient models	26
Table 4-1. Levee failure modes and their relation to woody vegetation. Source: USACE (2012, International Levee Handbook)	34
Table 5-1. Approximate time required to fill holed with cement-bentonite grout	84
Table 5-2. Index soil properties for Sandy Levee test site	85
Table 5-3. Index soil properties for the Clayey Levee test site	91
Table 5-4. Summary of grout volumes	108
Table 6-1. Soil properties used for flow models	129
Table 6-2. Soil properties used for Twitchell Island flow models	137

ACKNOWLEDGEMENTS

There is a long list of people that made this dissertation possible. I have my family to thank: the love of my life, Libia Diaz for putting up with all the time invested in this project; my boy, Nico for keeping us up all night every night after May 2011, and of course my mother Patricia, father German and older brother Juan.

From the University of California at Berkeley, I am in eternal debt to my advisor, Professor Nicholas Sitar and co-advisor Raymond Seed. Thank you for all your guidance and advice both in engineering matters and matters of life. Professor Jonathan Bray for being a key part of the California Levee Vegetation Research Program and guiding my co-worker and me during several challenging field tests. Professor Michael Riemer for allowing me to work with him as assistant on the geotechnical laboratories during several years of my stay at the university. Professor William Dietrich for teaching me two of the most interesting classes I have ever attended and Professor William Nazaroff for introducing me to the beautiful world of environmental engineering. Finally, Professor Juan Pestana, my advisor during my master's studies, for allowing me to enter the program at Berkeley in the first place and allowing me to participate in the New Orleans investigations, as well as supporting me during personal challenges.

Also from UC Berkeley, my heart goes out to Shelley Okimoto, whose assistance allowed me to sort out the endless loops of academic life. My dear co-worker in the California Levee Vegetation Research Program, Michelle Shriro: it has been a pleasure to work with you.

It was my utmost pleasure to have worked with or shared with my french brother Julien Waeber, officemates Justin Hollenback and Hamed Hamedifar, Gabriel Candia, Joe Webber, Roozbeh Grayeli, Tonguc Deger, Catherine Jones and all the other PhD students part of 'GEOBEARS', our small group of graduate students. I would also like to thank the Masters class of 2010. Finally, my old friends from the 2005 Masters class, and specially the teaching assistants I had the opportunity to learn from: Xavier Vera, Adda Athanasopoulos, and Jennifer Donahue.

The California Levee Vegetation Research Program provided funding for the second part of this dissertation; this was a very challenging project which allowed us to integrate engineering concepts with environmental conservation. Peter Buck and Mick Klasson from the Sacramento Area Flood Control Agency provided part of our funds and platforms to showcase our findings, Roy Kroll, Cassandra Musto and Al Romero from the California Department of Water Resources facilitated permitting, equipment and even hand labor during the field phase of our work. Richard Marck, Tim Kerr and the staff from the American River Flood Control District, who allowed us to destroy one of their levees and allowed me to accompany them during regular levee inspections. Same goes for Jack Bailey and Max Sakato of Reclamation District 1500, your levees provided the most interesting field site.

I also extend my gratitude to the external advisors and other members of the California Levee Vegetation Research Program; Don Gray from the University of Michigan, George Sills from Sills Engineering, Doug Shields from the USDA, Les Harder from HDR, Gerald Bawden from USGS for all the superb LiDAR work you provided for the program, Allison Berry, Dirk Van Vuren, Shih-

Ming Chung, Richard Evans from UC Davis, and John Lichter from Tree Associates. Thank you for your invaluable advice, help and suggestions on our project.

My friends at URS Corporation helped me every step of the way, thank you Lelio Mejia, Said Salah-Mars, Phil Meymand, Bob Green, Sathish Murugaiah, Kanax Kanalalingam, Camilo Quiñones, John Paxton, Khaled Chowdury and the folks from the Oakland and Sacramento offices of this great company.

The numerical models presented in this dissertation were performed using GEOSTUDIO®. Curtis Kelln, Carola Preusser and all the folks at technical support from this amazing company provided me with invaluable support and a license for their 3D package.

Finally, my gratitude and respect to my friends Scott Shewbridge from the USACE and Juan Perri from Exponent. You truly are an inspiration.

Chapter 1

INTRODUCTION

The American Society of Civil Engineers (ASCE) has rated the current US flood defense systems as having the lowest levels of adequacy and reliability among all types of infrastructure (Seed et al., 2012). A dominating factor for this rating is the very high vulnerability of many levees to seepage induced failures. These types of failures, particularly failures due to underseepage and/or piping phenomena have historically been recognized as the most common failure mechanisms (Turnbull and Mansur, 1956).

The effect of increased pore water pressures on slope stability is well recognized (see e.g. Terzaghi, 1950) and it is particularly important with respect to levee stability. Many levees, especially “legacy” levees, were built directly on a relatively thin blanket comprised of fine-grained materials deposited when flows overtopped or breached the natural or man-made levees. In many settings this thin fine-grained layer (or blanket) is frequently underlain by a thicker coarse grained layer, which, if “open” to the riverside, behaves as a confined aquifer layer that conveys water beneath the embankment with relatively low head loss.

Current levee analysis and design standards require the assumption of fully developed steady-state flow conditions. Consequently, steady state seepage calculations are used to estimate the susceptibility of a given levee to underseepage and/or piping via calculation of average uplift gradients through the top stratum and exit gradients near the toe. The computed pore pressures are in turn employed in a slope stability calculations that assume fully drained effective stress shear strength conditions for all layers in the profile coupled with the generated pore pressures from the seepage analysis. This is detailed in *Analysis Case III* from the U.S. Army Corps of Engineers (USACE) EM 1110-2-1923 (USACE, 2000). The use of steady state analysis conditions is generally considered the most critical scenario in terms of the development of pore pressure through and under the embankment, and generally results in very low factors of safety (Perri et al., 2012). However, steady state seepage is not necessarily representative of real flooding conditions and, depending on geometric and hydrogeologic conditions, transient conditions can be as critical for relatively short duration flood loading.

Another levee performance issue related to time dependency is the influence of woody vegetation and animal activity within a levee embankment and its foundation on seepage. It has been observed that biotic activity increases the risk of levee failure by adding preferential seepage paths along the large, continuous voids left by the roots or burrows, which lead to piping and altering of wetting front patterns. In fact, loading duration, degree of saturation of

the levee materials and other environmental conditions can dictate whether the discontinuities left by biotic activity pose a greater threat than liquefaction, waterside erosion, underseepage and other types of loading.

1.1. OBJECTIVES

The main objective of this dissertation was to look at the abovementioned performance issues considering time-dependency as a potentially more adequate loading condition to assess levee instability. In particular, the efforts were focused on answering the following questions:

- 1) What is the role of transient loading on levee underseepage and blanket heave? Many levees protecting certain areas hold high water for months or years at a time, making the establishment of steady state conditions almost a certainty; however, many other levees are loaded for days or weeks at the most, thus assuming steady state conditions may not necessarily be the most adequate design consideration. To this end, a set of comparison steady state and transient, finite element analyses of uplift gradients was developed for a wide range of levee geometries, soil conductivities and flood durations to create a framework for the assessment of the adequacy of steady state assumptions for a given levee profile.
- 2) What are the effects of root and animal activity on the seepage performance of a levee? Can the voids left by roots and animals allow the development of a progressing wetting front into a discontinuity so water that flows fast enough that the walls of the hole are eroded and a pipe failure ensues? A field, laboratory and analytical programme was undertaken to analyze the effects of these issues and to evaluate their influence on transient flow through a levee embankment.

Chapter 2

INFLUENCE OF SEEPAGE ON LEVEE PERFORMANCE: STATE OF PRACTICE

2.1. INTRODUCTION

Seepage under levees (underseepage) and the associated decrease in effective stress are considered the most common causes of failure of levees. Turnbull and Mansur (1961) identified this failure mechanism as the uplift effect from increased pore pressures on a pervious stratum under the levee and/or fine-grained top stratum, which can generate heaving or rupture of surficial layers, and can lead to piping and internal erosion. In the years following Hurricane Katrina, analysis and design methods have been updated and now recommend the use of steady state water pressures generated from seepage calculations (USACE, 2000). This approach is believed to yield overly conservative pore pressure fields and, therefore, very low factors of safety for relatively short duration flood loadings. However, because of its simplicity and because steady state seepage parameters are easier to determine than the corresponding time-dependent parameters (Peter, 1982), steady state analysis is far more common than transient analysis.

This chapter describes the basic equations for steady and transient seepage analyses and then presents a review of the mechanism of heave and piping, including the currently recommended USACE and Dutch underseepage and heave susceptibility analysis methods.

2.2. UNDERSEEPAGE BASICS, SAND BOILS, AND BLANKET HEAVE

Many levees are built as a barrier to rising waters next to rivers or canals. Consequently, high water levels on the waterside create a hydraulic gradient that can induce seepage under the levee and emerge from the ground on the protected side (USACE, 2003). Given certain geometric and hydraulic conditions, this flow of water may induce movement of particles and

formation of volcano-like features, widely known as sand boils (Figure 2-1). This phenomenon occurs when coarse-grained particles are dragged by the water and carried to the surface by the fast flowing water beneath the levee toe and is referred to as piping. Piping ultimately produces voids (or pipes) in the sand under or within the levee, beginning at the mouth of the sand boil downstream of the levee toe and extending upstream a certain distance.



Figure 2-1. Sand boil. Image from USACE (2011a)

A levee subject to a change in hydraulic loading from an increase in water elevation on the canal or river side will develop underseepage pressures if a pervious layer is hydraulically connected to the river channel. Increased hydraulic head propagates from the riverside towards the landside within the more pervious layer at a rate faster than along the overlying fine-grained blanket and levee, which can induce heave of the blanket and gradual static liquefaction of the coarse grained layer (Ozkan, 2003).

The methods of analysis for underseepage commonly deal with the solution of partial differential equations to estimate hydraulic heads and flow or Darcy velocities across a flow media. A brief summary of these equations is provided in the following paragraphs. For more details, common references are included in classic groundwater texts (Freeze and Cherry, 1979; Cedergren, 1997)

STEADY STATE CONDITIONS

Steady state flow occurs when at any point in a flow field the magnitude and direction of the flow are constant with time (Freeze and Cherry, 1979). The solution for Darcy flow in three

dimensions through an anisotropic saturated porous medium and is given by Laplace's equation:

$$\frac{\partial}{\partial x} \left(K_x \frac{\partial h}{\partial x} \right) + \frac{\partial}{\partial y} \left(K_y \frac{\partial h}{\partial y} \right) + \frac{\partial}{\partial z} \left(K_z \frac{\partial h}{\partial z} \right) = 0 \quad (2.1)$$

Where K is the value of saturated hydraulic conductivity in the x , y and z directions. This equation yields the value of hydraulic head h at any point in the flow field, and is widely used in analytical and numerical processes to solve steady-state groundwater problems. By simplifying Equation 2.1 assuming isotropic conditions and flow in two dimensions, flow nets can be constructed using graphical solutions or hand calculations (see e.g. Cedergren, 1997).

TRANSIENT CONDITIONS

Transient flow occurs when at any point in a flow field the magnitude or direction of the flow velocity changes with time (Freeze and Cherry, 1979). Time-dependent conditions are commonly used to analyze unsaturated problems where saturation increases as a wetting front advances from a source of hydraulic loading, but can also be employed to model the development of pressure pulses from short duration storms along saturated aquifer layers below levees and dams that can lead to potential heave or piping. The formulation for transient flow for a saturated anisotropic medium is given by an expanded form of Equation 2.1:

$$\frac{\partial}{\partial x} \left(K_x \frac{\partial h}{\partial x} \right) + \frac{\partial}{\partial y} \left(K_y \frac{\partial h}{\partial y} \right) + \frac{\partial}{\partial z} \left(K_z \frac{\partial h}{\partial z} \right) = S_s \frac{\partial h}{\partial t} \quad (2.2)$$

Where S_s is specific storage. This equation relates changes in head with a mass rate of water produced by an expansion of the water under a change in density, and a mass rate of water generated by a volume change (porosity) of the medium. For an isotropic saturated porous medium and strictly horizontal flow, Equation 2.2 reduces to:

$$\frac{\partial^2 h}{\partial x^2} + \frac{\partial^2 h}{\partial y^2} = \frac{S}{T} \frac{\partial h}{\partial t} \quad (2.3)$$

where S , is storativity and T , is the transmissivity of the aquifer. For unsaturated conditions, the Laplace equation is modified to consider the changes in hydraulic conductivity that a material experiences as it becomes unsaturated, by including the soil water characteristic curve (SWCC) functions. This modified equation (Equation 2.4) is often called *Richards equation*, after Richards (1931).

$$\frac{\partial}{\partial x} \left(K(\psi) \frac{\partial \psi}{\partial x} \right) + \frac{\partial}{\partial y} \left(K(\psi) \frac{\partial \psi}{\partial y} \right) + \frac{\partial}{\partial z} \left(K(\psi) \left(\frac{\partial \psi}{\partial x} + 1 \right) \right) = C(\psi) \frac{\partial \psi}{\partial t} \quad (2.4)$$

Where ψ is the matric suction, and $C(\psi)$ is the characteristic curve function describing the changes in volumetric water content with suction, sometimes written as $\theta(\psi)$. Note that the hydraulic conductivity is a non-linear function of matrix suction, which makes the choice of parameters and solution of the problem more challenging than assuming fully saturated conditions.

Equation 2.1 through Equation 2.4 are the governing relationships available in finite element or finite difference software for the numerical computation of underseepage problems (see e.g. Geo-Slope International, 2008).

BLANKET HEAVE AND PIPING

The mechanisms of blanket heave (uplift) and piping are closely related and are controlled by forces acting on a soil grain in a porous medium subject to water flow in response to an energy gradient and the resulting seepage forces acting on the grain. The Netherlands Technical Advisory Committee on Flood Defenses (Technical Advisory Committee on Flood Defences, 1999) describes the process of heave and piping as follows:

- Uplift of the covering layer on the inside of the levee (dike): a high outside water level will cause the water pressures in the sand layer (aquifer) to increase. When the water pressures at the site of the covering layer on the inside become greater than the weight of that layer, this will start to push up. In practice, uplifting is sometimes, but not always to be observed via weak wave movements on the surface when it is trod upon.
- Cracking of the covering layer and the creation of boils: cracks in the covering layer can occur due to uplift, through which the seepage water finds its way to the surface. Due to the erosion capability of this seepage flow, a channel is created between the sand layer and the surface (crack channel). The eroded material from the crack channel is borne by the seepage flow and deposited around the outflow opening. The diameter of the crack channel can vary substantially depending on the flow speed and the erodibility of the material in the covering layer (blanket).
- Erosion of the sand layer: Sand particles are transported from the sand layer to the crack channel by seepage exiting the sand layer. The crack channel is thus filled with sand in a fluidized state. The flow resistance in the crack channel rises. There are now two possibilities, namely (1) the flow speed at the site of the exit point decelerates to such a degree that the erosion process stops due to increased resistance, or (2) the flow speed decelerates insufficiently, so that the transport of sand to the crack channel continues in

the first case the boil will start to produce 'clean' water. In the second case sand will be transported by the seeping flow via the crack channel to the surface and be deposited around the boil, where a sand crater is created. In the sand layer small channels (pipes) are created at the top of the sand layer directly under the top layer, which expand upstream.

- *Creation of through pipes: In the case of sufficient hydraulic head over the defense, the erosion channels will continue to grow until they reach the outside water. There is then an open connection between outside water and exit point, which means that the flood defense has become sensitive to piping.*
- *Collapse of the flood defense: As a consequence of the creation of through pipes, they will continue to erode at an accelerated rate, so that their dimensions increase. Ultimately it is assumed that this will lead to hollow spaces under the flood defense which are so large that subsidence and cracking of the dike body occurs. Factual observation of this collapse process and its duration, at least at dikes are not available however. In small-scale tests it has been observed how the further erosion of the sand layer after the creation of a through pipe occurs very quickly, that is in around a minute. Although the creation of through pipes cannot be immediately identified with the actual collapse of the dike itself, this is assumed in the current design philosophy. The limit state 'creation of through pipes' is accordingly interpreted as limit state in relation to collapse.*

In addition to established flow regime, piping susceptibility is also a function of geometry of the subsurface layers and material properties. A typical subsurface profile beneath a levee consists of a fine-grained top layer, generally deposited over long periods of time as fines settled after high flows overtopped existing levees and left low energy clay and silt deposits atop coarser alluvial fans. Alternatively, this top layer may have been placed as part of a reclamation or engineering project. If this fine-grained top (blanket) layer is present, heave and cracking of the blanket (Figure 2- 2) is necessary to initiate sand boils and piping (Figure 2-3), unless open paths are present from penetrations, ditches, decomposed roots or animal burrows.

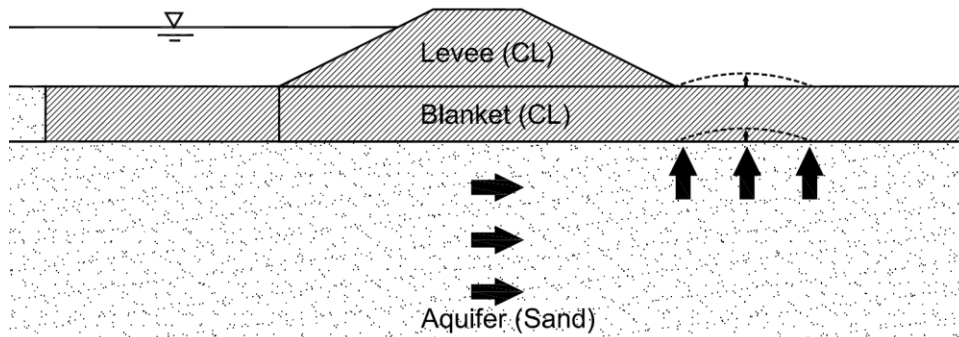


Figure 2- 2. Schematic diagram showing heave mechanism

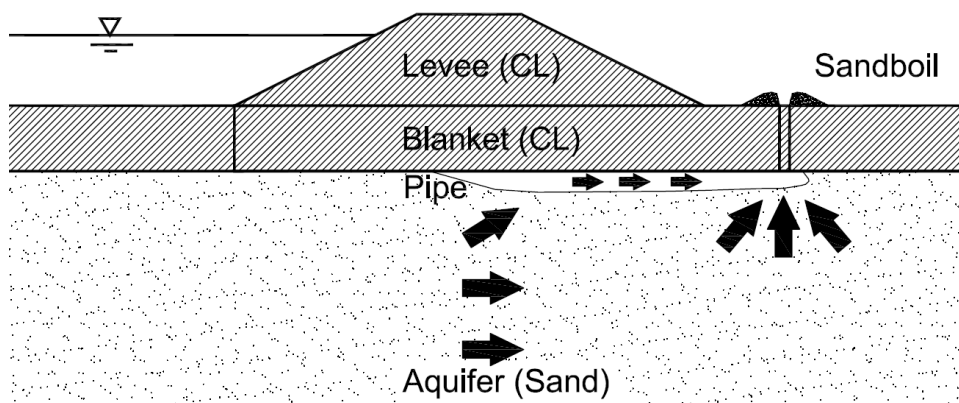


Figure 2-3. Piping mechanism

HEAVE CALCULATION

The parameters controlling heave susceptibility are the unit weight of the surficial stratum and the hydraulic heads developed across the aquifer layer. The Netherlands Technical Advisory Committee on Flood Defences (TAW, 1998) proposed a limit equilibrium calculation for the heave and cracking susceptibility of blanket layers, and set a limiting value of head (potential limit) equal to the hydraulic head that yields an uplift pressure equivalent to the value of downward pressure from the blanket layer. Several texts (TAW, 1998; USACE, 2003) express the heave potential simply as the ratio of buoyant unit weight of the top stratum and the water pressures exerted by underseepage flow. Other calculation methodologies include the estimation of the heave gradient, which is the ratio of the residual hydraulic head and the thickness of the blanket (Figure 2-5). On this figure, gradient is estimated by setting an arbitrary datum along the ground surface adjacent to the landside toe, and the residual hydraulic head (h_o) is defined as the total head above the datum measured beneath the blanket layer if a piezometer was placed on the aquifer. In other words, the gradient through the top blanket is the rate of change of total head with respect to vertical distance (USACE, 2003), or:

$$i = \frac{h_o}{z} \quad (2.5)$$

Where i is the heave gradient, h_o is the difference between the hydraulic head at the bottom of the blanket and the elevation of the ground surface near the levee toe (residual head), and z is the thickness of the blanket. A similar estimate is provided by TAW (1998) for Dutch levees (Figure 2-4) and was employed in the WATEX software (Deltares, 1999) developed for the computation of the flow field beneath the blanket.

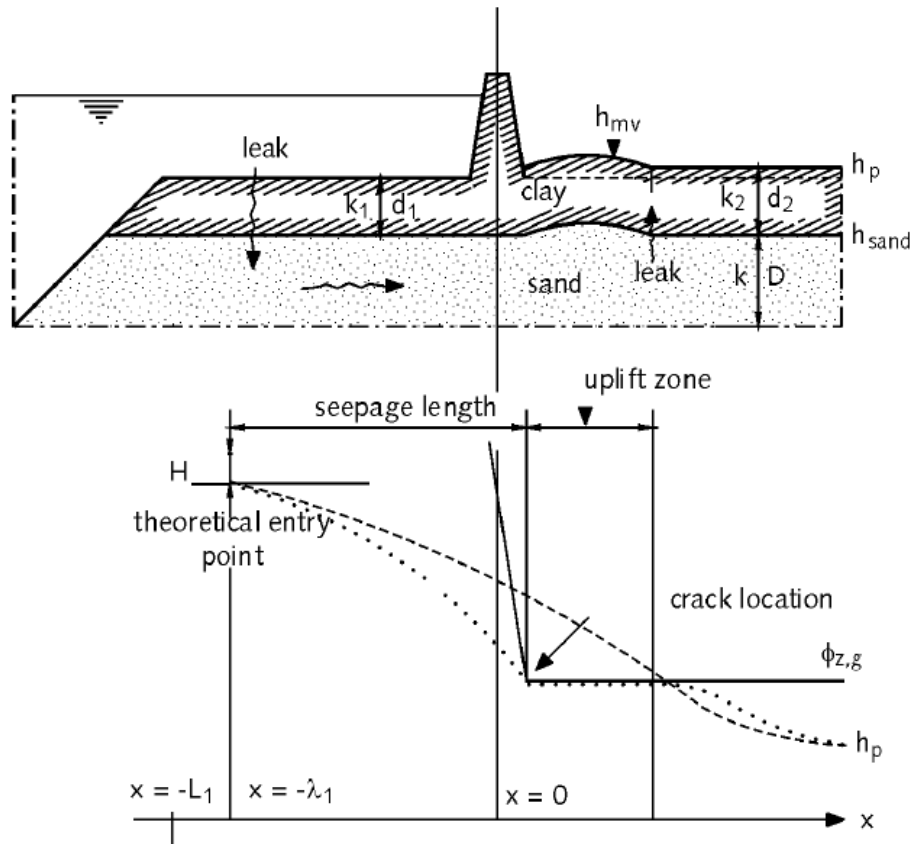


Figure 2-4. Calculation of heave potential (TAW, 1999)

Along the h_{sand} surface on Figure 2-4 the weight of the blanket layer works vertically down, and is counteracted by the water pressure from the aquifer layer. Equilibrium is reached when:

$$(\phi_{zg} - h_{sand})\gamma_w = (h_{mv} - h_p)\gamma_{dr} + (h_p - h_{sand})\gamma_{nat} \quad (2.6)$$

Where ϕ_{zg} is the limiting hydraulic head or potential, h_{sand} is the elevation of the top of the aquifer layer, h_{mv} is the ground surface elevation, h_p is the phreatic head at the bottom of the blanket layer above the ground surface (or residual head), γ_w is the unit weight of the water, γ_d

is the dry unit weight of the blanket, and γ_{nat} is the moist unit weight of the blanket layer. Equation 2.6 is valid for total heads beneath the blanket lower than the elevation of the ground surface at the levee toe. For heads greater than the ground surface elevation, the second term on this equation changes to $(h_p - h_{mv})\gamma_w + (h_{mw} - h_{sand})\gamma_{nat}$

The limiting value of head is then expressed as:

$$\phi_{zg} = h_p + d \frac{\gamma_{nat} - \gamma_w}{\gamma_w} \quad (2.7)$$

Where d is the thickness of the blanket layer. Similarly, the USACE defines heave potential in terms of a heave gradient (Figure 2-5), as the ratio between the residual head (h_o) and the thickness of the blanket (z). Heave occurs when the heave gradient exceeds a critical value, often defined as:

$$i_{crit} = \frac{\gamma_{sat} - \gamma_w}{\gamma_w} \quad (2.8)$$

Where γ_{sat} is the saturated unit weight of the soil. Critical gradient is often assumed to be 0.85, but in fact this factor is a function of the unit weight of the soil. This principle is derived from the concept of total and effective stress acting at the plane along the bottom of the blanket. The pore water pressure along this plane is described by:

$$u = \gamma_w(h_o + z) \quad (2.9)$$

The conditions at which boiling occurs can be determined by setting the water pressure equal to the total stress:

$$\begin{aligned} \gamma_w(h_o + z) &= \gamma_{sat}z \\ \frac{h_o}{z} &= \frac{\gamma_{sat} - \gamma_w}{\gamma_w} \end{aligned} \quad (2.10)$$

The critical gradient is given by the right hand side of Equation 2.10, and is a function of the saturated unit weight of the layer, assuming the density of the water is constant (Figure 2-6).

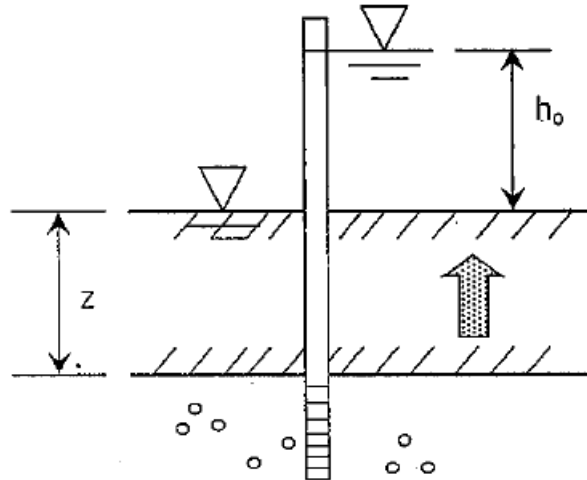


Figure 2-5. Estimation of heave gradient (USACE, 2003)

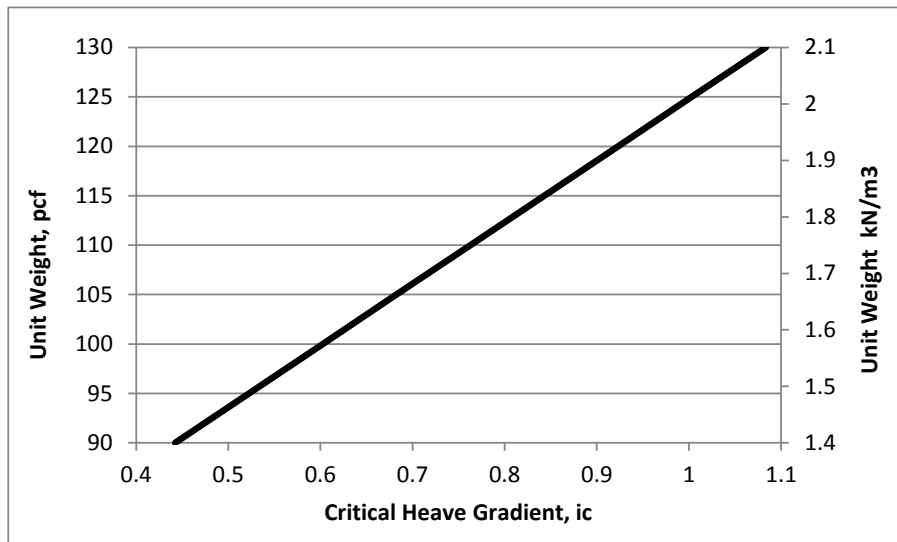


Figure 2-6. Critical gradient i_c in relation to unit weight

PIPING CALCULATION

Once heave or uplift potential has been established, movement due to uplift may generate cracks on the blanket layer and piping can initiate. Common methods to estimate piping potential are based on work by Terzaghi as cited by Peter (1982), in which a critical porosity-dependent hydraulic gradient is estimated as follows:

$$i_c = \frac{\gamma_{sat} - \gamma_w}{\gamma_w} (1 - e) \quad (2.11)$$

Where i_c is the critical gradient, e is the clean bed porosity, and γ_{sat} and γ_w are the saturated unit weight of the soil and water unit weight, respectively. Other available models include porosity as for example Khilar et al. (1985):

$$i_c = \frac{\tau_c}{2.878\gamma_w} \left(\frac{e}{K_h} \right)^{0.5} \quad (2.12)$$

Where K_h is the saturated horizontal hydraulic conductivity, τ_c is the critical shear or tractive stress at the onset of piping. Common correlations for critical shear stress are a function of a representative grain size (d_{50}): $\tau_c = c \cdot d_{50}$, where c is often assigned a value of 10.

Singh et al. (2002) proposes a porosity-based model for critical head and gradient after reviewing available methodologies (Equation 2.13), defining two parameters, m and n based on a statistical analysis of laboratory tests performed by Weijers and Sellmeijer (1993).

$$i_c \propto \left(\frac{(1-e)^m}{e^n} \right) \quad (2.13)$$

Bligh (1910) proposed perhaps the first model for piping under hydraulic structures. This model 'checks' for heave on the top layer and piping along the underlying aquifer, by defining a qualitative characterization of the aquifer soil, known as creep factor.

$$\Delta H \leq \Delta H_c = \frac{L}{C_{creep}} \quad (2.14)$$

Where ΔH is the hydraulic head on the riverside, ΔH_c is the maximum permissible gradient, L is the minimum seepage length, commonly defined as the footprint of the levee embankment, and C_{creep} is the creep factor. Similarly, Lane (1934) proposed a modification to Bligh's model to account for vertical features that add resistance or head loss through the aquifer layer:

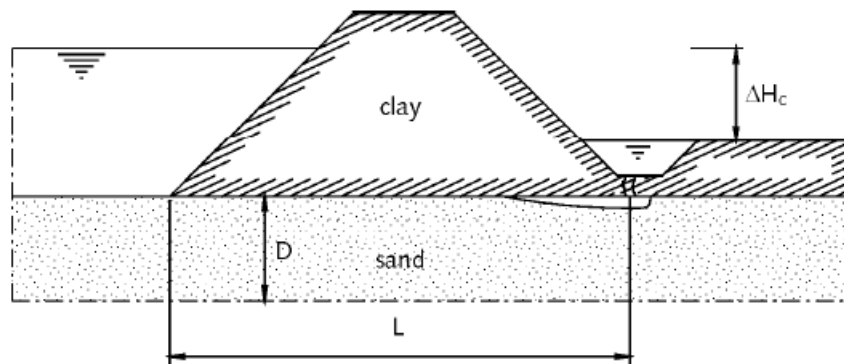
$$\Delta H \leq \Delta H_c = \frac{\left(\frac{1}{3}L_h + L_v \right)}{C_{creep}} \quad (2.15)$$

Where L_h is the total length of the horizontal seepage path, and L_v the total length of the vertical seepage paths. The vertical component is important when cutoff walls, sheetpiles or other vertical features exist in the cross section. Table 2-1 summarizes the creep factors for the methods by Bligh and Lane.

Table 2-1. Seepage factors for piping (Rijkswaterstaat, 1999)

Soil Type	Median Gran Diameter (μm)	C_{creep} (Bligh, 1910)	C_{creep} (Lane, 1934)
Extremely fine sand	<105	-	8.5
Very fine sand	105 – 150	18	7
Very fine sand (mica)	150 – 210	15	7
Medium coarse sand	210 – 300	-	6
Very coarse sand	300 – 2000	12	5
Fine gravel	2000 – 5600	9	4
Medium coarse gravel	5600 – 16000	-	3.5
Very coarse gravel	>16000	4	3

More recently, Sellmeijer (1989, 1993) developed a mathematical model for piping calculations based on three governing principles: (1) the groundwater (Darcy) flow through the soil, (2) water flow through the eroding pipe, and (3) a state of limit equilibrium of the particles along the bottom and sides of the pipe (Sellmeijer, 2006). With this model, a maximum head on the waterside can be estimated at which point the sand grains within the aquifer are still in equilibrium. This value of head is a function of the pipe length to levee footprint length ratio (l/L) in Figure 2-7, the hydraulic conductivity of the aquifer, the coefficient of drag of the sand particles.

**Figure 2-7. Sellmeijer (1989) piping model (TAW, 1999)**

Sellmeijer's method assumes that for a head below the critical value, an erosional fissure will develop and stabilize at a certain point. The corresponding gradients decrease as the fissure or pipe lengthens, and the sand grains along the fissure offer no further resistance to drag forces. If the head increases the fissure will grow again until a new state of equilibrium is reached (Figure 2-8). Following this assumption, Sellmeijer's model was developed:

$$\Delta H_c = \alpha c \frac{\gamma_p}{\gamma_w} \tan(\theta) (0.68 - 0.1 \ln(c)) L \quad (2.16)$$

$$\alpha = \left(\frac{D}{L}\right) \left(\frac{0.28}{\left(\frac{D}{L}\right)^{2.8} - 1}\right)$$

$$c = \eta d_{70} \left(\frac{1}{\kappa L}\right)^{1/3}$$

Where ΔH_c is the critical hydraulic head on the waterside, γ_w and γ_p are the unit weight of the water and submerged unit weight of sand grains, respectively, θ is the rolling resistance angle of sand grains, η is the drag coefficient, κ is the intrinsic permeability of the aquifer, d_{70} is the particle diameter coarser than 70% of the soil, D is the thickness of the aquifer, and L is the length of the seepage path, measured horizontally.

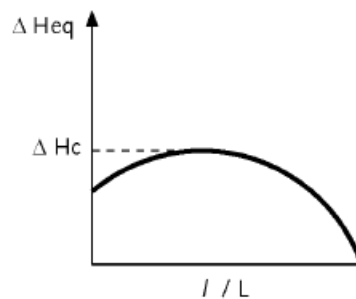


Figure 2-8. Equilibrium hydraulic head in Sellmeijer's model (TAW, 1999)

2.3. CURRENT USACE AND CALIFORNIA DWR SEEPAGE GUIDELINES

Technical Letter 1110-2-569 (USACE, 2005) provides a summary of current levee design and analysis underseepage guidance, including the rationale for selection of critical gradients. Derived from the work by Turnbull and Mansur (1956) and reproduced in TM 3-424 (USACE, 1956), Figure 2-9 presents a relationship between gradient and severity of seepage for 16 sites along the Lower Mississippi River during the 1950 flood. From this figure trends have been adopted for the triggering and/or reactivation of sand boils, as follows: (a) for gradients between 0 and 0.5, 'light to no seepage' is expected; (b) for gradients between 0.2 and 0.6 'medium seepage' can result; (c) gradients between 0.4 and 0.7 'heavy seepage' can result, and (d) gradients 0.5 to 0.8 likely will result in 'sand boils'. The ranges specified in TL 1110-2-569 indicate that there is a large variation in the value of gradient that may cause sand boils to form, but the letter indicates that occurrence of sand boils under gradients of 0.5 or lower may be due to reactivation of existing boils rather than genesis of new ones. Gradients specified in this technical letter, TM 3-424 and other USACE publications are computed using the ratio of residual hydraulic head and blanket thickness in Equation 2.5, and hydraulic heads beneath the blanket are computed using *blanket theory* (USACE, 2000). Blanket theory is an analytical

procedure developed for underseepage analysis presented in TM 3-424. It assumes a two-layer system of uniform thickness and horizontal boundaries, comprised of a semi pervious top blanket and a pervious sand stratum. Flow in the pervious substratum is assumed to be horizontal and flow through the blanket layer is assumed to be vertical. Current practice allows the use of finite element or finite difference software to estimate the values of residual hydraulic heads beneath the blanket.

This is reflected in the following criteria (USACE, 2005):

“These current requirements apply to all projects, existing and new construction. If the computed upward gradient through the blanket at the landside toe of the levee is greater than 0.8, a seepage berm should be designed with an allowable upward gradient of 0.3 through the blanket and berm at the landside toe of the levee (approximately equivalent to a factor of safety of 2.8 at the 0.3 gradient). A lower factor of safety could be used if there were sufficient soil data and past performance information to justify it. The berm width would be designed to lead to an allowable upward gradient of 0.8 at the berm toe, with a maximum width of 300 to 400 feet.”

The technical letter emphasizes gathering past performance data to corroborate the computed values, as well as instrumenting the levees and conducting detailed geotechnical investigations to obtain detailed information and minimize the uncertainties in gradient calculation. Under such conditions, the technical letter allows for a lower factor of safety:

“The allowable factor of safety for use in evaluations and/or design of seepage control measures should correspond to an exit gradient at the toe of the levee of $i = 0.5$. In general, this would provide a factor of safety of about 1.6. This change will standardize all levee seepage requirements to one exit gradient of 0.5. Landside drainage ditches (along the toe of the levee), seepage berms, and relief wells should all be designed to the same exit gradient of 0.5.”

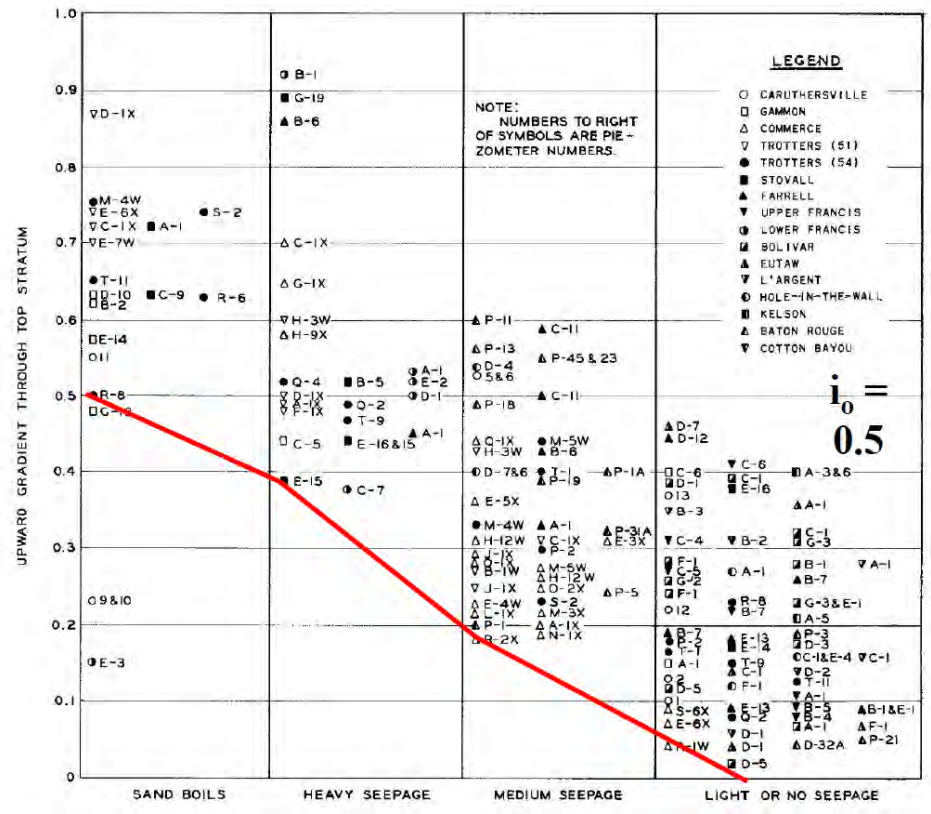


Figure 2-9. Historical review of underseepage history, USACE (1956)

Common practice in the Netherlands includes the determination of piping potential using common empirical formulas developed by Bligh (1910), Lane (1934), Sellmeijer (1989), and the fragment method contained in TAW (1999), which recommends simple flow charts to decide whether a given levee is in need of heave (Figure 2-10) or piping (Figure 2-11) remediation, by applying the methodologies by Lane, Bligh and Sellmeijer in conjunction with secondary studies if needed. Similar to United States practice, the Dutch standards also require gradients be kept below 0.5.

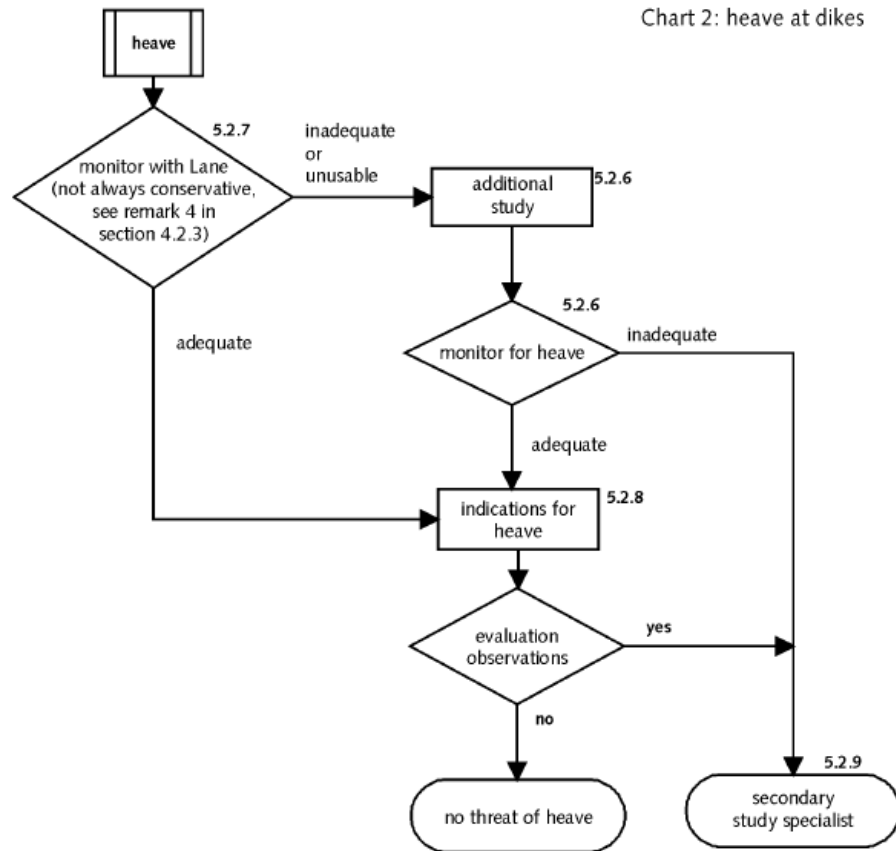


Figure 2-10. Flow chart for heave susceptibility on Dutch levees (TAW, 1999)

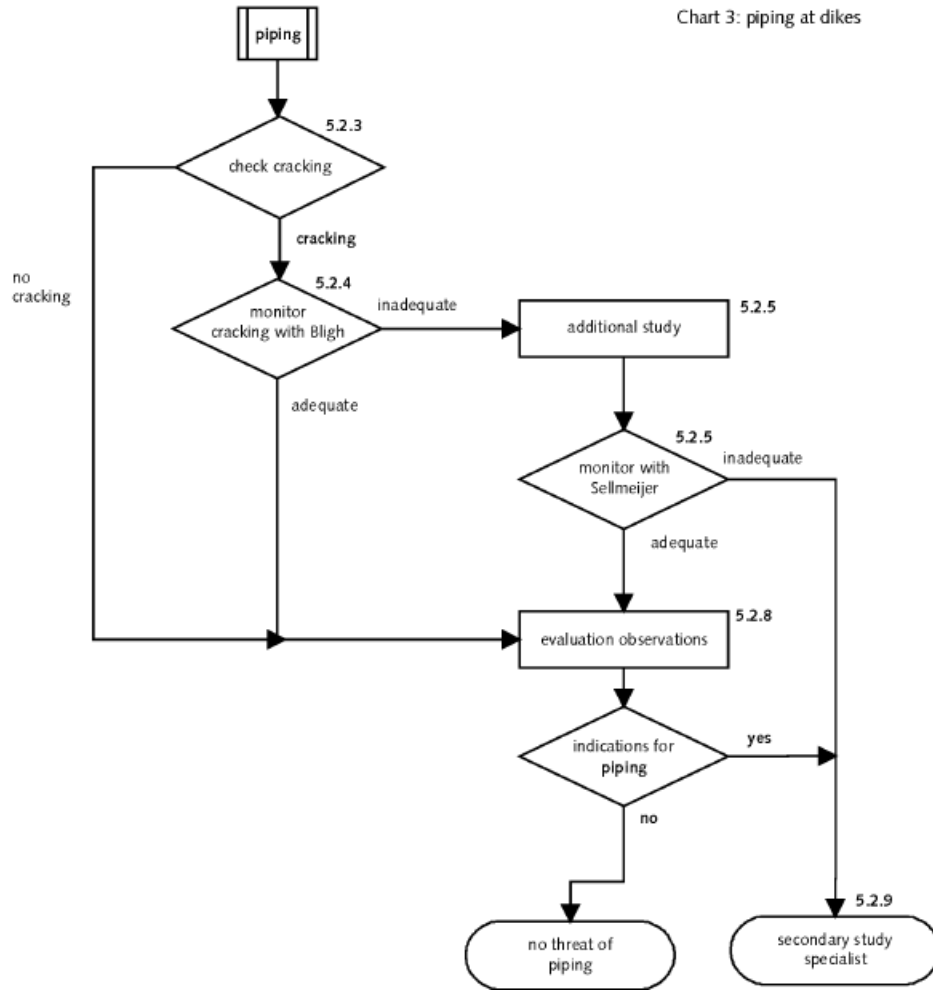


Figure 2-11. Flowchart for piping susceptibility on Dutch levees (TAW, 1999)

Chapter 3

TRANSIENT ANALYSIS OF LEVEE UNDERSEEPAGE

3.1. INTRODUCTION

As already discussed, underseepage is one of the primary causes of levee failure during floods and the current regulatory guidance recommends assuming steady-state seepage as the critical condition. However, given the complexity of layering at individual sites, there has been a growing interest in evaluating whether transient conditions, especially during the rising stage of the flood, could produce hydraulic gradients that are more severe than would be estimated from a steady-state calculation. To this end a suite of transient analyses was performed to identify conditions under which the transient effects may be significant.

The analyses focus exclusively on underseepage and not on seepage through the embankment material (through seepage), as the latter problem which essentially deals with saturation times of embankment materials is highly dependent on initial conditions and unsaturated flow, and is not a cause of uplift or heave failures. The results of the simulations are presented as a set of isochrones with their corresponding transient values for a wide range of parameters, flood durations and initial conditions. These isochrones provide a simple measure for evaluating the accuracy of the steady state simulations and, by implication, the corresponding slope stability estimates.

Also, the models were used to calculate total hydraulic heads at certain locations beneath the landside toe and blanket, and the heave potential was estimated using the ratio between residual head and thickness of the blanket layer:

$$i = \frac{h_o}{z} \quad (3.1)$$

Where i is the heave gradient, h_o is the difference between the hydraulic head at the bottom of the blanket and the elevation of the ground surface near the levee toe (residual head), and z is the thickness of the blanket.

The relationship in Equation 3.1 yields the heave or uplift gradient acting vertically up against the resisting downward pressure exerted by the submerged unit weight of the blanket (Figure 3-1). As described in Chapter 2, these heave gradients are considered critical when above 0.7 to 0.8 (USACE, 2003), but depending on the properties of the surficial clay layer this critical value can be significantly lower.

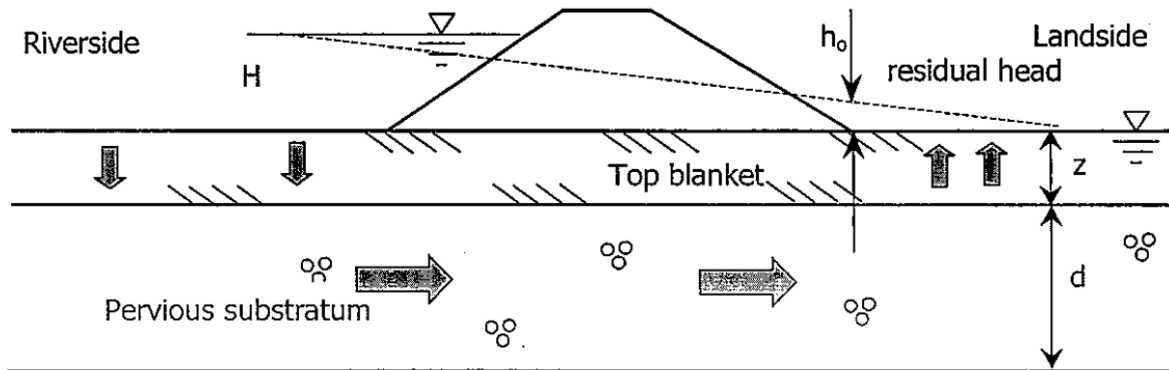


Figure 3-1. Definition of residual head used in underseepage analyses (USACE, 2003)

All analyses were performed using the finite element code SEEP/W, part of the GEOSTUDIO® 2012 Office (Geo-Slope, 2008), which is a conventional finite element formulation of the saturated-unsaturated flow equation given in Equation 2.3 in Chapter 2. The details of the finite element formulation are well known and are omitted herein. However, the details of the material parameter estimation are discussed in detail, as these are critical to the understanding of the results.

3.2. CROSS SECTION AND MODEL PARAMETERS

A typical river levee cross section was used for the analyses (Figure 3-2), consisting on three main layers: (1) a compacted clay embankment, (2) a thin clay layer beneath the embankment, and (3) a thick sandy aquifer extending to the bottom of the model. The aquitard was modeled as a 'no flow' boundary beneath the sand layer. The following variables were used in the models:

- Hydraulic conductivity of blanket layer (K_{bl})
- Hydraulic conductivity of aquifer layer (K_{aq})
- Duration of peak storm surge
- Distance from waterside levee toe to aquifer entrance (X_e)

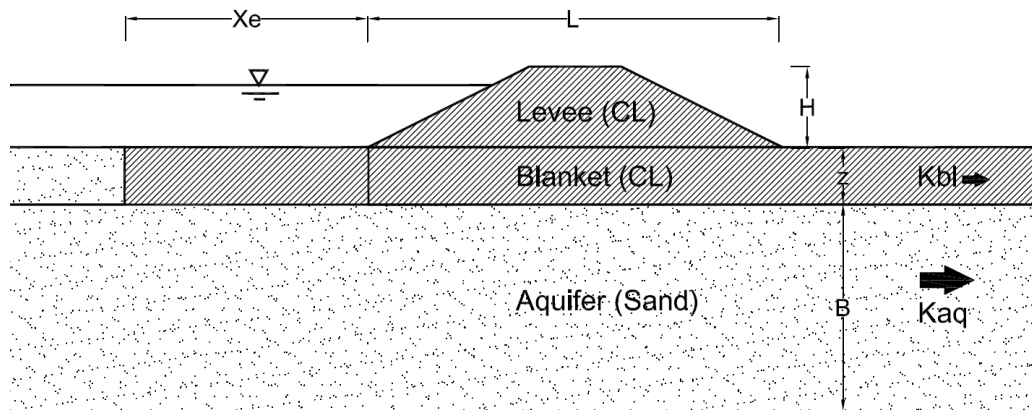


Figure 3-2. Cross section used for transient models

The parameters listed above were found to have the largest influence on the computed pore pressure fields and development of pressure pulses through the aquifer layer, while other parameters were found to have lesser influence on the computed heads and gradients, and were therefore left unchanged, i.e.:

- Blanket thickness (z)
- Compressibility of aquifer (M_v)
- Hydraulic conductivity of levee (K_l)

The analyzed cross section (Figure 3-2) consists of a 7-meter high clayey levee embankment with landside and waterside slopes of 2:1 (Horizontal to Vertical) resting atop a clay blanket. The model extends 100 meters towards the waterside, and 500 meters towards the landside to minimize the effects of lateral boundary conditions. Element size was set to 1 meter to achieve the desired level of accuracy and to satisfy convergence and error tolerances.

The distance from the waterside toe to the aquifer entrance (X_e) was varied by horizontally moving the nodes left of the blanket (blue region in Figure 3-3) to distances of 0, 10, 30, 50, 80 and 100 meters, yet for the generation of the resulting isochrones, this value was normalized by the footprint length of the levee (L) with the intent of eliminating units. Blanket thickness (z) was set at three meters and aquifer thickness (B) was set at 20 meters. An arbitrary vertical datum was set so that the bottom of the model was located at elevation 0 m. Initial conditions were created by performing a steady state calculation assuming an established phreatic surface corresponding to the elevation of the bottom of the blanket ($H=20$ m), meaning that the blanket and levee soils were unsaturated prior to the flood.

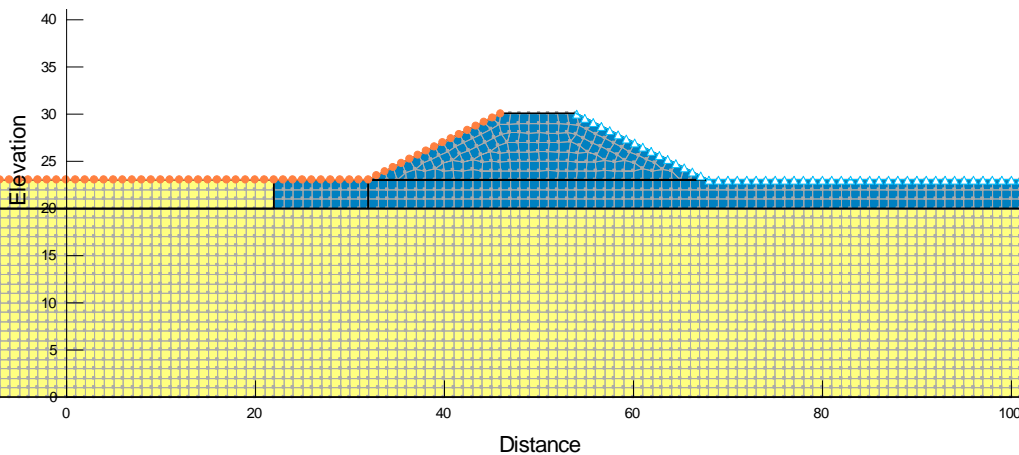


Figure 3-3. SEEP/W input section. All dimensions in meters

Waterside boundary conditions (orange nodes on Figure 3-3) were applied along surface nodes and the waterside (left) vertical edge to represent a sudden increase on river stage from the initial steady state conditions to a total head corresponding to one meter below the levee crest ($H=29$ m), which is a typical design freeboard. The idealized hydrograph is shown on Figure 3-4. The peak duration of the modeled flood was one of the key parameters in the increase in transient gradients; therefore a wide range of values was modeled.

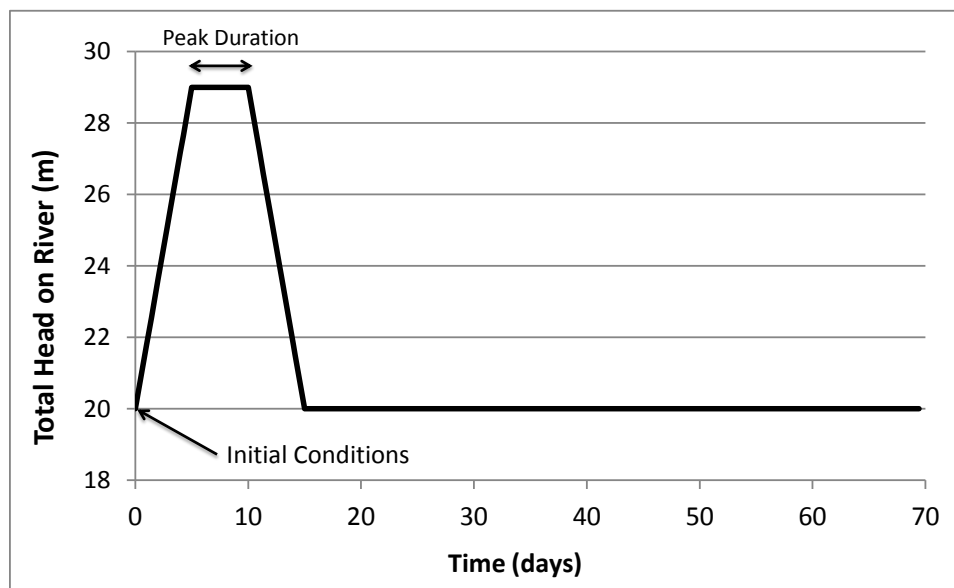


Figure 3-4. Base hydrograph used in transient analyses

Boundary conditions on the protected side consisted of (1) a fixed total head on the vertical edge of the model corresponding to the same steady state condition at the base of the blanket ($H=20$ m). A seepage boundary condition was specified along the nodes on the landside levee slope and along the ground surface. The seepage boundary condition sets the pressure head equal to zero (atmospheric) at the specified node and corresponding flux is computed.

3.3. MATERIAL PROPERTIES

3.3.1. Volumetric Water Content

Values of volumetric water content, or the volume of water contained in the pores of the soil were assumed at saturation conditions, as 0.35 for sand layers, and 0.45 for fine-grained layers. For the estimation of the decrease of these values under unsaturated conditions, the Van Genuchten (1980) relationship was used to estimate the soil water characteristic curves of each material (Equation 3.2).

$$\Theta = \Theta_r + \frac{\Theta_s - \Theta_r}{\left[1 + \left(\frac{\Psi}{a}\right)^n\right]^m} \quad (3.2)$$

Where:

Θ_s , Θ_r = saturated and residual volumetric water contents, respectively

a, n, m = fitting parameters

$n = 1/(1-m)$

Ψ = suction [M/L²]

Figure 3-5 shows the resulting soil-water characteristic curves using the Van Genuchten (1980) method for the main soil types considered on the transient models. The sandy materials have a low air entry value of about 1 kPa, which allows for the rapid saturation of unsaturated portion of these materials under relatively small changes in pore pressure. Conversely, the fine grained materials have an air entry value close to 60 kPa, consistent with higher suction values and the longer time to saturate these materials.

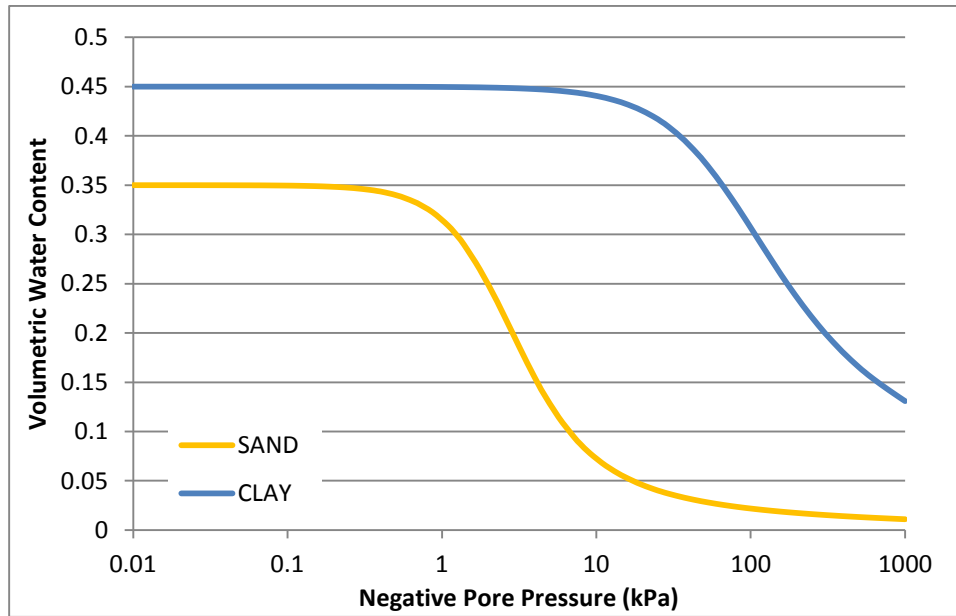


Figure 3-5. Soil Water Characteristic Curves for clayey and sandy materials in transient models

3.3.2. Hydraulic Conductivity

Hydraulic conductivities were estimated for the different materials in the profile using available literature for the conductivity values in the positive pore pressure realm, and the Van Genuchten (1980) relationship (Equation 3.3) was used to estimate the conductivity decrease under unsaturated conditions.

$$K(\Psi) = K_s \frac{[1 - (a\Psi^{n-1})(1 + (a\Psi^n)^{-m})]^2}{[(1 + a\Psi^n)^{m/2}]} \quad (3.3)$$

where:

K_s , K = saturated hydraulic conductivity and conductivity for a given value of suction [L/T]

a , n , m = fitting parameters

$n = 1/(1-m)$

Ψ = suction [M/L²]

The saturated hydraulic conductivity for the clay levee and blanket was set at 1×10^{-6} cm/s (10^{-8} m/s), and the saturated hydraulic conductivity for the aquifer layer was varied between 1×10^{-3} , 1×10^{-4} and 1×10^{-5} cm/s to create different possible geologic scenarios that resulted in different isochrones. With the saturated hydraulic conductivities known, the Van Genuchten (1980) (Equation 3.4 and 3.5) uses the volumetric water content (or soil water characteristic curve) function to estimate the parameters a , n and m , as follows:

$$m = 1 - \exp(-0.8 Sp) \text{ [for } 0 < Sp < 1] \quad (3.4)$$

$$m = 1 - \frac{0.5755}{Sp} + \frac{0.1}{Sp^2} + \frac{0.025}{Sp^3} \text{ [for } Sp > 1\text{]}$$

$$a = \frac{1}{\Psi} \left(2^{\frac{1}{m}} - 1 \right)^{(1-m)}$$

Sp is the slope of the water content function, and is defined as:

$$Sp = \frac{1}{(\Theta_s - \Theta_r)} \left| \frac{d\Theta_p}{d(\log \Psi_p)} \right| \quad (3.5)$$

where:

Θ_s, Θ_r = saturated and residual volumetric water contents, respectively

Θ_p = volumetric water content at the halfway point of the volumetric water content function

Ψ_p = matric suction at Θ_p [M/L²]

The conductivity functions shown on Figure 3-6 contain values for the clay blanket and levee (blue series), and a changing function for the aquifer (orange series), to accommodate saturated hydraulic conductivity ratios (K_{aq}/K_{bl}) of 1,000, 100 and 10. A set of isochrones was developed using each one of these conductivity ratios.

Layer compressibility is encompassed in aquifer storativity and transmissivity properties. Internally, the program calculates transmissivity as the product of hydraulic conductivity and layer thickness. Another parameter used in the transient calculations is the coefficient of compressibility of the aquifer layer (M_v), which can be estimated from consolidation tests for fine grained soils, or derived from storage coefficients estimated in aquifer pumping tests. This value was left unchanged from the program default of 1×10^{-5} 1/kPa for all layers in the profile. All other material properties are summarized on **Table 3-**.

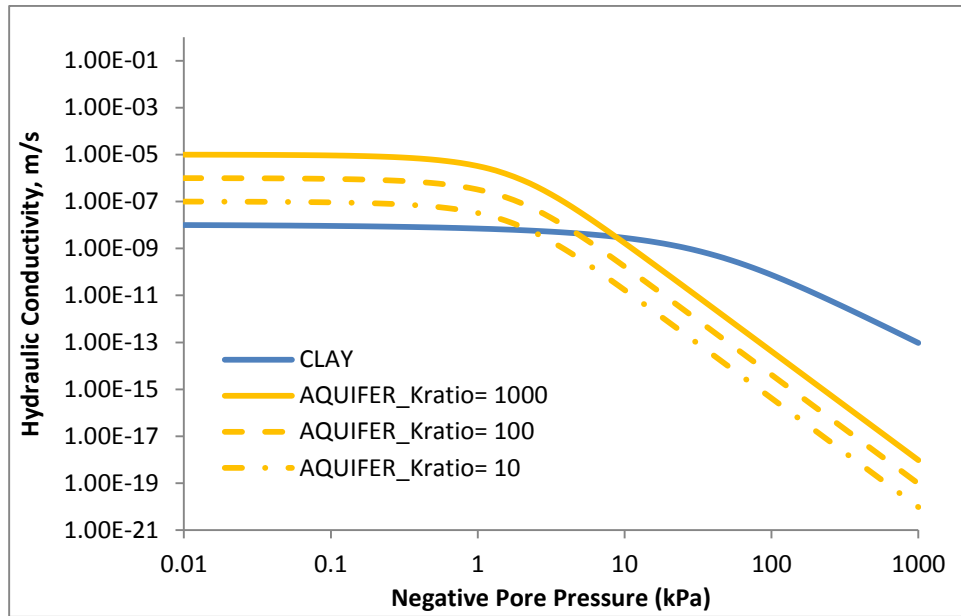


Figure 3-6. Hydraulic conductivity functions used in the transient models

Table 3-1. Summary of material properties for transient models

Layer	$K_{h,sat}$ [m/s]	Anisotropy Ratio K_v/K_h	θ_{sat} [-]	M_v [1/Kpa]	Color
Clay Levee	1×10^{-8}	0.25	0.45	0.00001	
Clay Blanket	1×10^{-8}	0.25	0.45	0.00001	
Sand Aquifer_1	1×10^{-5}	0.25	0.35	0.00001	
Sand Aquifer_2	1×10^{-6}	0.25	0.35	0.00001	
Sand Aquifer_3	1×10^{-7}	0.25	0.35	0.00001	

Note: Each one of the 'Sand Aquifer' layers was used for a separate model to yield different K_{aq}/K_{bl} ratios.

3.4. RESULTS

A total of 126 transient simulations were performed to create the isochrones presented in the results section. A summary of the variables used in the models is contained in Table 3.2.

Table 3-2. Summary of transient models

Model Run	K_{aq}/K_{bl} [-]	Peak Flood Duration [days]	X_e/L [-]
1-1	1,000	5, 10, 15, 20, 30, 40, 60	0
1-2			0.3
1-3			1.0
1-4			1.4

1-5			2.4
1-6			3.0
2-1	100	5, 10, 15, 20, 30, 40, 60	0
2-2			0.3
2-3			1.0
2-4			1.4
2-5			2.4
2-6			3.0
3-1			10
3-2	0.3		
3-3	1.0		
3-4	1.4		
3-5	2.4		
3-6	3.0		

The analyses were used to obtain a time series of total heads at a node beneath the base of the blanket, aligned vertically with the landside levee toe. This value was then compared the pore pressure obtained by performing a steady state calculation using the peak value from the input hydrograph. Figure 3-7 shows the evolution of heads for the case of a five day peak storm and a conductivity ratio of 1,000 and varying length of waterside blanket. For this case, computed total heads range between 95% and 88% of the steady state values for the cases of 'entrance at toe' ($X_e/L=0$) and 'entrance 100 m' ($X_e/L>3$), respectively. Figure 3-8 shows steady-state total head contours for the case of $X_e/L=0$ and $K_{aq}/K_{bl}=1,000$, showing essentially no head drop across the aquifer and a significant head differential across the fine-grained blanket, indicative of very high steady-state heave or uplift gradients. Using Equation 3.1 results in a steady state heave gradient of 1.84.

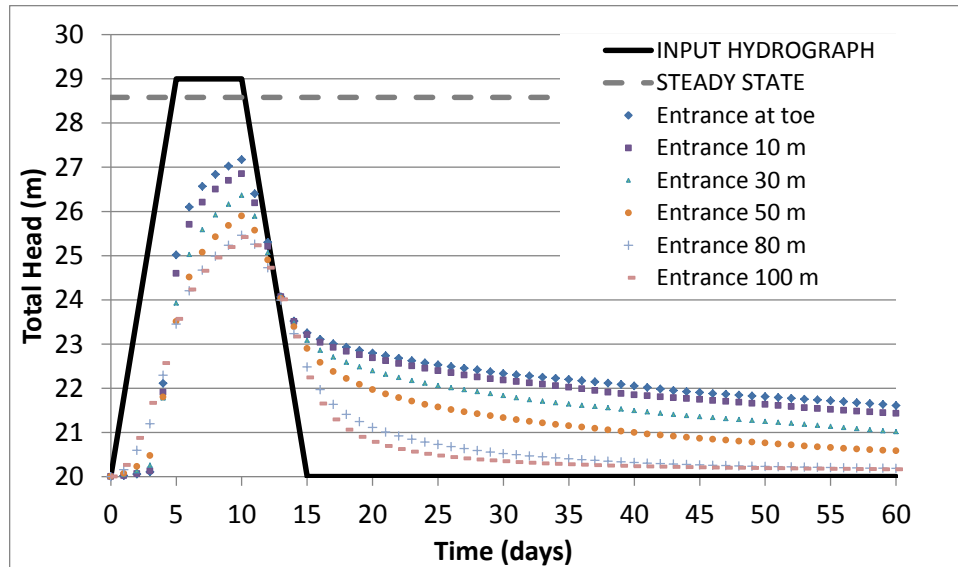


Figure 3-7. Example of evolution of total heads beneath clay blanket, $X_e/L=0$, $K_{aq}/K_{bl}=1,000$, peak duration= 5 days

The results of the transient analysis yield slightly smaller total heads beneath the blanket, approximately 1 meter less than the steady state condition near the landside toe (Figure 3-9), and while the heads are smaller than the steady-state case, they are approximately 95% of the steady state value, which is equivalent to a heave gradient of 1.77, still significantly larger than the critical gradient for heave. The head contours shown on Figure 3-9 indicate that the levee and blanket layers have not reached saturation during the duration of the peak, as evidenced by the tightly arranged head contours near the bottom of the blanket and waterside slope, yet the aquifer is pervious enough to allow the development of critical gradients and heave potential.

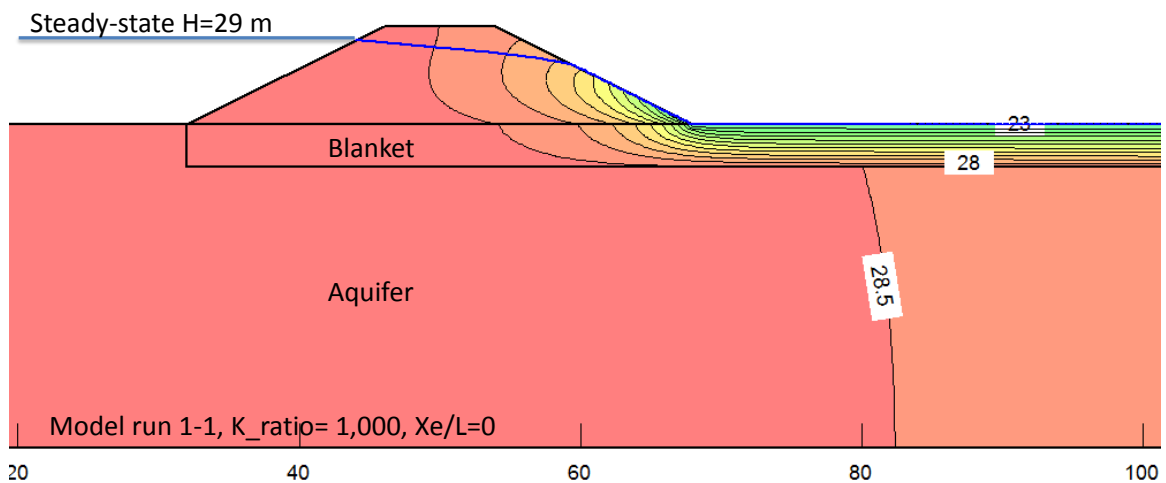


Figure 3-8. Steady-state base case $X_e/L=0$, $K_{aq}/K_{bl}=1,000$

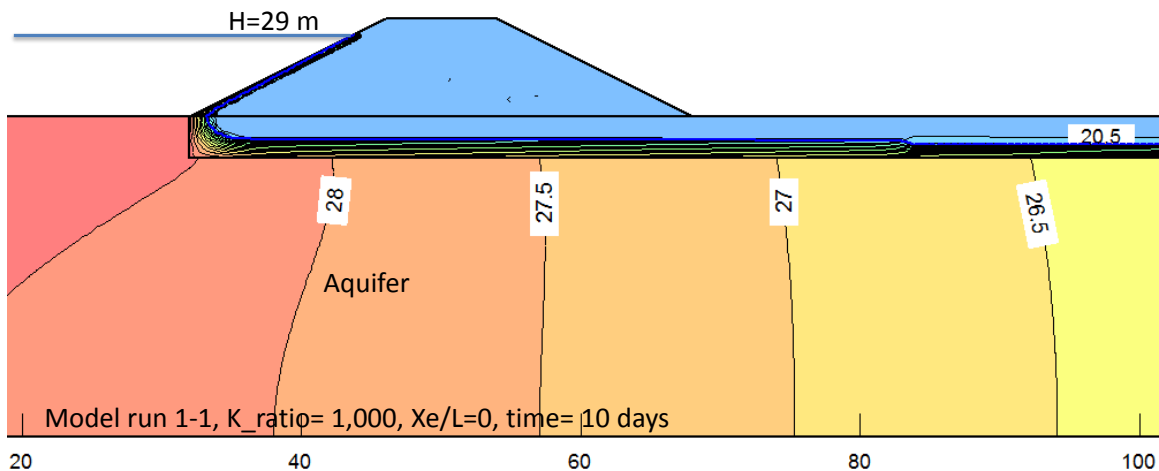


Figure 3-9. Transient head contours, $X_e/L=0$, $K_aq/K_{bl}=0$, $time=10$ days

Figure 3-10 shows the time histories of gradients for the case mentioned before. Using the maximum value of total head reported in the time history for each analysis case, a normalized heave gradient was computed by dividing the transient gradient by the corresponding steady-state value.

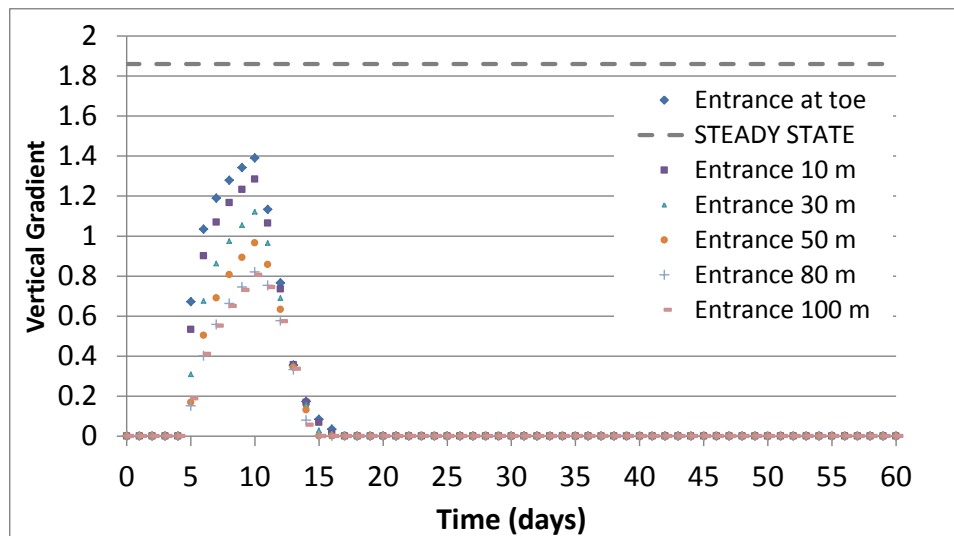


Figure 3-10. Example of time series of heave gradients, $X_e/L=0$, $K_aq/K_{bl}=1,000$, peak duration= 5 days

3.4.1. Isochrones for Hydraulic Conductivity Ratio = 1,000

The isochrones consist of lines of equal peak storm duration relating the ratio of transient to steady-state heave gradients to the distance of the waterside levee toe from the point where the river flood is charging the aquifer.

Figure 3-11 shows the isochrones for the case of a hydraulic conductivity ratio of 1,000. The plot indicates that after a X_e/L value larger than 2.5 to 3.0, the ratio of transient to steady-state

heave gradient stabilizes, and decreases as a function of increasing X_e/L and decreasing storm duration.

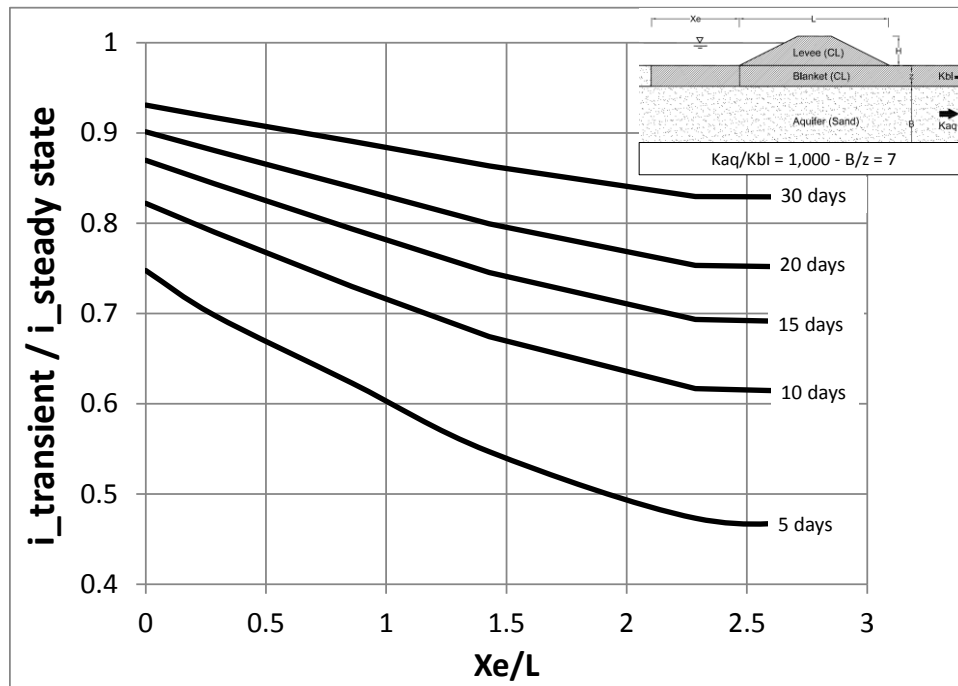


Figure 3-11. Isochrones for $K_{aq}/K_{bl}=1,000$

3.4.2. Isochrones for Hydraulic Conductivity Ratio = 100

Isochrones for a hydraulic conductivity ratio of 100, obtained by decreasing the conductivity of the permeable layer by a factor of 10, are shown on Figure 3-12. The 10-fold decrease in hydraulic conductivity of the aquifer layer yields a slower response of the aquifer layer and higher total head losses.

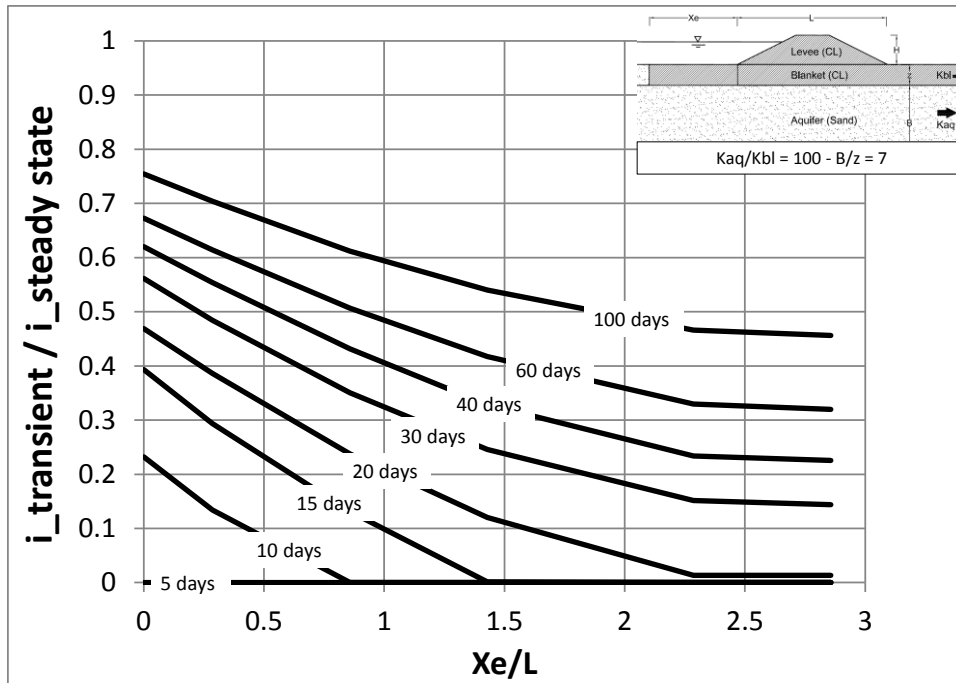


Figure 3-12. Isochrones for $K_{aq}/K_{bl}=100$

3.4.3. Isochrones for Hydraulic Conductivity Ratio = 10

Isochrones for a hydraulic conductivity ratio of 10 are shown on Figure 3-13. This case with this low ratio barely starts to yield any type of gradient after a flood duration larger than 100 days.

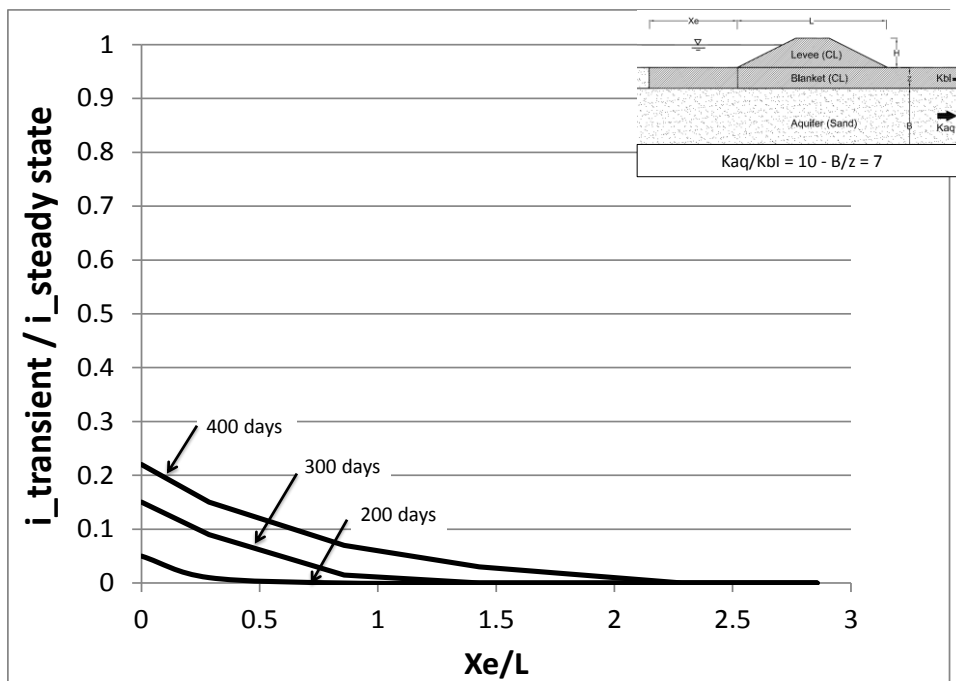


Figure 3-13. Isochrones for $K_{aq}/K_{bl}=10$

3.5. SUMMARY

The simulations and isochrones presented in this chapter are intended to provide a basis for comparison between steady state and time dependent seepage analyses of flood protection systems. Generally, transient analyses are considered troublesome and thus steady state conditions are assumed for all cases. However, depending on the geometry of the layers and flood duration, transient conditions may be as critical as their steady state counterpart, particularly when the hydraulic loading is connected to the aquifer layer close to the waterside levee toe. For a high conductivity aquifer, transient gradients may be as high as 75% to 92% of the steady state value for an aquifer entrance at the toe of the levee, for flood durations of 5 and 30 days, respectively. These percentages are reduced to 47% and 84% for an entrance located more than 2.5 times the width of the levee. The numbers greatly reduce as the conductivity of the aquifer decreases, to the point where no transient gradients are generated after more than 100 days of flood duration.

In summary, time dependency does play an important role on seepage induced levee instability; given certain geometric and hydraulic characteristics, critical conditions may be generated within a matter of days or weeks.

Layer thickness plays an important role on the determination of transient gradients, particularly the thickness of the surface blanket, which is the denominator in the formula for estimating the heave gradient (Equation 3.1). However, by normalizing the transient gradients by their steady state value, the influence of layer thickness is eliminated and the isochrones can be used for any set of layer thicknesses, as long as a corresponding steady state analysis using the peak flood as boundary condition is performed.

Other parameters, such as unsaturated properties of the levee and blanket layers do not have an influence on the resulting gradients and isochrones, since the driving force on this problem is the development of pore pressures beneath the fine-grained blanket overlaying the aquifer. However, these unsaturated properties do have an influence on the stability behavior of the structure, as the suction induced apparent cohesion present in the fine-grained embankment will be reduced as the levee saturates.

Finally, the slope of the hydrograph rise was found to have an insignificant impact on the results, and only seems to affect the time lag between the peak of the hydrograph and the arrival of the pressure pulse beneath the levee. However, the results show that steady state seepage analysis may be overly conservative in certain settings. Therefore, transient seepage analysis should be considered when levees are being remediated or new levees are being constructed, assuming that the site is adequately characterized.

Chapter 4

INFLUENCE OF WOODY VEGETATION AND ANIMAL BURROWING ON LEVEE SEEPAGE

4.1 INTRODUCTION

The current state of knowledge about the influence that live and decomposing vegetation and mammal burrows have on the performance of embankments is reviewed here to provide a basis for the analyses performed as part of this research. In particular, the focus is on the changes that vegetation and animal activity have on the wetting patterns and hydrogeological response of embankments when subject to hydraulic loading.

Most available research literature has focused on the effects of clear-cutting vegetation on natural slopes (Sidle, 1992), which results in long-term rise in the water table. As a result slope failures tend to increase when vegetation is removed. Furthermore, root decay causes the previously resisting tensile forces added by root systems to diminish (see e.g. Grey and Megahan, 1981) and in some cases large voids form allowing subsurface water to flow faster and trigger piping erosion (Ziemer, 1992).

In the context of levee performance, the importance of quantifying the effects of vegetation and animal activity on hydrogeologic performance of embankments resides in the potential for internal erosion or piping due to concentrated flow along potential preferential seepage paths within the embankment. The following is a summary of available case histories where vegetation and animal burrows have had some type of influence on a reported levee breach or distress.

4.2 REPORTED DETRIMENTAL EFFECTS OF WOODY VEGETATION IN LEVEES

A review of historical data and performance reports from levees in the United States was performed focusing specifically on reports where negative impacts were documented. Sources of information were the literature review performed by the USACE's Engineering Research and Development Center (ERDC) in 2011, levee performance reports by USACE between 1993 and 2009 (USACE, personal communications in 2012) and other available sources. Generally, the

reported negative impacts of vegetation on levee performance were related to overtopping and scour around tree trunks and root systems, which resulted in exacerbated scour around the tree or root. Several instances of sand boils around live trees on the landside toe area were reported, but no reports of water seeping through or along live or decomposed root systems were encountered in levee literature. Several post-failure investigations reported the presence of large woody vegetation through the embankments after failure had occurred. The USACE along with several national and international agencies are currently working on the International Levee Manual and describe several levee failure modes in relation to the presence of woody vegetation (Table 4-1).

The following paragraphs document some of these cases and describe the reported failure (or distress) mechanism and the influence from woody vegetation.

4.2.1 URS (2011) LITERATURE REVIEW

The California Department of Water Resources (DWR) has funded the Urban Levee Evaluation Project (ULEP) and Non-Urban Levee Evaluation Project (NULEP), where more than 2,000 miles of levees in California have been logged in a database which includes past performance information, soils reports, geotechnical testing and analyses, known breaches, levee penetrations, etc. URS (2011) performed a literature review using this database with the objective of generating records of past performance instances where some mention of vegetation was available.

The performance records evaluated by URS included records where vegetation was identified as a factor that negatively, or positively, affected levee performance. Also, records where vegetation influenced levee operations and maintenance (O&M) instances, records that had incidental description of vegetation and did not have an association with O&M nor performance; and records that identified the occurrence of vegetation in association with performance data but no clear cause-effect relationship between performance and vegetation (URS, 2011).

Table 4-1. Levee failure modes and their relation to woody vegetation. Source: USACE (2012, International Levee Handbook)

No.	Failure Mode Category	Sub-Category	Load Factors	Failure Mechanism	Effect Leading to failure	Potential Role of Woody Vegetation
1	Under seepage	-	H	Water seeps through the top stratum and increases the hydraulic pressure in the aquifer and raises the exit gradient.	Liquefaction occurs at the base of the protected side where the exit gradient is the highest. Water flows to the protected side, and stability of the levee structure is weakened.	Woody vegetation may affect soil permeability on both sides of the embankment. A critical location is at the toe on the protected side.

2	Through seepage	Saturation	H	Levee embankment becomes saturated and pore water pressure builds. Phreatic line advances to the protected side.	Water seeps out on the protected side of the embankment.	Woody vegetation reduces the distance between the phreatic line and inner slope of the levee.
3	Through seepage	Internal erosion and piping	H	Preferential flow paths develop due to internal cracks, low strength soil zones, conduits, inclusions, or water-restrictive soil layers.	Levee or foundation loses soil particles, eventually deforming and weakening the levee structure and causing breaching.	Living tree roots may channel water along the root-soil interface. Dead tree roots may decay, leaving defects in the levee. Woody vegetation may attract animals that burrow into the levee.
4	Uplift and piping	-	H	Excessive hydraulic head creates excessive hydrostatic pressure in a confined pervious stratum below the embankment.	Levee structure is weakened, and preferential seepage paths develop underneath the levee.	The effects of woody vegetation with respect to this failure mode are unclear.
5	Foundation instability	-	H	Lateral force from hydrostatic water level difference exceeds net shear strength of the foundation.	Levee structure is weakened and deforms, displacing the structure from its foundation. A breach in the levee may result from displacement of the structure.	Roots that penetrate into engineered foundations may weaken or reinforce the foundation.
6	Oversettling	-	M _L , M _S	The foundation fails to support the levee as designed and the levee settles so that the actual crest elevation is below the design crest elevation.	The levee no longer prevents overtopping during those flood events for which it was designed to prevent overtopping.	The weight of a large tree on an embankment could conceivably cause excessive settlement of the levee, but this scenario is regarded as unlikely.
7	Scour and erosion	Protected side	H	(A) Laminar overtopping: Water level exceeds the crest of the levee and water flows down the protected side.	Erosion may alter levee geometry and weaken the structure. Severe erosion may cut through the levee.	Tree stems interrupt the laminar or wave flows, creating currents and eddies that may enhance the erosive force of the water. Root structures may reduce the erodibility of the

				(B) Wave overtopping: Waves overtop the levee crest and water flows down the protected side.		soil. Canopies may inhibit the growth of herbaceous ground cover.
8	Scour and erosion	Flood side	H, V	Levee is undercut on the flood side, altering the geometry of the levee structure.	Slumping on the floodside. Erosion removes soil material. Erosion may alter the geometry and weaken the levee structure.	Woody vegetation on the stream bank (roots and or stems) may create local currents and eddies that increase the erosive force of water. Embedded roots may stabilize banks and side slopes.
9	Slope instability	Deep slip plane	H, W, M _s	Opposing forces in the levee structure become unbalanced. Internal levee forces and moments exceed the soil strength along a horizontal, vertical or rotational slip plane.	Levee slumps (collapses), causing a breach. If water levels are high, water may flow to the protected side.	Woody vegetation may add weight to the slope and may transfer the force of wind to the slip plane, increasing or decreasing the ability to withstand downward force along the slip plane.
10	Slope instability	Surficial	H, M _s	Surface soil layer becomes saturated and weakened.	Surficial slope failure (shallow slumping) may reduce the ability to withstand other failure modes.	Shallow root systems may reinforce shallow soils (root depth, spatial extent, and tensile strength). Canopy cover may reduce side slope water runoff. Root systems may enhance the percolation of water into the levee structure.
Load Factors: H= hydraulic head, W= wind velocity, V= fluvial velocity, M _L = Mass of the levee, M _s = Embankment surcharge						

The results of the URS analysis of over 10,000 records showed that 6,970 performance records contained some observations with respect to vegetation. Of these, 348 were levee breaches resulting in water flooding the protected side, but none of the records identified vegetation as an influence on the reported breaches. The remaining 6,622 records contained 95 performance reports that indicated the presence of vegetation in the vicinity of an identified performance issue (Figure 4-1). From these 95 records, 11 identified vegetation as a factor influencing performance, 25 indicated vegetation had an influence on O&M (Operation and Management),

39 had references to vegetation in a way that was not relevant to O&M or performance issue; and finally, 20 referenced vegetation but had insufficient information to assess its role.

The report by URS (2011) indicates that those reports that discuss vegetation in the context of O&M were described as “...inability to visually determine levee performance during high water events.”

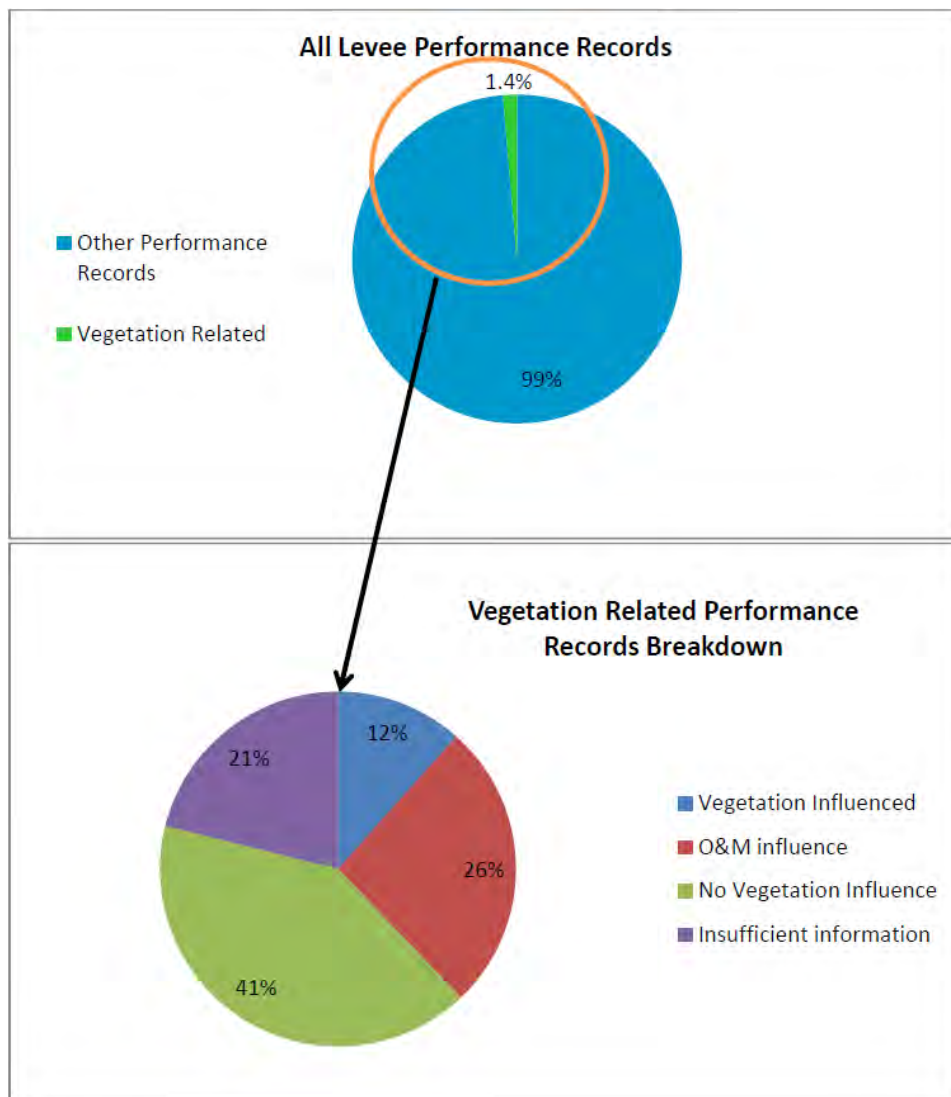


Figure 4-1. Performance records related to vegetation in California levees (URS, 2011)

4.2.2 INSTANCES REPORTED BY THE USACE

The USACE in its evaluation of the influence of woody vegetation on levee performance reviewed data from across the US and identified 15 cases in which vegetation was implicated in some fashion (USACE, 2012). From these reports, seven were identified by field personnel as ‘causing damage’; eight were identified as ‘inhibited inspection or maintenance’ and only one was identified as ‘contributed to failure’.

Most of these incident reports were documented by personnel from different districts of the USACE, and none was associated with a levee failure. In fact, most incidents only dealt with lack of visibility or localized erosion due to tree toppling. These incidents were not investigated in great detail and consequently not all levee performance information might have been discovered.

1993 LEVEE BREACH ON DES MOINES RIVER (IA)

The 1993 flooding in the Mississippi River basin has been catalogued as one of the most severe events in recent years, with a 500-year recurrence interval. A levee breach was reported by a USACE engineer along the descending bank of the Des Moines River in Iowa, north of the town of Des Moines. This site breached once again during a 2008 flood described in subsequent paragraphs.

The event in 1993 was reported to have crested one to two days before the breach occurred, and the breached levee was known for having been constructed with poor compaction, having no under or through seepage measures, steep slopes under constant erosion from the river and heavy tree growth (Figure 4-2 and Figure 4-3). Once the waters began to recede, the engineer in charge of the report states that *“saturated levee embankments in this reach began a catastrophic failure, with large segments of the levee material slumping into the river. Several massive root balls were observed in the area where the levee failed. Ultimately the levee slumping passed through the levee crown and into the landside of the levee...the heavy tree growth hindered levee inspections and monitoring during the flood fight as well as the remedial constructive measures that were undertaken on the landside of the levee”*. The inspection report goes on to state that *“the large trees located on these saturated slopes added to the non-stability of the levee with dead and wind loads contributing to the failure of the levee. While original construction standards on material compaction were inadequate, the failed areas of the levee revealed significant root growth throughout the levee, which likely further facilitated the saturation of the levee embankment when record river stages were occurring”*.

This last statement suggests the possibility of saturation of the levee prism enhanced by seepage paths along the roots, but no direct or specific evidence was provided. The fact that the failure occurred while the waters were receding and progressed from the waterside slope to the landside indicates that these failures may have been related to a rapid drawdown slope instability condition rather than root-driven seepage forces.



Figure 4-2. 1993 Des Moines River breach (USACE, 1993). Red oval highlights root system



Figure 4-3. Downstream view of Des Moines River levee break (USACE, 1993). Red oval highlights root system

WATER SKI PARK LEVEE DAMAGE, CARBON RIVER (WA)

An August 2007 USACE report describes localized waterside levee slope damage near Orting, WA, after an alder tree was toppled in a windstorm and removed surficial soil and erosion armoring from the surface. No measurements of the hole left by the root system were provided, but it appears that the tree lifted a very shallow 'slab' of soil (Figure 4-4). No levee failure or distress was reported at this site.

PUYALLUP LEVEE DAMAGE, TACOMA (WA)

Vegetation-induced levee damage in December 2005 was reported by the USACE on the levee along the Puyallup River near Tacoma, WA. This incident report indicates that soft soil conditions, along with wind loads and river incision contributed to a cottonwood tree toppling over and removing soil from the waterside slope (Figure 4-5). No further indication of damage or reconstruction is provided in the incident report, but the report indicates that this type of occurrence is common in the area and toppled trees pull out material adjacent to the levee prism. In this case, the root ball pulled a mass of soil near the waterside toe the levee.



Figure 4-4. Erosion on waterside slope after tree toppling (USACE, 2007)



Figure 4-5. Cottonwood toppled on Puyallup River (WA). Image courtesy USACE

LEEVE DAMAGE ON LINDLEY LEVEE NEAR WAITSBURG (WA)

Similar to the case on the Puyallup River (Figure 4-5), in 2008 high wind caused several trees to topple and remove soil and erosion protective riprap from the waterside slope (USACE, 2008). The levee appeared to have had very little maintenance and trees and shrubs grew uncontrolled on the waterside slope (Figure 4-6). The report does not give an indication as to how deep the hole left by the root system was as the tree toppled, nor how many of these incidents occurred along the Touchet River. A failure or breach of the levee did not occur.



Figure 4-6. Damage on waterside toe, Touchet River (USACE, 2008)

LEEVE DISTRESS, SAINT GENEVIEVE (MO)

The St. Genevieve #2 levee along the Mississippi River was subjected to severe water loading during June 2008. USACE post incident inspection report provides a description of the levee distress that seems to have been related to presence of woody vegetation near the landside toe. On 28 June, 2008, several active sand boils were reported in a heavily vegetated area (Figure 4-7) which were observed to be flowing water and soil. Flood fighting activities lasted over five days, local authorities built sand bag rings around the active boils (Figure 4-8) and allowed the toe area to flood several feet to reduce the hydraulic head differential and stop the flow of material through the sand boils.

According to the incident report, the largest boil was approximately 1 meter (3 ft) in diameter and most of the boils were encountered in a low spot with a dense line of trees. After the fifth day of flood fighting some boils were still active and a 200 m (600 ft) long rock berm was placed to increase the stability of the toe area, but new sandboils developed upstream of the berm.



Figure 4-7. View of landside toe area, St. Genevieve levee distress (USACE, 2008)

No information on the levee and foundation conditions are given in the incident report, but the levees in the area along the Mississippi River in Missouri are known for their underseepage susceptibility because of relatively thin landside blankets (fine-grained soil layers). Several other sand boils were reported during the same flood event in other areas as described by Harder et al., (2009). The incident report concludes that tree roots and associated animal activity (the animal activity was not reported) likely attributed to the intensity of the seepage, and that

vegetation made it difficult to place the mitigation rings around the boils; however, it seems likely that some boils would have occurred without the presence of vegetation.

MAINTENANCE AND REPAIR, GRAND TOWER LEVEE (IL)

Several shallow landslides along the protected-side toe of the Grand Tower and Degognia levee in Southern Illinois occurred in 2008. At this location, trees were present along long stretches of the landside toe (Figure 4-9). Landslides appear to be a common occurrence in the area and are associated with high-plasticity clays used for embankment material and not necessarily associated with the presence of woody vegetation near the toe of the levee. The report indicates that the trees inhibited maintenance and did not allow for staging materials and equipment for repairs to be performed, but no direct relation to the observed failure was given.



Figure 4-8. Active sand boils around trees, St. Genevieve levee distress (USACE, 2008)

However, the USACE report concludes that *“without a vegetation clear zone at the toe of the levee, the slides in the affected levee stretches cannot be repaired. If the slides are not repaired the integrity of the levee is affected by a decrease in the factor of safety which puts the protected area at increased risk for flooding. If the trees were removed and a vegetation clear zone of 15 feet was maintained the existing and future levee slides could be repaired”*.



Figure 4-9. Trees along landside toe. Grand Tower Levee (USACE, 2008)

MAINTENANCE INHIBITION BY VEGETATION

Well documented potential detrimental impact that dense woody vegetation has on levee performance is the interference with regular maintenance and inspection activities. A levee along the Kuskokwim River in Alaska was reported to be so densely vegetated that visual inspection was impossible during routine inspection in 2008 (Figure 4-10).

Similar cases were reported in May and September 2008 on the Klutina River (Figure 4-11) and Tanana River in Alaska (Figure 4-12). The slopes of the levees were covered with large and small diameter trees and brush, and the levee owner was directed to maintain the levee in accordance to USACE guidelines. However, no indication of poor performance or negative influence from the trees was reported.



Figure 4-10. Dense vegetation inhibiting visual inspection along Aniak levee in Alaska (USACE, 2008)



Figure 4-11. Vegetation covered slopes, Klutina River levee, Alaska (USACE, 2008)



Figure 4-12. Vegetation covered slopes, Tanana River levee, Alaska (USACE, 2008)

DAMAGE TO CORRALES LEVEE, CORRALES (NM)

The landside drainage system of the Corrales levee unit along the Rio Grande in New Mexico is protected from underseepage by a system of subdrains comprised of a PVC pipe parallel to the levee toe and risers every 1/10th of a mile. An inspection in October, 2008, found several trees, including Siberian elms, cottonwoods, Russian olive and salt cedar growing next to or inside the risers (Figure 4-13). In some cases the roots of these trees damaged the risers and most likely penetrated the slotted PVC pipe near the toe of the levee. The inspection team deemed that the subdrain system would not function as designed and recommended removing all trees and roots from the toe subdrain system and an investigation of the extent of intrusion by the woody vegetation.

TREES AND TREE-INFLUENCED ANIMAL ACTIVITY, ALAMOSA LEVEE, RIO GRANDE (CO)

A USACE incident report for the Alamosa levee along the Rio Grande in Colorado from September 2008, describes the waterside toe area to be populated by numerous large trees within 5 meters (15 feet) of the toe (Figure 4-14). The inspector reported that the trees were of different size and health, as some of them had been damaged by recurrent beaver activity in the area.



Figure 4-13. Tree growing inside landside subdrain system. Rio Grande, New Mexico (USACE, 2008)



Figure 4-14. Trees at waterside toe and channel dug by beaver, Alamosa levee, Colorado (USACE, 2008)

A channel had been dug by the animals from the river to the waterside toe (apparently there is a waterside berm separating the levee from the river) and two large beaver den entrances were encountered, as well as several smaller holes along the waterside slope (Figure 4-15).



Figure 4-15. Beaver tunnel on waterside slope, just below tree line. Alamosa levee, Colorado (USACE, 2008)

The report attributes the existence of beaver dens to the presence of woody vegetation because *“these trees on the riverside provide shelter, protection and food for the beavers”*.

COFFEYVILLE LEVEE (KS)

The USACE (2007) reported a small erosional feature on the landside slope of the Coffeyville levee in central Kansas following the storms of May and June of 2007. According to the incident report, the compacted clay levee was overtopped by approximately 1.2 m (four feet) of water and no breaches were reported, but an erosional feature was discovered during post flood inspections (Figure 4-16). The erosion exposed roots from a large tree near the landside toe extending upslope and reaching the crown of the levee. However, it is not clear how the roots might have contributed to the removal of approximately 1 to 1.5 meters (3 to 5.5 feet) from the area near the landside hinge point of the embankment.



Figure 4-16. Levee distress, Coffeyville levee, Kansas (USACE, 2007)



Figure 4-17. View of exposed roots on Coffeyville levee distress, Kansas (USACE, 2007)

The images show that the erosional feature roughly coincides with the zone of densest roots (Figure 4-17). However, there is no information on soil properties and their variability along the levee.

4.3 EVALUATIONS OF LEVEE DISTRESS AND LEVEE BREACHES BY OTHERS

4.3.1 EAST SAINT LOUIS LEVEE SYSTEM, JUNE 2008 FLOOD

Harder et al. (2009) performed inspections of the levee distress and breaches during the June 2008 floods in the Midwestern United States. Twenty-two breaches were reported, mainly due to overtopping along levee systems spanning the states of Iowa, Illinois and Missouri. The sites studied were selected because of the presence of trees and/or animal burrowing activity. Their descriptions, conclusions and findings are summarized on this section.

The distressed site is located on the left descending bank of the Mississippi River across from St. Louis (MO). The levee is approximately 8 meters (25 ft) high with slopes of 3:1 (horizontal to vertical). Two berms and a system of relief wells were observed by Harder et al. (2009), indicating a known history of seepage and stability issues for this levee reach.

Animal burrows were observed near the crest and on the lower part of the landside slope, and several trees that were apparently uprooted some time before the 2008 floods were also observed. The root balls (Figure 4-18) were still in evidence showing that there was apparently disturbed ground near the landside toe and most likely including roots in the soil.



Figure 4-18. Uprooted trees and root balls at the East St. Louis site. (Harder et al., 2009)

Sand boils (Figure 4-19) were observed between the relief wells, in some instances as close as 20 ft from a well, and the occurrence of the boils appeared to coincide with the ground disturbance produced by the uprooted trees. A previous flood event in 1993 did not produce any sand boils, despite the fact that recorded river levels were about 11 ft higher than the 2008 flood. The report by Harder et al. (2009) indicates that improper tree removal might have

disturbed the top soil enough to allow the triggering of the observed levee distress in the form of sand boils.

The reported levee distress at this site seems to have been exacerbated by anthropogenic activities rather than by the presence of woody vegetation detrimental to the performance of the levee. The fact that during previous flood events with significantly higher hydraulic loading the existing remediation measures performed adequately (relief wells, stability and seepage berms) indicates that the problems presented on this site were likely a direct consequence of the ground disturbance generated by the removal of the tree and root balls near the landside toe. The report does not provide information on the presence or absence of a landside fine-grained blanket, but it is likely that the removal of root balls had damaged the blanket or created discontinuities that allowed the formation of sand boils.



Figure 4-19. Sand boil at East St. Louis site (Harder et al., 2009)

4.3.2 CAP AU GRIS LEVEE BREACHES, MISSISSIPPI RIVER, WINFIELD, MO

Harder et al. (2009) describe two breaches that washed away the embankment at low spots along the alignment, coincident with road access or structure encroachments. The breaches occurred along a levee near Winfield (MO) along the Mississippi River.

Post failure reconnaissance of the eroded embankments indicated the presence of several large (5 to 7 inches in diameter) live roots, extending across most of the embankment width. The first breach (Cap Au Gris – Site 1 in Harder et al. 2009) of a relatively low levee (9 feet high) with slopes between 3:1 and 4:1 (Figure 4-20) developed as water overtopped and concentrated on a low spot where a road access joined the levee crown. A witness account described no (through or under) seepage shortly before the failure, therefore the failure was likely due to

concentrated overtopping that washed away the levee material and resulted in a 30 ft wide breach extending down to the foundation.

The roots encountered in the eroded area ranged from less than 1 inch to about 5 inches in diameter (Figure 4-21), and seemed to originate from two stumps encountered near the waterside toe of the eroded levee with diameters of 3 and 4 feet. The larger roots appear to have reached distances greater than 50 ft from the stump towards the embankment. A smaller stump and a live cottonwood were also present in the vicinity of the breach.



Figure 4-20. Cap Au Gris - Site 1 (Harder et al., 2009)



Figure 4-21. View of eroded levee at Cap Au Gris - Site 1 (Harder et al., 2009)

A second breach in the area (Cap Au Gris – Site 2), located approximately one mile downstream of Site 1 was also triggered by concentrated overtopping around a low spot on the levee crown. This breach was approximately 105 m (350 ft) wide and destroyed several houses. Post failure reconnaissance also encountered a large number of roots coming from live trees located at or near the waterside toe and a single burned stump near the landside toe.

Harder et al. (2009) examined the interface between the clay embankment and roots along intact sections of the levee, showing no visible gap between the roots and the soil that could potentially serve as a preferential seepage path. They noted that the downstream edge of the breach coincides with the root system of the burned stump, suggesting the possibility that the breach width was limited by the reinforcing effect of this root system. No evidence other than the coinciding locations exists for this hypothesis.

The two failures along the Cap Au Gris levee as reported by Harder et al. (2009) present important observations on the extents and size of intrusions created by roots coming from live trees in the Midwest. Several roots with diameters larger than 5 inches were observed going from the waterside toe to the landside toe, however, there was no evidence that presence of the roots had any effect on the levee breach except, possibly, to inhibit the depth of scour during overtopping.

4.3.3 1993 MISSOURI RIVER FLOOD

Allen et al (2003) investigated a series of levee breaches along the Missouri River after the 1993 floods, and concluded that vegetation played a significant role in the reduction or prevention of damage of levees. Their study of a 353 mile long segment along the Missouri River concluded that areas where vegetation corridors were present exhibited a smaller number of levee failures, and that the length of the failures or breaches was almost halved when a vegetated corridor existed (Figure 4-22). Moreover, they concluded that discontinuities within these corridors can be weak links for initiation of failures. The figure shows number of levee failures based on incremental increases in the width of woody corridors for levee mile 0-226. The numbers above each bar correspond to the cumulative percentage of levee failures occurring with the addition of each increase in woody corridor width.

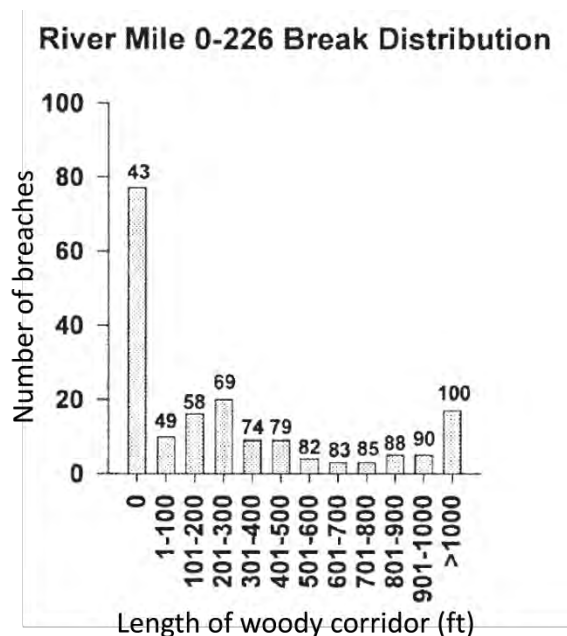


Figure 4-22. Number of breaches as a function of woody corridor length (modified from Allen et al., 2003) [1 ft: 0.3048 m]

4.4 BURROWING ANIMAL ACTIVITY

Historically, animal burrowing has been well recognized as a cause of levee failures. VanBaars (2009) reports that approximately 4% of all levee failures in the Netherlands from 1134 until 2006 have been the consequence of animal activity. Depending on the animal species, burrows in levee embankments tend to form tunnels, galleries and dens that can form complex interconnected systems extending for hundreds of feet. These voids then pose a threat to the integrity of the levee in several ways (DWR, 2009):

- The large voids can provide a preferential seepage path during high stages on adjacent water bodies, altering the saturation front through the embankment and potentially generating higher water tables and/or through seepage that triggers surface erosion of the landside levee slope. Higher phreatic surfaces represent higher pore pressures across the levee prism, that in turn reduce the effective stress of the soil and can contribute to slope stability failures;
- If the voids are large enough and several of them are connected, localized collapses of the embankment can occur and generate loss of protection elevation leading to possible overtopping;
- If the embankment is composed of erodible materials, large burrow systems that extend through the full width of the levee can become conduits for piping and rapid erosion of the levee materials.

For dams, which share some characteristics with levees, FEMA (2005) identifies potential risks from animal burrowing as (1) hydraulic alteration, (2) structural integrity losses, and (3) surface

erosion. Hydraulic alteration (Figure 4-23) is a distortion of the phreatic surface established through the embankment, as burrow dens and complexes located on the waterside can allow water from the waterside to enter inner portions of the embankment with no loss of hydraulic potential. If the burrows are on the protected side (landside), burrows that extend below the phreatic surface can concentrate the flow lines and potentially lead to piping. This phenomenon is most often cited as the greatest concern because it is progressive and can rapidly lead to failure (FEMA, 2005). Structural integrity losses occur when a large number of burrows or dens collapse, generating a localized loss of freeboard or flood protection elevation (Figure 4-23) or slope instability in the vicinity of the collapse. Finally, surface erosion by the downslope biogenic movement of soil ejected from the animal burrows eliminates vegetal cover that provides erosion protection.

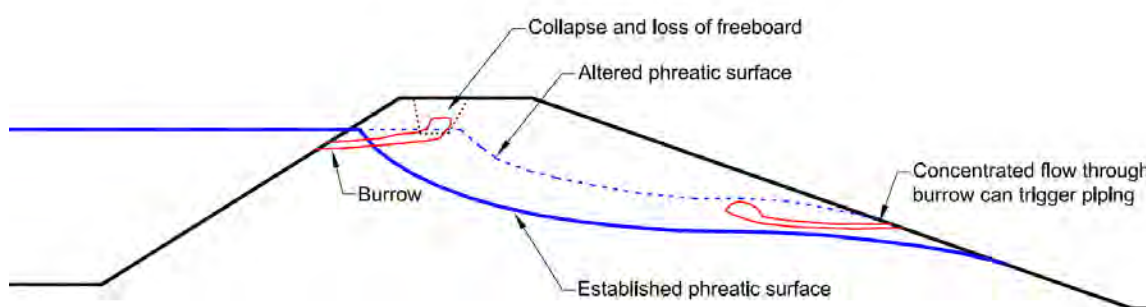


Figure 4-23. Effects of animal burrows in embankments

Current efforts to quantify the extents of animal burrow-induced damage to levees in California are being undertaken as part of the California Levee Vegetation Research Program and by the California DWR. In 2009 DWR conducted an *Animal Burrow Hole Persistence Study* on Sacramento area levees using data from biannual inspections spanning twenty four years (DWR, 2009). The variable employed to measure the activity of mammals was the cumulative occurrence of documented burrows over time, which suggests animal persistence in a given levee reach. Repeated reports were then related to a higher degree of structural damage in comparison with sites that had none or few reported instances of mammal intrusions. The study categorizes the level of activity using statistical analysis, and assigned low, medium and high persistence to levee miles within the lower, middle and upper third of the statistical distribution. Of the 1,567 miles analyzed by DWR, 543 miles (35%) were classified as having a high persistence of animal activity data with eight or more recurrent events, 382 miles (24%) as having medium persistence (four to seven recurrences), 350 miles (22%) had low persistence (one to three recurrences), and the remaining 292 miles were considered to have no recurrences or no available data to classify them.

The presence and recurrence of animal intrusions in levees are a direct function of available food sources, levee material, vegetation and maintenance practices. The latter is of particular

importance as local districts generally have different funding depending on the characteristics of their protected basin (e.g. urban vs. non-urban levees). Therefore, each district applies animal control and vegetation management practices that are deemed affordable and specific to the habitats of the burrowing species. Typical animal control measures consist of cement-bentonite grouting, trapping, baiting with zinc phosphide, fumigation, anticoagulant baits, carbon monoxide injections, biological control, contraception, and shooting (Ventura County Watershed Protection District, 2006).

Typical burrowing rodent species in levees are Botta's Pocket Gopher (*Thomomys bottae*) known for creating shallow networks of burrows parallel to the ground surface (4 to 6 cm in diameter). Gophers have been reported to burrow through irrigation ditch embankments (Dixon, 1922) and are commonly found in North and Central America. This species is known for displacing as much soil as 18 m³/ha per year (Bayoumi and Meguid, 2011). The California Voles (*Microtus californicus*) are another small rodent that tends to remain in the upper foot of soil and dig holes similar to voles, generally between 3 to 5 cm in diameter.

California Ground Squirrels (*Otospermophilus beecheyi*) are a common burrowing mammal and tend to dig relatively large burrows (6-15 cm in diameter), averaging 10 cm in diameter and between one and ten meters in length. The longest squirrel burrow on record had a total length of 222 meters with 33 openings, indicating that despite their relatively small size, squirrels can burrow completely through a levee section (Bayoumi and Meguid, 2011). Squirrel burrow complexes can become preferential paths for seepage and carry floodwaters and sediment and in general provide pathways for internal erosion of levee embankments. Van Vuren (2011) indicates that the presence of woody vegetation has a negative influence on the occurrence of squirrel population.

Larger species such as beavers (*Castor Canadensis*), muskrats (*Ondatra zibethicus*) and certain carnivores (coyotes, gray foxes and skunks) may excavate significantly larger burrows that can result in collapse of a levee embankment (Van Vuren, 2011). Beavers obstruct waterways by constructing dams; their dens generally extend from several feet below the waterline toward the landside. Dens tend to be between 0.5 and 3 meters in diameter and extend several meters into the levee embankment. Two recent levee failures in the United States have been attributed to beaver intrusions (Clevenger, 1999): one in Southern Hinds County (MS), where "*a levee almost breached within a few hours from the first spotted landside leakage. Upon inspection by the division of dam safety in the state of Mississippi, beaver dens and tunnels were exposed and the levee segment appeared to be badly damaged*". The second failure was reported in DeSoto County (MS) and involved a large beaver den near a populated area (Clevenger, 1999).

Muskrats are another large burrowing species known for creating large burrows and extensive damage to levees and earthen dams. Typical muskrat burrows are between 13 and 15 cm in diameter and can extend between three and fifteen meters (Bayoumi and Meguid, 2011), converging in one or several nest chambers above the water level. Muskrat burrows have been classified as a threat to the security of dike and levee systems in the Netherlands (Van Troostwijk, 1978; Kadlec et al., 2007) because of their large size, which similar to beaver dens;

can trigger collapses of large portions of a levee embankment. Other species such as Marmots, Nutria and Armadillos have also been linked to levee damage.

In terms of potential damage to levees, gopher and voles are considered to have little influence as their burrows tend to be shallow and parallel to the levee face; therefore, their effects are more of a maintenance issue as soil is transported downslope but the potential for collapse of the embankment is low. California ground squirrels dig larger, deeper and longer burrow complexes that can threaten levee performance (Daar et al. 1984). These three species were the focus of a recent study by Van Vuren et al., (2011). He performed a statistical study of habitat association for mammal intrusions on levees in California, by analyzing data collected in 166 50-ft long segments. His team counted 33,678 gopher burrows and 5,705 squirrel burrows. Larger species were found to be too few for the statistical analysis (16 large carnivore holes). However, the size of a single large beaver intrusion might be large enough to produce a collapse of the embankment.

Personal communications with staff from the American River Flood Control District (ARFCD) allowed the author to obtain several undocumented incidents of beaver intrusions, which were successfully found and repaired during normal (summer) canal water elevation. These intrusions were generally encountered near the water line, and where there is a waterside berm present the dens tend to remain within the berm and away from the levee. However, once beaver populations increase and there are periods of prolonged high water, some animals will move upslope and dig dens at or above the waterside toe, thus jeopardizing the safety of the levee or potentially causing it to fail.

Typically, the ARFCD and other levee maintenance districts find beaver damage during routine patrol and levee inspections. Mitigation of these incidents is achieved by excavating the dens and re-compacting the excavated portion of the levee. No population control is currently undertaken for beavers by ARFCD.

The author joined personnel from ARFCD on a day-long inspection of several levees near Sacramento, CA, where infestations from different species were observed. During this inspection, several remediated beaver den sites were visited where active beaver dams were present, indicating recent activity from these animals. A new den 'in progress' was also encountered at a site with more than twenty years of reported beaver activity and constant den mitigation. The American River Flood Control District is considered to have a successful squirrel control program, which consists of regular baiting and yearly cement-bentonite grouting of the largest burrows. In some years more than 25,000 pounds of cement grout is used (ARFCD, 2012 – personal communication). Nevertheless, year after year new burrows will be opened necessitating ongoing, costly levee repair and maintenance.

The following section describes several well-documented animal intrusion case histories that have resulted in extensive damage to levees in order to set the stage for the experimental program performed in this dissertation.

4.4.1 PIN OAK LEVEE BREACH

The Pin Oak levee protects the city of Winfield, MO, from the backwaters of the Mississippi River and has a history of poor performance, as two breaches had previously occurred at this site during the 1993 floods (Harder et al., 2009).

During the 2008 flood several landside slope failures were observed, as well as through-seepage (flow of water through the levee embankment exiting on the landside slope) at two locations. A breach occurred at one of the through-seepage sites on 27 June, 2008 (Figure 4-24). The heaviest seepage was observed near the landside toe where a landside ditch parallels the toe. Sandbags were placed around the heavy seepage area (Figure 4-25) in an attempt to minimize the seepage quantities but the through seepage 'broke through' the levee material above the top of the sandbags. Subsequent emergency response included the construction of a larger sandbag ring and placement of a tarp on the waterside slope; all to no avail as this levee breached several hours later.

The post-breach reconnaissance by Harder et al. (2009) reports several 5 to 8 cm (2 to 3 inch) diameter rodent holes in the vicinity of the breach along the waterside slope, extending from the toe to a few feet below midslope. Witness accounts report the presence of muskrats diving into the area where the tarp was placed during the flood and chunks of clay being ejected from the protected side. The extent of the animal activity appears to coincide with the eroded mass, as it only extended down to the elevation of the toe.



Figure 4-24. Pin Oak Levee breach (Harder et al., 2009)



Figure 4-25. Animal burrows on Pin Oak Levee breached section (Harder et al., 2009)

4.4.2 TRUCKEE CANAL BREACH, FERNLEY, NV

This levee breach was originally documented by URS (2008) in a report for the U.S. Bureau of Reclamation. The failure occurred on 5 January, 2008, near Fernley, Nevada. The breached levee lined the Truckee Canal, which serves as a diversion for excess flows from the Truckee River as well as a water conveyance for miscellaneous uses. The embankment was about eight feet high, with slopes of approximately 1.5:1 (horizontal to vertical) (Figure 4-26). Embankment materials were mainly silts and clays dredged from the bottom of the Truckee Canal and piled over the years (URS, 2008).

The breach developed early in the morning and water flowed into the city of Fernley for about nine hours before it could be plugged, flooding the adjacent areas to depths up to eight feet (Figure 4-27). The investigative team concluded that because the embankment and foundation materials were composed by silts and clays of medium to high plasticity (ML, CL, MH and CH), underseepage or through seepage was an unlikely cause of the failure. Other potential failure modes, such as wave erosion, lateral instability, overtopping and seismic activity were also ruled out because of lack of evidence. The most likely failure mechanism was judged to be a piping failure due to rodent activity, as evidence of active rodent (muskrat) activity had been reported in the area by local personnel, and several rodent tunnels were observed during the forensic investigations. A previous smaller failure in 1996 was also related to animal burrowing in the area (Benedict, 2008).

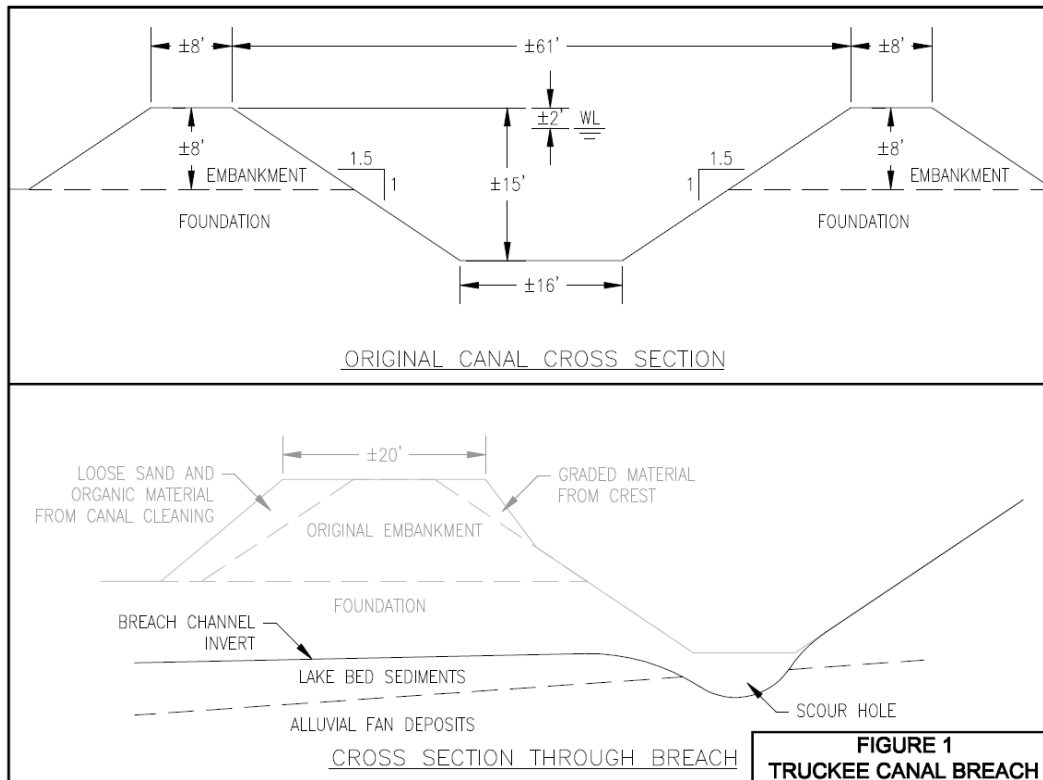


Figure 4-26. Truckee Canal cross sections (URS, 2008)

URS also performed chemical grouting at a site 250 ft downstream of the breach in order to assess the extents of the Muskrat burrows present in the area. The investigation revealed a complex system of interconnected burrows (Figure 4-28) extending from the waterside slope to near the landside slope, reaching what the investigative team called a 'collapse feature' (Figure 4-29) with a fan of sand apparently coming from internal erosion along the burrows. The findings indicate that even if the holes did not fully extend to the face of the landside slope, such openings could have collapsed at some point during the failure.

For these reasons, the specific cause of the breach was attributed to Muskrat burrows, given the presence of the networks exposed and documented by URS (2008) and the fact that a previous (smaller) failure in 1996 was also related to animal burrowing in the area.



Figure 4-27. Developed breach looking downstream (URS, 2008)



Figure 4-28. Exposed grouted burrows 250 ft downstream of breached site (URS, 2008)

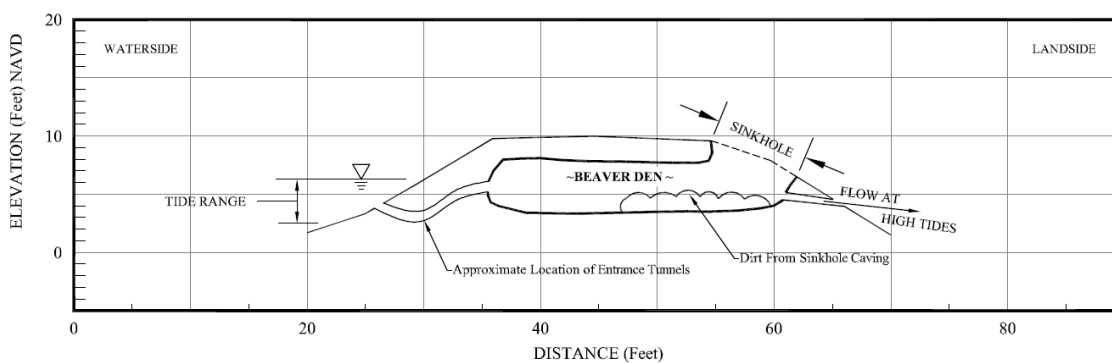


Figure 4-29. Collapse feature at the landside edge of burrow complex (URS, 2008)

4.4.3 MEDFORD ISLAND LEVEE, CA

On 24 January 2009 a cave-in was reported on the southern end of Medford Island in the Sacramento-San Joaquin Delta, exposing a large Beaver den. The levee is approximately 2.5 to 3 meters (8 to 10 ft) high and 6 meters (20 ft) wide at its crown (Figure 4-30).

A survey of the den showed that it extended 4 meters (12 ft) from the landside hinge point of the levee towards the waterside. The void was 1.5 m (5 feet) high by 3 meters (9 feet) wide (MBK, 2009). The den extended from the landside to within 0.6 meters (2 feet) of the waterside face.



EMERGENCY REPAIR JAN. 25-26, 2009

Figure 4-30. Schematic of beaver den cave-in (MBK, 2009)

After the measurements were taken, less than two feet of soil remained above the ceiling of the den and the surface of the crown (Figure 4-31), posing a high risk for the collapse of the structure. Water was seen entering the den from two tunnels (Figure 4-32), and flowing out of the den through a single tunnel (Figure 4-33) that exited the slope at about mid-slope on the landside (MBK, 2009).

The locations of the entrances and exit to the den appeared to be within the range of tidal water fluctuations; therefore, during the daily high tides water would flow in and out of the den possibly worsening the already critical conditions. Emergency repairs included using an excavator to collapse a series of Beaver tunnels along the waterside slope over a distance of 15 m (50 ft) upstream and downstream of the cave-in. Subsequently, the cave-in was excavated and filled with compacted material, slopes were reshaped and riprap was installed to protect the area. The characteristics and extents of the additional collapsed tunnels were not documented during the emergency repair activities.



Figure 4-31. Beaver den cave-in, Medford Island, CA. Photo Courtesy Dustin Sanoski (DWR)

4.4.4 AMERICAN RIVER FLOOD CONTROL DISTRICT, SACRAMENTO, CA

Several recent instances of beaver intrusions have been reported by inspection personnel from the American River Flood Control District (ARFCD) in Sacramento (CA). Repairs were necessary at least eight locations along the 40 miles of levees maintained by this flood control district between 2004 and 2011. Figure 4-34 shows a collapse near the waterside toe of the levee at Arcade Creek (north of Sacramento) found in June of 2004. The damage was spotted during one of the levee inspections, extending from the waterside edge of a 5 m (15 ft) wide berm approximately 4 to 5 meters towards the toe of the levee. The intrusion was between 30 and 35 cm in diameter (12 to 14 inches) at its entrance, which coincided with the root system of a tree. The burrow extended between 1 and 2 meters below the elevation of the berm.



Figure 4-32. Internal view of the den showing access tunnels from the waterside (MBK, 2009)



Figure 4-33. View of the landside cave-in from the levee crown (MBK, 2009)

Similar beaver activity has been recurrent along Arcade Creek (Figure 4-35 through Figure 4-42). The beaver tunnels and dens are generally found in the waterside berm and sometimes extend to the waterside toe of the levee and beyond. However, when there are prolonged periods of

high water some of these animals burrow above the berm and into the levee (Figure 4-42), or when no berm exists between the canal and the levee these animals dig directly into the levee embankment (Figure 4-31 and Figure 4-36) creating potential for collapse, internal erosion and accelerated saturation of the levee under high water.



Figure 4-34. Waterside berm collapse at Arcade Creek levee. Images courtesy of Richard Marck (ARFCD)

The beaver den shown on Figure 4-36 was found at the waterside toe of the levee along Arcade Creek in 2004. This levee segment did not have a waterside berm and the animal dug directly into the levee material. Obviously, this type of situation has the potential to inflict more damage than dens encountered along the waterside berm. The beaver den shown on Figure 4-37 is of particular interest because of its great size (at least 3 meters in length and 35 cm in diameter) and because it is located in an area historically known for beaver intrusions. The levee borders Arcade Creek near Sacramento and it too is part of the ARFCD maintained area, which is known for rapidly mitigating this type of animal intrusion. Mitigation consists of excavating the distressed or collapsed area and backfilling it with large rocks and soil so re-burrowing is discouraged. However, this type of practice does not eradicate the problem; rather it simply makes the burrowing animals dig new dens just a few meters upstream or downstream of the repaired levee section. During the first weeks of 2012, a new den was encountered between previous mitigated burrows (Figure 4-38). The new den was only 1 to 1.5 meters in length and about 35 cm in diameter, and given the presence of a recent waterline

and fresh claw marks inside the walls of the burrow it was concluded that this burrow was likely under construction and repairs were required before the waters rose in the creek.

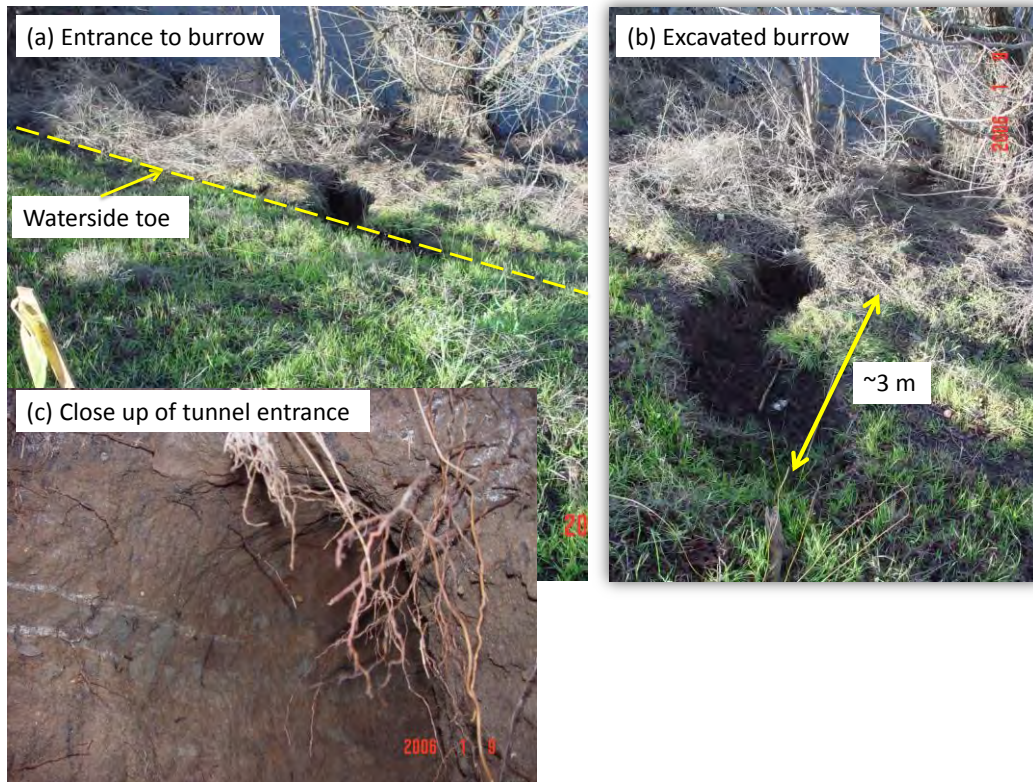


Figure 4-35. Beaver den at Arcade Creek levee in 2006. Images courtesy of Richard Marck (ARFCD)



Figure 4-36. Beaver hole at waterside toe in 2004. Image courtesy of Richard Marck (ARFCD)



Figure 4-37. Beaver den at Arcade Creek. Images courtesy of Richard Marck (ARFCD)



Figure 4-38. Reoccurrence of beaver intrusion in Arcade Creek

The burrow shown on Figure 4-39 near the southern end of Arcade Creek was located in the vicinity of a tree, which was removed during mitigation activities. The beavers seemed to have used large roots at the roof of their burrows, as shown on Figure 4-40.



Figure 4-39. Beaver den at the southern end of Arcade Creek in 2004. Images courtesy of Richard Marck (ARFCD)

Other types of reported beaver damage do not necessarily threaten levee integrity but, if left unattended, can evolve into larger issues. For example, beaver induced damage was found on a paved bike path atop a waterside berm along the north levee of the American River in Sacramento (CA); ARFCD inspection personnel found a sinkhole on the edge of the pavement and some deformations on the paved bike path. Upon inspection, a large beaver entrance was found near the waterline, approximately 1.5 meters below the pavement level. Figure 4-41 shows the sinkhole, which extended vertically down until reaching the burrow connecting to the canal.

Another instance of beaver damage was also reported by ARFCD in 2006 along the Natomas East Main Drain Canal (NEMDC), an interior drainage canal bordering the Natomas basin north of Sacramento (CA). According to reports from ARFCD staff, this area is generally subject to beaver intrusions, but after sustained high waters in the winter of 2006, some beavers dug tunnels from the waterside trench and extended up the waterside slope until less than two meters (measured vertically down) from the crest of the levee (Figure 4-42). The tunnels

collapsed over time, exposing a large hole approximately 50 centimeters in diameter and about one meter below the slope of the levee. The holes seemed to remain parallel to the waterside slope and about one meter below ground surface, and did not extend towards the landward slope.

The levee in this area is composed of compacted clays of medium to high plasticity, which may have allowed the beaver(s) to extend the den from one side of the levee to the other without collapsing. Emergency remediation consisted in excavating the sinkhole area, exposing tules, a small cavern and the tunnel extending to the waterside toe (Costa, 2012), and constructing temporary earthen plugs on both levee toes. Final remediation took place by drilling several holes along the top of the levee and filling them with concrete. Flares were placed at the entrance of the beaver den before the concrete was poured to verify that the drilled holes had in fact intersected the tunnel (Figure 4-44).



Figure 4-40. Beaver burrow collapse at waterside toe near Arcade Creek in 2004. Images courtesy of Richard Marck (ARFCD)



Figure 4-41. Beaver burrow below paved bike path along north levee of American River in 2006. Images courtesy of Richard Marck (ARFCD)



Figure 4-42. Waterside slope collapse from beaver burrow along NEMDC in 2006. Images courtesy of Richard Marck (ARFCD)

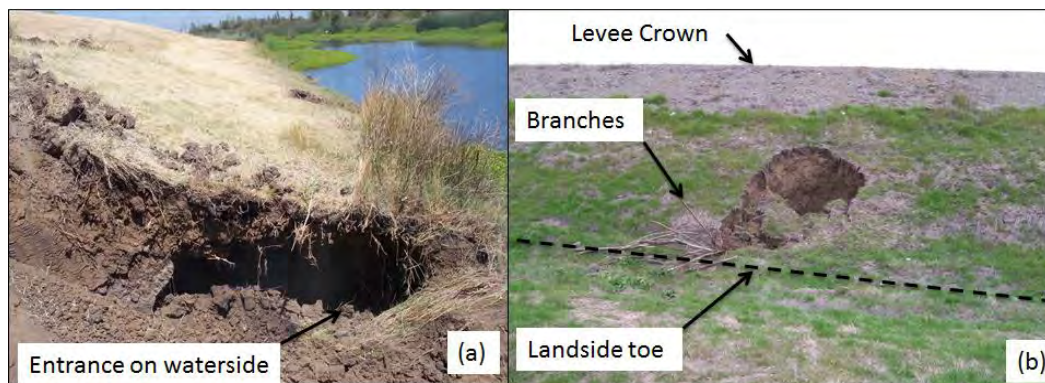


Figure 4-43. Beaver den collapse at PGCC levee near Sacramento, CA. Photo courtesy Ray Costa (2012)



Figure 4-44. Remediation activities on beaver den at PGCC near Sacramento, CA. Photo courtesy Ray Costa (2012)

After excavation, the sink hole was determined to be a collapse feature from the beaver tunnels dug from the waterside of the levee extending horizontally toward the landside toe. To prevent further damage, a 10-foot-deep concrete, steel or vinyl sheet pile cutoff wall near the levee waterside toe was proposed (SAFCA, 2010).

4.5 SUMMARY

The available case histories and data indicate that both vegetation and animal activity can impact levee performance. The severity of this impact depends on tree and animal species, location of the tree, levee district maintenance practices, soil types and hydraulic loading the levee is subject to; thus it is not appropriate to consider all trees as imposing the same level of risk to all levees. As observed from USACE incident reports, majority of the reported vegetation related case histories point to vegetation as inhibiting maintenance and inspection, with none directly tied to an actual cause of levee failure. Conversely, several cases where vegetation was present along the waterside levee slope were reported to have limited erosion and fewer failures when compared to reaches without vegetation. In comparison, levee failures associated

with animal burrowing appear to be well documented and apparently common, given the larger, more continuous openings within an embankment produced by the burrowing activity.

The available data show that the size, extent of the burrows and associated damage is highly dependent on the burrowing species, levee material, maintenance practices and surrounding habitat. Burrows created by pocket gophers and voles seem to be very common in the United States, but their potential for levee damage or breach is minimal since generally the burrow complexes created by these two species are of small diameter (5 to 10 cm), and tend to remain shallow and parallel to the surface, making the damages related to gophers more of a common surface maintenance issue than a structural issue. Holes from California ground squirrels are less frequent (but also very common). Van Vuren (2011) reports a six-fold difference on the occurrence of gopher burrows compared to squirrel burrows. However, the size, extents and potential damage from squirrel networks is much greater than smaller species. Most periodic burrow maintenance and animal eradication activities in California levees are aimed at controlling squirrels. Common squirrel burrows can be between 10 and 15 cm in diameter and the cumulative burrow network lengths have been reported to extend for several tens of meters inside a levee embankment. Muskrat burrows tend to be larger and deeper than squirrel, and have the potential to extend from the waterside toe to the landside toe, as evidenced by the failure on the Truckee Canal in 2008.

Finally, larger species such as beavers, skunks or some carnivores tend to generate the largest burrows and consequently the highest potential for levee damage. Dens of the size as reported at Medford Island (CA) generally result in collapse of the levee and immediate loss of flood protection, which during a flood, can result in widening of the collapsed area and breaching of a much longer levee segment. No reported incidents of breaches from beaver holes were encountered during the literature review, but several collapses under normal (summer) water were encountered. Van Vuren (2011) found no beaver intrusions in 2009 and 2010, most likely because beaver burrow entrances are dug under water and were difficult to find during the field portion of his study.

Chapter 5

FIELD EVALUATION OF BURROWING ANIMAL IMPACTS AND EFFECTIVENESS OF REMEDIAL MEASURES

5.1 INTRODUCTION

As already shown, animal burrowing is a serious threat to the performance of dams and levees, as the voids created by the animals can contribute to shortening of the seepage path, piping, and collapse of parts of the embankment. To learn more about the extent of mammal burrow networks two separate field investigations were performed as a part of the California Levee Vegetation Research Program (CLVRP). One levee section was a sandy levee along the Sacramento River with an active California ground squirrel (*Otospermophilus beecheyi*) infestation, which had only minimal maintenance and mitigation practices in place. The second site was a clayey levee along Cache Creek where yearly maintenance activities are undertaken by the California Department of Water Resources (DWR) and, consequently, the effects of the burrowing activity were considered minor. Thus these two sites were selected for field studies to achieve two objectives:

- Assess the extent and architecture of burrow networks under the two limiting conditions of: (1) no maintenance and regular (yearly) baiting; and (2) regular (yearly) grouting.
- Study the efficacy of current DWR grouting technique of injecting a cement-bentonite grout into the largest burrows by a follow up chemical grouting to fill remaining void spaces missed by the cement grout.

Two grout campaigns were performed at each site: first, the California Department DWR used their regular grouting procedure by injecting a cement-bentonite grout into the largest burrows. Subsequently, a chemical grout was injected through a grid spaced in a triangular grid pattern in an effort to fill remaining void spaces missed by the cement grout.

Upon completion of the grouting activities, the levees were excavated and the grouted burrows were exposed and surveyed using Tripod Light Detection and Ranging (T-LiDAR) scans. This data was then used to estimate the volume of voids within the embankment created by the burrows, and to evaluate the efficacy of the grouting procedures by differentiating between the two types of grout.

5.2 METHODS OF INVESTIGATION

5.2.1 SITE SELECTION

The selection of the sites was based on the following criteria:

- Degree of infestation: A site with an active infestation was desired to show the effect of minimal maintenance or animal control on the size and extent of the burrow system, while a site where periodic maintenance takes place was selected in order to observe the effects of regular maintenance practices.
- Burrowing species: California ground squirrels and Botta's pocket gophers (*Thomomys bottae*) were the target species at both sites. Smaller species are likely to have less influence on the performance of a levee, and larger species with potentially larger burrow systems have been found to be much less frequent than squirrels and gophers (VanVuren, 2011).
- Soil conditions: The sites were targeted so the infestations were encountered in different materials. The embankment at the site with minimal animal control measures consisted mainly of loose sands with interbedded clay layers, while the maintained site consisted of a clay embankment.

5.2.2 SITE SURVEY

The first step in the site evaluation at each location consisted of surveying all existing active and inactive burrows by laying out a coordinate grid along the levee slopes and crown, measuring the size of the main holes encountered, and documenting all other important features, such as stratigraphic contacts, cracks along the levee crown and slopes, and the presence of vegetation.

After the grid was laid out, survey flags were placed next to each hole and an initial high-resolution ground based T-LiDAR base scan was performed so a three dimensional image of the levee prior to the test was available. A local reference frame was established for the T-LiDAR systems by installing several benchmarks using one meter threaded rod pushed to refusal, and a set of six 4-inch PVC crosses outside the study area such that a minimum of six spherical (Figure 5-1) or PVC targets could be seen in each scan to optimize post-processing and aligning processes. Two types of T-LiDAR systems were used: an *Optech* ILRIS device, which captures infrared contrasts on the soil at a scan density of 2 to 3 millimeter spot spacing, or 2,500 data points per square meter; the second device employed was a *Faro* device, which is able to capture real RGB color of each scanned point, generating a 3D colored representation of the scanned area. The flags next to each hole were installed with a two to three centimeter long reflective strip that produces a signal spike on the T-LiDAR data (Cobos Roa et al., 2012) so the exact location of the holes in the study area were captured by the baseline laser scan.

5.2.3 GROUTING PROGRAM

The first round of grouting was performed using the typical cement-bentonite grout mix employed by the DWR and local maintenance districts in their periodic grouting campaigns, which consists of injecting a relatively viscous grout containing 5-10% bentonite. This phase of the grouting program used a portable grout rig (Figure 5-2), which consisted of a small drum fixed to a board, so a small forklift could transport it, and fitted with a pump, hoses and valves to allow the desired amount of mixed grout to flow by applying a small amount of pressure (approximately 0.5 psi [3.4 kPa]). Inside the drum, the mix of cement, bentonite and water was achieved manually; alternatively, a mix on-site cement truck can be used to pour the cement into the mix.



Figure 5-1. Reference targets used for aligning T-LiDAR scans



Figure 5-2. DWR portable grout mixer for field tests

Once the cement-bentonite mix was prepared, holes typically targeted during regular grouting operations (8 cm in diameter and larger) were filled until grout flowed back out of the hole or out of a nearby hole, at which point the hole was plugged using a burlap bag (Figure 5-3).

The approximate time it took for each hole to be filled was recorded and using average flow quantities coming from the pump, the volume of grout used was estimated. If cement-bentonite grout was observed flowing out of one or more holes around the injection point, the locations were recorded.



Figure 5-3. Typical DWR grouting procedure

Several days after the cement-bentonite grouting program was completed, another round of grouting was performed, this time using a polyurethane-based grout. The chemical mixture and injection procedure was similar to that used in 2008 after the levee failure in Fernley, Nevada (described in Chapter 4). Grout consisted of a mixture of ten parts pink-dyed water and one part additive composed of Stratathane ST-504 injection resin from Strata-Tech Inc. and Sika® concrete bonding adhesive.

The result was a very fluid hydrophilic solution capable of flowing through the pores of coarse-grained materials and fissures in the fine-grained soil until a large discontinuity such as a burrow was encountered, at which point the polyurethane flowed into the opening and quickly filled it. The mixture expanded while curing thus creating a tight seal.

The polyurethane grout was injected into the soil using 2 cm diameter, 1.5 meter (5 feet) long steel tubing with holes drilled along the lower 1 meter (3 feet) of tube (Figure 5-4). The pipes were inserted into the soil using a jackhammer on a 1.2 m (4 feet) spacing in a triangular grid pattern (Figure 5-5). Several additional pipes were inserted near large active holes where large amounts of cement-bentonite grout were used during the first phase of the grouting program.

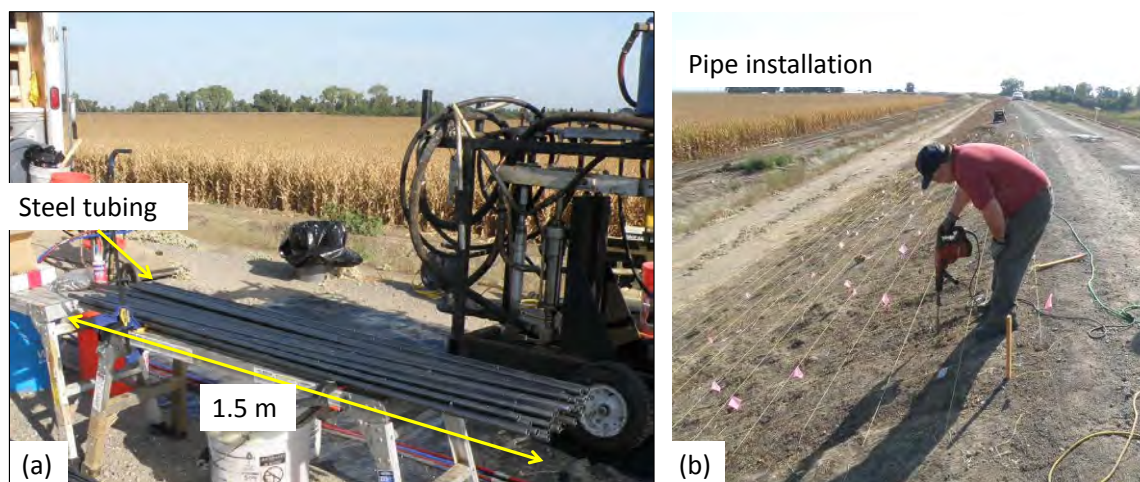


Figure 5-4. Experiment setup: (a) injection tubing prior to installation, (b) installation of tubing using jackhammer

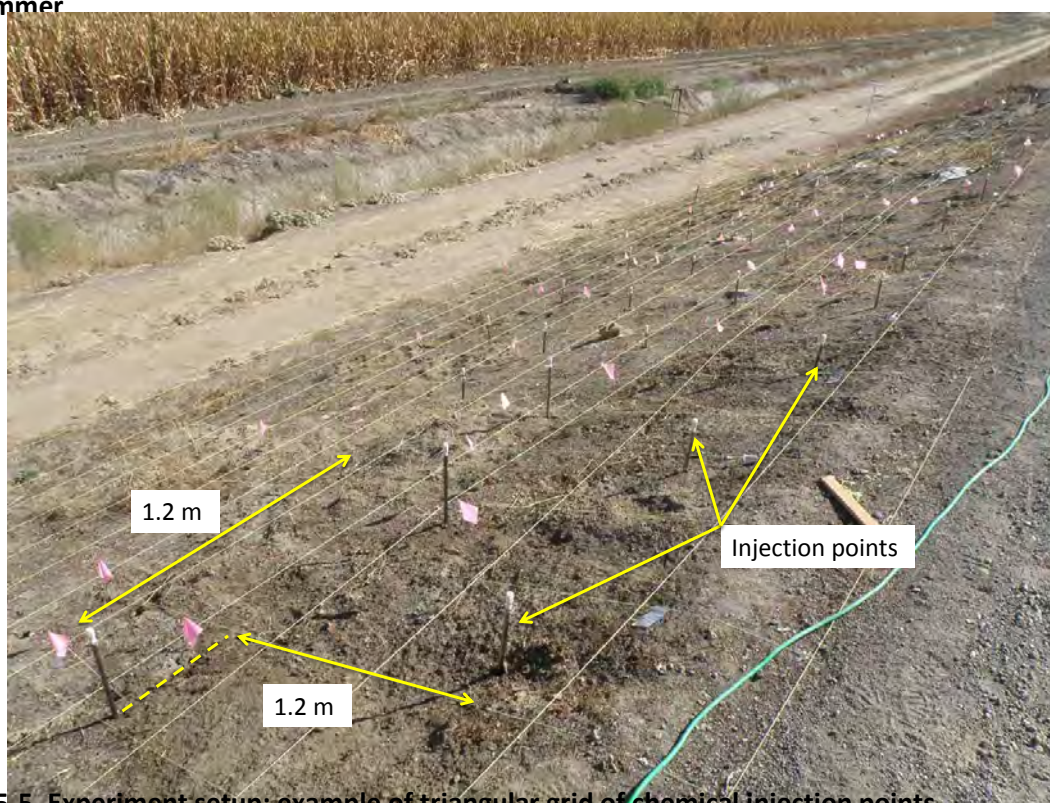


Figure 5-5. Experiment setup: example of triangular grid of chemical injection points

The polyurethane grout was pumped using a double stroke pump (Figure 5-6a) which regulates the amount of water and additive being transferred to the injection gun, commonly known as an 'F assembly' (Figure 5-6b). This gun joins the water and additive lines in a 0.5 cm diameter tube which mixes the two flows prior to entering each injection tube (Figure 5-7).

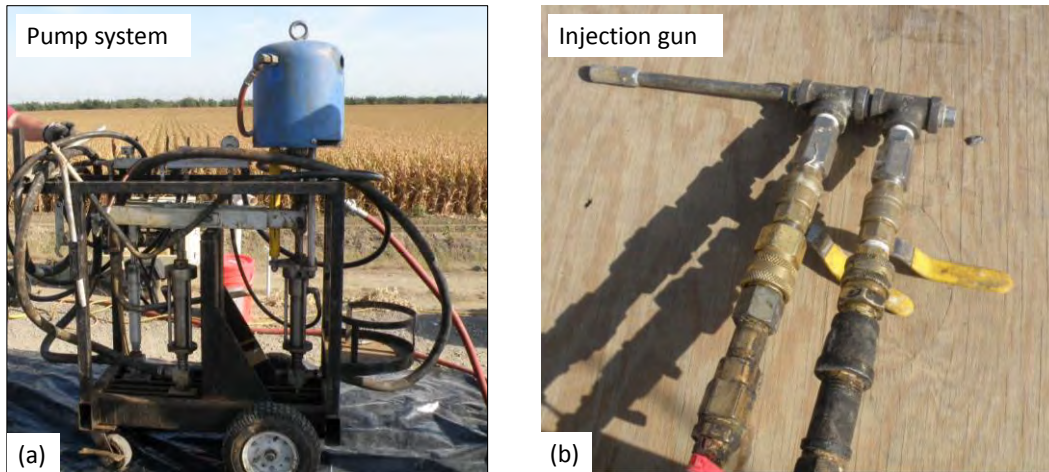


Figure 5-6. Experiment setup: (a) double-stroke pump system, (b) 'F assembly' injection device

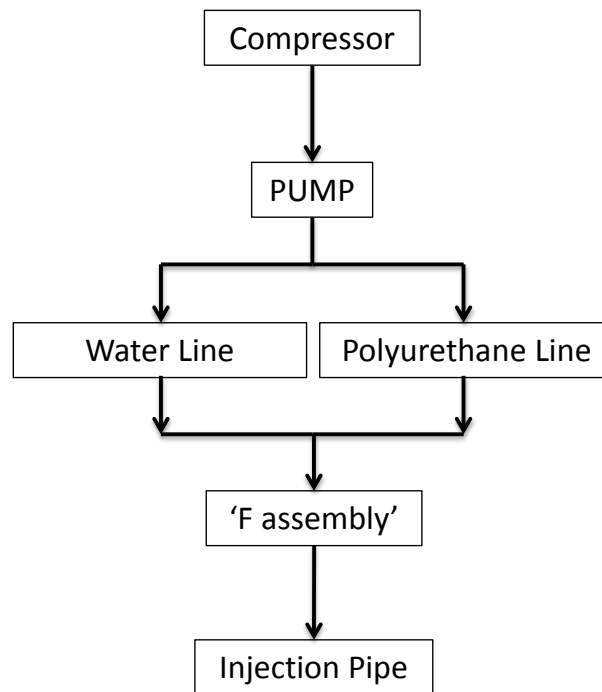


Figure 5-7. Flow chart of polyurethane grout injection process

The polyurethane grout was pumped into each injection point (**Error! Reference source not found.**) until grout flowed back up around the tubing, out of the soil near the injection port, or out of a nearby burrow. Injections started at the lower line of pipes and moved upslope to form a barrier and decrease the amount of grout and water mix flowing downslope and away from the levee toe. This process generally took one to three minutes for each injection point, but some areas near the largest burrows took up to ten minutes per point.



Figure 5-8. View of chemical grout injection procedure

5.3 SITE 1: SANDY LEVEE

The sandy levee borders the eastern margin of the Sacramento River, several miles upstream of Sacramento, California. Figure 5-9 shows the cross section and the relative location of the embankment from the river and the available food source present approximately ten meters from the landside toe.

No periodic grouting or baiting practices have been in place at this site. Rodent control measures typically performed by the reclamation district in charge of maintaining this levee consist of using a propane gun to internally collapse active burrows, filling the blasted hole using hand tools, and occasional baiting. During the inspection of the area several large active California ground squirrel burrows were encountered along a stretch of the levee adjacent to a cornfield, and a 20 meter (60 feet) long segment encompassing some of the largest burrows within this reach was selected for the evaluation.

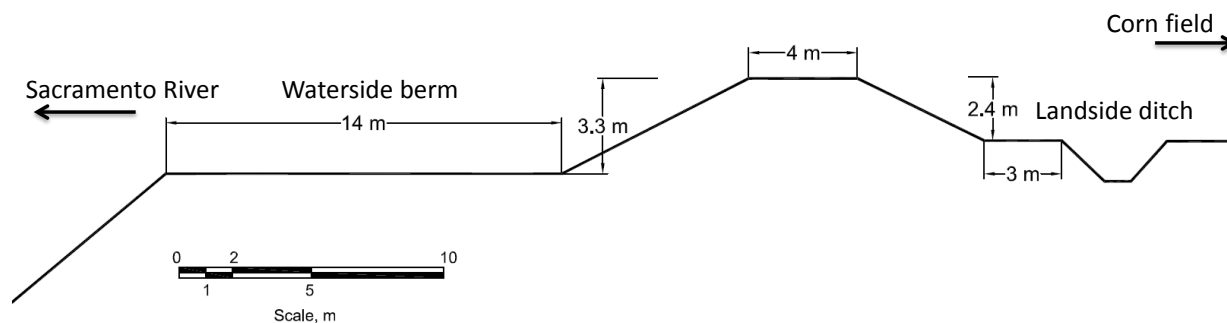


Figure 5-9. Cross section at Sandy Levee Site [1 m: 3.28 ft]

On the landside slope (Figure 5-10), several large active burrows were observed mid slope and towards the levee crown, with ‘porches’ of ejected material exceeding one meter in downslope length. Typical active burrow diameters ranged between 8 and 20 centimeters (0.3 and 0.7 ft), indicating the burrowing species was ground squirrel, which was confirmed later when several squirrels were observed emerging from nearby burrows. The upper bound of the diameter appears to be large for the common California ground squirrel, and can be explained by the fact that the levee material lacks cohesion or cementation and collapses easily; therefore the large size of some holes is likely the result of re-digging of previously smaller burrows (Van Vuren, 2012).

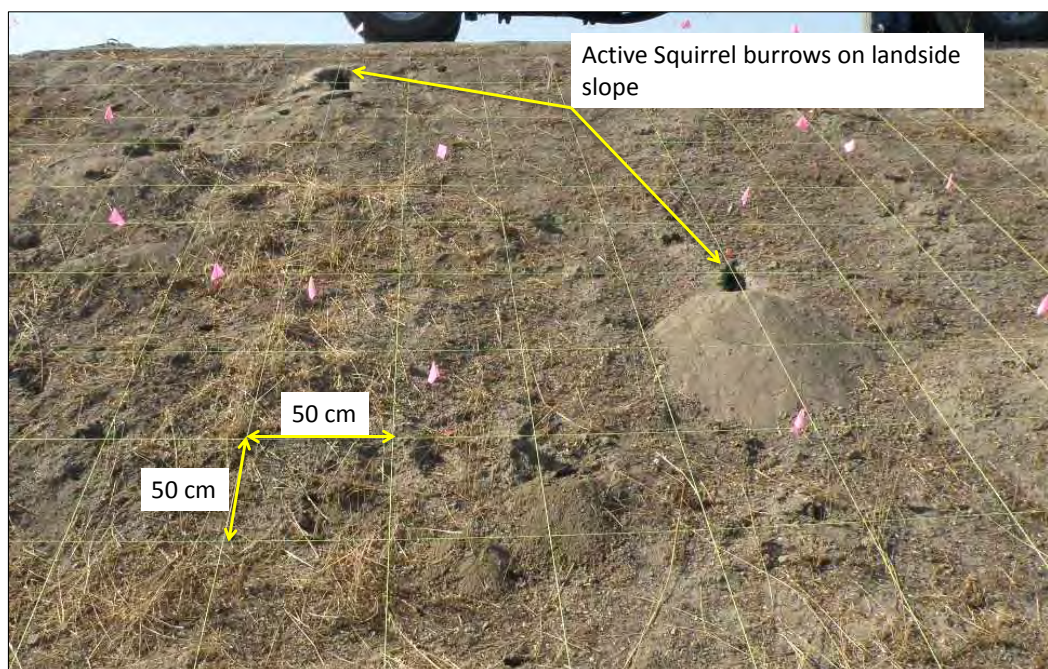


Figure 5-10. Typical active squirrel burrows on landside slope at Sandy Levee Site

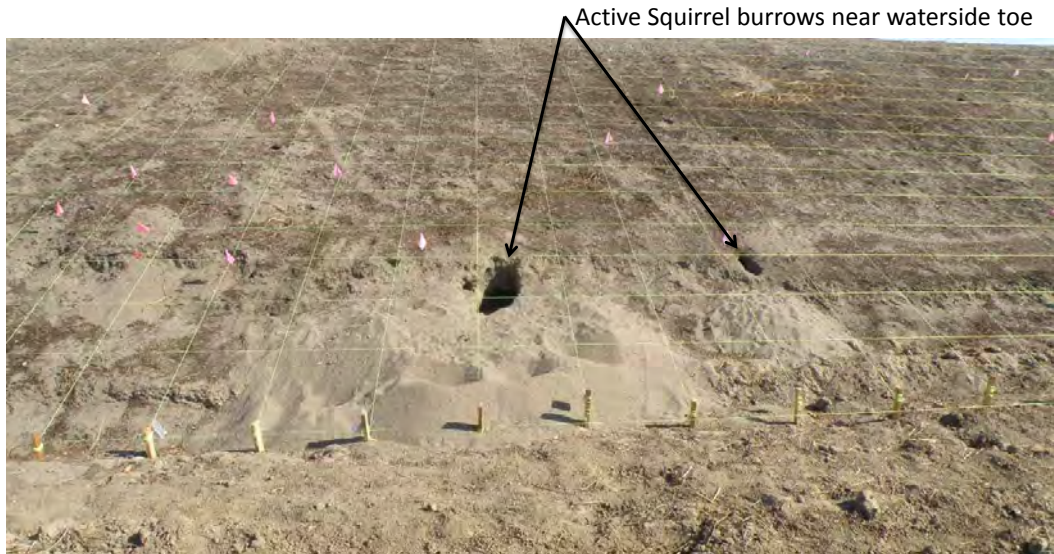


Figure 5-11. Largest active squirrel burrows on waterside slope at Sandy Levee Site

Figure 5-11 shows a view of the main burrows on the waterside slope. Two large burrows with an entrance diameter between 20 and 30 centimeters (0.7 and 1 ft) were observed near the waterside toe, and showed a large cone of ejected material. Other burrows along the waterside slope were generally small or inactive. Seventy-two burrows were surveyed on the landside slope; thirty-four burrows were encountered on the waterside slope, and six along the crown of the levee. The marked difference between landside and waterside slope is likely attributable to the proximity of the food source near the landside slope, and to layering of the levee embankment. The surveyed holes are indicated by pink flags on Figure 5-10 and Figure 5-11, and are shown in plan view on Figure 5-12. The plan view shows active squirrel burrows and all other holes where no differentiation of activity and species could be made because of recent burning of the levee slopes, which might have removed the material from the porches, and partially or completely collapsed some holes.

A burrow was classified as active based on the presence of material ejected downslope of the entrance, food waste and/or footprints in the vicinity of the entrance. A total of 14 active squirrel holes were surveyed on the landside slope, one on the crown near the landside hinge point and six on the waterside slope. Inactive burrows showed a similar trend; 58 inactive or collapsed holes were observed on the landside slope, while 19 were found on the waterside slope.

Figure 5-13 overlays the surveyed burrows and the injection points for the two types of grout used in this study. The green squares indicate the fourteen burrows where cement-bentonite grout was injected, and green arrows indicate instances when grout flowed out of holes adjacent to a burrow being grouted. The time required to fill every hole was recorded, and volumes were estimated using average flow quantities from the portable equipment ($0.01 \text{ m}^3/\text{s}$) used by DWR (Table 5-1). Typical DWR grouting activities target the largest holes with a clear and open surface expression; consequently only fourteen holes were grouted using this

technique and all other holes were dismissed because they were either too small or collapsed near the entrance.

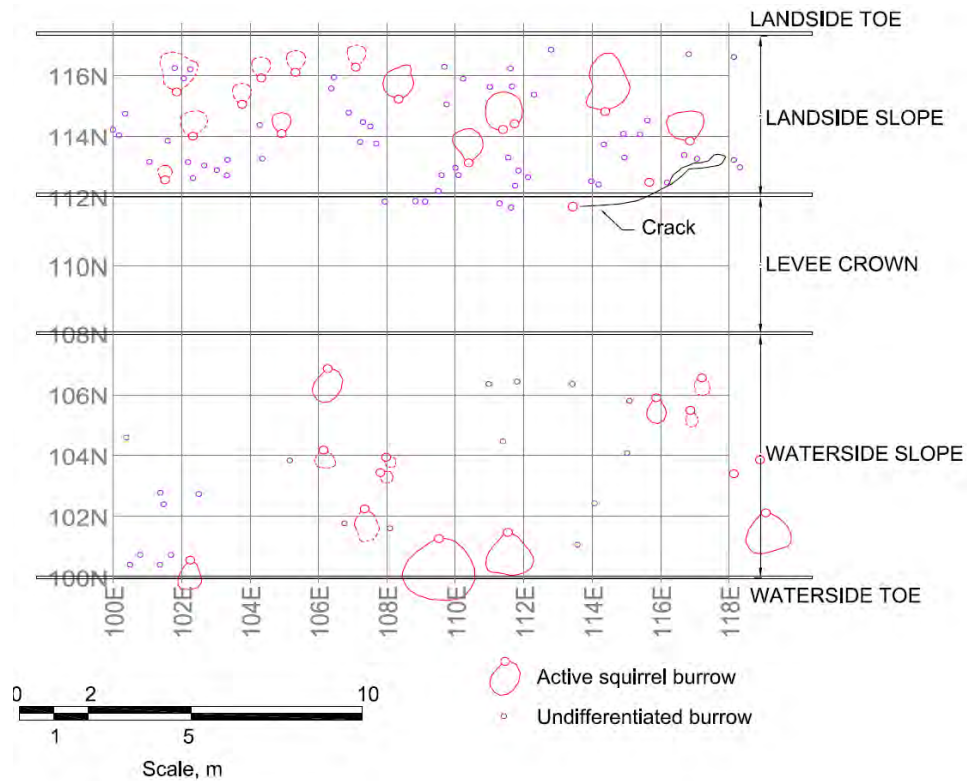


Figure 5-12. Plan view of surveyed burrows at Sandy Levee Site

A total of 140 polyurethane injection points were used at the Sandy Levee Site to cover the area under study (Figure 5-13). Similar to the cement-bentonite grout, times (and consequently volumes) of injection varied between injection points and were recorded.

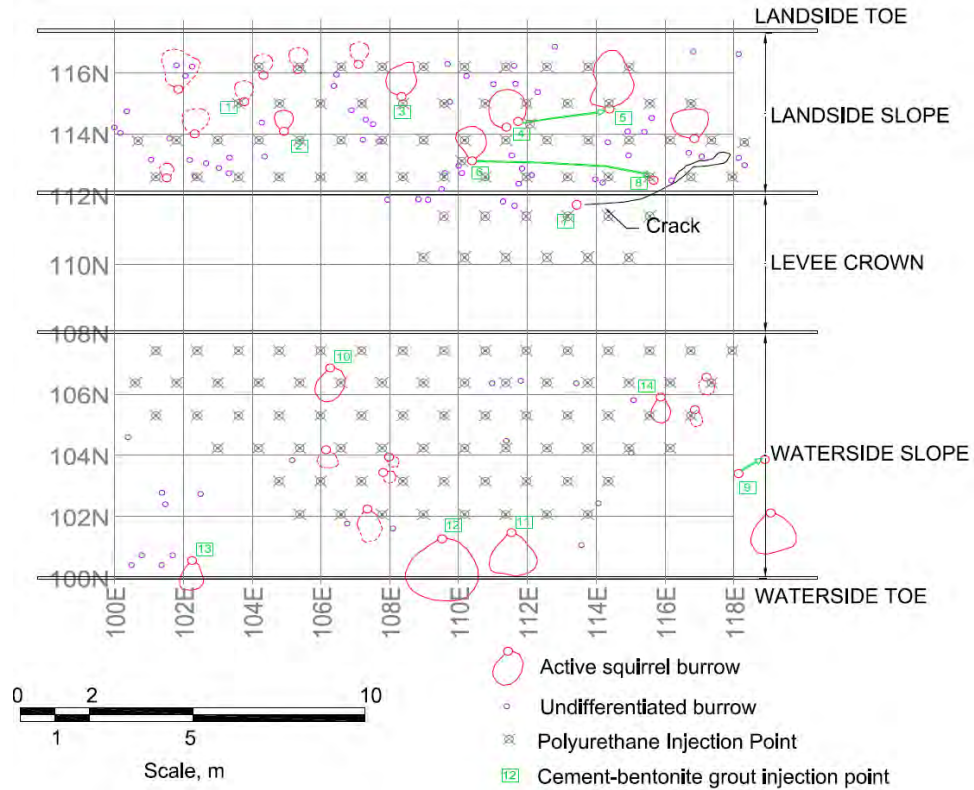


Figure 5-13. Plan view of cement-bentonite and polyurethane injection points at Sandy Levee Site

Table 5-1. Approximate time required to fill holed with cement-bentonite grout

Hole Number	Time required to fill hole (sec)
1	15
2	35
3	15
4	900
5	25
6	10
7	20
8	420
9	180
10	60
11	210
12	60
13	20
14	30

Index soil properties were estimated for the site prior to excavation. Disturbed soil samples were retrieved using bag samples. The objective was to obtain general index properties that allow basic geotechnical characterization of the levee embankment at the test site.

Table 5-2 shows the summary of index properties estimated from four samples obtained at different points on the levee embankment.

Table 5-2. Index soil properties for Sandy Levee test site

Sample	% Fines	% Sand	% Gravel	Water Content (%)	USCS
LS-1	10	90	0	16.5	SP-SM
LS-2	15	85	0	-	SM
WS-1	17	83	0	-	SM
WS-2	61	39	0	23.0	ML

LS: Landside slope, WS: Waterside slope.

Samples LS-1, LS-2 and WS-1 correspond to the majority of the levee material, composed of silty sand with a mean grain size of 0.3 millimeters and 13 percent fines. The last sample was retrieved from a thin stiff silt seam near the waterside toe slope area. Most of the long burrows found during post-grouting excavation were encountered along the interface between the stiff seam and the loose sands. A simplified cross section for the Sandy Levee Site is shown on Figure 5-14.

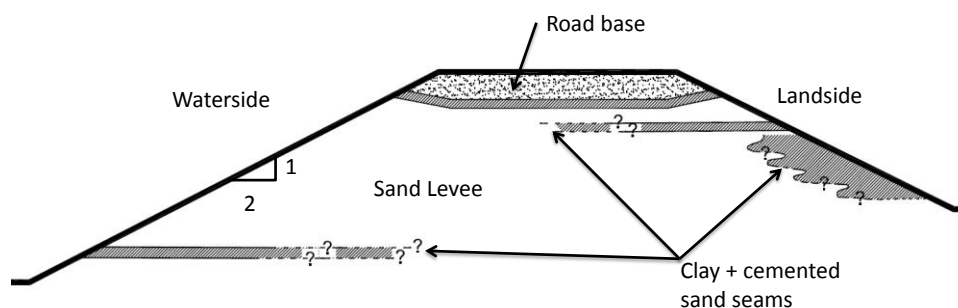


Figure 5-14. Simplified cross section at Sandy Levee Site

5.3.1 SITE 2: CLAYEY LEVEE SITE

The clayey levee is located along the west bank of Cache Creek north of Woodland, California. Similar to the other site, this site also had an active small mammal food source very near the landside toe of the levee; Figure 5-15 shows the approximate cross section at this site. The creek channel is located 20 meters away from the levee and is deeply incised; therefore the levee is infrequently wetted during the flood season.

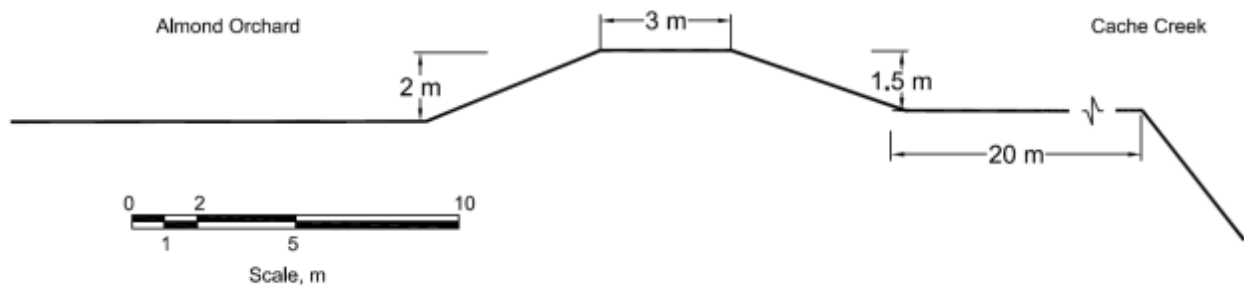


Figure 5-15. Cross section at Clayey Levee Site

This site is of great importance to the history of grouting practices in California. During the floods of March 1998, this levee experienced water levels within 0.5 meters of the levee crown (Figure 5-16a). Sustained high water resulted in several sandboils and through-seepage on the clayey embankment (Figure 5-16b, c and d). This near failure was attributed to the presence of mammal burrows, which led to the beginning of current DWR grouting and maintenance programs. Since 1998, this levee has been used as a test site by the DWR, to perfect grouting techniques and mix compositions. Grouting takes place at the end of the spring season, and records of grouting volumes and number of burrows have been kept and were provided by DWR personnel (Figure 5-17). The figure shows that the volume of grout required to fill active or new burrow holes along this stretch of levee decreased every year despite having a food source next to the levee. The fact that several holes were flowing muddy water during the 1998 flows indicates that some of these burrows were completely penetrating the embankment and piping was occurring.

DWR (2009) concluded that there were holes completely penetrating the levee prism in the study area, and these holes tended to be located in the upper portion of the levee representing a significant risk for stability if not remediated. That study provides several important observations:

- *“Rodent colonies and individual holes appear to increase in size each year if not backfilled.*
- *Surface treatments such as dragging and track walking levee slopes leave hidden voids within levees. Consequently, such activities should be performed after grouting is completed.*
- *Levee reconstruction to address rodent damage is not economically practical for individual holes given the scope of the rodent problem.*
- *Squirrel population varies greatly from year to year and is dependent on weather. High concentrations of squirrels are observed after mild winters.*
- *After a colony of squirrels is eradicated, the burrow systems are quickly filled with juvenile squirrels from adjacent locations.*

- *Best eradication results are achieved when State efforts have been coordinated with activities of local growers”.*

The data in Figure 5-17 suggests that even though the number of burrows encountered along the levee reach under study had increased by approximately 300%, the amount of grout used per hole has declined five-fold. Not shown on the plot is the amount of labor hours per hole, which declined from about two man-hours in 2000 to less than 0.5 in 2004. These results suggest that the adoption of a periodic burrow grouting program can mitigate the likelihood of a large burrow or network of burrows from penetrating a levee, and decrease the maintenance cost.

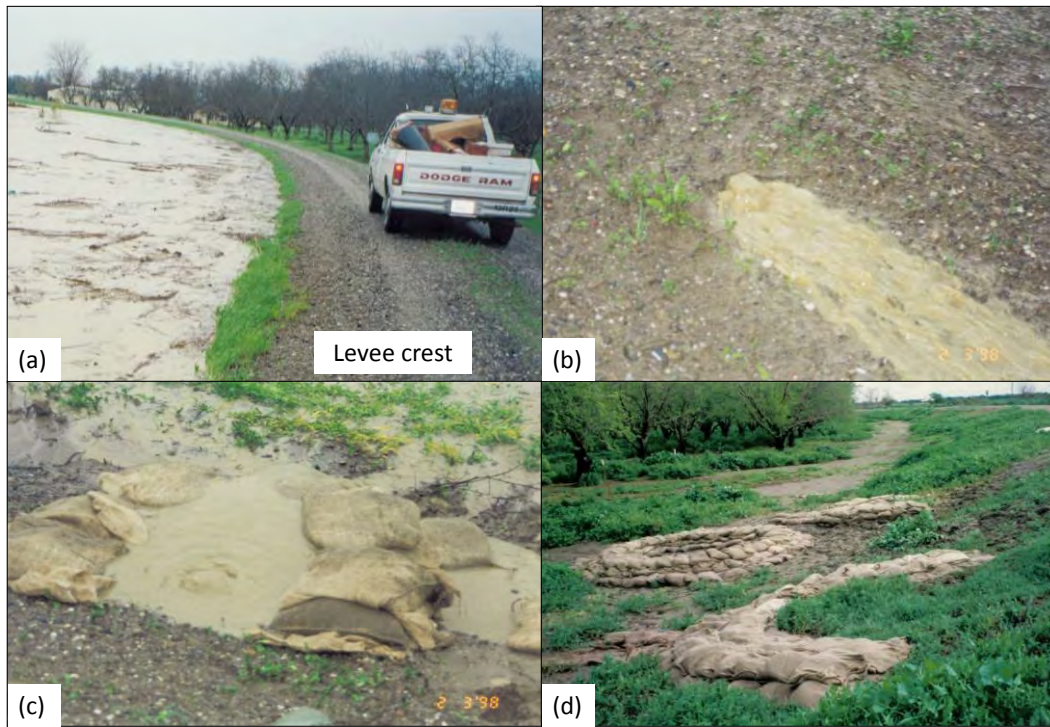


Figure 5-16. High water on Clayey Levee Site during 1998. Images courtesy Al Romero, DWR

In general burrowing activity observed during the present study was mainly by gophers, with a few isolated squirrel burrows. Typical burrows had diameters ranging from five to ten centimeters, and were mostly concentrated in the upper half of both landside and waterside slopes, coinciding with a strip of grass that was not mowed by the landowner. Most evidence of recent small mammal activity was unfortunately lost shortly before the site work commenced because of mowing and burning of the slope surfaces, but the entrances to the main burrows remained relatively intact. Figure 5-18 shows the landside slope prior to excavation, indicating the location of burrows and one of the sandbag rings shown on Figure 5-16d.

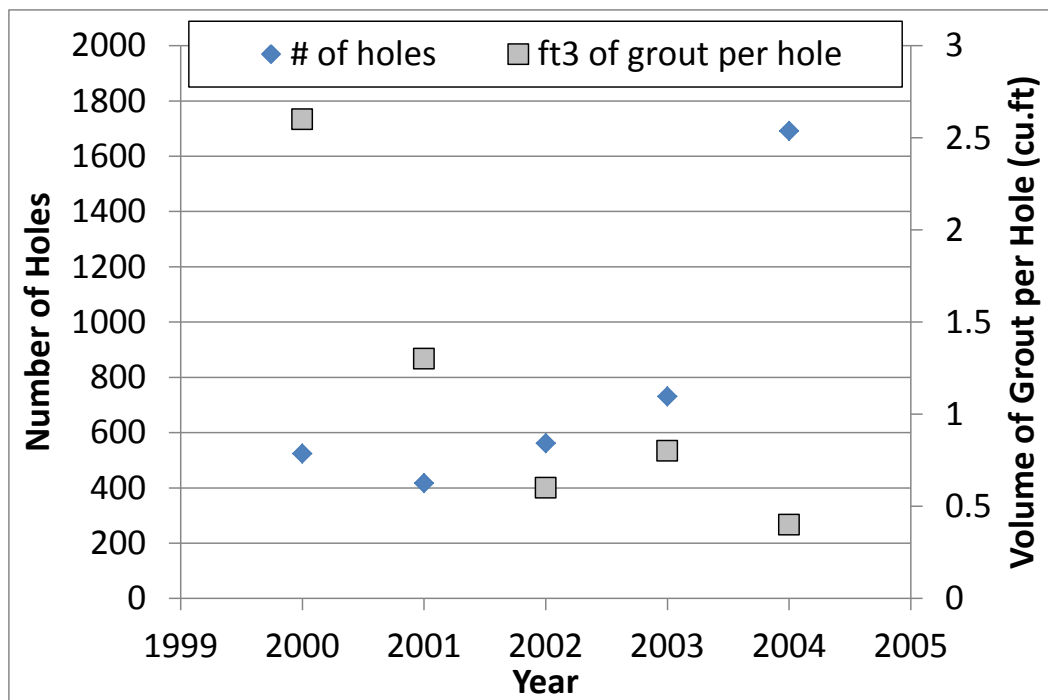


Figure 5-17. Volume of grout used on the Clayey Levee Site from 1995 to 2004 (data provided by Al Romero, DWR)

Similar level of burrowing activity was observed on the waterside slope, with most of the burrows concentrated on the upper half of the slope (Figure 5-19). In contrast with the sandy levee, the few remaining ejected soil ‘porches’ were composed of chunks of clay and few gravel particles, representative of the material composing the levee embankment. The site was surveyed following the same procedure as described for the other site, but differentiation of active and inactive holes was more challenging on this site because of the previously mentioned mowing and burning. A plan view of identified burrows is shown on Figure 5-20. Twelve active squirrel burrows were encountered along the 20-meter long test section; fifty-two unidentified burrows were logged on the waterside slope, and seventy such holes on the landside. Based on conversations with Dr. Dirk Van Vuren of UC Davis, most of these small, unidentified holes were classified as gopher holes. The urethane grout injection plan (Figure 5-21) included seventy five ports distributed in a grid pattern and spaced at 1.2 meters (four feet).



Figure 5-18. Location of burrows on landside slope at Clayey Levee site. Pink flagging indicates location of undifferentiated burrows, green flagging indicates burrows historically grouted with cement-bentonite by DWR.

Since this site was last grouted by DWR during late summer of 2011 (10 months before this study) it was deemed unnecessary to re-inject cement-bentonite grout before injection of the polyurethane based grout.

Index soil properties were determined prior to excavation. Disturbed soil samples were retrieved using bag samples. Table 5-3 shows the summary of index properties estimated from five samples obtained at different points on the levee embankment; namely, near each toe, mid-slope and near the levee crest.



Figure 5-19. Typical squirrel burrows on waterside slope at Clayey Levee Site

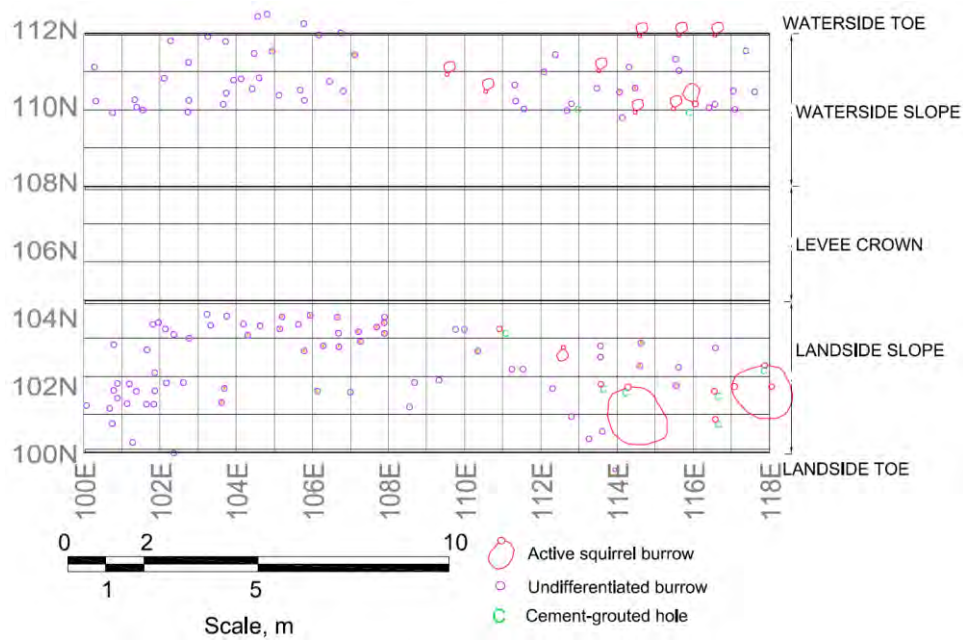


Figure 5-20. Plan view of identified burrows at the Clayey Levee Site

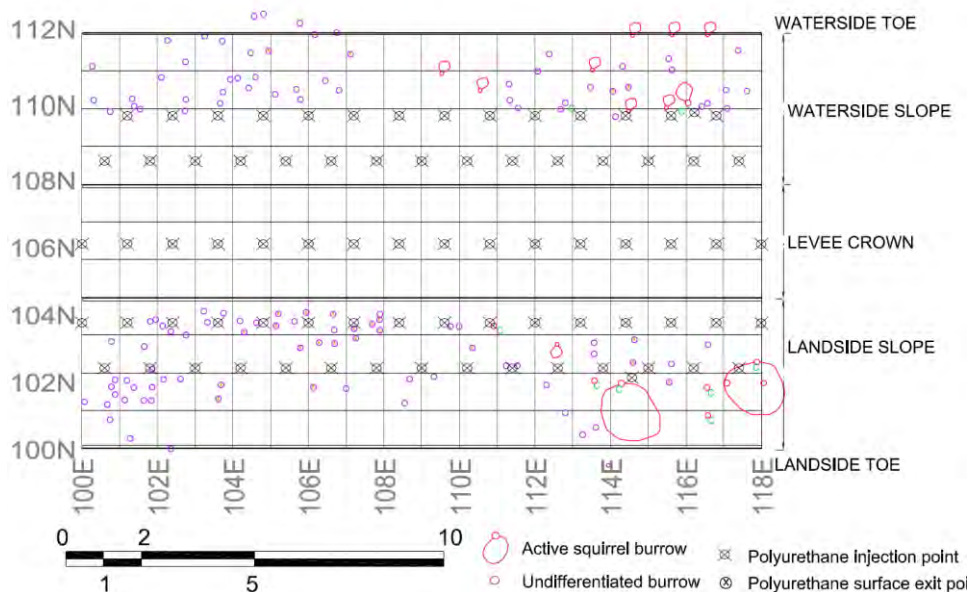


Figure 5-21. Map of grout injection points at the Clay Levee Site

Table 5-3. Index soil properties for the Clayey Levee test site

Sample	% Fines	% Sand	% Gravel	LL (%)	PI (%)	Water Content (%)	USCS
LS-1	67	30	3	-	-	35	ML
LS-2			-	-	-	49	ML
WS-1			-	-	-	41	CL-ML
WS-2			-	40	15	29	CL-ML

LS: Landside slope, WS: Waterside slope

The material composing the embankment is a clayey silt, average moisture content at the end of the 2012 winter was 39% and average Atterberg limits were 40% and 15% for Liquid Limit and Plasticity Index, respectively. The embankment is uniform with very few sand lenses or layering. A simplified geologic cross section for the Clayey Levee Site is shown on Figure 5-22.

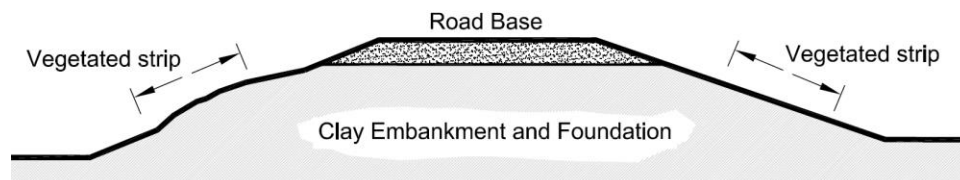


Figure 5-22. Embankment cross section at Clayey Levee Site.

5.4 EXCAVATION AND SURVEYING OF GROUTED BURROW GEOMETRY

5.4.1 SITE 1: SANDY LEVEE SITE, SACRAMENTO RIVER

Excavation was performed using a combination of a compressed air-powered wand, commonly known as 'air knife', hand labor and backhoe operation. The excavation started by removing approximately 50 centimeters (1.6 ft) of gravel base and compacted clay material from the top using a backhoe. Then the air knife was used to remove thin lifts of soil, typically between 20 to 30 centimeters (0.7 to 1 ft) or until a grouted burrow was encountered, at which point the equipment was stopped and hand tools were used to carefully expose the entire burrow.

Once a grouted burrow system was exposed, the surrounding soil was removed using hand tools and, the grouted burrows were cleaned with paint brushes and spray-painted for easy recognition in logs, pictures and T-LiDAR scans. A bright green paint was used for all cement-bentonite grouted burrows, and polyurethane grouted burrows were colored with a pink spray paint. A small area near the landside slope was colored with orange paint because it exhibited both types of grout in comparable quantities.

Personnel from the US Geological Survey Sacramento office visited the site every day after burrows were exposed and painted, and performed T-LiDAR scans of the exposed burrow systems (Bawden et al., 2012). A minimum of six scans were performed per day from different angles with the objective of minimizing shadows in the point clouds and obtaining volumetric representations of the burrows.

The excavated material on the waterside levee slope was mostly sand and, therefore, the air knife was very effective in quickly removing a large portion of the slope. After exposing a large burrow near the waterside toe, no additional grouted burrows were found; therefore, the backhoe was used to remove the remaining soil along this slope. In contrast, the landside levee slope proved to be more challenging to excavate, and several large burrow complexes were encountered just below a stiff silt layer located below the crown and extending to approximately mid-slope on the landside levee slope.

WATERSIDE BURROW SYSTEM

As noted above, a single large burrow was encountered on the waterside slope, approximately one meter above the levee toe. This burrow extended parallel to the toe between the two large active openings shown on Figure 5-11 and had two main arms extending into the levee. Figure 5-23 shows the initial excavation of this burrow, which extended approximately 2.5 meters in the direction parallel to the toe and was mostly filled with cement-bentonite grout between the two burlap bags indicating the cement-based grout injection points, except for a 40 centimeter (1.3 ft) segment filled with polyurethane that seemed to join the ends of the cement-bentonite grout. A 1.5 meter (5 ft) urethane-filled burrow was encountered to the western end (upper left side of Figure 5-23) of this system, extending approximately normal to the levee toe alignment.

Finally, the largest and more important component of this burrow system was observed near the eastern edge of the burrow (bottom right of Figure 5-23), where a large diameter burrow mainly grouted with cement extended from the burlap bag approximately 2 meters (6.6 ft) into the levee with an average diameter of 40 centimeters.

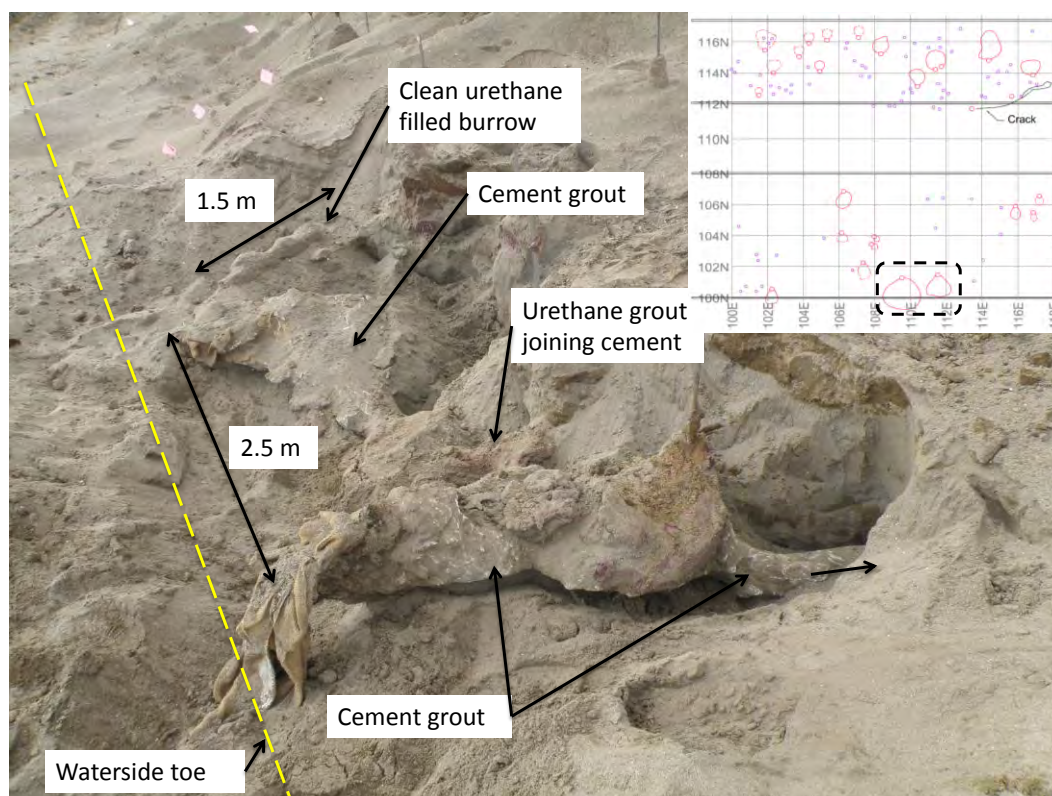


Figure 5-23. Exposed burrow system near waterside toe, Sandy Levee Site

The diameter of the burrow decreased to approximately 20 centimeters and continued into the levee for an additional 2.4 meters (7.9 ft) (Figure 5-24). It terminated in a disc-shaped den of approximately 35 centimeters in diameter and 20 centimeters in thickness. A 30 centimeter long tunnel was observed extending below the den (Figure 5-25), which could have been used as a disposal for droppings by the burrowing animal (Van Vuren personal communication, 2012).

The location of the main burrow and den coincided with the interface between the silty material and the loose sand composing the majority of the levee. The stiffer fine-grained soil apparently provided a stable roof for the burrow and allowed the animal to dig efficiently in the loose sand. This observation was consistent for almost all burrows at this site.

Evidence of the persistence of burrowing activities was observed during the grouting: sometime during the two weeks between the end of the cement-bentonite grouting and the start of the polyurethane grouting programs, a new hole was observed between the two large active burrows near the waterside toe shown on Figure 5-11. Excavation revealed that this new hole followed the previously grouted linear burrow into the levee and likely reached the disc-shaped

den; but it is unclear whether it was created as a new burrow or if it was dug as an escape route by an animal trapped in the adjacent grouted tunnel. Figure 5-26a shows the location of the new burrow entrance relative to the previously grouted large burrows. Figure 5-26b is a close up of the 10 centimeter-diameter (0.3 ft) ungrouted new burrow below the cement grouted burrow.

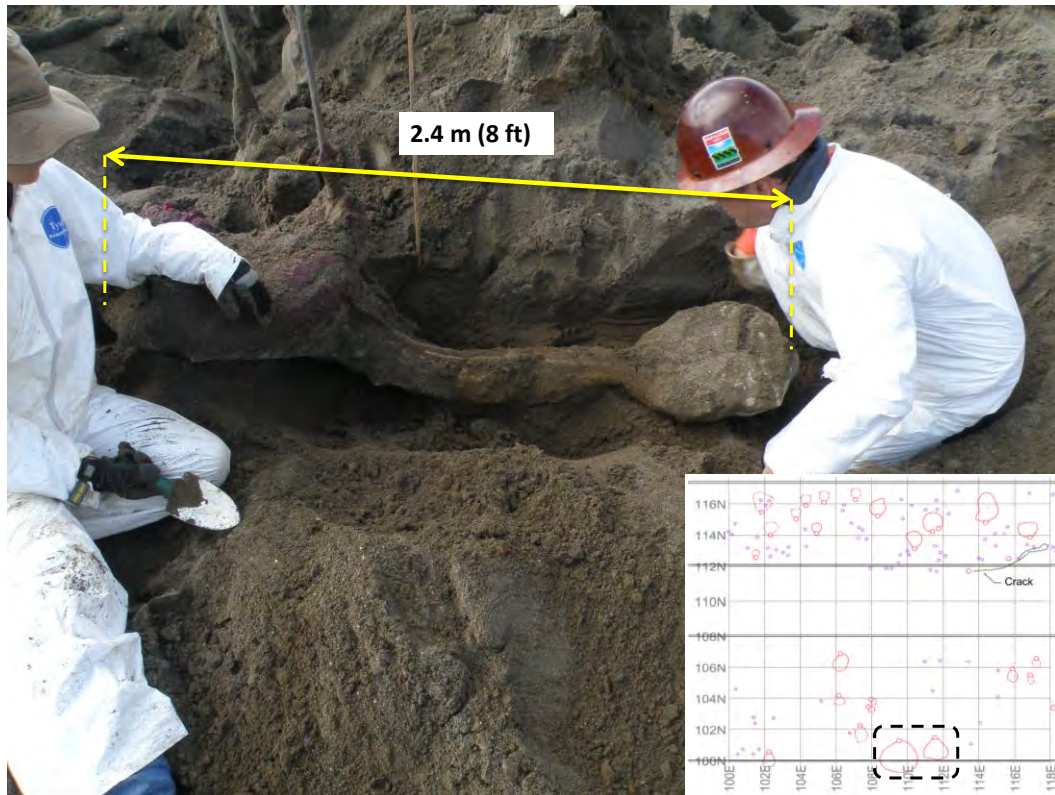


Figure 5-24. Continuation of waterside burrow into the levee, Sandy Levee Site

The total length of the waterside burrow system was measured to be 5.2 m, and its approximate volume was 0.3 m^3 (10.5 ft^3). Approximately 70% of this volume was comprised of cement-bentonite grout, and the remaining 30% of polyurethane grout. The void left by the new burrow was not considered in these volume estimates.



Figure 5-25. Close up of den (grout mass) near waterside toe, Sandy Levee Site. The wooden stake points to a short burrow below the den

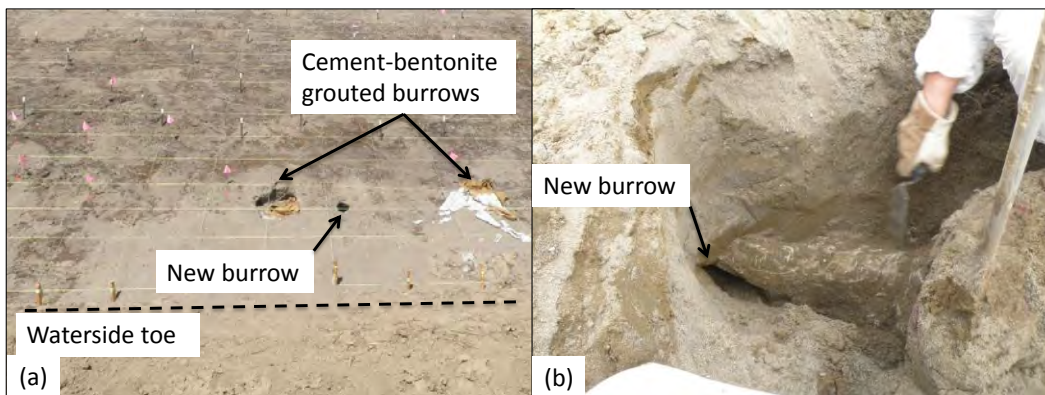


Figure 5-26. New hole after cement-bentonite grout on waterside toe, Sandy Levee Site. (a) shows the location of the new burrow and (b) shows the partially excavated open burrow below the cement-grouted main tunnel

LANDSIDE BURROW SYSTEM

The burrow systems encountered on the landside were longer and much more complex than the linear feature found near the waterside toe. A multi-level complex was observed from

approximately one meter below the landside edge of the crown of the levee near the eastern end of the test site, and extended west for approximately ten meters parallel to the levee alignment. This complex connected all the large active burrows grouted using cement-bentonite and was measured to be 56.4 meters (178 ft) in total length and approximately 1.1 m³ (38.8 ft³) in volume. 75% of the estimated volume corresponded to cement-bentonite grout and the remaining 25% to polyurethane grout.

Several smaller burrows were observed away from the main complex, one near the levee toe, extending for approximately two meters parallel to the levee alignment, and a second burrow west of the edge of the complex. Both of these burrows were entirely grouted with polyurethane, and the latter might have been part of the main burrow complex at some point.

Figure 5-27 shows a view from the top of the eastern edge of the main burrow complex, which consisted of a series of intertwined tunnels ranging from five to fifteen centimeters in diameter occupying an area of approximately 2.5 meters (8.2 ft) in the direction parallel to the slope (left to right of photo) and 1.7 meters (5.5 ft) in the normal direction. This area contains the largest volume of grout in the study and coincides with cement-bentonite injection point number 4 in Table 5-1, which took approximately 25 minutes to fill.

The colored grout on Figure 5-27 indicates a large portion of the complex was filled with cement-bentonite grout (green color), and several large pieces were filled by the polyurethane grout (pink color). Several additional polyurethane injection ports were installed in this area with the objective of effectively filling all voids; however, some of these ports were inadvertently pushed through the already hardened cement-bentonite grout, causing it to break and allowing polyurethane to flow through the cracks and generate a mixed grout area, colored with orange spray paint (right edge of burrow complex).

The burrow complex extended upstream (top of Figure 5-28) and divided into two main tunnels of approximately 15 centimeters (0.5 ft) in diameter; the alignment of these tunnels dipped down approximately 50 centimeters (1.6 ft) and converged into a single tunnel that sharply increased in elevation at the end of the burrow system. Figure 5-29 shows a lateral view of the landside burrow complex at the end of the excavation activities, at which point the main intertwined portion (Figure 5-27) had been removed to expose deeper portions of the system.

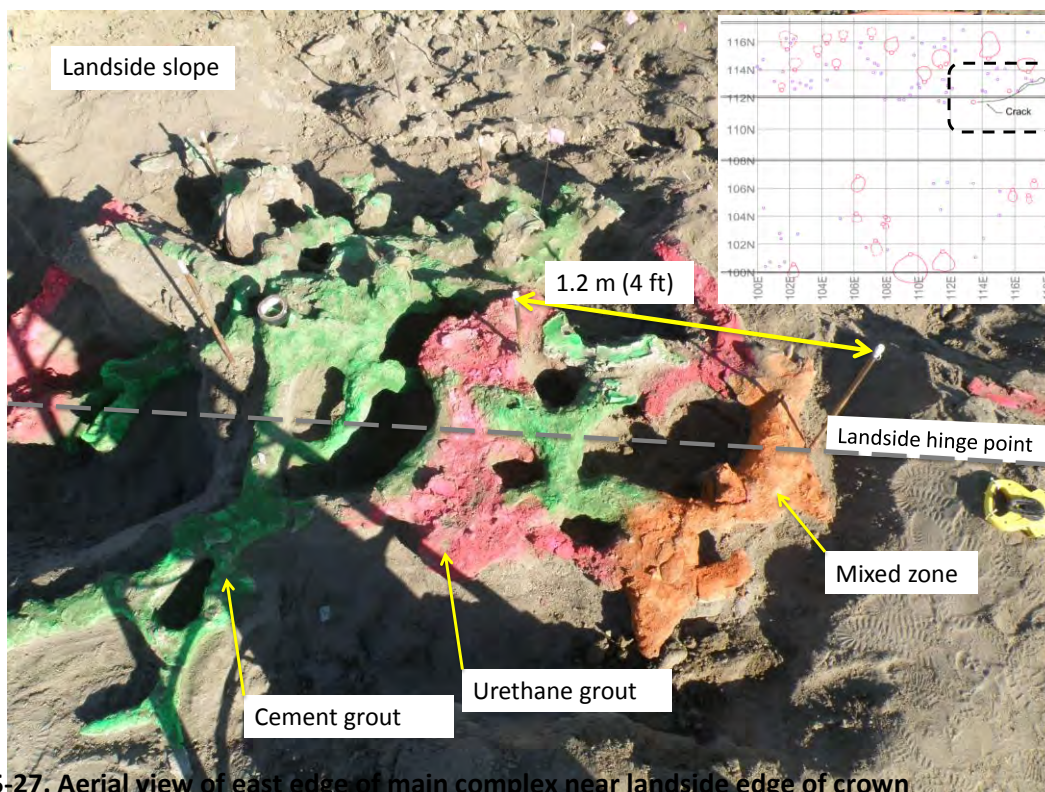


Figure 5-27. Aerial view of east edge of main complex near landside edge of crown

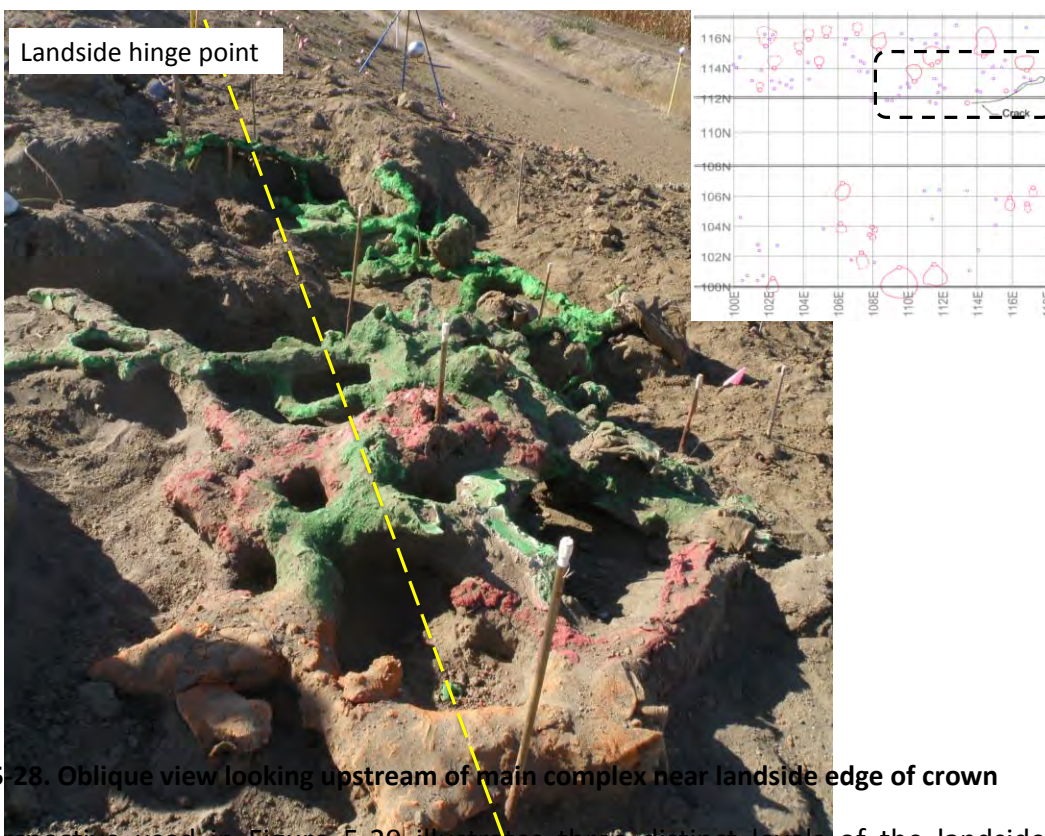


Figure 5-28. Oblique view looking upstream of main complex near landside edge of crown

The perspective used in Figure 5-29 illustrates three distinct levels of the landside burrow system: (1) the shallowest portion of the complex coincides with the very dense and

intertwined zone previously described, which connected all the cement-bentonite grout injection points; (2) a deeper level, where the system of burrows is composed by two main tunnels, and (3) a single tunnel that sharply rises to an elevation similar to level 1. An isolated burrow grouted exclusively with polyurethane was observed near the landside toe (bottom of Figure 5-29); approximately 1.5 meters (4.9 ft) below level 2 of the main complex and extended 2 meters (6.6 ft) parallel to the levee alignment, with a sharp turn towards the interior of the levee.

T-LiDAR data collected by USGS was processed using the program IMVIEW, allowing the differentiation of the different types of grout and consequently estimating lengths and volumes. For estimation of grout volumes, individual burrow segments were exported as point clouds to AutoCAD, and a three-dimensional surface was fitted along the points on the surface of the burrow. Figure 5-30 shows a cross sectional view of the T-LiDAR data, with the waterside slope to the right of the figure. This image allows visualizing the extension of the landside burrow system from the toe to essentially the centerline of the embankment. Figure 5-31 and Figure 5-32 contain close-ups of the landside and waterside burrow systems, respectively.

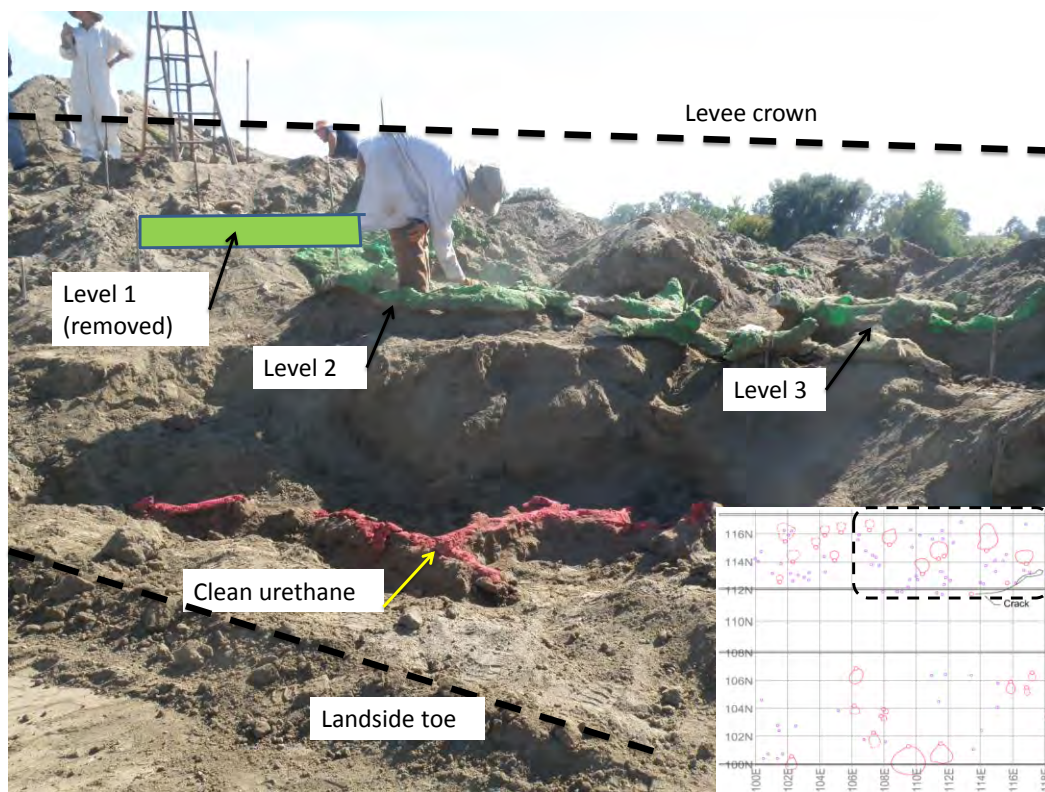


Figure 5-29. Lateral view of landside levee slope burrow system

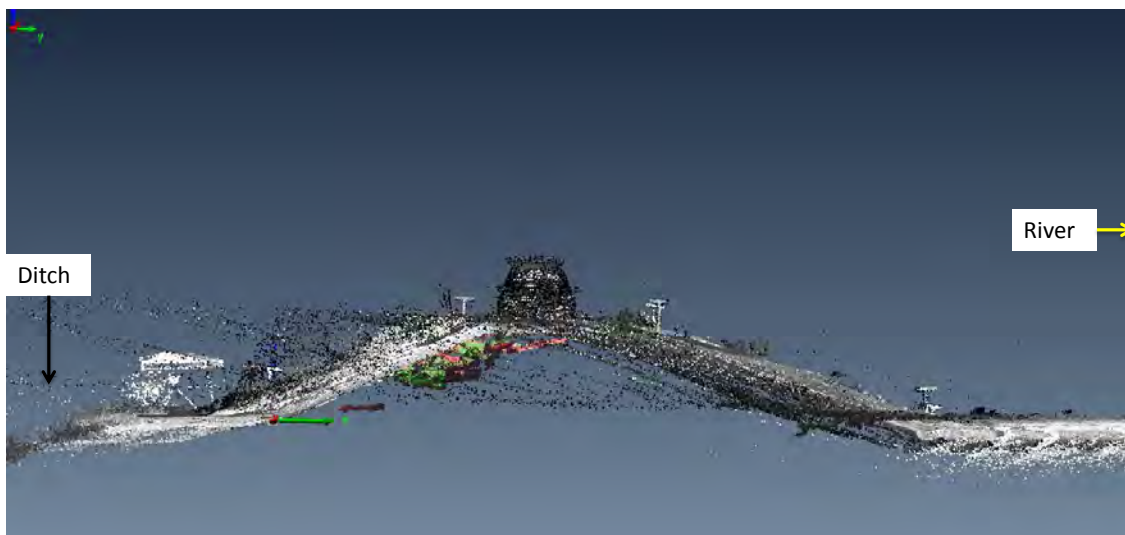


Figure 5-30. Cross section showing LiDAR data on Sandy Levee Site

The figures below illustrate how intricate and large burrow systems can become if no grouting (or void filling) or species control is performed on a levee. The surveyed burrows extend for several meters in all directions. Even though a burrow extending from one side of the levee to the other was not encountered, the potential for wetting front penetration and rapid saturation is clear given the large volume of voids generated within the embankment.

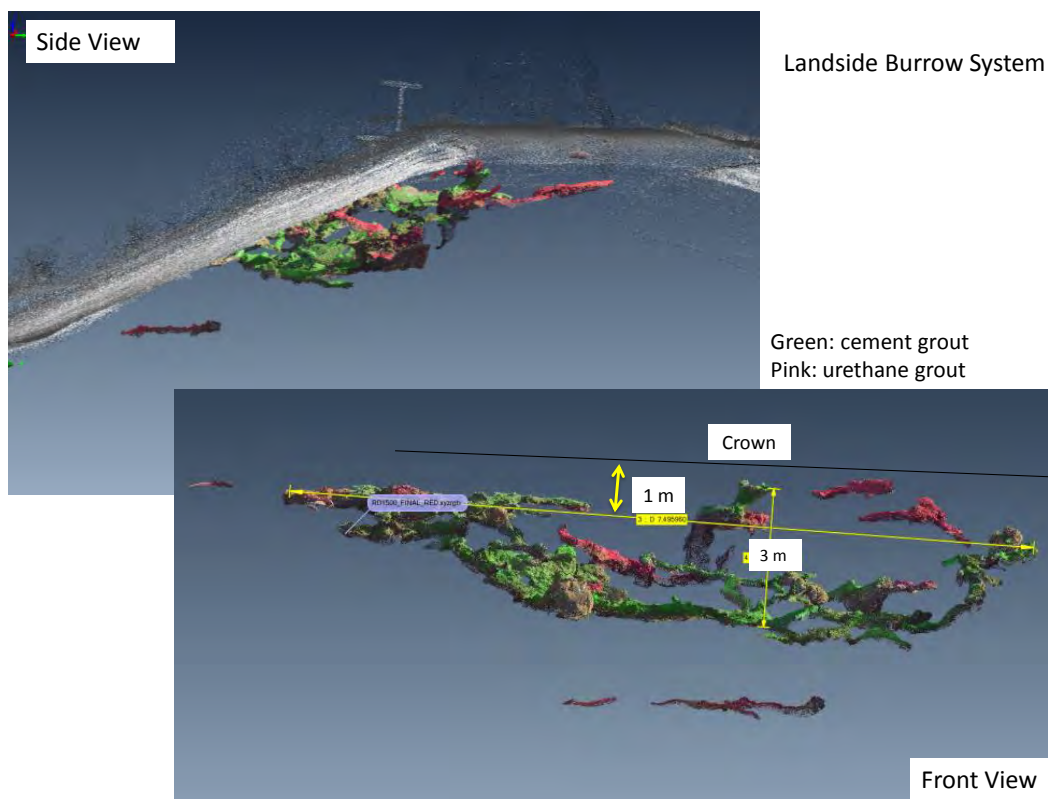


Figure 5-31. Close-up of landside burrow system (a) shows a cross section view, (b) a front view [1 m: 3.28 ft]

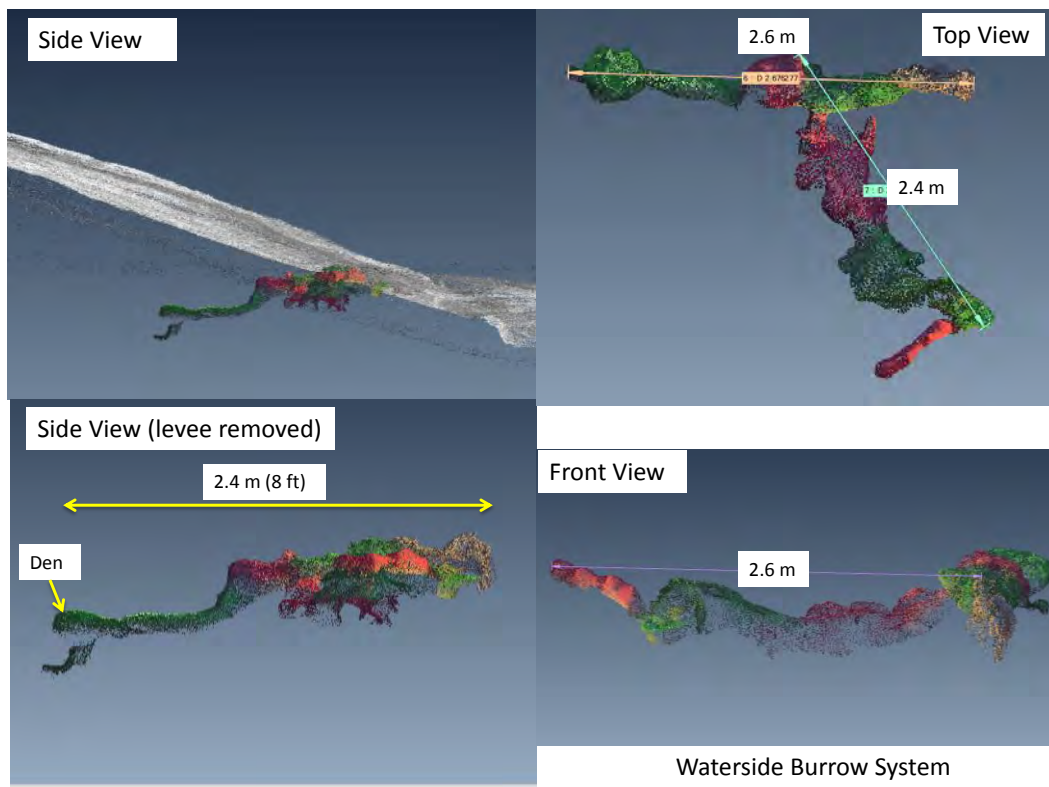


Figure 5-32. Views of the waterside burrow system [1 m: 3.28 ft]

5.4.2 SITE 2: CLAYEY LEVEE, CACHE CREEK

LANDSIDE BURROW SYSTEM

The burrow system encountered on the landside slope was similar to that observed at the sandy levee site, with intricate and interconnected multi-level systems created by squirrels and gophers. Most of the burrows coincided with a strip of grass (Figure 5-22) that is not mowed by the adjacent land owner, making it a food source for the gophers. Squirrels, on the other hand, created larger burrows (10-15 cm in diameter) extending landward from the strip of grass toward the levee toes.

The majority of the burrows were found approximately 0.5 to 1.0 meters (1.6 to 3.3 ft) below the surface of the slope and crown, and only a few isolated burrows extended landward into the toe area, as shown on the right hand side of Figure 5-33. A single burrow was encountered extending from the waterside toward the landside slope (Figure 5-34 and Figure 5-35), approximately one meter below the elevation of the crown. This burrow was approximately 12 to 15 cm in diameter, and was grouted during a previous maintenance campaign with cement-bentonite grout. The grout was observed broken up and relatively easily friable, suggesting that the grout filling this hole belongs to early practices, when DWR used a higher percentage of

bentonite (about 10%), which made the mix more friable upon drying. The location of this penetrating burrow on Figure 5-34 coincides with one of the flood fight sites from 1998.

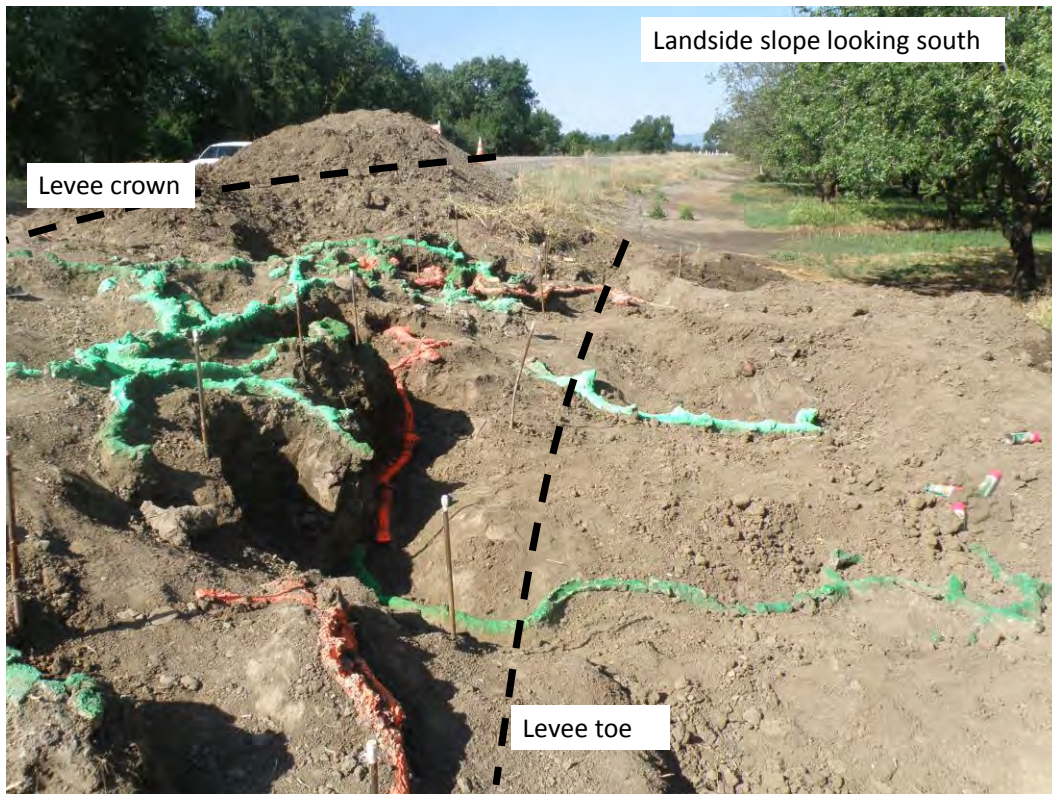


Figure 5-33. View of excavated landside slope at Clayey Site

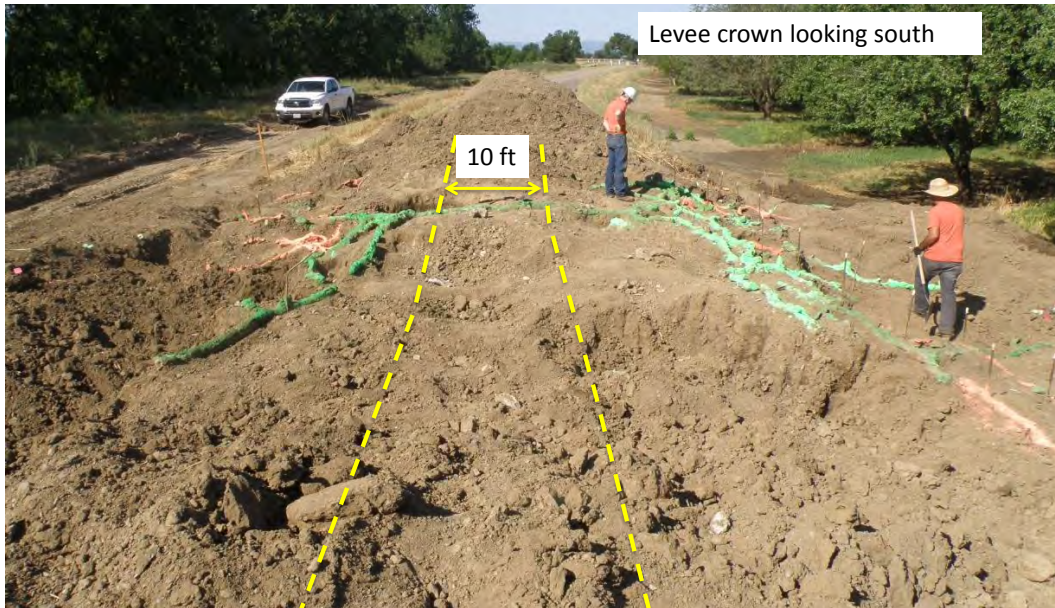


Figure 5



Figure 5-35. View looking north of completely penetrating burrow

WATERSIDE SYSTEM

The waterside levee burrow system (Figure 5-36) was not as extensive as the landside and was comprised of a few isolated burrows, mostly filled with polyurethane grout. This trend is consistent with the observations from the sandy levee, where the majority of the burrows were encountered on the landside levee slope, which coincides with the slope nearest to the food source.

The waterside 'edge' of the completely penetrating burrow was encountered approximately 1 to 1.2 m (3.3 to 4 ft) below the levee crown, and connected to a series of short burrows also filled with cement-bentonite grout.

5.5 SIGNIFICANCE OF THE COMPLETELY PENETRATING BURROW

Numerical simulations are employed in the following chapter to assess the influence of animal burrows on the seepage performance of embankments, from the point of view of wetting front instability and soil piping. Piping, which is considered an important threat to levee safety is highly dependent on three factors: (1) flow through the porous media around the pipe, (2) length and size of the pipe, and (3) particle stability. The fact animal burrowing has the capacity to create completely penetrating burrows eliminates the variable of flow through the porous media, since the full hydraulic heads from the riverside are charging along the entire cavity with minimal energy loss, and piping potential is reduced to a function of flow velocity inside the pipe, which in turn is dependent on the head differential between the water surface on the riverside and the entrance to the pipe. Figure 5-37 and Figure 5-38 show a cross section and plan views of the completely penetrating hole and burrow system. The penetrating burrow was approximately one meter below the top of the levee, almost perpendicular to the levee alignment.



Figure 5

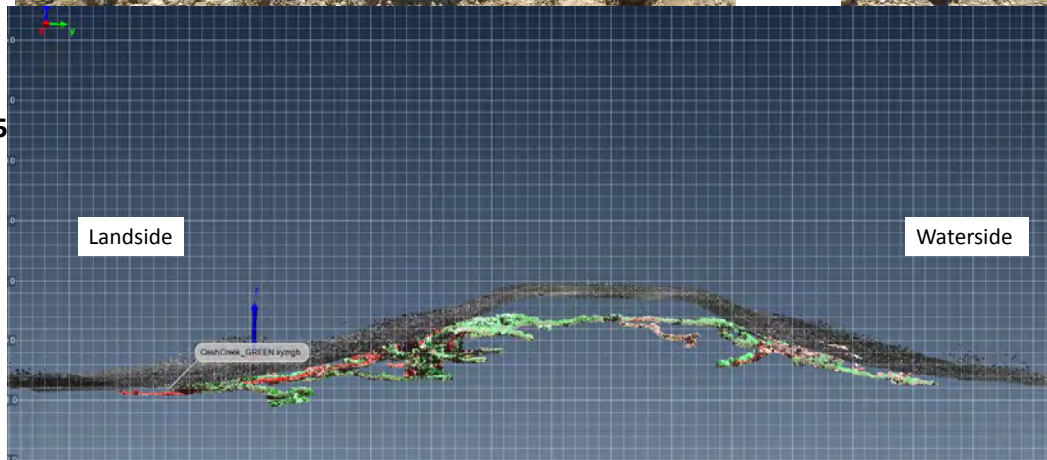


Figure 5-37. Cross section view of completely penetrating burrow at Clayey Levee Site

5.6 SUMMARY OF RESULTS AND OBSERVATIONS

The burrowing activities by the California ground squirrel at the sandy levee site were found to be very strongly correlated to proximity to a food source very near the landside levee toe, as evidenced by the amount of active and inactive burrows on the landside slope as compared to the waterside slope. This was observed not only for the 20 meter (60 ft) long test site, but along the entire stretch of this levee adjacent to a large corn plantation. The number of burrows on this surface was twice the number observed on the waterside slope, and the volume of voids created by the burrowing activities over the years was significantly larger on the landside (1.0 to 0.3 m³).

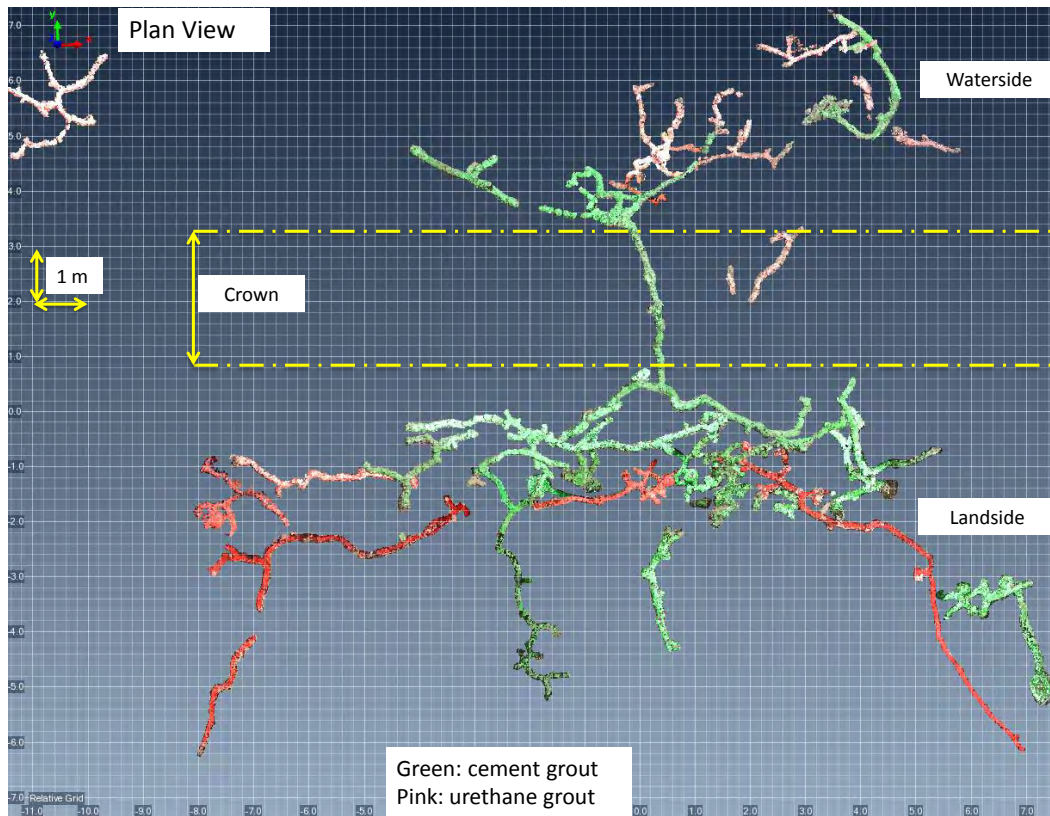


Figure 5-38. Plan view of burrow system at Clayey Levee Site

Layering was also observed to have a strong influence on the amount and extent of burrowing at the site. Figure 5-39 shows two instances where the burrows follow an interface between a stiff fine-grained or cemented sand layer overlying the loose sand material composing most of the embankment, most likely because the animals prefer to dig through the loose materials, while at the same time having a stiff and stable roof. This was the case for most of the burrows observed at the site as well as other sandy levees. Similarly, Harder et al (2012) investigated root penetrations into a slurry wall and found a squirrel burrow penetrating the slurry wall from the crown of the levee and extending several feet below the crown along the interface of the slurry wall and surrounding sandy embankment.

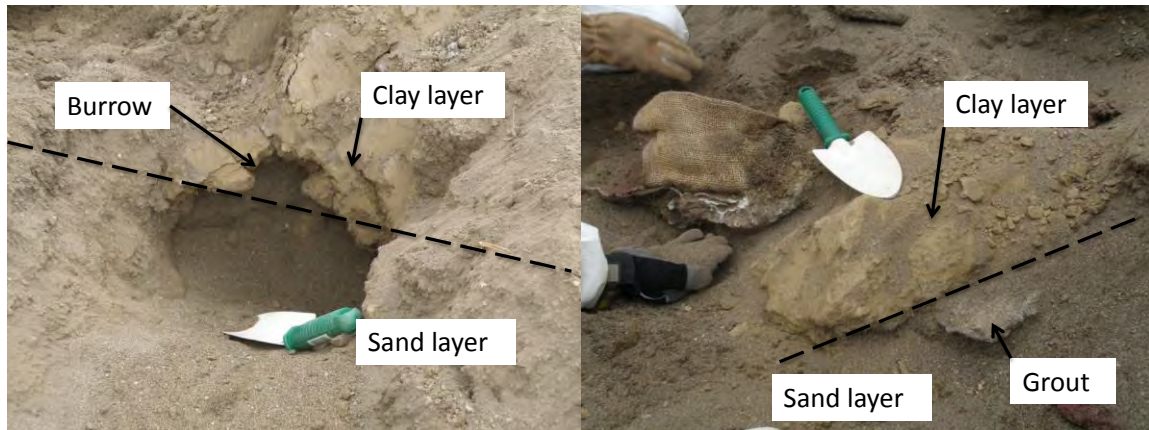


Figure 5-39. Layer interface facilitating burrowing at Sandy Levee Site

Another key observation is the persistence of burrowing activities, as shown on Figure 5-26, a new burrow was dug between the two large burrows near the waterside toe after the cement-bentonite grout was injected, and followed the alignment of the grouted burrow. Furthermore, during a field visit several months after the test was completed and the levee had been rebuilt, new burrows were observed within the repaired levee section (Figure 5-40) and on the landside berm.

Despite the relatively large amount of cement-bentonite and polyurethane grout injected into the embankments, several ungrouted burrows were encountered during excavation of both sites, especially at the sandy levee site, which, as discussed earlier, does not have a regular grouting program in place by the reclamation district. Figure 5-41 shows two ungrouted burrows encountered during excavation. These once again coincided with the interface between a stiff fine-grained layer and the sandy embankment (Figure 5-41a) and the contact between the compacted road base and underlying levee material (Figure 5-41b).



Figure 5-40. New burrows on landside slope of reconstructed Sandy Levee Site



Figure 5-41 UngROUTED burrows on Sandy Levee Site. (a) shows a burrow near Level 1 of the large landside burrow complex, and (b) is an ungrouted burrow to the west of the same complex

Similar conclusions can be drawn from the observations at the clayey levee site. The main difference between the two sites was that this site had a history of piping and, therefore, is regularly grouted. However, despite these efforts approximately 20% of the holes created by burrowing mammals had not been grouted. The percentages of cement to polyurethane grouts were similar to the sandy site (80 to 20%), yet the volume was slightly smaller given that the levee prism was also smaller.

5.7 EFFECTIVENESS OF CEMENT-BENTONITE GROUT

The effectiveness of current DWR grouting practices was studied by quantifying the volume of grouted burrows using this technique, and comparing it to the total volume of burrows documented in the field program. The estimates are given below (Table 5-4) differentiating the two test sites.

Table 5-4. Summary of grout volumes

	STUDY SITE	
	Sandy Levee	Clayey Levee
Cement-Bentonite Grout, m ³	1.02	0.96
Urethane Grout, m ³	0.37	0.21
Total Volume, m ³	1.39	1.17
% Cement-Bentonite	74%	82%
% Urethane	26%	18%
% of Levee Soil Removed by Burrowing Activity ¹	0.24%	0.31%

¹Calculated as percentage of the total volume of levee soil in the test section [1 m³: 35.3 ft³]

Current DWR grouting practices were successful in filling between 70 and 80% of the existing burrows in the two test sites. While the two sites were widely different in terms of levee material and maintenance practices, there are similarities that point to how effective the cement-bentonite grout methodology is, as well as some of its shortcomings.

Most of the large, open burrows were effectively grouted with cement-bentonite and most of these burrows appear to be connected forming large complex burrow systems, making complete filling of these systems a difficult task due to the viscosity of the fluid. Several instances of partially filled holes with voids within the hardened grout were observed in both sites. Moreover, maintenance crews limit grouting efforts to large (10 cm diameter or larger) open burrows, leaving potentially large holes ungrouted if their entrances collapsed prior to grouting.

The total volume of cement-bentonite grout was 8% larger for the site with regular maintenance, which at first glance may not appear to be a significant difference to warrant yearly grouting. However, the data on Figure 5-17 suggests that through the implementation of a regular, ongoing grouting program the amount of cement bentonite grout needed to fill burrows decreases over time, which would correspond to reduced maintenance effort and reductions in yearly materials and manpower costs over time.

An important unknown is the long-term performance and effects of grouting on seepage and stability of a levee. After decades of injecting grout into levees, the conditions of the embankments will surely change as the levee material is replaced by grout.

5.8 CONCLUDING REMARKS

Large burrow complexes were encountered at both test sites extending for several tens of meters on both landslide and waterside slopes. Location and extent of the burrow networks were dominated by the presence of interface between loose and stiff layers where a stiff layer formed a stable roof while an underlying loose sandy material contributed to easy digging. Similarly, burrow systems were found to be concentrated closest to an available food source. The majority of exposed burrows were grouted by the cement-bentonite mix and a small number of burrows were filled exclusively with the chemical grout, likely because no surface expression of the burrow was present at the time of grouting. One completely penetrating burrow was encountered on the second field test, extending from the waterside to the landside slope at approximately mid-slope elevation. The volume of burrows measured during the field tests accounts for approximately 0.3% of the total volume of the tested levee segment, with the majority of this volume grouted by the conventional cement-bentonite grout.

Overall, current cement-bentonite injection practices prove a useful tool in grouting most of the large active burrows on a levee, as long as regular maintenance is performed. However, there is always a possibility that some holes are missed and that these holes may completely penetrate a levee embankment. Thus, grouting activities have to be supplemented by regular patrolling and by maintaining activity databases for best effectiveness.

Chapter 6

ANALYSIS OF THE INFLUENCE OF ROOTS AND BURROWS ON SEEPAGE THROUGH LEVEES

6.1 INTRODUCTION

The influence of the woody vegetation on seepage through levees was evaluated by performing a series of transient seepage analyses using data obtained from the field seepage tests performed as a part of the California Levee Vegetation Research Program (CLVRP) on two different levee segments by Shriro et al. (2014a, b) and Cobos et al (2014a, b). A separate series of analyses was carried out to assess the influence of burrows on seepage through levees using the data obtained from the field mapping of burrows also performed as a part of the CLVRP effort as described in Chapter 5. The details of the analyses and their results are presented in this chapter.

6.2 CAL EXPO FIELD TEST

The Cal Expo site is located along the north (right bank) levee of the American River in Sacramento (CA). A detailed description of the site and the seepage experiment is presented by Shriro et al. (2014a) and only the aspects pertinent to the seepage analyses are presented herein. The test section consisted of a silty levee, approximately 4.5 m high (16 ft) with landside and waterside slopes of 2:1 (horizontal to vertical). Groundwater level was located several meters below the area subject to the test; therefore, the test focused on the evolution of negative pore pressure values as a wetting front was generated by the test.

The principal objective of the field test was to study the influence of woody vegetation on the seepage patterns through the unsaturated portion of an embankment. Figure 6-1 is a simplified cross section showing the main elements of the test. Parallel trenches were excavated above (near the landside levee crown) and below (near landside levee toe) of a decomposing stump of a eucalyptus tree that was cut down around 1993. An additional set of trenches was excavated

away from the stump to provide control conditions (Figure 6-2). The wetting front test consisted on filling the upper trenches with water, establishing a pressure head condition of 60 to 90 cm (2 to 2.5 ft) and monitoring the progression of the wetting front from the upper to the lower trench using an array of tensiometers and piezometers.

Three lines of instruments (Lines A, B and C on Figure 6-2) were laid out with nests of tensiometers installed in depths ranging from 45 cm to 150 cm and vibrating wire piezometers from 150 to 210 cm, with the objective of covering the shallower soil layers where most of the root mass was located. Figure 6-3 shows a detailed instrumentation layout, with the location and name of each instrument installed at this site. The nomenclature used to name the instrument is as follows: the first letter indicates the type of instrument (T: tensiometer, P: piezometer), the following number indicates the row the instrument was located at (1 through 4 – line 1 was located near the upper trenches, and line 4 just above the lower trenches), the following letter indicates the instrument line (A through C), and the last number indicates the depth of the instrument in inches. Instrument Line A was located through the decomposing stump, Instrument Line B was located approximately 2.5 m left (east) of Line A, and Instrument Line C was located through the control trenches.

Vibrating wire piezometers were installed to measure positive pore pressures in case a saturated condition was achieved in the soil and, therefore, were installed at greater depths than the tensiometers. The piezometers were installed using the grout-in method (E. Mikkelsen personal communication), with the porous stone pointing upward, to avoid rapid draining and desaturation of the porous stone and diaphragm. This procedure allowed measuring of suction values comparable to those recorded by the tensiometers.

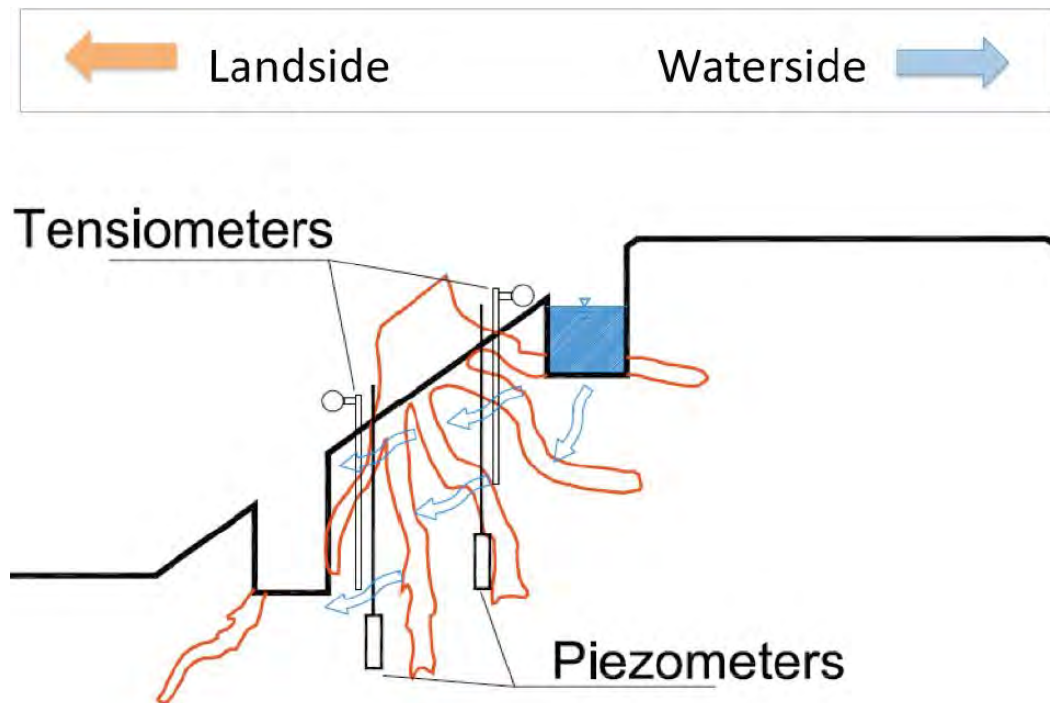


Figure 6-1. Generalized cross section of wetting front test (Shriro et al., 2011)

A mammal burrow was encountered approximately 2.5 meters east (left) of instrument Line A, which was later found to connect upper and lower stump trenches; surficial evidence of burrowing activity was also observed along the test area, as shown by the red circles on Figure 6-3. The existence of these holes proved to be a dominant factor on the wetting front test, as will be described in subsequent sections.

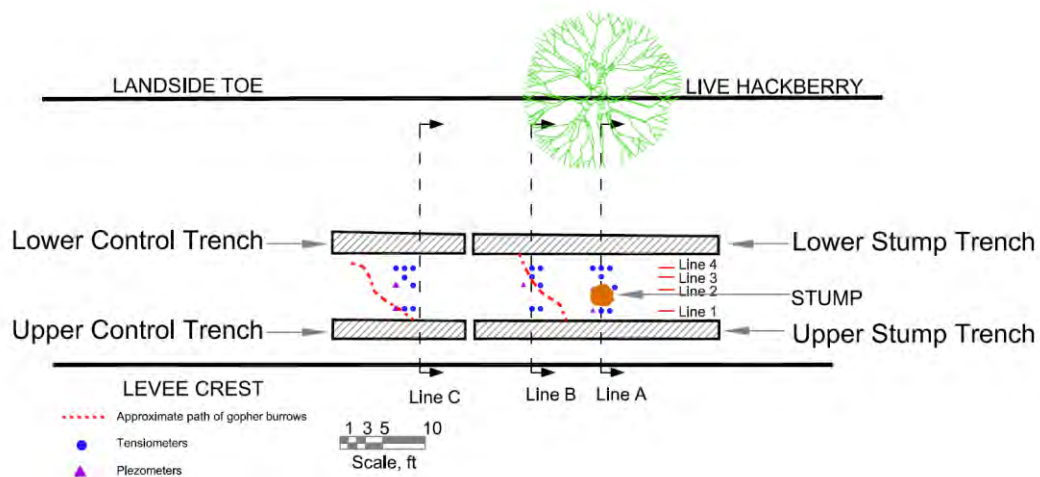


Figure 6-2. Plan view of wetting front test (Cobos et al., 2012) [1 ft: 0.31 m]

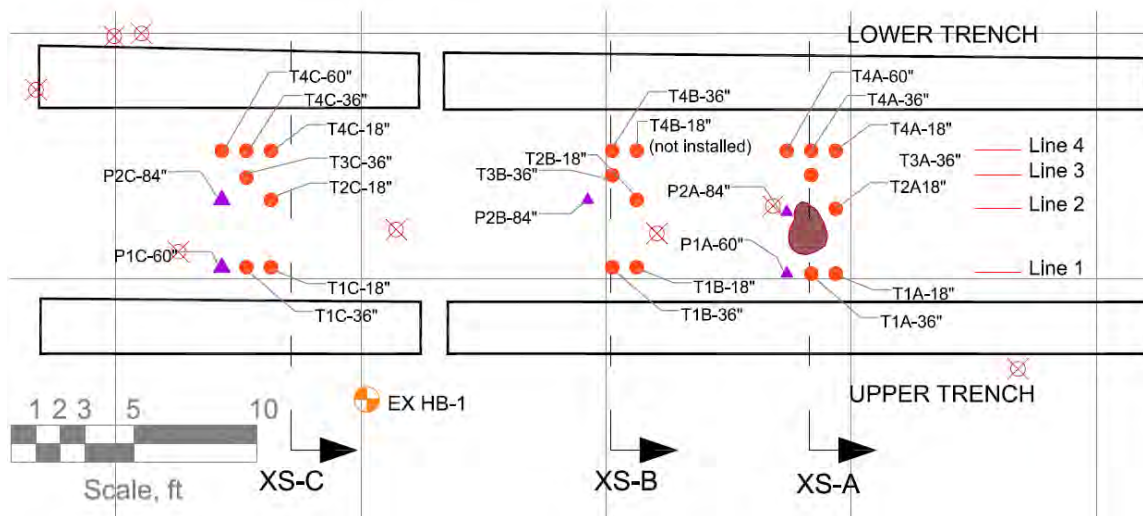


Figure 6-3. Instrument layout of wetting front test. T: tensiometer, P: piezometer, EX: hand augered boring [1 ft: 0.3 m]

6.2.1 SUMMARY OF RECORDED DATA

Suction values from tensiometers were recorded using Campbell Scientific® CR3000 Microloggers, which allowed automatic data collection during the entire test using a collection interval of 30 seconds. Piezometers were monitored using a Geokon® portable readout device every two to five minutes; therefore, the amount of data collected for each piezometer was significantly less than the tensiometers.

The electronic pressure transducers used to measure suction values on the Soil Moisture Equipment® tensiometers were calibrated after the test was completed in the laboratory. Calibration consisted of inserting each tensiometer/transducer assembly as it was used in the field (with the same cable lengths and splices) into a jar filled with loose, moist Monterey Sand, and applying controlled values of suction through the top of the tensiometer probe. Voltages recorded in this process were plotted against suction values from the dial pressure gage so a calibration curve was generated for each instrument (Figure 6-4). Applied suction values ranged from a few Kilopascals to approximately the cavitation value for each tensiometer length. Once the maximum value was reached on a tensiometer, the sand specimen was saturated so the voltage and suction values at saturation were determined for each instrument. This 'zero' value is a key calibration parameter as different length tensiometers have different saturation values.

Calibration Sheet - 18" Long Tensiometers

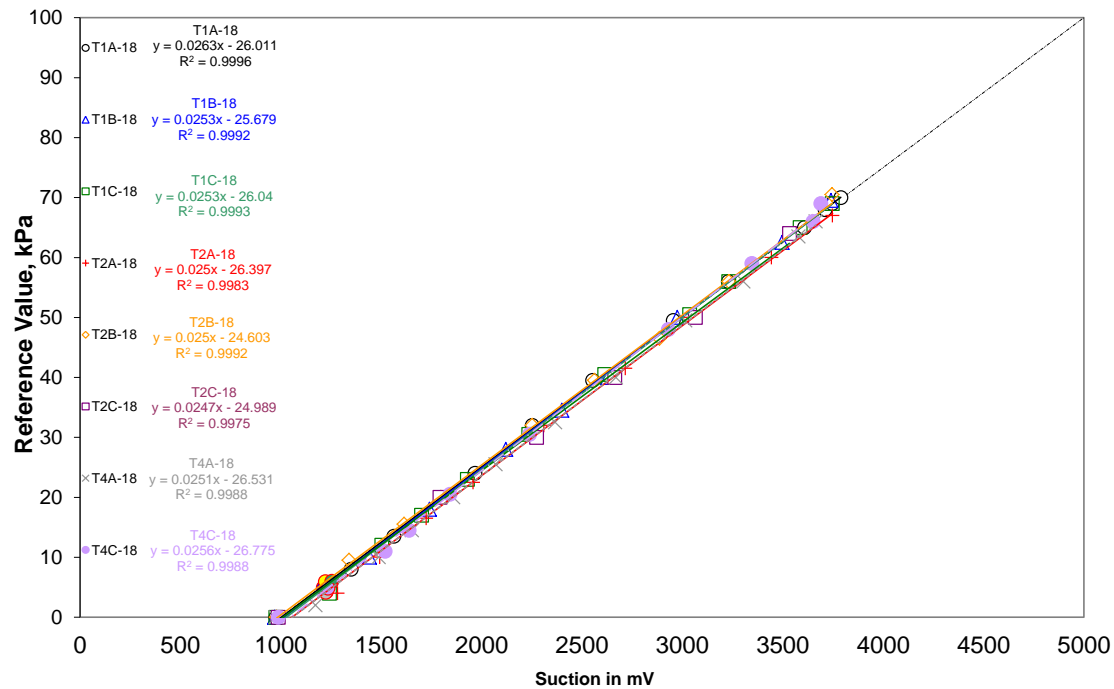


Figure 6-4. Calibration for 18" long tensiometers

Prior to commencing the wetting front test, a 'test run' was performed to assure all devices, power sources and loggers were functioning correctly. Figure 6-5 and Figure 6-6 show the tensiometer data for the test run. Suction values ranged between 30 and 70 kPa during the 40 hours of the test, and temperatures ranged from 60 to 100 degrees Fahrenheit. Sudden drops on recorded data represent times when the tensiometer tube was refilled with water, therefore losing the vacuum inside the tube and gauge throat. During the test run refilling was performed several times given the high suction and temperatures that contributed to the quick emptying of the tensiometers.

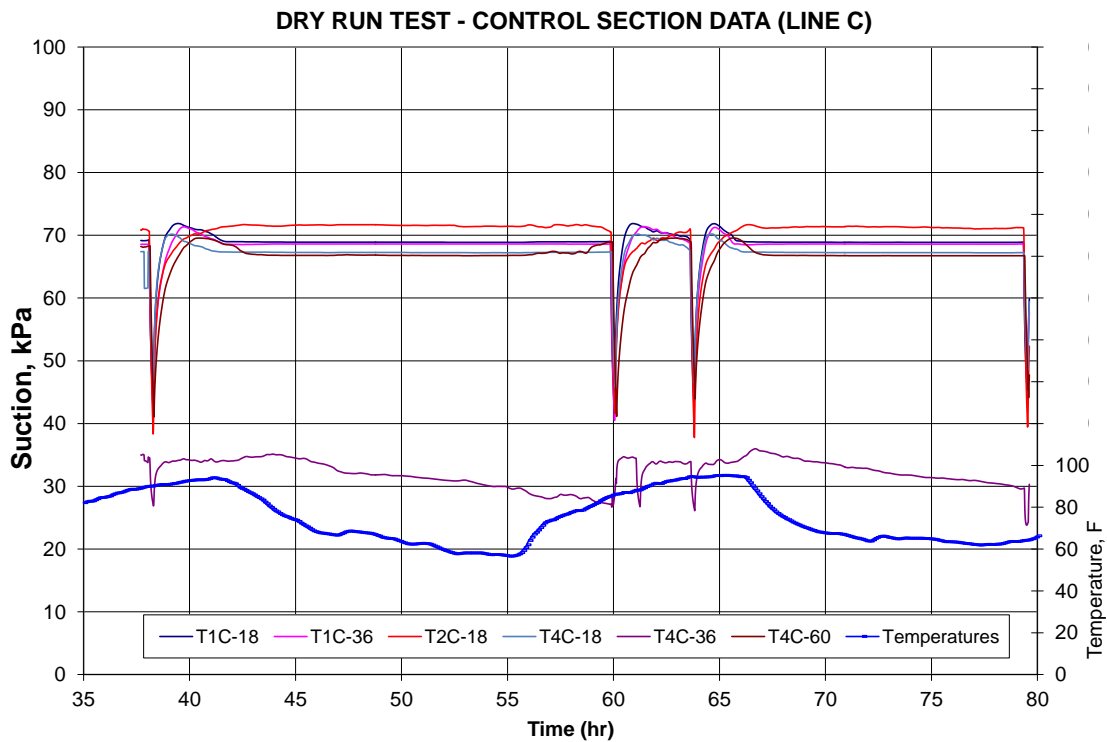


Figure 6-5. Test run data for control trench

The wetting front test started on September 7, 2010 at 10:57 am, some minutes after times were reset to zero and tensiometers were refilled and given enough time to re-equilibrate. Approximately 500 thousand data points were recorded during the test and data reduction required significant smoothing of each tensiometer data series.

Data recorded along each instrument line is shown on the following figures. Each time series contains a relatively flat segment near the start of the test, corresponding to the time prior to the arrival of the wetting front to the ceramic tip. The drop on tension values indicates that the wetting front reached the instrument and, therefore, suction values rapidly decreased to almost zero.

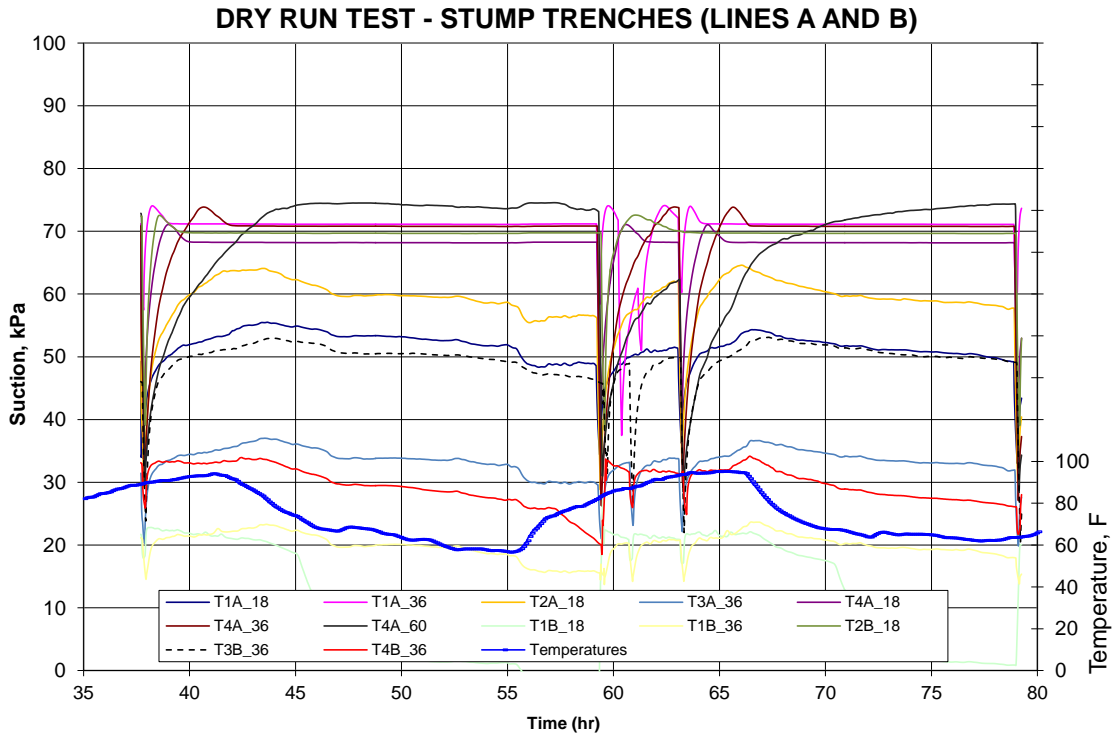


Figure 6-6. Dry run data for stump trench

After all instruments were saturated, the upper trenches were allowed to empty and the soil mass between the two trenches started to slowly drain. This is evidenced by the slight increase in suction after time = 120 hours. Figure 6-7 through Figure 6-9 show the entire suction time histories for Lines C, B and A, respectively.

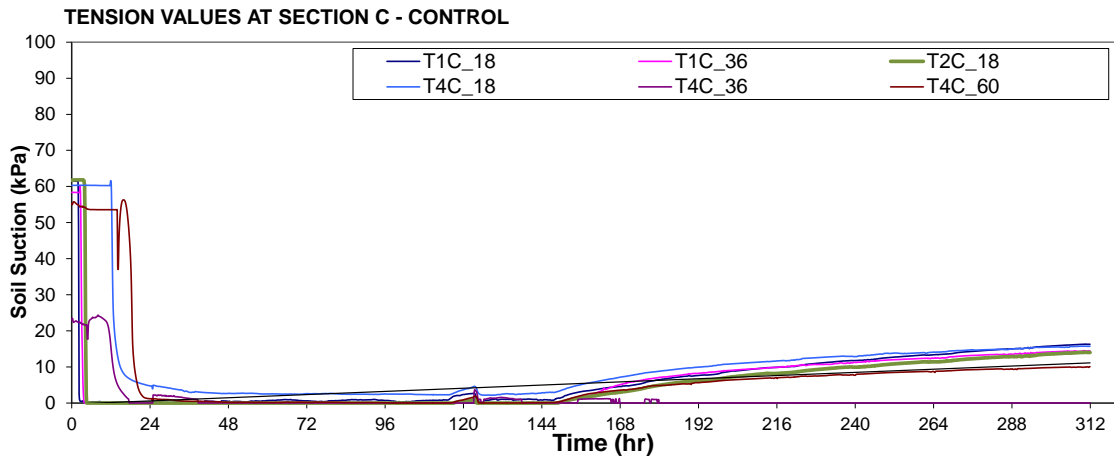


Figure 6-7. Test data for control section (Line C)

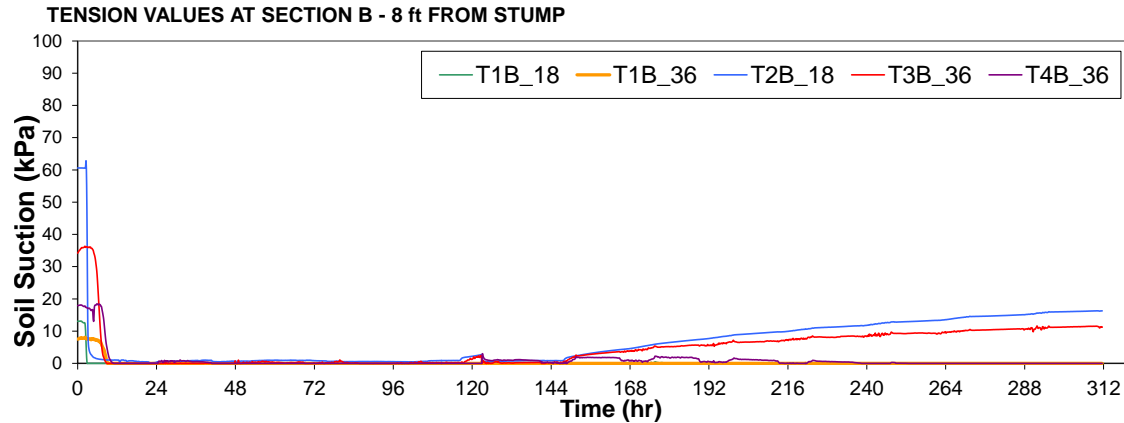


Figure 6-8. Test data for section away from stump (Line B)

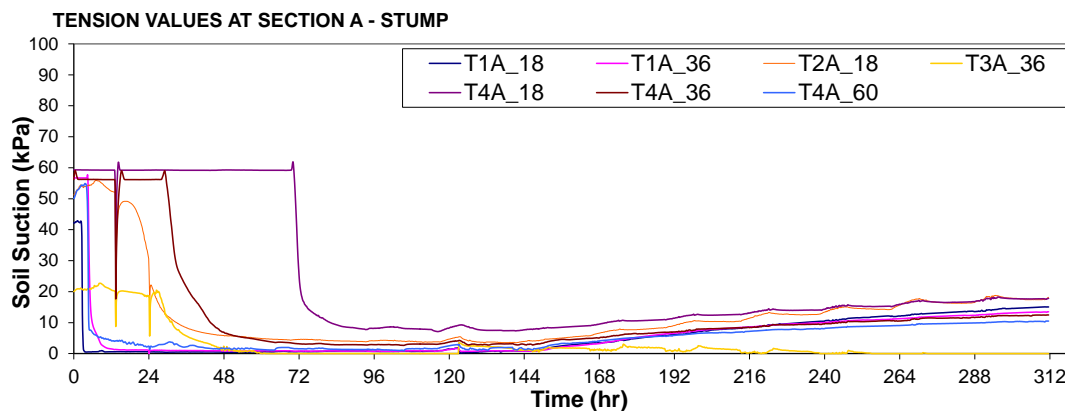


Figure 6-9. Test data for stump section (Line A)

INSTRUMENT LINE B SATURATION

The measured progression of the wetting front was significantly different between the three instrument lines. Instruments on Line B (Figure 6-10) saturated in less than twelve hours, mainly because of the presence of a mammal burrow extending from the upper to the lower trench. This burrow was directly connected to the source of water and was able to transmit the full hydraulic head applied on the upper trench throughout the levee material, causing some surface seeps and small collapses on the lower trench wall within 30 minutes of start of test. The saturation path on this instrument line extended from upper to lower trench and radially out from the continuous burrow. The first instrument to saturate was T1B-18, located 30 cm downslope from the upper trench wall, and 45 cm (18 inches) below slope surface. Suction values on this instrument went to zero approximately two and a half hours after the start of the test. The next instrument to saturate was T2B-18, located approximately 1.2 m (4 ft) downslope from the upper trench wall and 45 cm deep. This instrument saturated in three hours as flow from the pressurized burrow saturated this area.

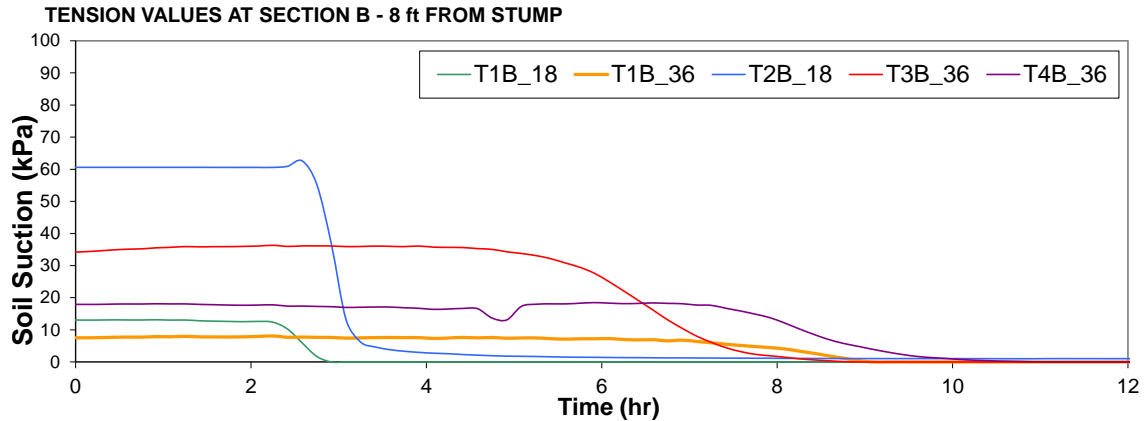


Figure 6-10. Saturation times of Line B

The remaining three instruments saturated between six and ten hours from the start of the test, driven by the fact that the burrow was essentially at the same head as in the upper trench, thus allowing for a faster saturation of the mass of soil between the two trenches.

INSTRUMENT LINE C SATURATION

Instrument Line C (Figure 6-11), located through the control section showed a similar behavior to line B, as a small burrow was encountered extending from the upper trench to approximately halfway between the upper and lower trenches. A small seep was encountered on the lower trench wall a few hours after the test started (Shriro et al, 2013), but did not expel as much water as the burrow on Line B. Saturation times for instruments on this line ranged between two and 22 hours, with the instruments in the vicinity of the small burrow saturating in less than four hours, and the remaining devices achieving saturation between 12 and 22 hours.

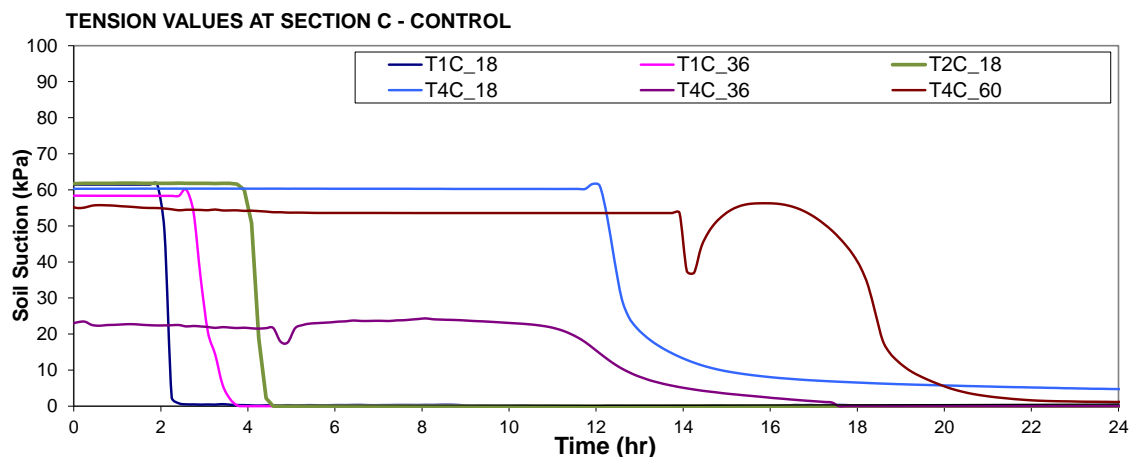


Figure 6-11. Saturation times for Line C

INSTRUMENT LINE A SATURATION

Instruments along Line A (Figure 6-12) exhibited significantly longer times to reach saturation when compared to the other two instrument sections on the field test. Devices near the upper trench (T1A-18 and T1A-36, located 18 and 36 inches deep and approximately 30 cm from the upper trench wall) saturated between two and six hours from the start of the test, while most of the remaining instruments saturated between 30 and 70 hours later. Instrument T4A-60, located 60 inches deep and less than half a meter from the lower trench wall also exhibited a rapid saturation, approximately five and a half hours after the start of the test; this can be explained by capillary saturation from the bottom of the lower trench, which was partially filled by the discharge flowing out of the mammal burrow near instrument Line B, located about 2.5 m east of the stump (on the same trench). The height of the water ponding on the lower trench was controlled using a pump, but 2-4 inches of water were present in the bottom of the trench as the pump was unable to drain it completely. Consequently, instrument T4A-60, which was almost at the same depth as the bottom of the lower stump trench was saturated from the bottom of the experiment section via capillary rise.

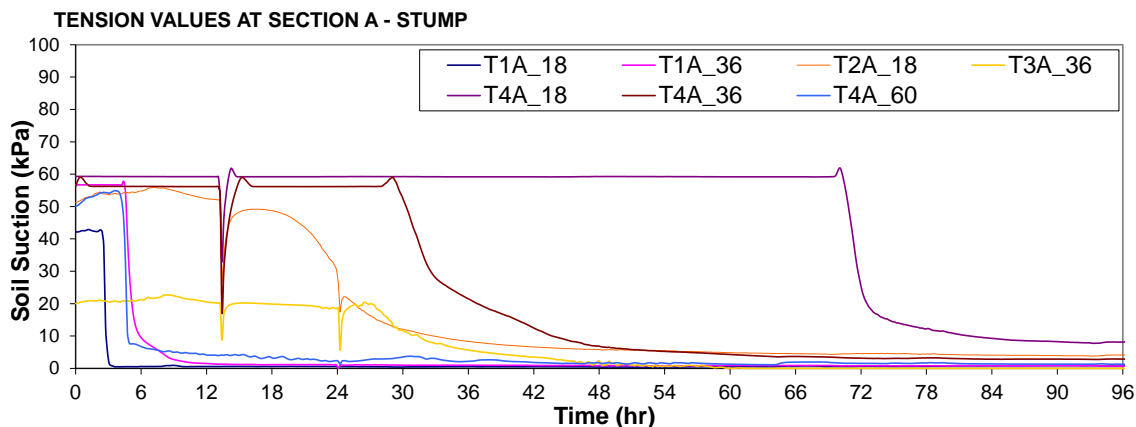


Figure 6-12. Saturation times for Line A

The instruments around and downslope from the stump consisted of lines 2, 3 and 4 (T2A-18, T3A-36, T4A-18 and T4A-36) appeared to reach saturation more than one day later, suggesting that the progression of the wetting front was delayed by the presence of the decomposing stump. Even though some short and isolated gaps between the soil and the decomposed roots were encountered during excavation activities (Shriro et al., 2011), no tensiometer or piezometer recorded increased pore pressures near these features.

6.2.2 EXCAVATION

After the wetting front test was completed and some suction had been recovered as the trenches were allowed to drain, the soil between the stump trenches was excavated with the

objective of exposing the root architecture and logging the different soil layers, root diameters, state of decomposition and presence of animal burrows.

Excavation was performed by removing thin slices between 30 to 60 cm in thickness starting from the lower trench, using a combination of a compressed air-powered wand (air knife) and delicate hand labor around decomposed roots. After a slice was excavated, the new excavation wall was logged using typical geological logging techniques (USBR, 1998), recording the configuration of each layer using a 30 cm square grid and photographic logs. Furthermore, the position and diameter of each root and animal burrow was recorded, and tags were placed next to them so they could later be digitally connected between trenches. The surveying and excavation procedures follow the methodology first presented by Chung et al (2012) and are described in Chapter 5. Following hand and photographic logging, a ground based LiDAR (T-LiDAR) device was employed to generate a three-dimensional model of the excavation wall and exposed root architecture. Reflective targets were placed next to roots and animal holes (Figure 6-13) and metallic paint was used to highlight the different geologic contacts, thus allowing the T-LiDAR to capture these features given the reflectance contrast between the reflective strips, metallic paint and moist soil. More details of the laser surveys and excavation process can be found in Cobos et al (2012).

The final stage of excavation is shown on Figure 6-14, at this point the soil between the trenches and around the stump had been removed and all roots and soil contacts had been logged. The mammal burrow along instrument Line B was grouted using a cement-bentonite mixture so its path would be conserved during excavation activities. This burrow is shown to the right of Figure 6-14, painted bright orange.

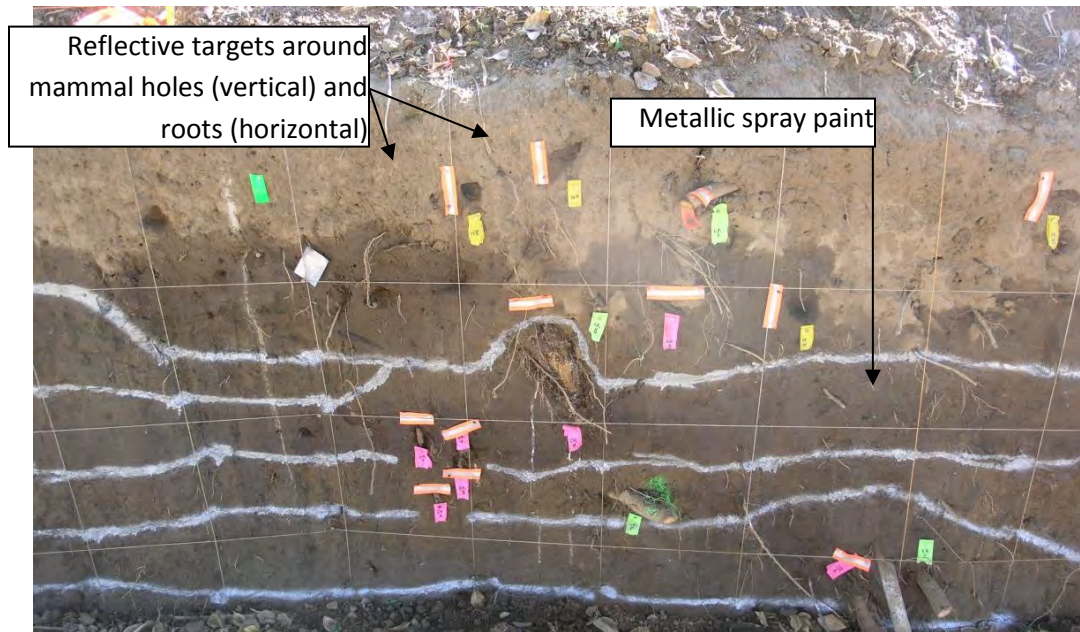


Figure 6-13. Reflective targets around mammal holes and decomposed roots, and metallic paint along stratigraphic contacts. Image modified from Cobos et al (2012).



Figure 6-14. Excavated stump

The results from the baseline T-LiDAR scans are shown on Figure 6-15. Some shadows from fence poles are still present on the dataset, but the four trenches and stump are visible. This dataset was used to generate the topography layer for the analyses presented in following sections. The different scans performed as excavation progressed are included on Figure 6-16. These are unfiltered surfaces created using the entire point cloud for each scan (a scan was comprised of at least five different setups and surveys to minimize shadows), which includes the excavated soil wall, exposed roots and reflective strips and paint. Personnel from the USGS-

Sacramento Western Remote Sensing and Visualization Center and the University of California at Davis Keck Caves used these data sets to isolate the enhanced soil layers and roots in separate files, allowing for relatively easy point cloud management.

Figure 6-17 shows the isolated soil layers as interpreted by the T-LiDAR from the enhanced (metallic-spray painted) geologic contacts in the first and second to last excavated slices. The left hand side of this figure superimposes the scanned root system and the highlighted soil horizons, and the right hand side shows the different layers without the root system. The logged layers appeared to be almost horizontal both parallel and perpendicular to the levee alignment.

Four views of the isolated decomposing stump are shown on Figure 6-18; the bottom view on the upper left corner of the figure is useful to understand the extent in plan view of the decomposed root system. The zone containing most of the root mass and stump is approximately circumscribed by a 2 m diameter circle. The other views in this figure are useful to discern the different geometric characteristics of the root system, including the tap root and the direction of the majority of large roots on this particular tree.

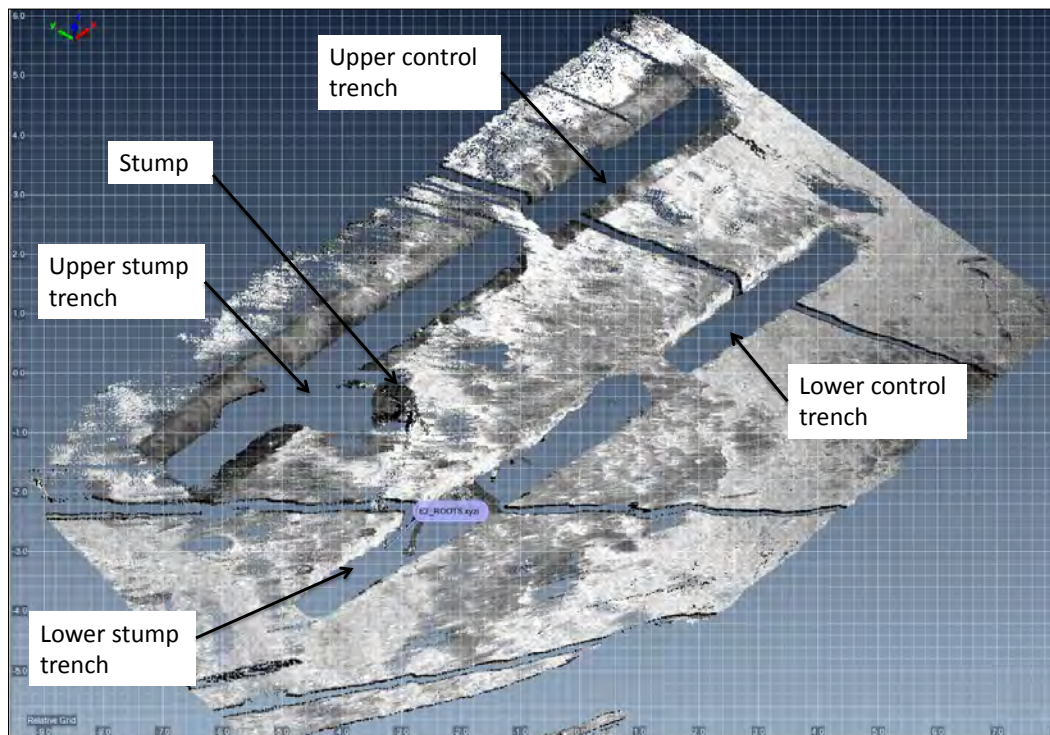


Figure 6-15. Baseline scan

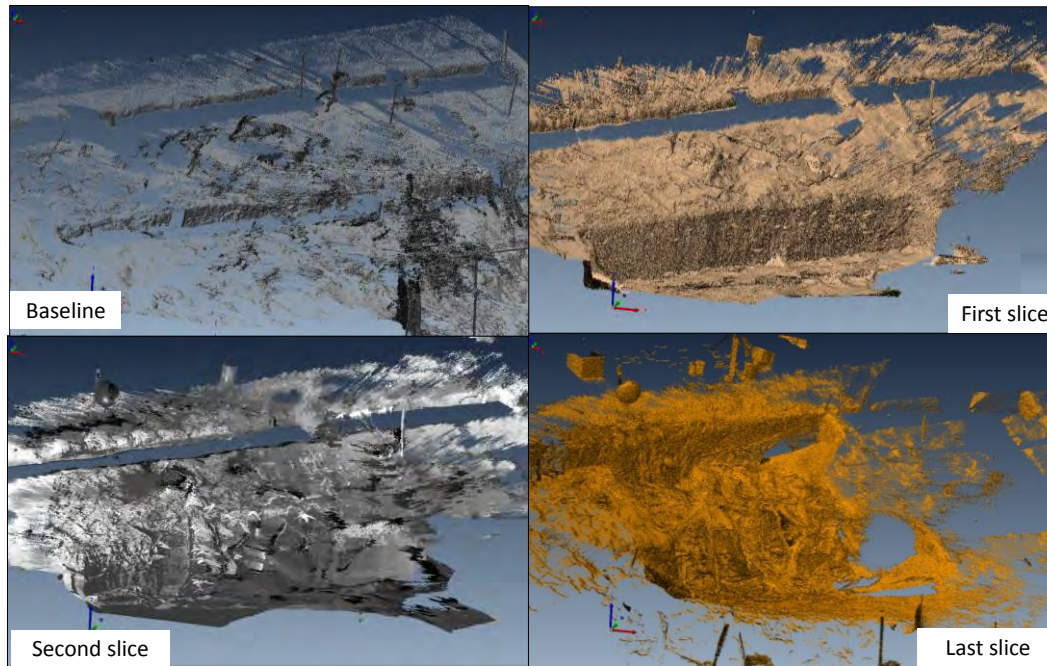


Figure 6-16. Scans of excavation progression

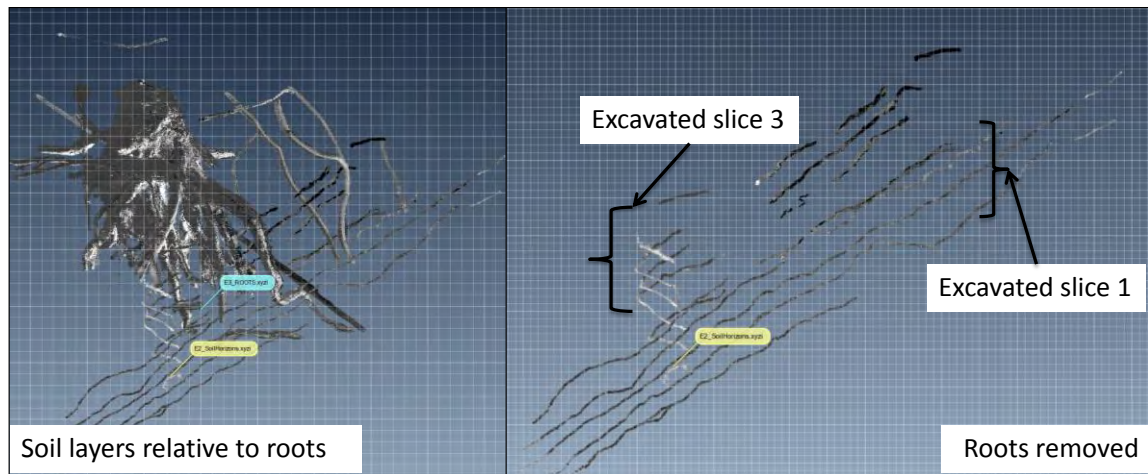


Figure 6-17. Soil horizons highlighted from LiDAR scans

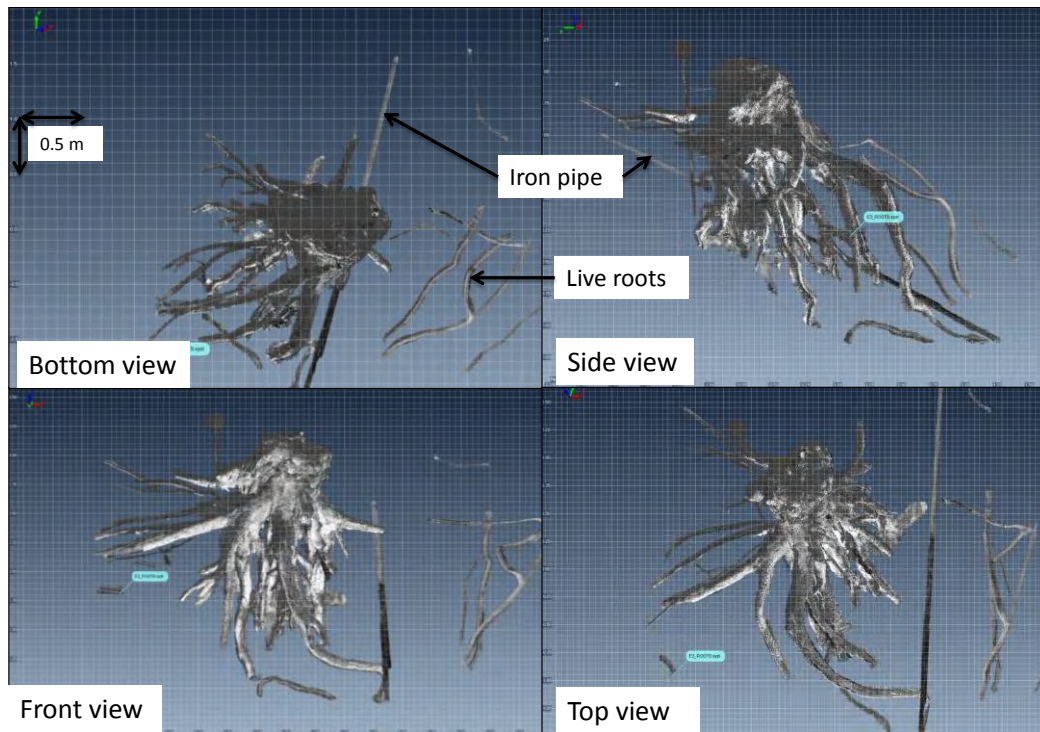


Figure 6-18. 3D views of stump

6.2.3 MODELING THE TREE ROOT SYSTEM

The root architecture was modeled using the point clouds (xyz files) from the T-LiDAR surveys. Gerald Bawden and Sandra Bond from the USGS kindly processed the data collected by the repeated scans, aligned the different datasets and provided a reduced 3D point cloud to be used in the models presented in this section.

The procedure used to generate a 3D representation of the root system was as follows:

- Using the software IMViewer, the root system was isolated and a .xyz file was generated for each root (Figure 6-19).
- The .xyz coordinate file for each root was imported into MatLab, and using a non-linear regression script, a 'best fit' polyline was generated to represent the centerline of each root.
- The different polylines were then imported by AutoCAD and assigned a diameter based on handwritten logs and photographic records.

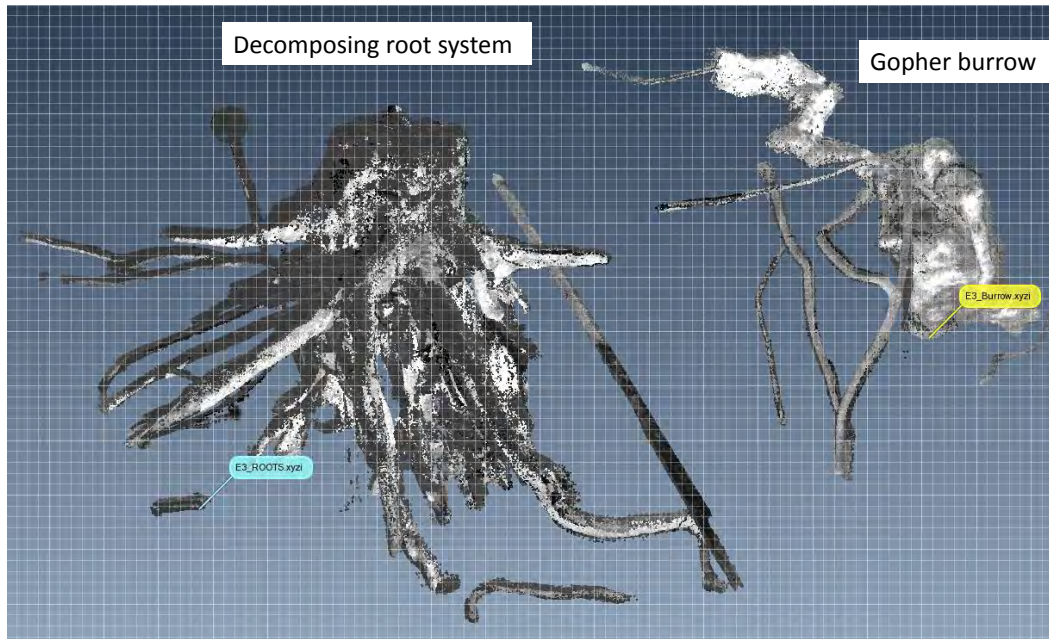


Figure 6-19. Root system point cloud

6.2.4 SOIL LAYERS

Using a similar procedure to that used for the roots, each stratigraphic contact was isolated from the point clouds (Figure 6-20), polylines created for each and imported by AutoCAD. Then a 3D surface was created joining the stratigraphy contacts from each excavated wall, and assumed horizontal outside the scanned areas (Figure 6-21).

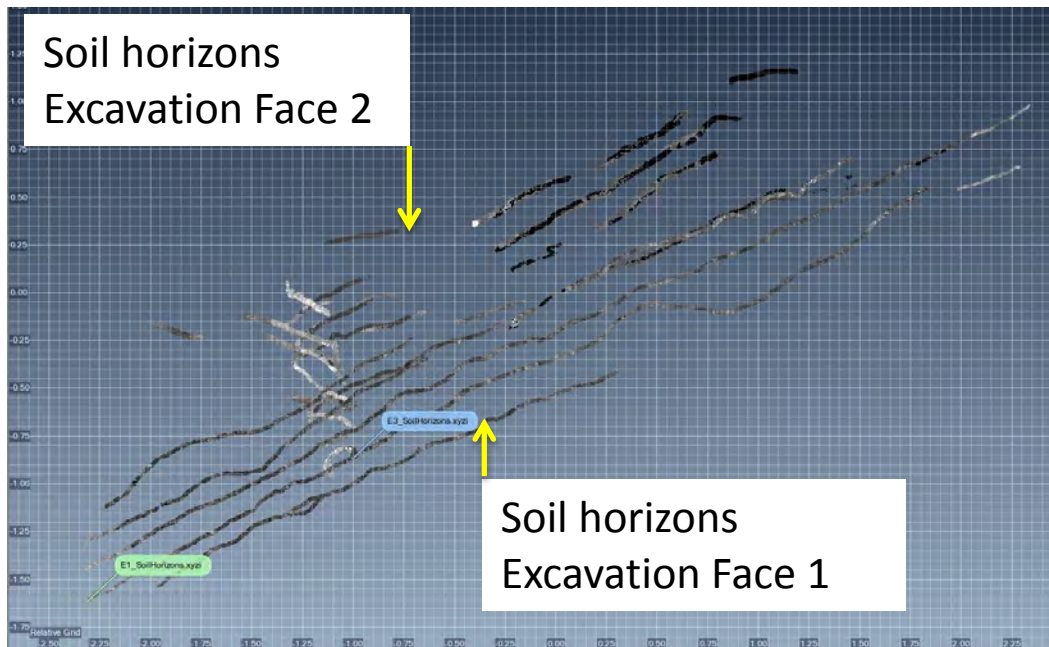


Figure 6-20. Isolated soil horizons

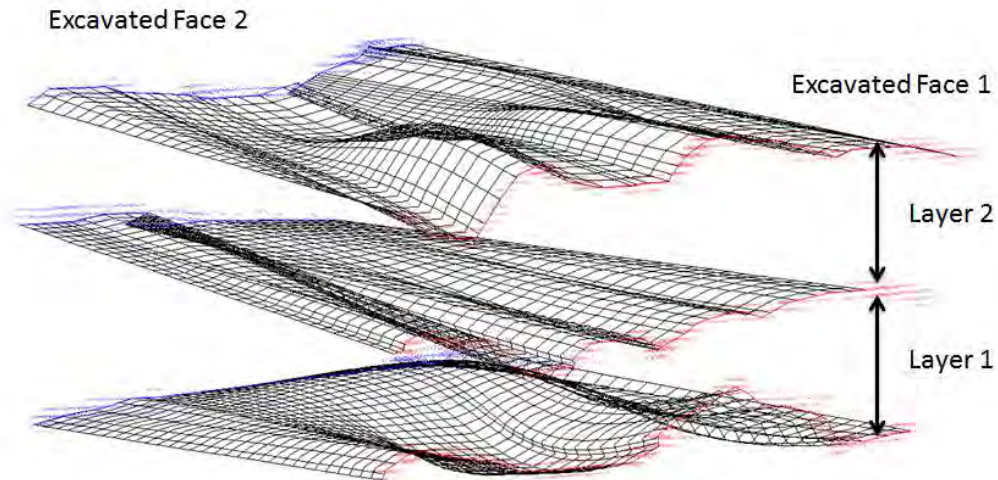


Figure 6-21. Generated stratigraphic contacts

The complexity of the root system and soil layers encountered in this field test proved to be greater than the capacity of the software employed to simulate three-dimensional features, therefore a simplification had to be made in order to model the field test. A cross section of the surveyed stratigraphy and root system next to the simplification used in the software is shown on Figure 6-22.

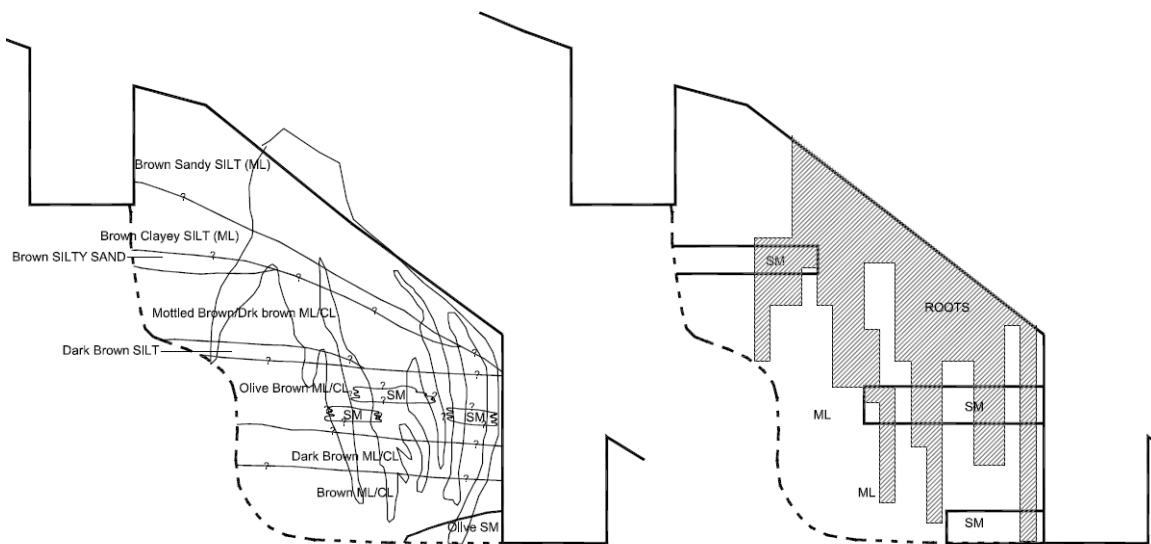


Figure 6-22. Simplified analysis section

6.2.5 SOIL PROPERTIES

Soil properties for the different layers were estimated using a combination of index tests (grain size, Atterberg limits, moisture contents) and matrix suction tests to determine the saturated and unsaturated properties of the profile on the test site.

Index tests were employed to determine soil texture and main type (Figure 6-23), and moisture contents were estimated before the test with the goal of having values of initial moisture contents for use with the unsaturated properties of the soil (Figure 6-24).

Matrix suction tests were performed using a Tempe cell from Soilmoisture Equipment Corp™ to estimate the soil water characteristic curve (SWCC) of each layer (Figure 6-25). Correlation developed by Chapuis (2004) was used to estimate the saturated hydraulic conductivity for each layer. Unsaturated values of hydraulic conductivity and volumetric water content relationships, i.e. the characteristic curves, for each material were estimated using the Van Genuchten (1980) relationship:

$$\theta = \theta_r + \frac{\theta_s - \theta_r}{\left[1 + \left(\frac{\Psi}{a}\right)^n\right]^m} \quad (6.1)$$

where:

θ_s , θ_r = saturated and residual volumetric water contents, respectively

a, n, m = fitting parameters

$n = 1/(1-m)$

Ψ = suction [M/L^2]

and

$$K(\Psi) = K_s \frac{[1 - (a\Psi^{n-1})(1 + (a\Psi^n)^{-m})]^2}{[(1 + a\Psi^n)^{m/2}]^2} \quad (6.2)$$

where:

K_s , K = saturated hydraulic conductivity and conductivity for a given value of suction [L/T]

a, n, m = fitting parameters

$n = 1/(1-m)$

Ψ = suction [M/L^2]

With the saturated hydraulic conductivities are known, the Van Genuchten (1980) (Equation 6.3 and 6.4) uses the volumetric water content (or soil water characteristic curve) function to estimate the parameters a , n and m , as follows:

$$\begin{aligned}
 m &= 1 - \exp(-0.8 S_p) \quad [for \ 0 < S_p < 1] \\
 m &= 1 - \frac{0.5755}{S_p} + \frac{0.1}{S_p^2} + \frac{0.025}{S_p^3} \quad [for \ S_p > 1] \\
 a &= \frac{1}{\Psi} \left(2^{\frac{1}{m}} - 1 \right)^{(1-m)}
 \end{aligned} \tag{6.3}$$

S_p is the slope of the water content function, and is defined as:

$$S_p = \frac{1}{(\Theta_s - \Theta_r)} \left| \frac{d\Theta_p}{d(\log \Psi_p)} \right| \tag{6.4}$$

where:

Θ_s , Θ_r = saturated and residual volumetric water contents, respectively

Θ_p = volumetric water content at the halfway point of the volumetric water content function

Ψ_p = matric suction at Θ_p [M/L²]

Layer compressibility is an important contributing parameter to layer storativity and transmissivity. Internally, the code employed for the modeling calculates transmissivity as the product of hydraulic conductivity and layer thickness. Another parameter used in the transient calculations is the coefficient of compressibility of the aquifer layer (M_v), which can be estimated from consolidation tests for fine grained soils, or correlated from storage coefficients estimated in pump tests. This value was left unchanged from the program default of 1×10^{-5} 1/kPa for all layers in the profile.

Table 6-1 summarizes the properties determined by the different tests and correlations. Gradation analyses performed in fifteen samples from the Cal Expo site are presented in Figure 6-23. Fines content in the soil ranged from 60 to 90% for thirteen of the samples, while two samples exhibited a percentage of fines between 35 and 43. The former represent sandy silt (ML) materials while the latter were classified as silty sand (SM) samples. Matrix suction tests performed to eleven of these samples show a similar pattern, with most of the samples clustered in a saturated volumetric water content between 40 and 50% and a water content ranging between 25 and 35% after applying a suction of 100 kPa, indicating the type of behavior

expected from a sandy silt sample. The remaining samples exhibited a more sand-like characteristic curve, with saturated content between 20 and 25% and 10% when 100 kPa of suction were applied to the sample. The dotted lines accompanying the two clusters of test results were created using the Van Genuchten (1980) relationship, employing the following parameters:

Table 6-1. Soil properties used for flow models

Material	K_{sat} (cm/s)	θ_s^1	θ_r	a (kPa)	n^2	m^2	K_y/K_z
Silt	1×10^{-5}	0.45	0.06	6.0	1.25	0.2	0.25
Sand	1×10^{-5}	0.20	0.08	0.3	3.0	0.67	0.25

¹Volumetric water content, ²coefficients used in the Van Genuchten (1980) equation for characteristic curves.

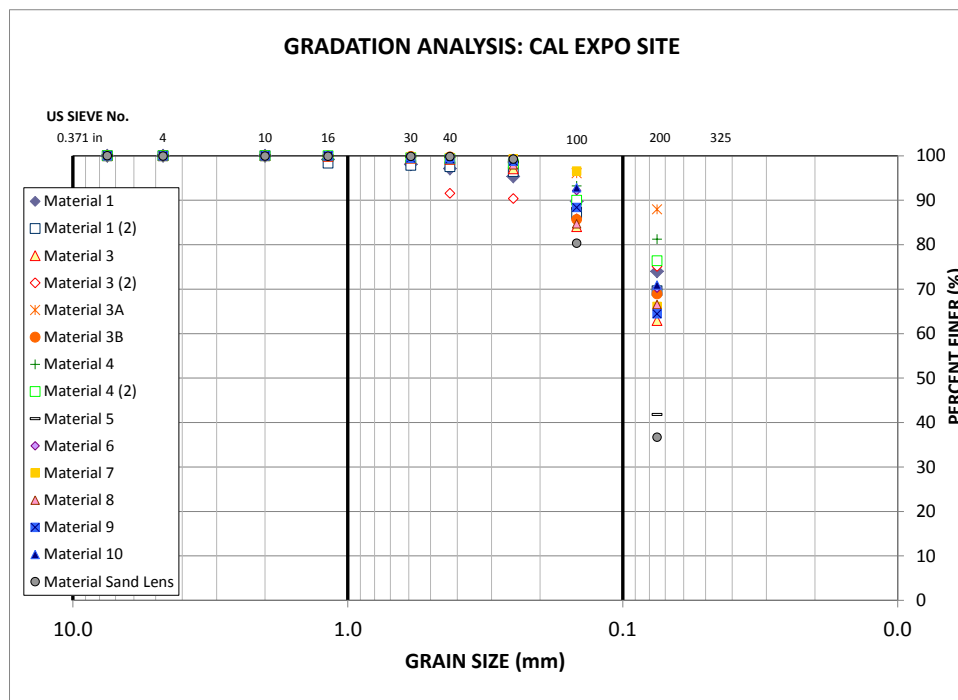


Figure 6-23. Gradation analyses for Cal Expo site

The volumetric moisture content values shown on Figure 6-24 were used as a guide for truncating the SWCCs used in the finite element flow models described in subsequent sections. These, in conjunction with the recorded suction values during the test run were instrumental in defining initial conditions for the different soil layers and avoiding the calculation of very low values of hydraulic conductivity during model solution.

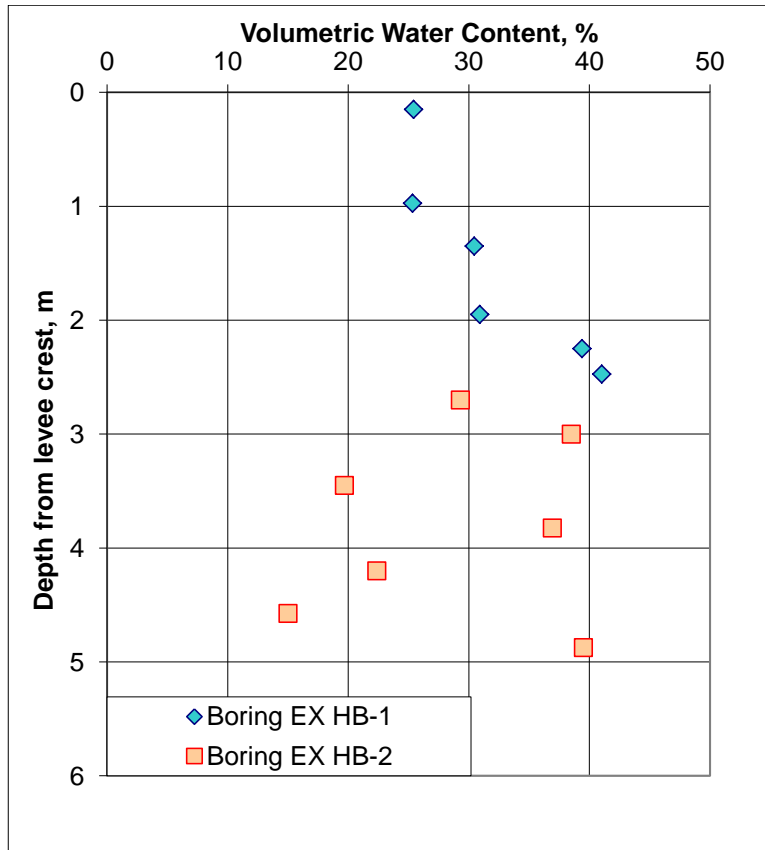


Figure 6-24. Initial moisture contents

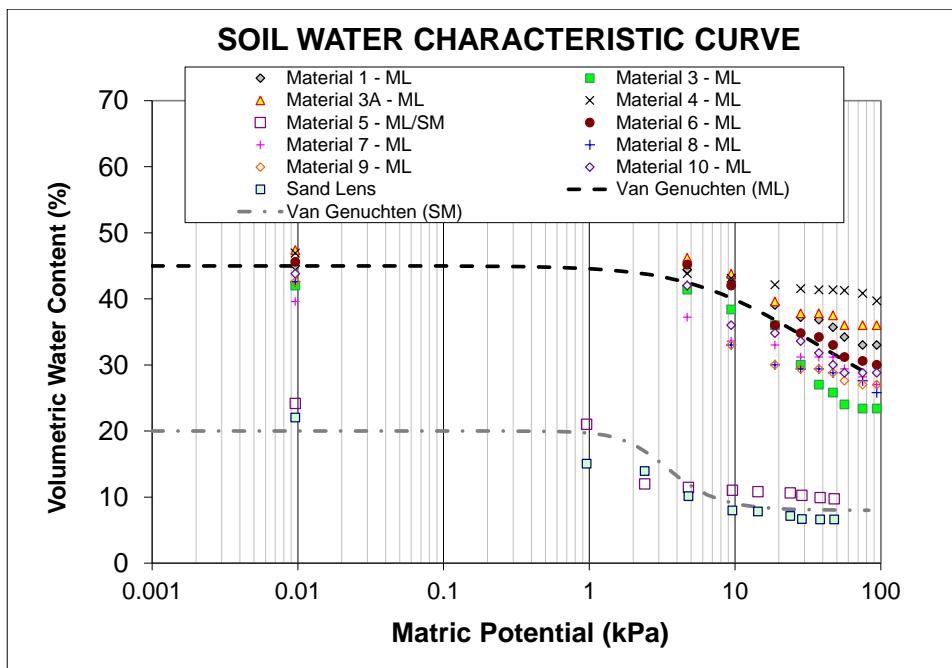


Figure 6-25. Soil Water Characteristic curves

6.2.6 3D FLOW MODEL

Seep3D, the three dimensional seepage package from GEOSTUDIO®, was used to develop a 3D finite element model that incorporated the root system and soil layers as described in previous paragraphs. The complexity of the problem and software limitations did not allow modeling the 3D geometry in its full detail, nor the presence of the finite and discontinuous spaces encountered between some roots and the surrounding soil as described by Shriro et al., (2011). Consequently, the decomposing root system was modeled as a homogeneous region with a value of hydraulic conductivity lower than the surrounding soil.

The domain was divided in 0.2 m cubic regions in the vicinity of the root system, and roots were simulated by assigning a lower hydraulic conductivity to the regions along the roots. Finite element size was 0.1 m in and around the decomposing root system. Away from the root system, cluster size increased to 0.5 m with finite element size of 0.25 m. The gopher burrow encountered along instrument Line B was modeled as an open space within the mesh.

INITIAL CONDITIONS

Initial conditions were defined using the values of initial moisture content and suction values measured during the dry run performed prior to the wetting front test. An initial finite element model was run by changing the position of the initial water table until suction values similar to the measured were computed by the software. Additionally, soil water characteristic curves were truncated at the maximum value of measured suction to avoid computation of very high

tension values by the software that could translate into uncharacteristically low values of volumetric water content and therefore very low values of unsaturated hydraulic conductivity.

BOUNDARY CONDITIONS

Boundary conditions were set to a constant pressure head for the duration of the wetting front test equal to 60 cm (2 ft) along the upper trenches and along the mammal burrow on instrument Line B; assuming that the burrow was not plugged and, therefore, no head loss occurred along its length. A seepage face (review nodes) type of boundary condition was assigned to the lower trench walls and levee slope to allow for flux seeping out of the surface without ponding on the surface. Finally, since visqueen sheets were placed along the bottom and back walls of the upper trenches to minimize flow towards the waterside (opposite) slope of the levee, a no-flow boundary condition was applied along these edges.

RESULTS

Model results are compared with tensiometer data series in Figure 6-26 for instrument Line A (stump) and Figure 6-27 for instrument Line B (gopher burrow). Continuous lines represent instrument data and dots represent model results. The resulting suction values from the 3D model compare relatively well with the measured values, especially for the instrument line along the animal burrow, given the short time that took to achieve instrument saturation. Along the instrument line across the stump the model values do not achieve a good match; however, the general trend of slower progression of the wetting front was captured by including a simplified representation of the root system using lower hydraulic conductivity clusters in the mesh.

The progression of the wetting front is represented by plotting a three-dimensional surface of zero pressure head ($P=0$) at different times during the simulation of the field test. Figure 6-28, Figure 6-29 and Figure 6-30 show these surfaces at time of 1, 10 and 50 hours from the start of the test, with the saturation front shown as a red surface on the stump trench. The effect of the gopher burrow (lower right corner of figures) is evident after just one hour of test simulation. The saturation front is not only extending from the upper trench towards the lower trench, but radially out from the burrow, which is acting like an open pipe with the same pressure head applied on the nodes along the upper trench.

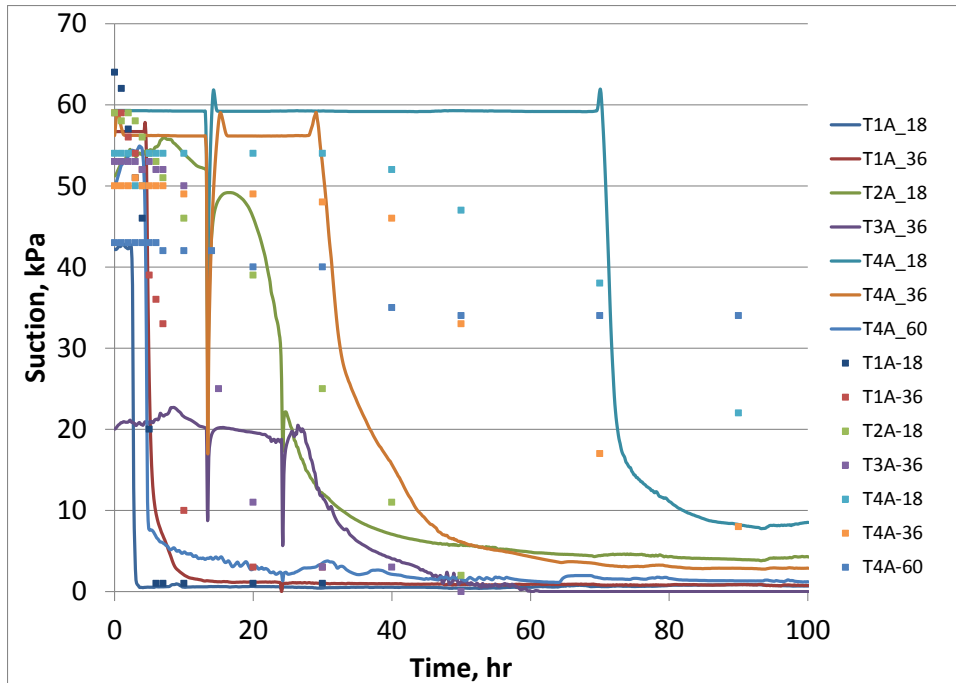


Figure 6-26. Model results for instrument Line A (stump). Solid lines: instrument data, Dots: model data

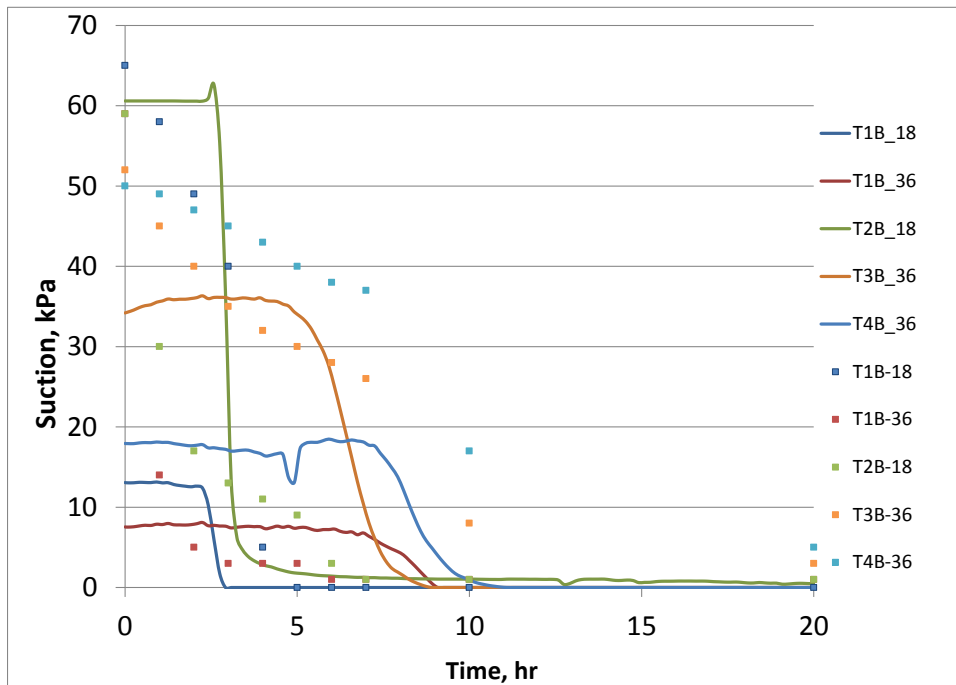


Figure 6-27. Model results for instrument Line B (gopher burrow). Solid lines: instrument data, Dots: model data

The simulations show that after one hour (Figure 6-28) the saturation front, or pressure head equals zero surface (shown in red) has advanced only a few inches from the upper trench,

consistent with values from tensiometers T1A-18, T1A-36 and T2A-18, which showed constant tension values for the first three hours of test. Figure 6-29 shows the simulated position of the wetting front after five hours, where the front has advanced approximately 50 centimeters downslope in the vicinity of the burrow and only a few centimeters along the rest of the trench. This is consistent with observed suction values along Line A (stump), which remained relatively constant between 20 and 60 kPa, depending on the instrument. The instruments along Line B (burrow) have started to saturate, particularly the instruments near the upper trench and the line situated 30 cm downslope.

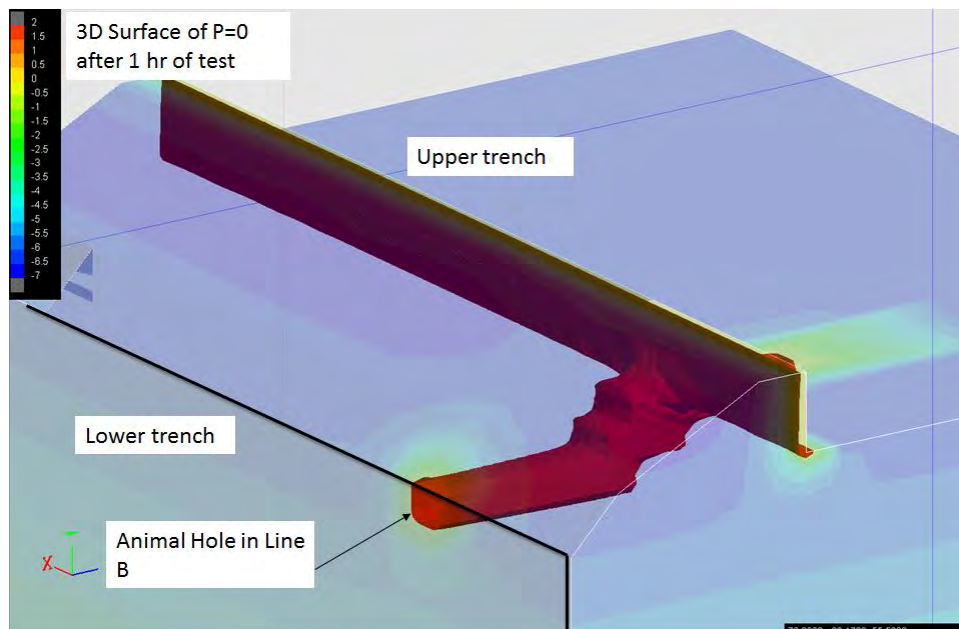


Figure 6-28. Saturation front after 1 hour of test simulation

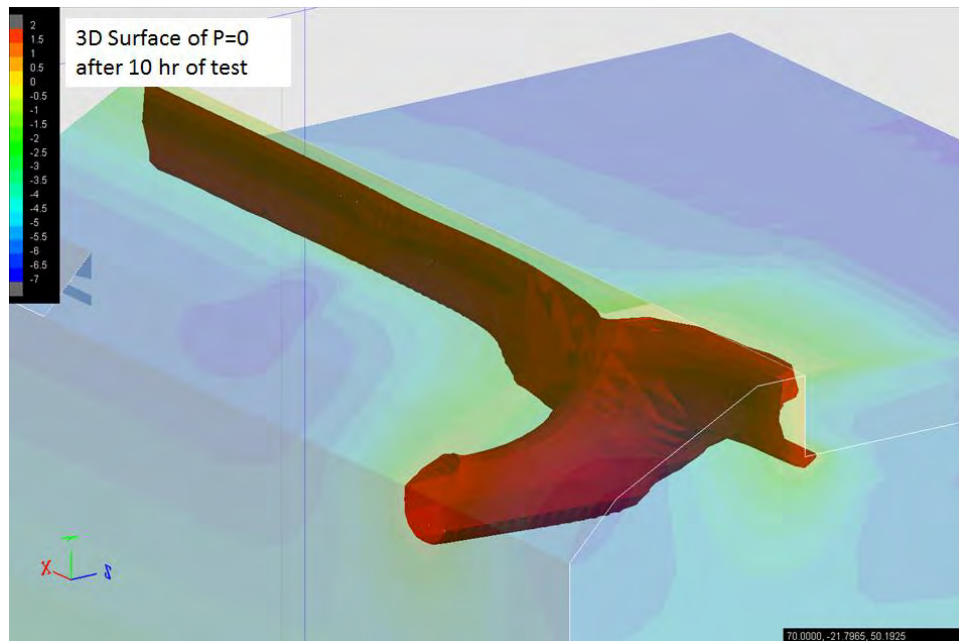


Figure 6-29. Saturation front after 10 hours of test simulation

The position of the wetting front after 50 hours of test simulation is shown on Figure 6-30. By this time the upper wall on the lower trench is saturated in the vicinity of the gopher burrow, and the wetting front is being delayed by the presence of the lower hydraulic conductivity clusters composing the tree root system. This is shown by the pronounced curvature on the P=0 surface on Figure 6-30 indicated by the arrow.

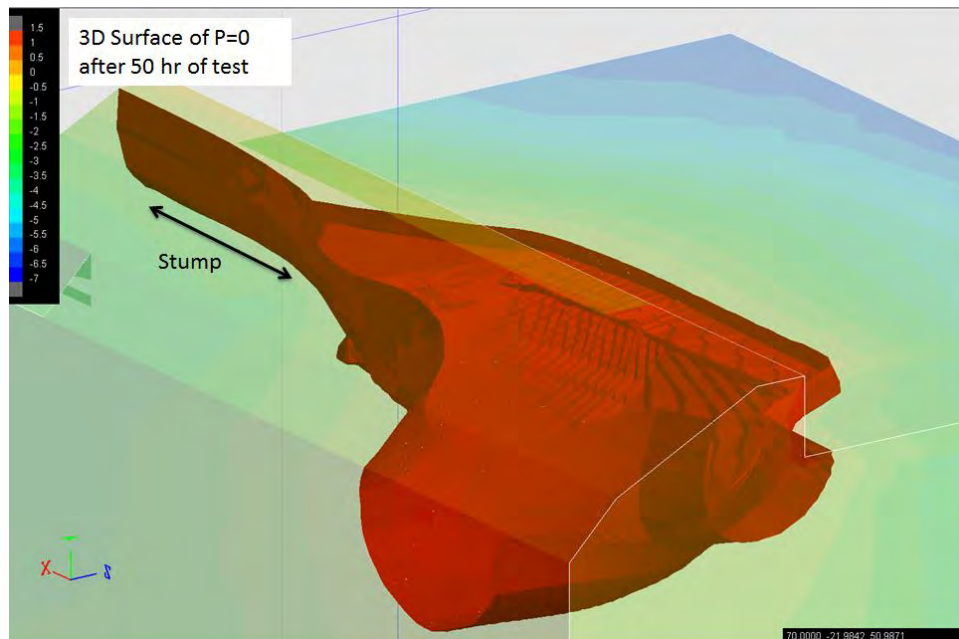


Figure 6-30. Saturation front after 50 hours of test simulation

Additional analyses were performed by changing the properties of the clusters representing the decomposing root system and the soil mass around it. In the first model a high value of hydraulic conductivity (1×10^{-3} cm/s) was assigned to these clusters. The results (Figure 6-31) show that despite the higher conductivity the influence on the saturation of the soil mass is negligible compared to that of a completely penetrating burrow. The fact that the high conductivity clusters (roots) are arranged in an irregular manner and are not directly connected to the water source means that the flux of water into these zones depends on the flux of water within the surrounding unsaturated fine-grained soil. The $P=0$ surface shown on Figure 6-31, corresponding to 50 hours of test simulation is very similar to the previously shown plot on Figure 6-30, with the difference that the marked curvature near the stump area is no longer present.

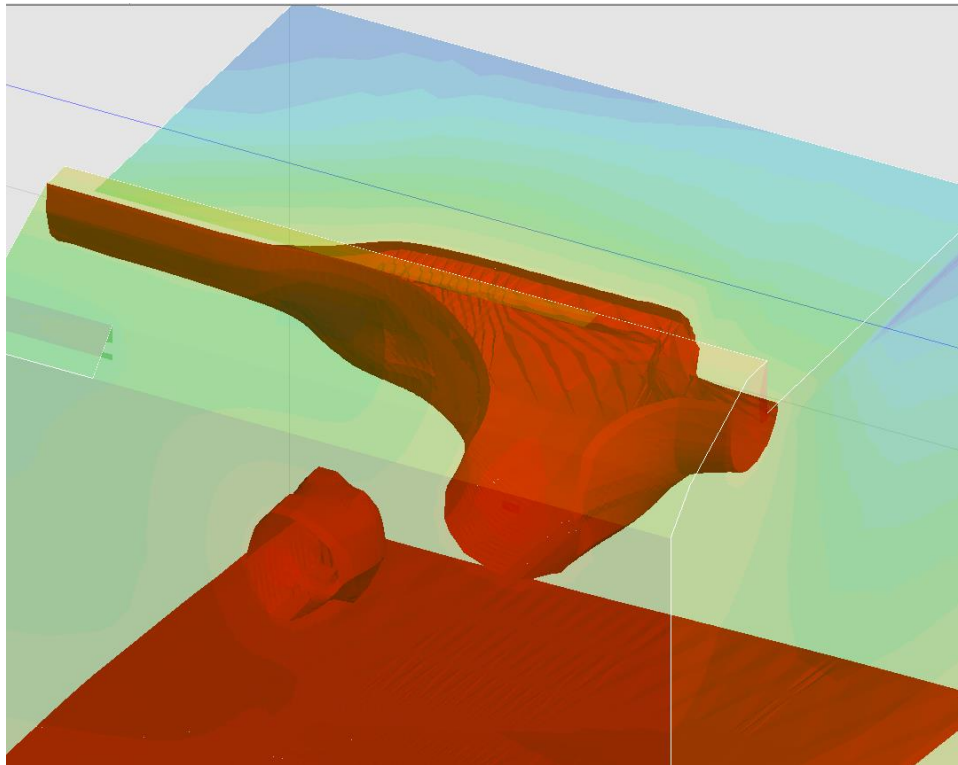


Figure 6-31. Simulation results changing conductivity of roots

6.3 TWITCHELL ISLAND SEEPAGE MODELING

The second seepage experiment to assess the influence of woody vegetation on transient seepage through a levee and on levee stability was performed at Twitchell Island and is described in detail by Shriro et al. 2013 and Shriro (2014a). The site is located at Rio Vista (CA) and the geometry of the site and the basic layout of the experiment is shown in Figures 6-32 and 6-33.

6.3.1 HYDRAULIC PROPERTIES AND CALIBRATION

The first step of the seepage modeling consisted of estimating hydrogeologic properties of the layers and calibrating these values to the recorded instrument data. Calibration was performed using the data from instrument line C (Figure 6-32), as it did not have a root system. After a reasonable agreement between simulation and instrument data was achieved, the soil properties were fixed and used in modeling of the other sections and analysis scenarios.

Saturated hydraulic conductivities were initially assumed based on recommendations in DWR's urban levee guidance document (URS, 2014). Unsaturated behavior was represented by creating SWCCs for the main soil types in the profiles and assuming Van Genuchten coefficients typical of each soil type. After the initial set of properties were defined for the layers in Section C, transient analyses to simulate the field experiment data were performed to calibrate the assumed properties. No specific laboratory tests were performed for the Twitchell Island site.

The transient calibration model started from an initial steady state simulation with the pre-experiment water level at -15 ft located along the vertical edges of the model (approximately 1000 ft away from the levee centerline), as measured by piezometers prior to the start of the centerline trench; and a canal water elevation of 1 ft (Figure 6-43). After the initial pore water pressure field was established, the initial suction values at each instrument location were compared to the instrument data, and through slight variations in the initial water levels a reasonable match between simulation and instrument data was achieved. Similar to the Cal Expo models described before, the SWCCs were truncated so realistic values of initial hydraulic conductivity were calculated by the software.

A transient simulation applying a head of 7.25 ft inside the excavated trench followed the generation of initial conditions to simulate the arrival of the wetting front to the different instruments in the section. Values of saturated hydraulic conductivity, saturated volumetric moisture content, air-entry value and slope of the SWCC were varied during the calibration process until a satisfactory calibration was achieved for a number of instruments in the profile. Table 6-2 shows the final parameter values result of the calibration process.

Table 6-2. Soil properties used for Twitchell Island flow models

Material	Color	K_{sat} (cm/s)	θ^1_s	θ_r	a^2 (psf)	K_y/K_z
Alluvial Sand		1×10^{-3}	0.3	0.05	0.5	0.33
Old clay levee		1×10^{-6}	0.42	0.1	100	0.2

Weak clay		1×10^{-6}	0.42	0.1	100	0.2
Sediment		1×10^{-8}	0.42	Assumed saturated		1.0
Levee silt		5×10^{-4}	0.4	0.1	5	0.2
Silty sand		5×10^{-4}	0.35	0.1	20	0.3

¹Volumetric water content, ²coefficients used in the Van Genuchten (1980) equation for characteristic curves.

Calibration results for each instrument are shown on Figure 6-34 to Figure 6-35. Calibration was successfully achieved for instruments TC2-36, TC4-24 and TC4-60; instruments TC4-36, and TC1-36 despite having similar initial suction values to those recorded during the test, achieved saturation in approximately half the time in the simulation than in the field test. Suction values on the waterside slope were not accurately predicted by the simulations, likely due to uncertainties in soil layering in the profile, loose pockets and burrows. The model predicts that shallow soils are moister than they were in fact observed to be in the field. In the transient simulations the final properties used in these and subsequent analyses were based on calibrations with landside instruments, whereas the waterside instruments focused on matching of positive pore pressures in piezometers for input into stability models.

Instrument Lines A and B included animal burrows and root systems. The burrows were modeled as open spaces within the finite element mesh and a total head boundary condition equal to the head on the test trench or canal was applied whenever the burrow was directly connected to the source of water; whereas discontinuous or plugged burrows were assigned a high value of hydraulic conductivity to allow continuity in the mesh and fast transmission of hydraulic heads from one end of the burrow to the other. The root systems were modeled as regions with constant hydraulic conductivity using a lower value equal to 1/5 of the saturated value of conductivity of the surrounding levee material.

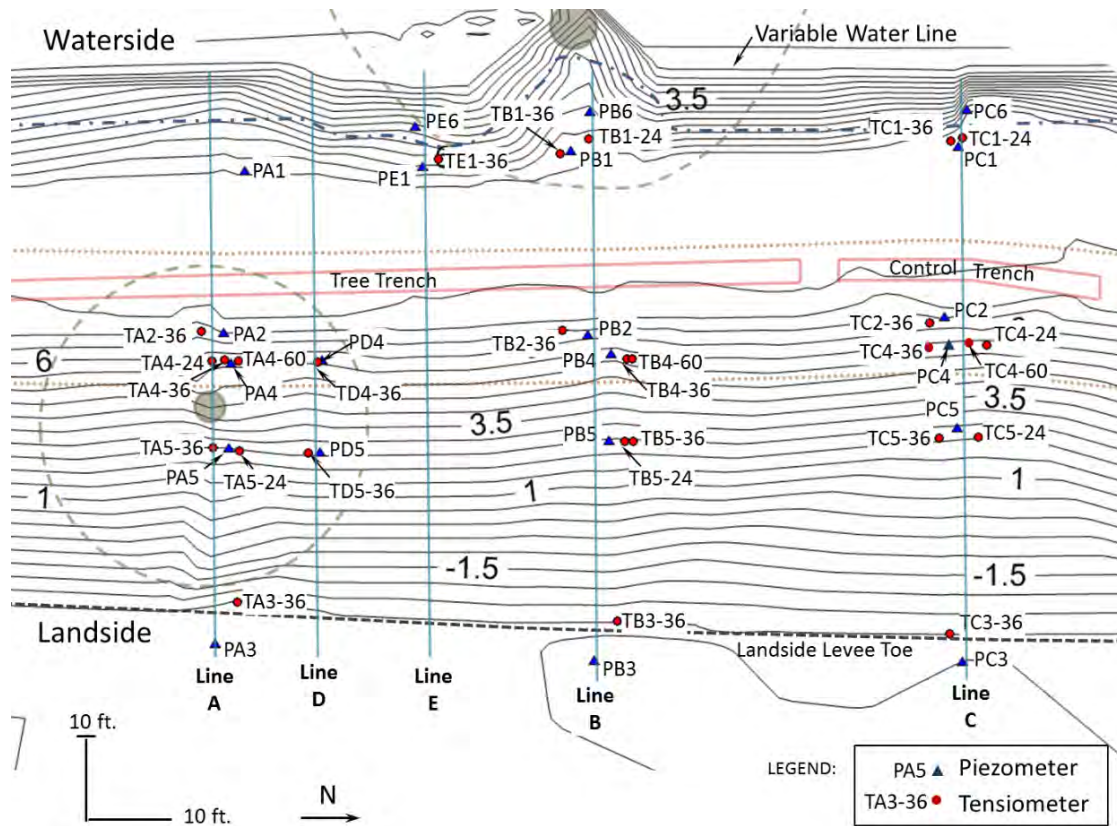


Figure 6-32. Location of instruments and analysis sections at the Twitchell Island centerline test site (Shriro, 2014)

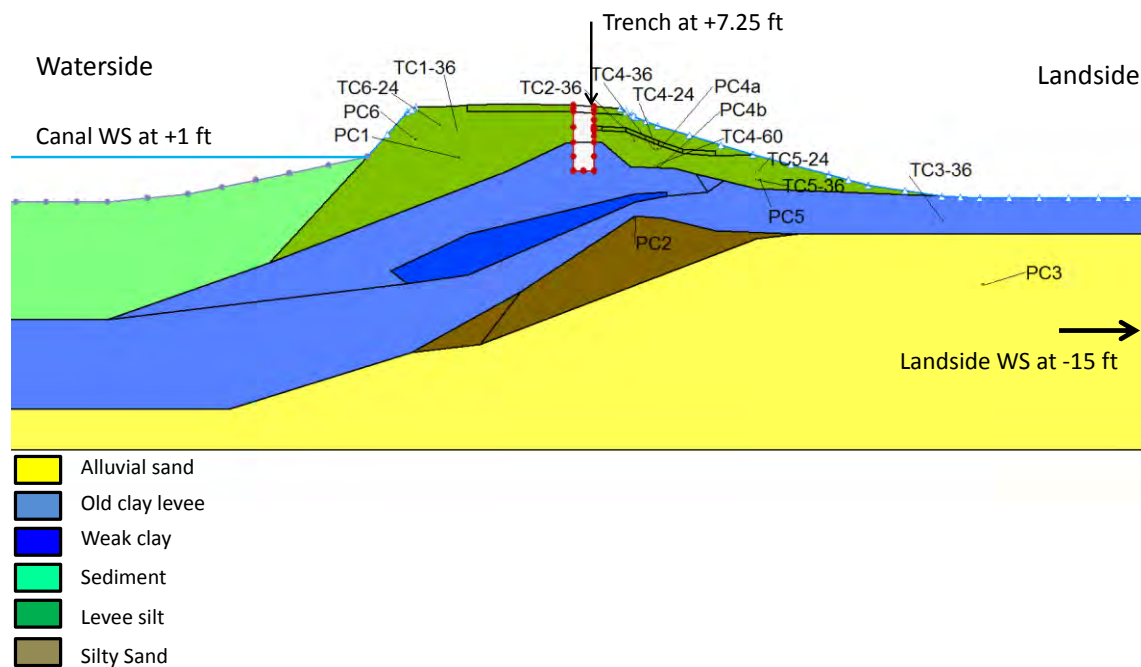


Figure 6-33. Instrument line C showing instrument location and boundary conditions

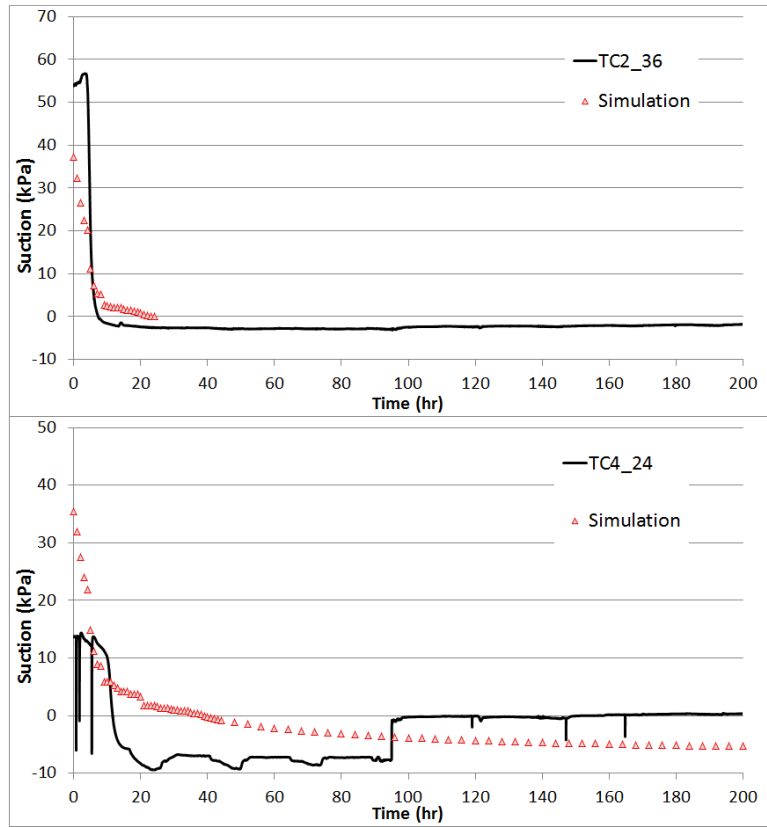


Figure 6-34. Instrument line C devices TC2-36 and TC4-24

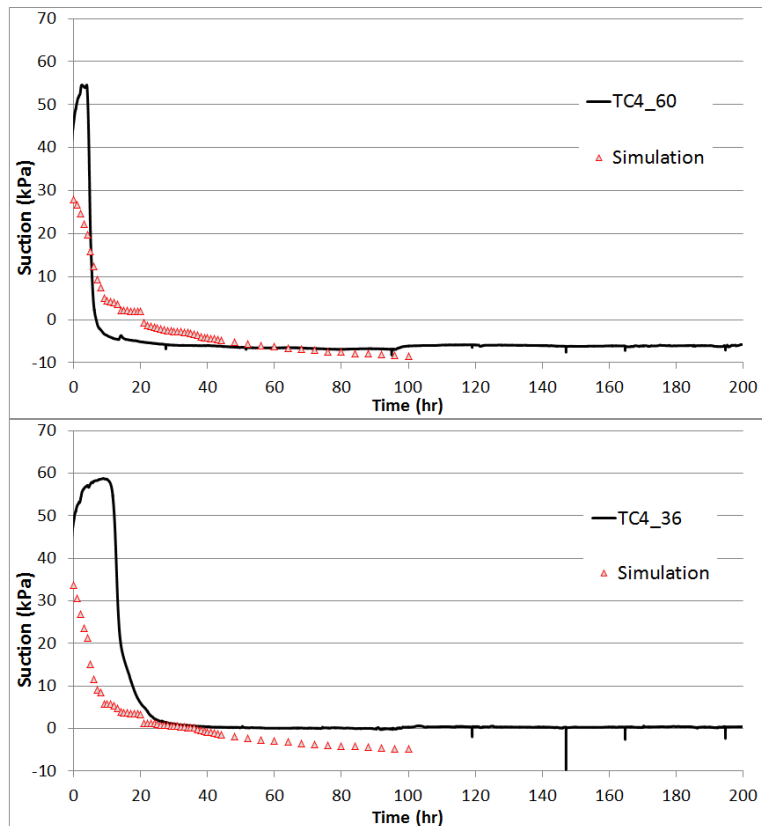


Figure 6-35. Instrument line C devices TC4-60 and TC4-36

Instrument Line B (Figure 6-36) includes a root zone on the waterside slope and a discontinuous animal burrow along the waterside half of the embankment. The transient simulation considers the same boundary conditions and time steps as control line C. The results are shown on Figure 6-37 and Figure 6-38. Similar to instrument line C, this section shows faster saturation of instruments on the waterside slope, given the much higher initial head condition of +1 ft on the canal side (compared to -15 ft on landside), making initial conductivity values on the waterside slope much higher and thus saturation times shorter than on the landside slope.

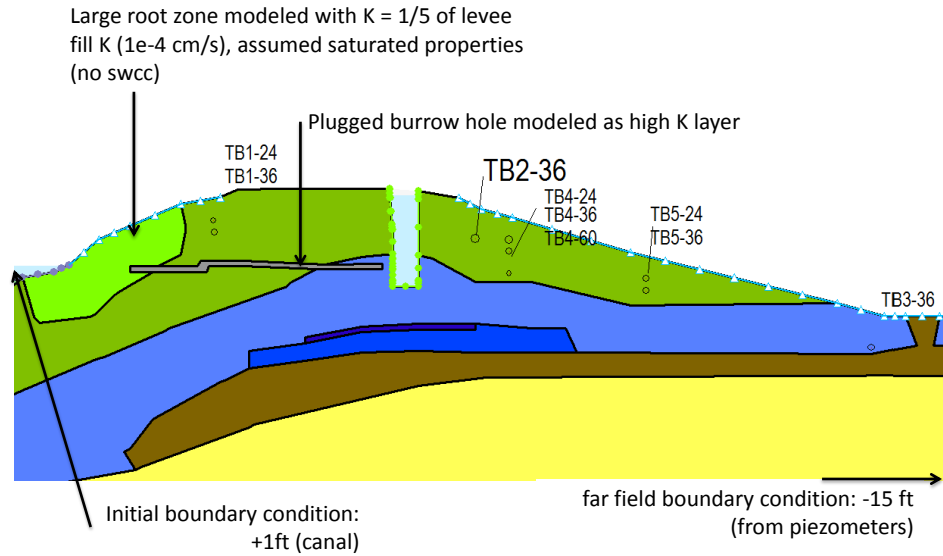


Figure 6-36. Instrument line B section and boundary conditions

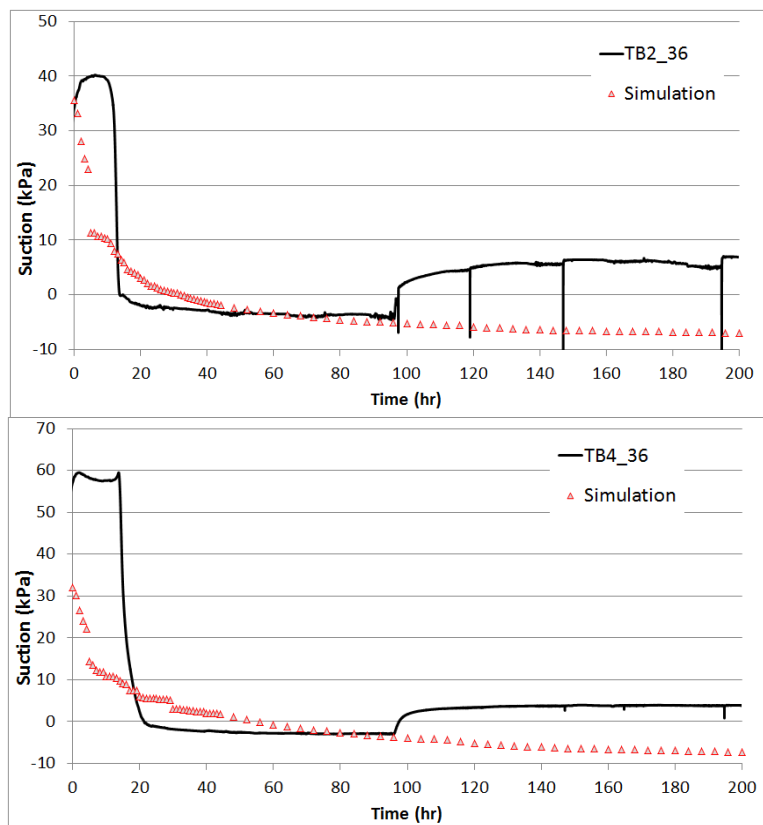


Figure 6-37. Instrument line B devices TB2-36 and TB4-36

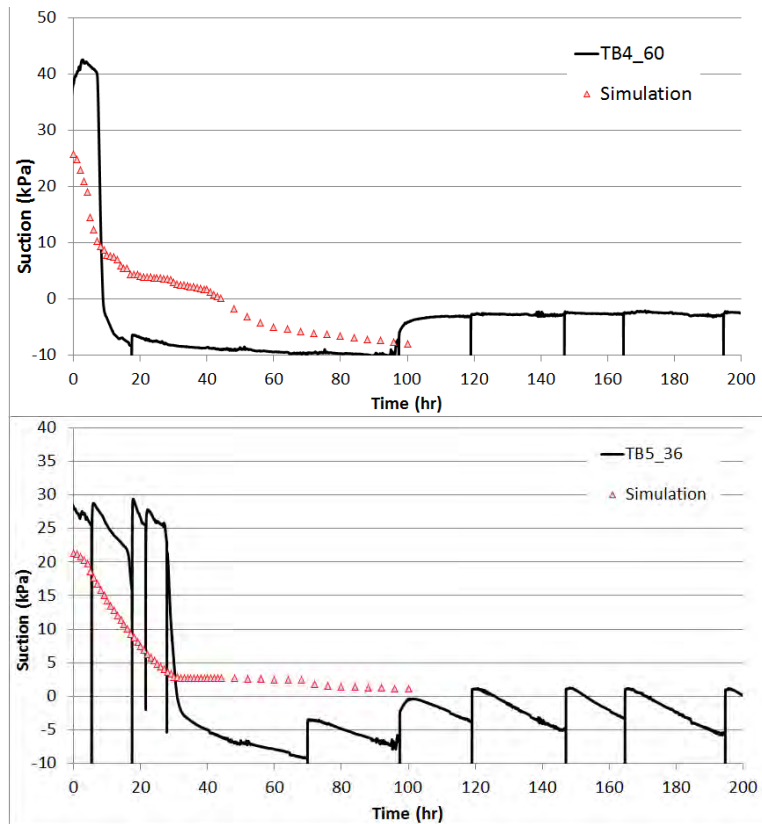


Figure 6-38. Instrument line B devices TB4-60 and TB5-36

Instrument Line A (Figure 6-39) includes a root zone on the waterside slope and a discontinuous animal burrow along the waterside half of the embankment. The transient simulation considers the same boundary conditions and time steps as control line C. The simulation results are shown on Figure 6-40 through Figure 6-42. As along instrument line B, this section shows faster saturation of instruments on the waterside slope, given the much higher initial head condition of +1 ft on the canal side (compared to -15 ft on landside), making initial conductivity values on the waterside slope much higher and thus saturation times shorter than on the landside slope.

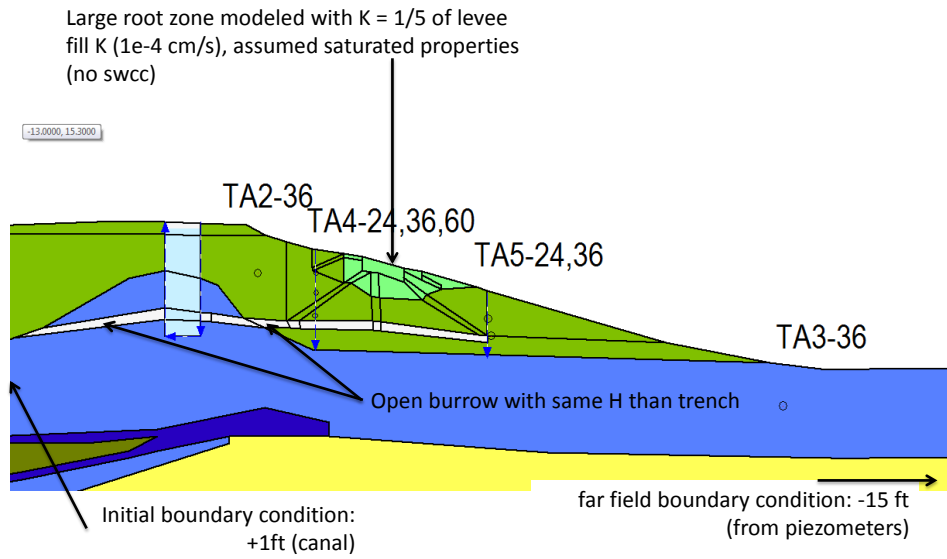


Figure 6-39. Instrument line A section and boundary conditions

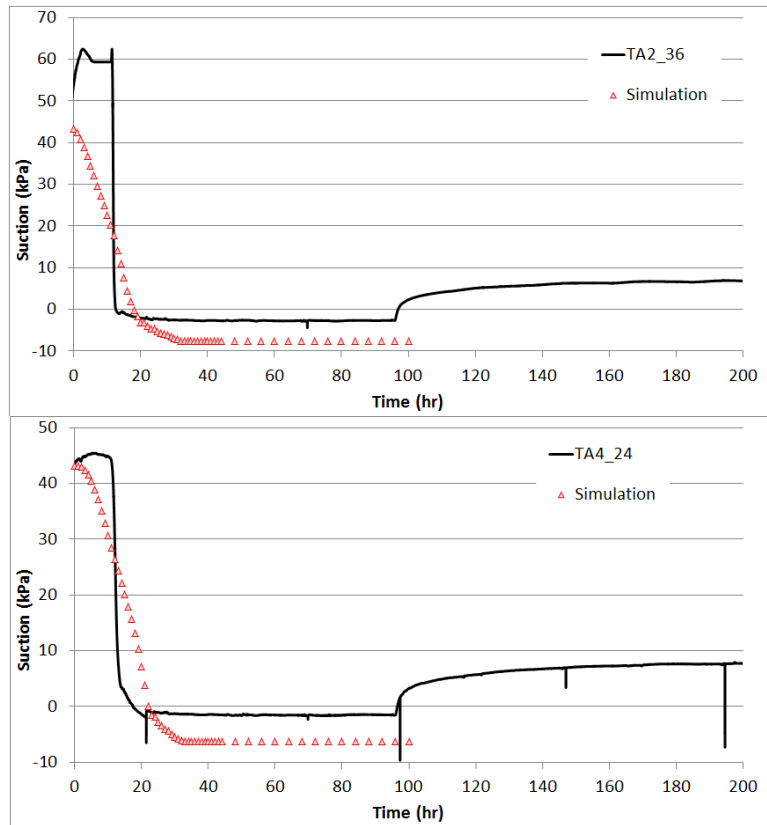


Figure 6-40. Instrument line A devices TA2-36 and TA4-24

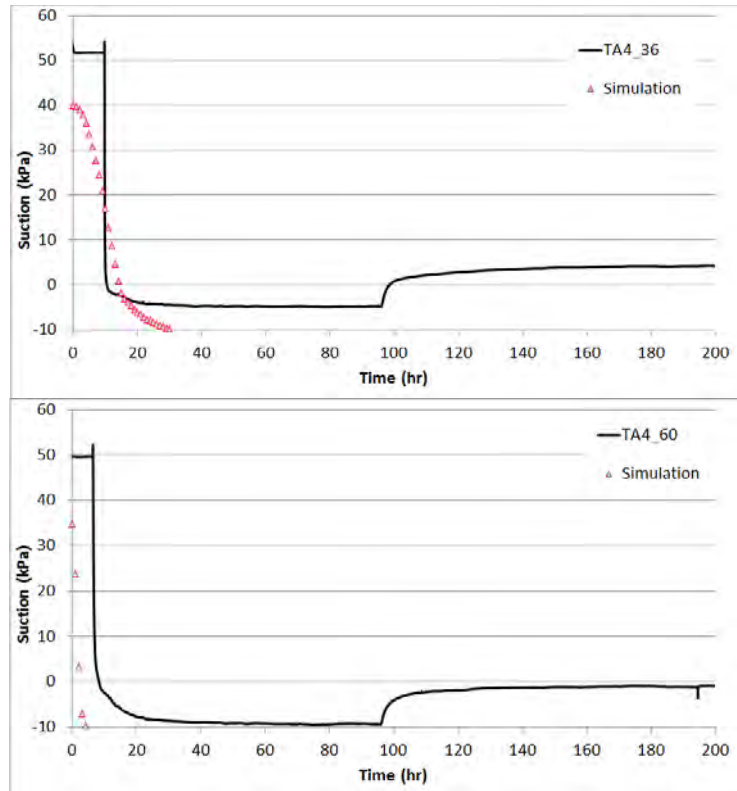


Figure 6-41. Instrument line A devices TA4-36 and TA4-60

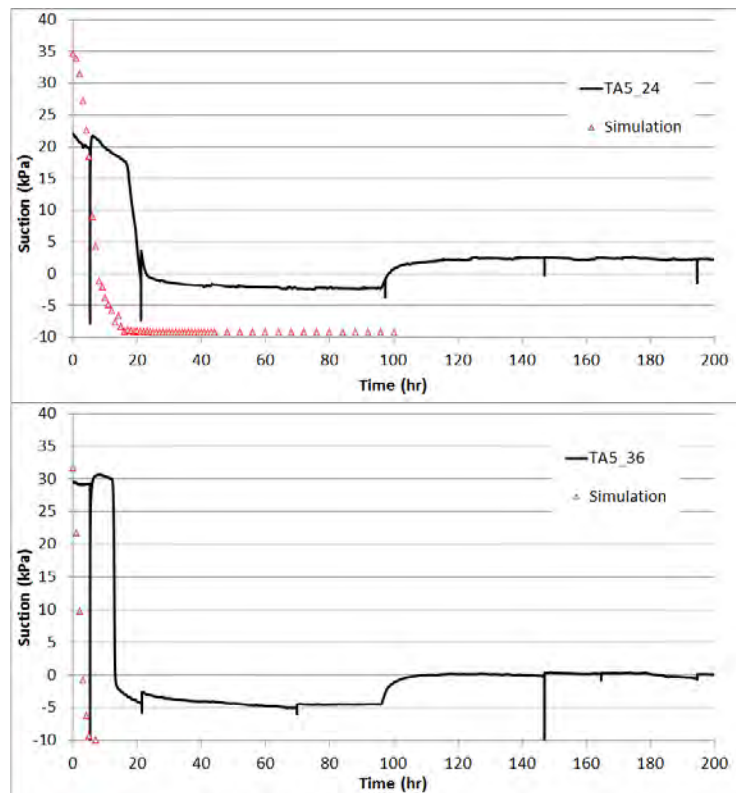


Figure 6-42. Instrument line A devices TA5-24 and TA5-36

The back-analyses of the Cal Expo and Twitchell Island field tests show that root systems delay the progression of saturation fronts, whereas the presence of animal burrows contribute to a fast saturation of the levee embankment.

6.4 MODELING ANIMAL BURROWS AND OTHER DISCONTINUITIES

6.4.1 IDEALIZED SIMULATIONS

The objectives of the simulations presented in this section were to examine whether a discontinuity or a macropore in a soil mass can become an important source of flow that may induce piping or faster saturation of a levee.

The base case of analysis is an idealized box of soil (Figure 6-43) with a circular discontinuity to simulate the presence of a burrow in cross-sectional view. Initial conditions for the model consist of a phreatic line near the base of the model so a profile of vertically increasing suction is generated within the soil column. Boundary conditions on the burrow are set by applying potential seepage nodes (setting pressure heads equal to atmospheric pressure for nodes where the pressure head is larger than zero) along the burrow walls. Transient conditions are achieved as a total head is applied along the nodes on the top of the model and a saturation front is created. Discharge into the burrow is estimated using a flux section across the discontinuity and saturation values are estimated on the nodes around the discontinuity for each time step of analysis. Results of the simulation are shown in Figure 6-44 by normalizing the flux into the discontinuity (void) by its discharge capacity and plotting it as a function of saturation (volumetric water content for each time step divided by saturated volumetric water content for the soil).

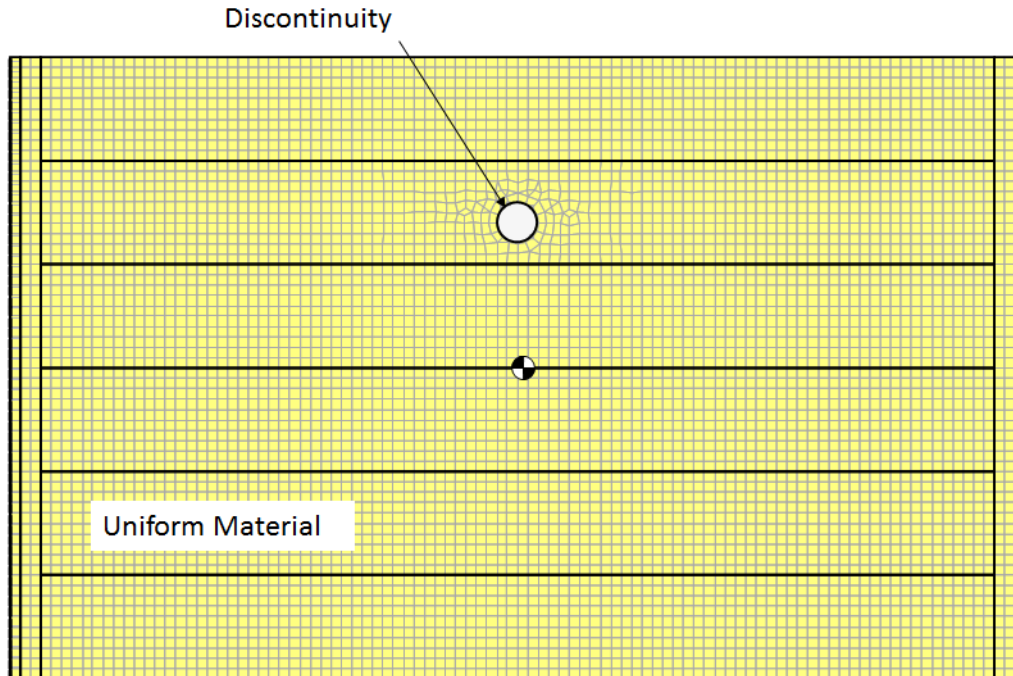


Figure 6-43. Idealized model section

The plot in Figure 6-44 illustrates a simple yet important point. A void within an unsaturated mass of soil will not become an important flow channel unless the soil around it is either saturated or directly connected to a source of water. The flux values for saturation values below 50% are less than 1% of its capacity at saturation and the flux becomes significant only after saturation exceeds 95% around the void. This is a similar concept to that derived by Phillips (1972).

The second conceptual model considered a single horizontal void shown in cross section view (Figure 6-45). This time, total heads are applied on the left vertical edge of the model to achieve a unit gradient across the idealized box of soil, and again flux into the cavity (grey cluster) was computed as a function of saturation and time. Right boundary conditions consist of a seepage face. Two sets of analyses were performed using this geometry. In the first simulation the soil was assigned sand-like properties and in the second the soil was assigned silt-like properties. The soil water characteristic curves used for both models are shown on Figure 6-46; saturated hydraulic conductivities were assumed as 1×10^{-3} cm/s and 1×10^{-5} cm/s for the sand and silt, respectively. Unsaturated properties were derived using the Van Genuchten (1980) relationship.

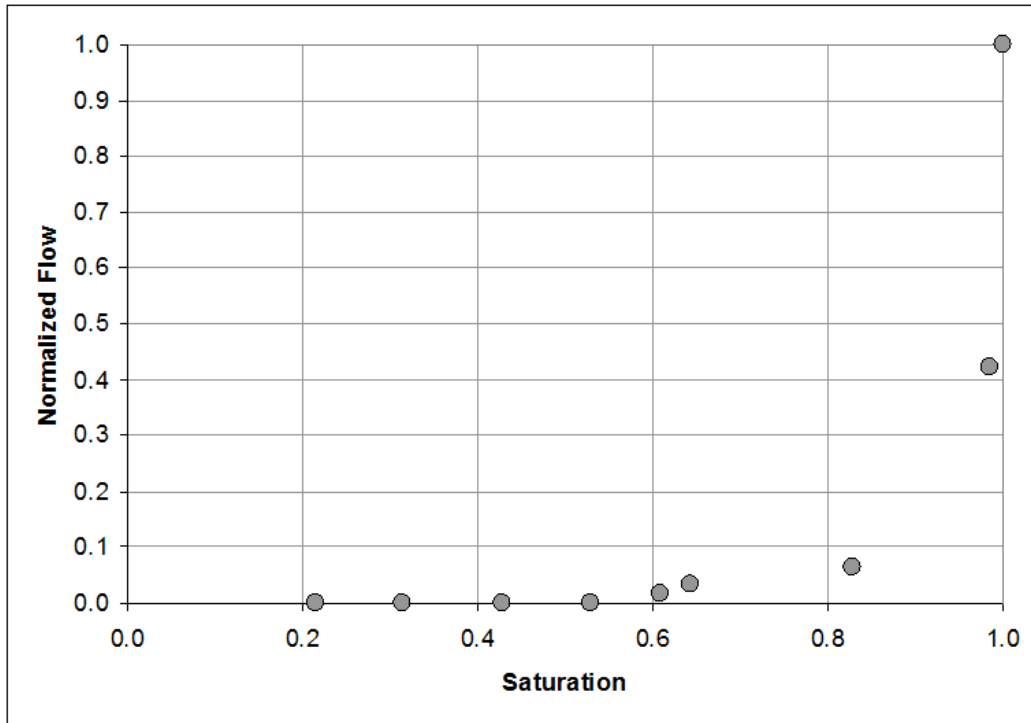


Figure 6-44. Results of idealized model

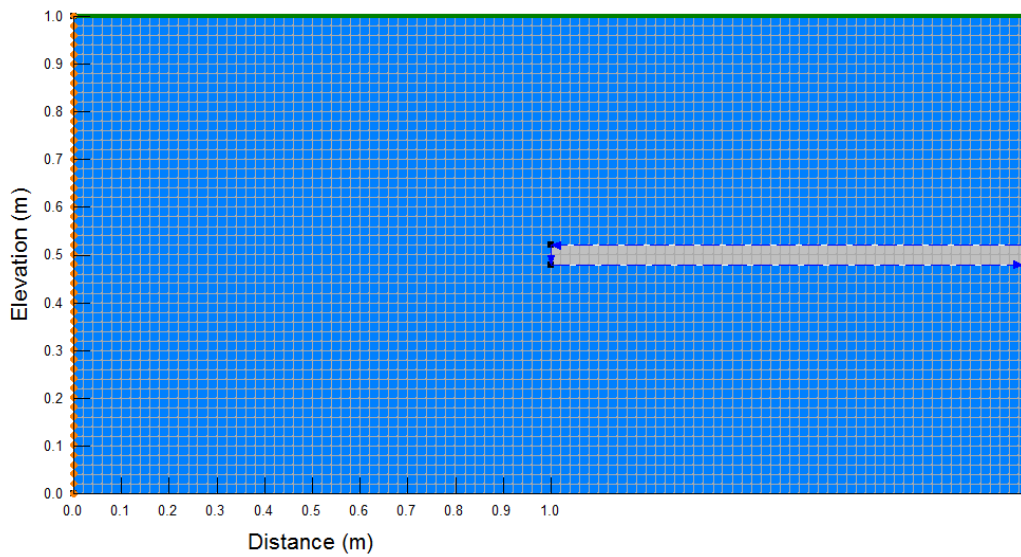


Figure 6-45. Idealized model for flow into a single cavity

The normalized values of discharge as a function of saturation are shown on Figure 6-47 and Figure 6-48 for the coarse-grained and fine-grained materials, respectively. As can be seen, the coarse-grained material, which started from an initial saturation of 10%, saturates rapidly given the high hydraulic conductivity and correspondingly the flux into the cavity rapidly increases. In contrast, the fine-grained material saturates more slowly and the flux also increases much more

slowly with its magnitude depending very much on the initial saturation. Maximum computed discharge for the sand model was on the order of 10^{-6} m³/s/m, and for the fine-grained model 10^{-9} m³/s/m. The hydraulic gradients exceeded a value of 10 which may be indicative of the potential for large deformations of the soil near the walls of a discontinuity and, consequently, may lead to the collapse of the void before saturated water flow initiates.

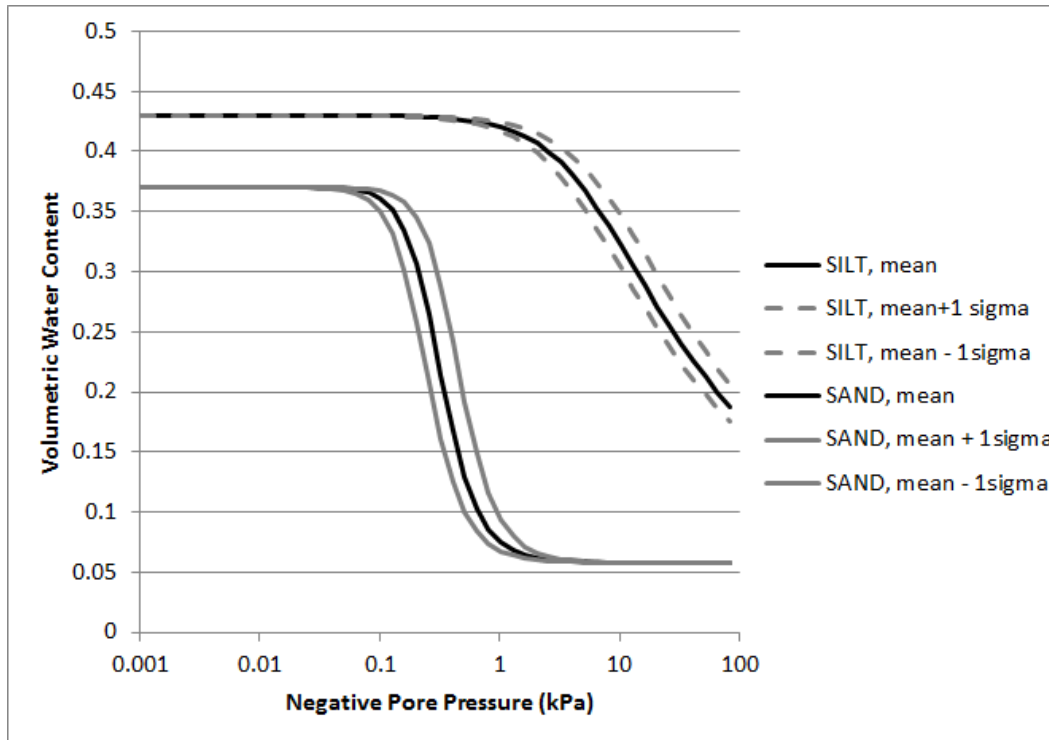


Figure 6-46. Material properties for single-cavity idealized model

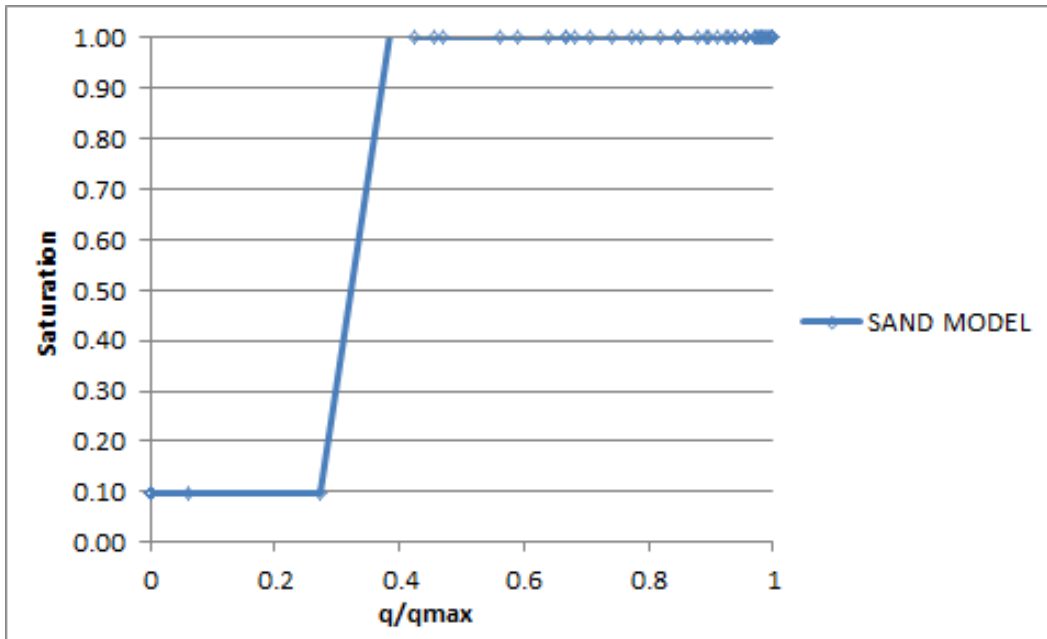


Figure 6-47. Results of the single-cavity idealized model using sand

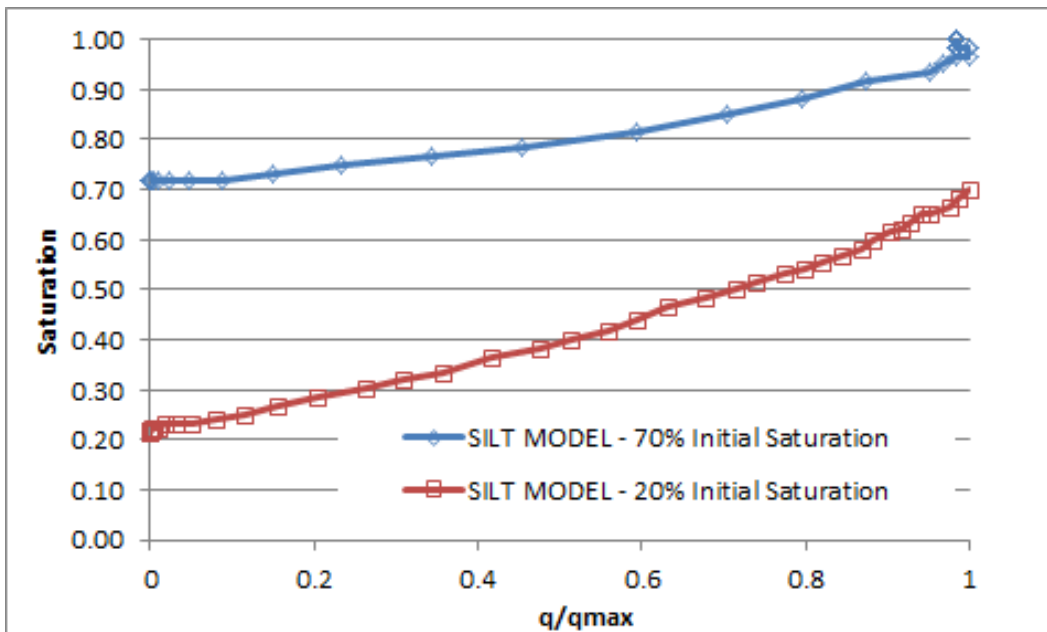


Figure 6-48. Results of the single-cavity idealized model using fine-grained soil

The third idealized simulation considered three discontinuities (green regions on Figure 6-49) within the mass of soil, two of these connected to the downstream 'seepage face', and the third on the upstream edge of the model. Boundary conditions are the same as previously described, and the total heads are also applied along the interface of the hole on the upstream edge of the model. The fluxes into each cavity (Figure 6-50) after 5 days of simulation were 5×10^{-8} and 5×10^{-6} $\text{m}^3/\text{s}/\text{m}$ for the upper and lower discontinuity, respectively. These are similar

to the computed flux through the entire cross section assuming no discontinuities were present (Figure 6-51), with a value of $1 \times 10^{-6} \text{ m}^3/\text{s}/\text{m}$. The blue line represents the position of the saturation front at the time indicated in the plot.

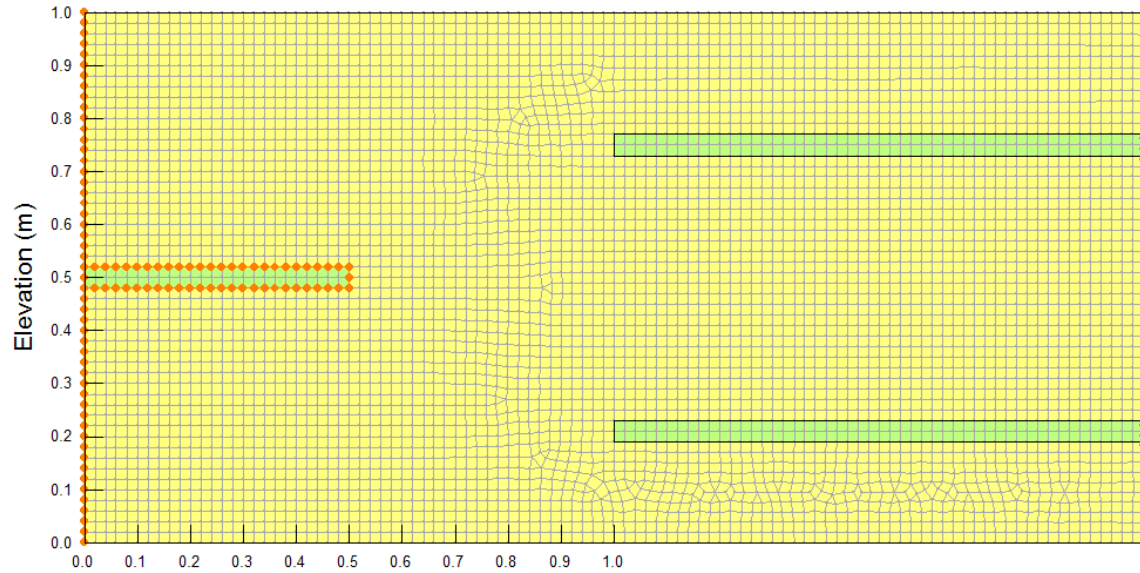


Figure 6-49. Multiple cavity idealized simulation

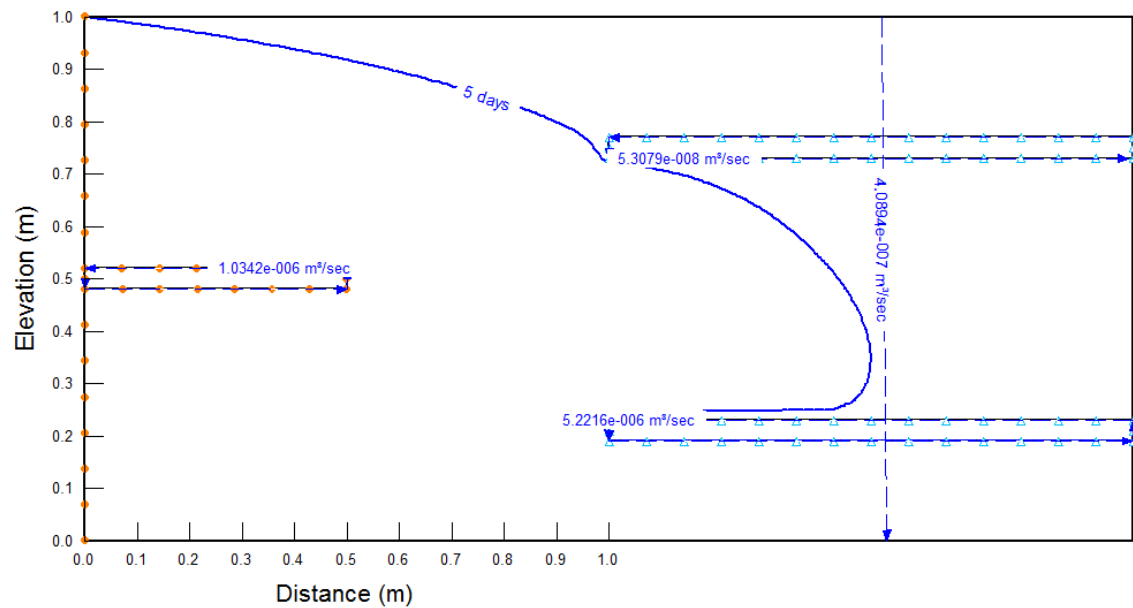


Figure 6-50. Multiple cavity simulation results

These idealized models are intended to show the influence of open discontinuities on the wetting patterns of unsaturated masses of soil, and whether a hole can potentially become an important flow channel within the soil mass. From the results of these analysis, it is evident that

the amount of water flowing into (and out of) a void depends on the amount of water flowing through the soil around the void and the degree of saturation of the soil mass. For the case shown on Figure 6-50, the computed discharges into the discontinuities are in the same order of magnitude as the flux through the entire cross section (Figure 6-51). The computed flux is shown by the dashed blue vertical arrow. Evidently, the effect that open discontinuities have on the behavior of the wetting front consists of controlling its geometry.

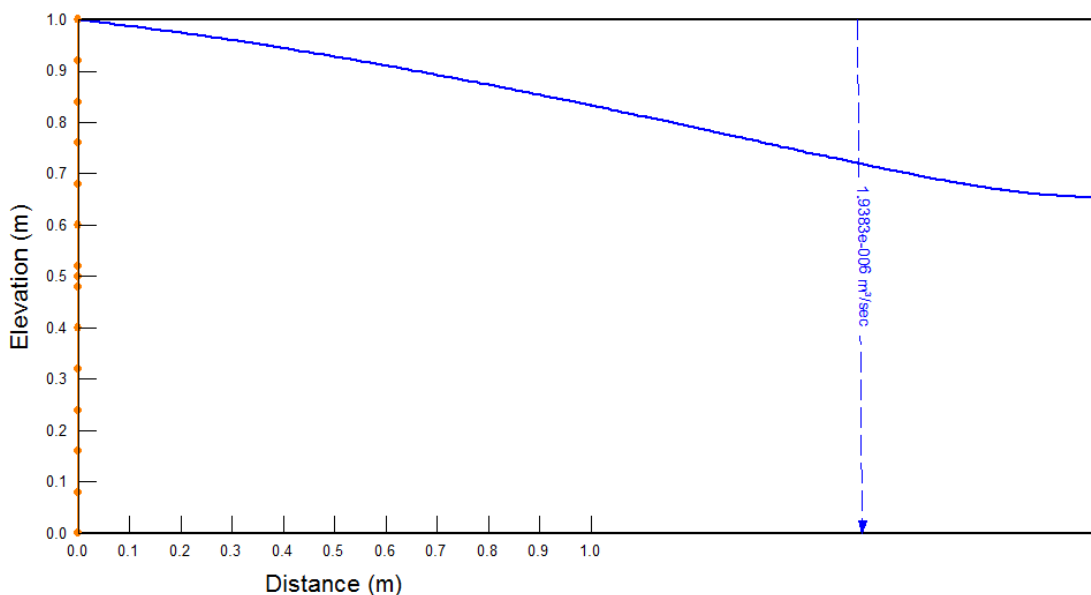


Figure 6-51. No cavity simulation results

6.4.2 ANIMAL BURROW FIELD TEST MODELING

The two animal burrow field studies described in Chapter 5 were used to as a basis for a series of simulations mimicking the discontinuous network of burrows. The first model is a two-dimensional representation of the burrows encountered in the sandy levee, where a single large burrow was encountered on the waterside toe, and a large complex of surficial burrows was found along the landside slope. For simplicity, the section was analyzed as a two-dimensional cross section, so the burrow system was ‘collapsed’ into a single cross section (Figure 6-52). The profile consists of a relatively clean sand levee with slopes of approximately 2H to 1V overlaying a silty foundation. Saturated hydraulic conductivities were assumed to be 1×10^{-3} cm/s and 1×10^{-5} cm/s for the sand levee and the silty foundation, respectively.

Boundary conditions consisted of a seepage face along the downstream levee surface and toe areas, as well as along the inner boundaries of the burrows open to atmospheric pressure on the downstream half of the embankment. Constant head boundary conditions were applied along the upstream levee slope and channel, assuming that the head was equal to the elevation of the levee crown.

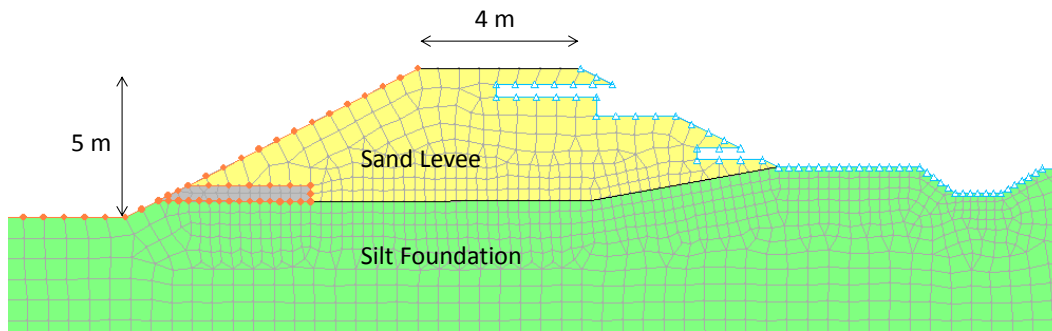


Figure 6-52. Simplified representation of animal burrow networks

The results from the steady state simulation are shown on Figure 6-53. The resulting flow field indicates that the combined effect of the waterside burrow and the burrow near the downstream toe of the levee is to shorten the seepage path and increase the gradient. The water side burrow allows the full water side head to reach into the levee and the landside burrow acts as a toe drain, concentrating flow paths and velocities toward the burrow. In contrast, the burrows located near the levee crown have little influence on the distribution of heads as the crown of the levee is likely to remain unsaturated even under steady state conditions

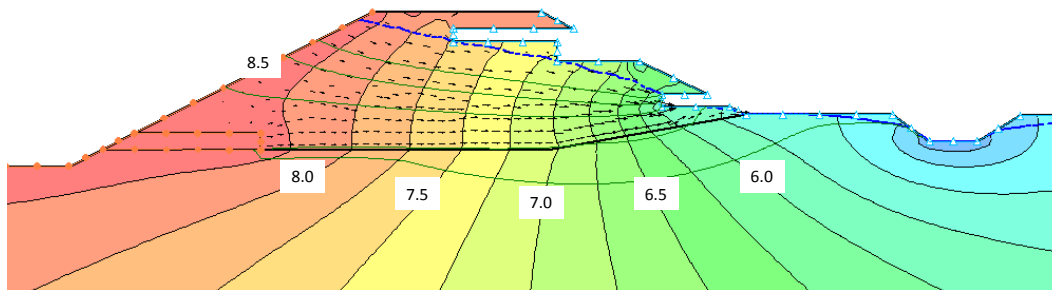


Figure 6-53. Steady state simulation of Sandy Levee Site burrows. Total head contour interval 0.25 m.

Second simulation was performed to analyze the influence that the location of a completely penetrating burrow has on the distribution of gradients within the embankment and on the piping potential. Figure 6-54 shows the section employed, with three model burrow locations labeled A, B and C, extending from one to three meters below the crown of the levee. Boundary conditions, material properties and model dimensions were kept the same as in the previous simulation.

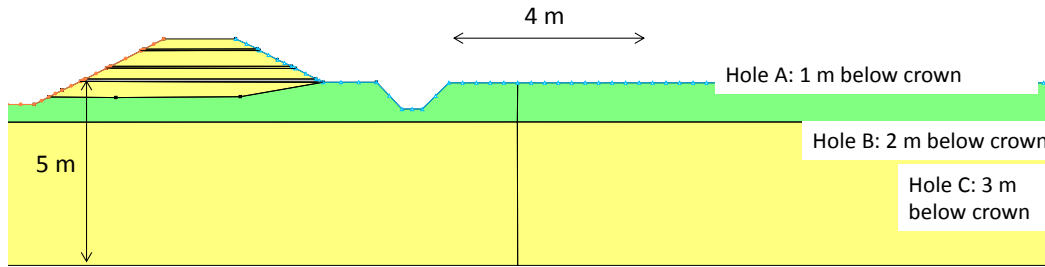


Figure 6-54. Geometry of the model section with completely penetrating burrows

Figure 6-55 shows the simulation results for model burrow C (3 m below levee crown) in terms of head distribution for a transient simulation of one day. At this point in time the geometry of the seepage front is similar to the saturation pattern observed in the case with no burrow (Figure 6-57). A pore pressure profile across a vertical section through the centerline of the embankment for this case is shown on Figure 6-56. The plot indicates that the presence of the burrow near the foundation level will produce a faster saturation of the embankment than if no hole were present (Figure 6-58). After two hours, the section with a hole near the bottom of the embankment has reached the maximum total head value (about 7.5 m), whereas the section with no holes reaches these values in about 20 hours.

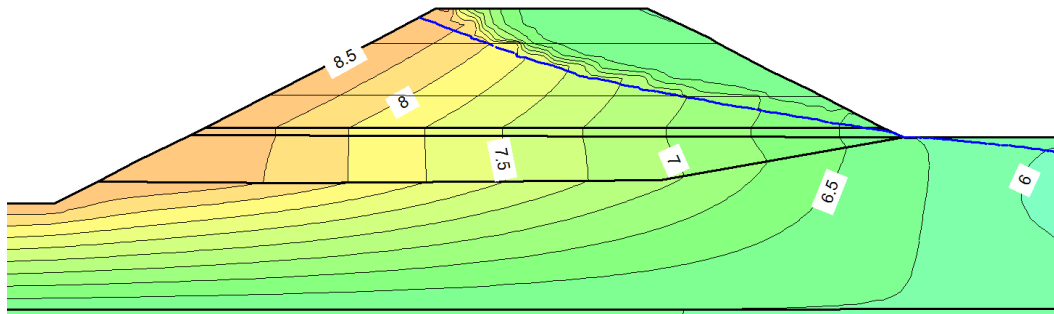


Figure 6-55. Results from transient analysis after one day of simulation with burrow at C. contour interval: 0.25 m

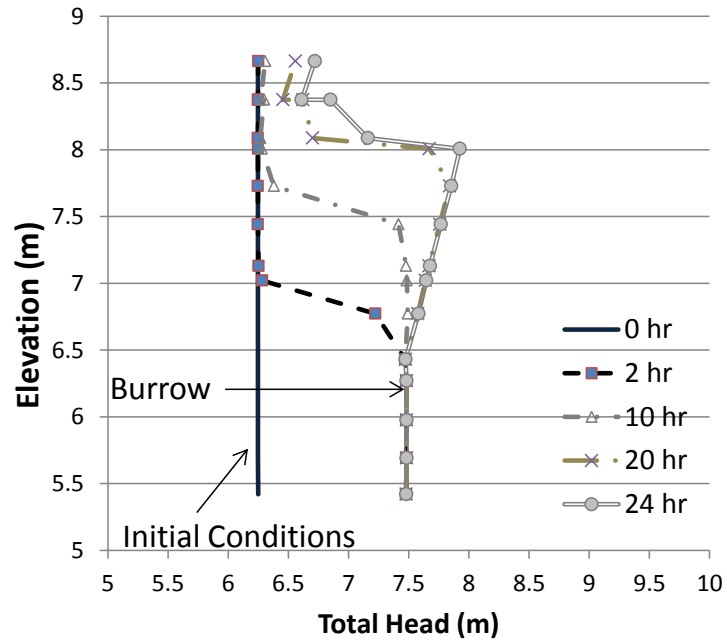


Figure 6-56. Evolution of pore pressures on a vertical section across the levee crown for Hole C

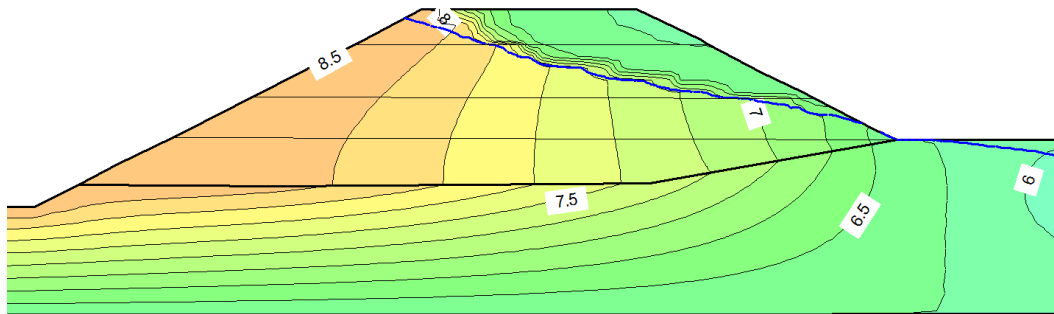


Figure 6-57. Results from transient analysis after one day of simulation. No holes present. Total head contour interval: 0.25 m.

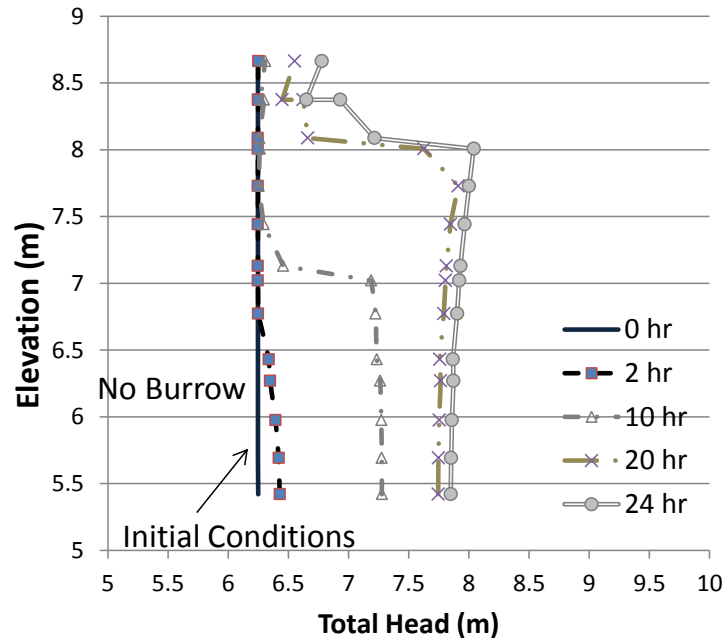


Figure 6-58. Evolution of pore pressures on a vertical section across the levee crown for the case of no hole

The results from the simulations with a burrow at location A (1 m below levee crown) and B (2 m below levee crown) are shown in Figure 6-59 and Figure 6-61, respectively. The pore pressure evolution across the centerline of the levee along A (Figure 6-60) and along B (Figure 6-62) indicates a similar behavior similar to that observed with the burrow located near the bottom of the embankment: the soil in the vicinity of the hole reaches its maximum head very rapidly (two hours) because of seepage from the burrow, which results in a shorter saturation time for the entire embankment along modeled section.

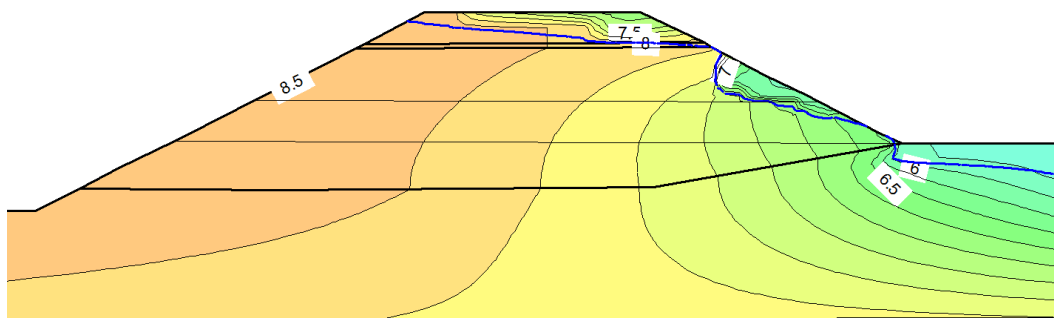


Figure 6-59. Results from transient analysis after one day of simulation with burrow at A. Total head contour interval: 0.25 m

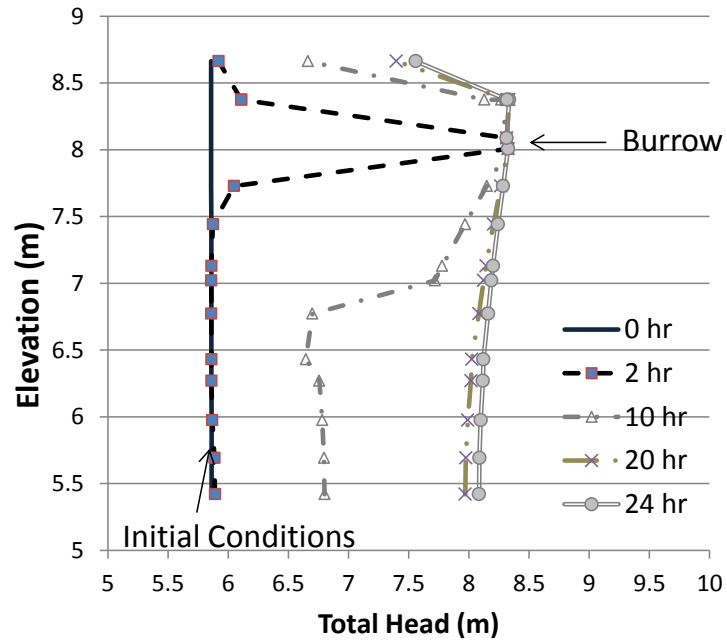


Figure 6-60. Evolution of pore pressures on a vertical section across the levee crown at burrow A

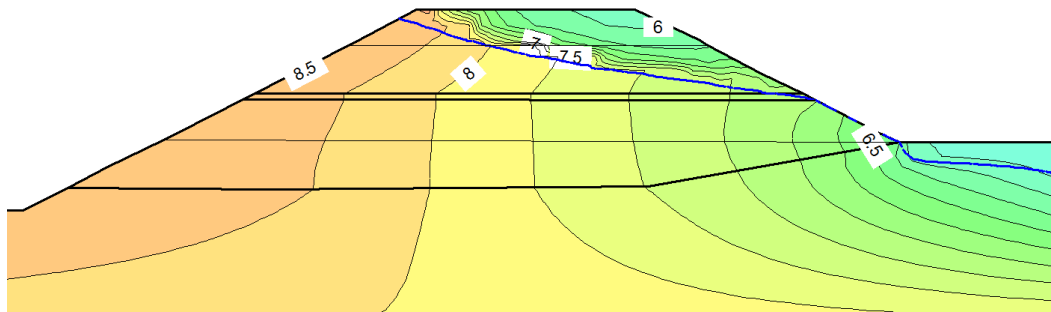


Figure 6-61. Results from transient analysis after one day of simulation with burrow at B. Total head contour interval: 0.25 m

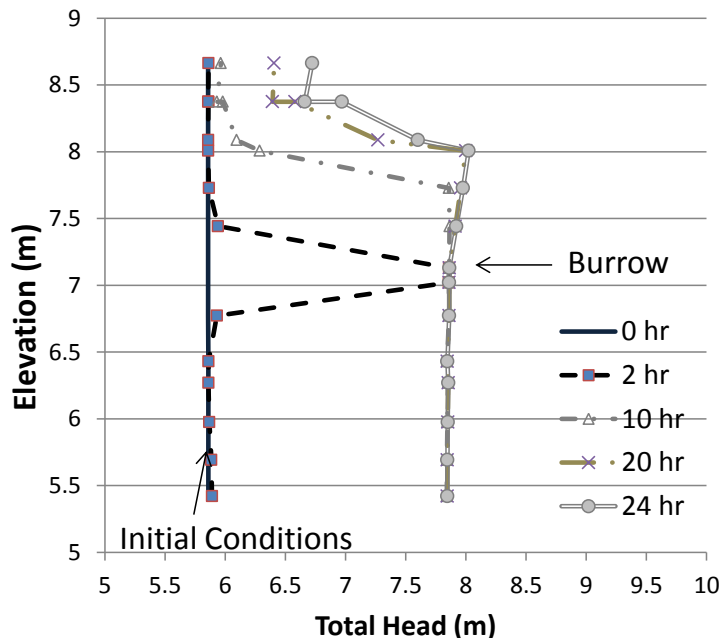


Figure 6-62. Evolution of pore pressures on a vertical section across the levee crown for Hole B

6.5 PIPING POTENTIAL OF COMPLETELY PENETRATING BURROWS

Piping is the development of a channel below or through a levee that is opened and widened by seepage force of groundwater flow concentrated along a discontinuity. Piping potential is related to three phenomena (Sellmeijer, 2006): (1) groundwater flow through the soil matrix, (2) water flow along the pipe or discontinuity, and (3) the state of limit equilibrium of the particles at the bottom of the pipe or discontinuity. A model that incorporates these phenomena is not commercially available, yet empirical formulae have been developed to assess the triggering of this issue. The Lane (1935) and Bligh (1910) methods relate the levee geometry with a series of coefficients to estimate a critical head over which piping would occur. Sellmeijer (1988) created a more robust procedure that incorporates particle characteristics as well as the geometry of the levee to estimate a ratio of critical head to the width of the embankment. More recently, Ojha (2003) developed a procedure based on flow velocity along the soil/void interface and particle diameter to estimate a critical traction velocity for initiation of the piping process. The results of the transient simulation for burrow C (3 m below levee crown) were used for piping potential estimation, employing the Ojha (2003) and Sellmeijer (1988) formulas.

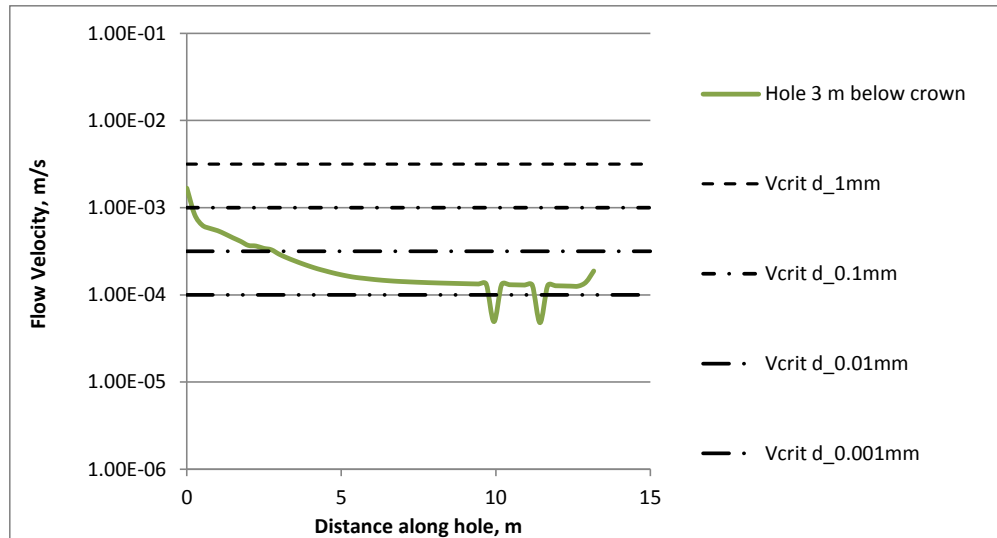


Figure 6-63. Piping potential evaluation using the Ohja (2003) formula

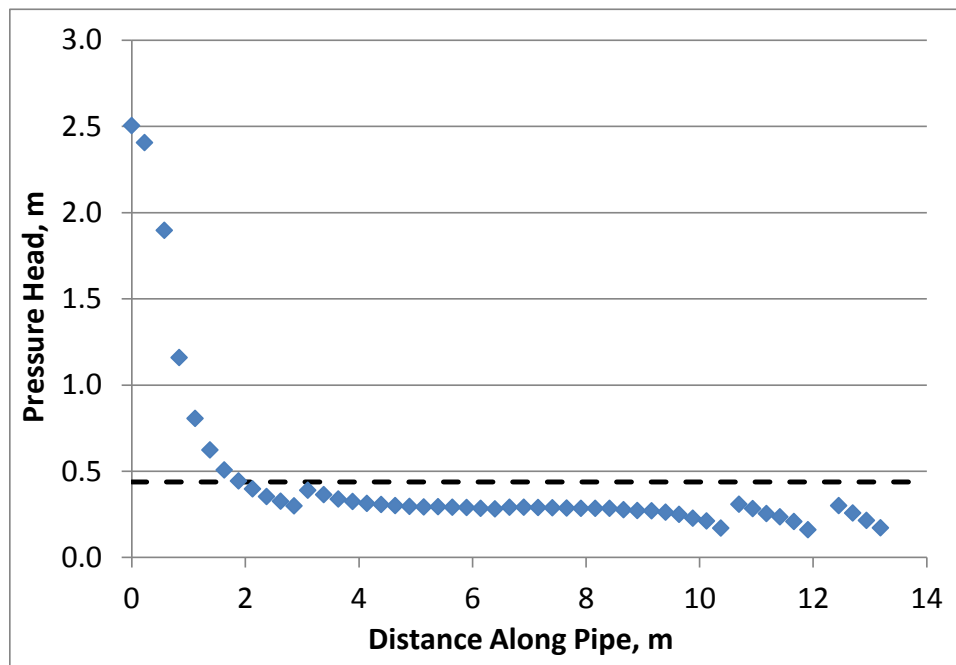


Figure 6-64. Piping potential evaluation using the Sellmeijer (1988) formula

The green series on Figure 6-63 represents the longitudinal profile of velocities along the soil/burrow interface. The data are compared to four critical velocity values according to Ohja (2003), for particle sizes ranging from 1 mm to 0.001 mm. The plot shows that the computed velocity field along the bottom of the burrow is sufficient for piping initiation. Similarly, using the Sellmeijer (1988) formula a critical potential head value (Figure 6-64) for a sandy soil with a D_{70} of 0.03 mm piping would initiate along the first several meters from the upstream entrance to the burrow.

6.5.1 CLAYEY LEVEE SITE MODELING

A simulation of the conditions in March 1998 during high water levels on the clayey (Figure 6-65) site was performed to further compare the simulation results to a well-documented case history. A 3D finite element model of the 2 m (6 ft) tall levee, with 2:1 slopes and 2.4 m (8 ft) wide crown (Figure 6-66) was constructed. The silty (67% fines) levee and foundation materials were assigned a saturated hydraulic conductivity of 5×10^{-6} cm/s, and unsaturated properties were estimated using the VanGenuchten (1980) equation as before.

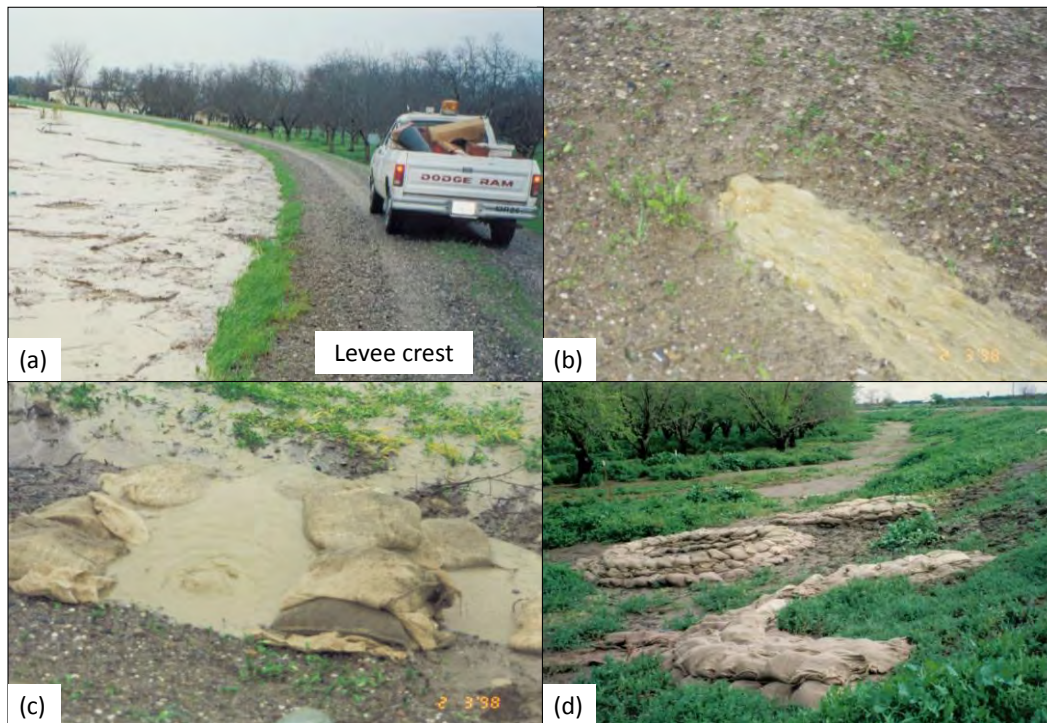


Figure 6-65. High water on Clayey Levee Site in 1998. Images courtesy Al Romero, DWR

Waterside boundary condition was constant head corresponding to water level located 0.15 m (0.5 ft) below the levee crown. Landside boundary conditions were represented with a constant head corresponding to water level 1 m (3ft) below the levee toe along the right vertical mesh boundary. The continuous burrow was modeled using saturated high conductivity elements located 1 m below the levee crown. Potential seepage faces were assigned along surfaces on the landside slope face and ground surface. Only steady state simulations were performed, as the burrow was connected to the riverside, thus making the analysis of saturation progression of the fine-grained embankment irrelevant.

The conductivity of the burrow was varied in the analyses and comparing the resulting velocities along the hole/soil interface were compared with velocity values for piping potential according to Ohja (2003). Figure 6-67 shows the range of flow velocities obtained by varying the

conductivity values of the burrow between 0.1 and 0.01 cm/s. Computed flow velocities along the hole range between 0.003 and 0.0003 m/s, which appear to be sufficient to trigger internal erosion for particle sizes above 0.01 mm. These velocity and piping potential estimations corroborate the observations during the high water in 1998 and show that a simplified approach to modeling burrows or other discontinuities in levees is adequate.

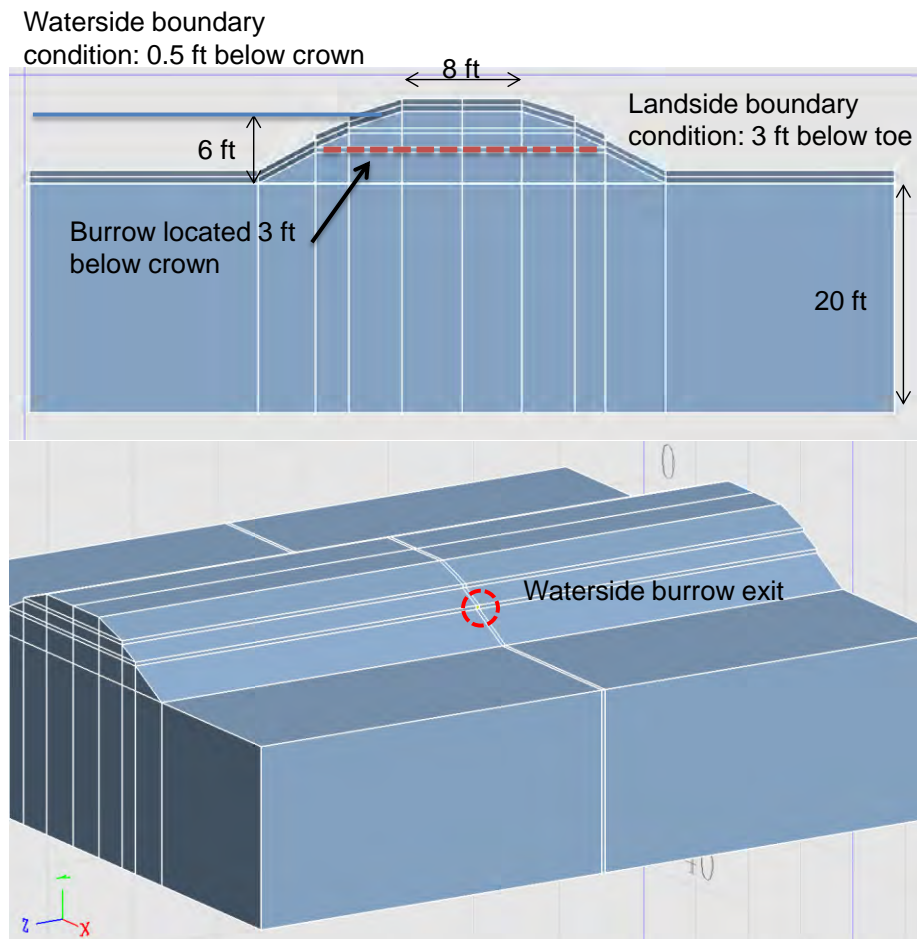


Figure 6-66. Clayey levee site 3D model

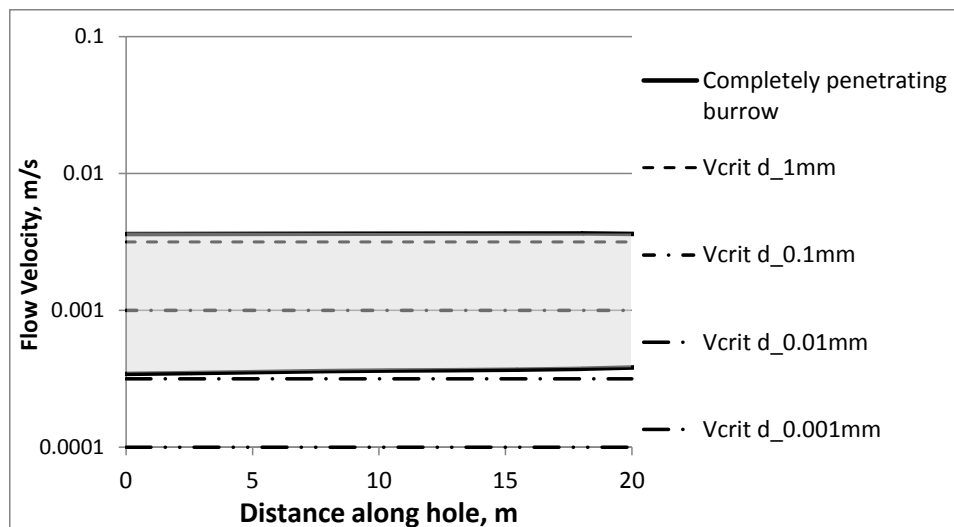


Figure 6-67. Critical flow velocities for different particle sizes compared to range of velocities along burrow

6.6 CONCLUSIONS

The effects of live and decomposing vegetation and animal burrowing on the seepage through levees were studied using data obtained from field experiments and field observations.

The simulations show that discontinuous voids, such as could be formed by decomposed root systems, do not provide a direct seepage path such that high flow velocities could develop. In cases where a given root is completely decomposed, its space is generally filled with decomposed matter, or *frass*, and tends to be looser than the surrounding soil, creating zones of higher hydraulic conductivity. However, while this condition could produce a faster advance of the wetting front, by relatively rapid saturation of localized zones within the levee, the flow quantities and velocities would not be high enough to trigger piping or internal erosion processes.

The data gathered during the seepage field test program showed that wetting fronts tend to progress slower through and around the root system than through sections with no roots, suggesting that the discontinuities found around some roots have little influence on accelerating groundwater flow and low likelihood of initiating erosion processes.

Animal burrowing has a much larger influence than roots given their larger diameter, length and continuity throughout the embankment than the live and decomposed roots observed in this research program. Of special interest are burrows or burrow systems extending from the waterside slope towards the landside slope, such as the one encountered on the clayey levee, which have the potential of eroding the levee material because the flow velocities can potentially reach critical values to trigger piping.

These observations are supported by numerical simulations performed to back-calculate the seepage tests and a historical account in one of the animal burrow sites. The models presented in this dissertation are relatively simple, yet intended to highlight the critical issues related to seepage performance of levee embankments when affected by biotic activity:

- Continuity and length of macropores: it seems unlikely that discontinuous macropores could trigger internal erosion on an embankment unless the discontinuity extends from the waterside levee slope to (or near to) the landside face of the levee. Depending on the hydraulic conductivity of the embankment, the flow into discontinuous cavities not extending to the landside slope will be very low making erosion unlikely. The likelihood of piping initiation and continuation increases with the length of the discontinuity and its position relative to the levee slopes.
- Location of the discontinuity: deeper animal holes or macropores connected to the waterside will be subject to larger hydraulic heads, and thus higher flow velocities than those located near the crest. Nevertheless, as depicted in the case history analysis of the clayey levee site, piping can be triggered even along relatively shallow discontinuities, as long as they are directly connected to the source of hydraulic loading and have an exit face. In this particular location, piping occurred along a burrow which experienced a head of approximately 80 cm (2.5 ft).
- Time dependency: discontinuous macropores such as those left by decomposed roots or small, collapsed animal burrows have an effect on time to saturation and wetting front stability. Isolated pockets of higher hydraulic conductivity will tend to accelerate the advancement of the saturation front, whereas root systems will tend to slow down this advancement.
- Saturation: the amount of water flowing into macropores not directly connected to the riverside is dependent on the hydraulic conductivity of the soil around it; an unsaturated fine-grained soil will have a very low conductivity and thus the flux of water into the hole will consequently be low. As saturation increases, the discharge into the discontinuity will increase. Conversely, for a discontinuity next to the source of hydraulic loading the saturation level of the soil around it is irrelevant, as the hole functions essentially as a pipe with flow velocity a function of the hydraulic head above it.

Chapter 7

FINDINGS AND CONCLUSIONS

The objectives of this dissertation were to assess the role of transient conditions on levee underseepage and blanket heave, and study the effects of root and animal activity on through seepage performance of a levee.

To this end, first part of this dissertation focused on an assessment of the adequacy of typical steady-state seepage analysis in the estimation of heave or uplift gradients in levees for cases where a fine-grained blanket overlays a coarse aquifer layer. The result of this assessment is a series of graphs that relate values of steady state and transient uplift gradients, as a function of site geometry, aquifer and blanket hydraulic conductivity and flood duration.

Depending on levee and subsurface geometry and storm duration, time dependency will play an important role on the performance of the embankment. As shown in the analyses, for some cases the transient gradient values are larger than 90% of the steady values given a certain set of geometric and flooding conditions; particularly when the flood duration is larger than 20 days and the aquifer presents a connection to the hydraulic heads from the river close to the waterside levee toe. However, for other geometries and flood durations, steady state seepage may be overly conservative, thus transient conditions should be evaluated when levees are being remediated or new levees are being designed.

Further work should be performed to assess the effects of this time dependency on static factors of safety, computing the corresponding factor of safety for each time step for all geometric configurations and boundary conditions considered on the seepage simulations. Challenges with this task include whether or not the effect of negative pore pressures in the estimation of shear strengths is essential. This framework will have to be validated using available case histories where transient loading is known to have contributed to failure.

The second part of this research was performed as a part of the California Levee Vegetation Research Program, with the objective of studying the effects of live and decomposing

vegetation and animal burrowing on seepage through levees. Seepage field experiments and mammal burrow studies performed as a part of a larger study (Shriro et al. 2014) were used to calibrate and analyze the potential for development of preferential seepage paths through levees.

Overall, the results of the field experiment and the corresponding seepage analyses show that:

- Live roots do not represent preferential seepage paths for water to flow through and erode the surrounding soil.
- For decomposed root systems, despite the presence of discontinuous gaps between the decomposed woody material and its bark or the surrounding soil, no increased flow quantities or velocities were observed in the field tests or simulations, in fact, wetting fronts tend to progress slower through and around the root system than through sections with no roots, suggesting that the discontinuities found around some roots have little influence on accelerating groundwater flow and low likelihood of initiating internal erosion processes.
- Field reports reviewed as part of the literature review portion of this project showed no evidence of woody vegetation serving as preferential seepage paths. Only one case history (Hodák, 2011) indicates a failure on a small dam due to vegetation related internal erosion, but little details are provided as to the position of the tree, species, soil conditions and the presence of animal activity.
- In terms of influence of seepage velocities, time of saturation, and piping potential, the presence of animal burrowing has a much larger influence than roots, given their larger diameter, length and continuity throughout the embankment. This is the case of the burrows observed on 1998 along the clayey site, where piping was observed on the upper half of the embankment, an area coinciding with the completely penetrating burrow described in Chapter 5 of this dissertation.

Chapter 8

REFERENCES

Allen, S., Dwyer, J., Wallace, D., Cook, E., 2003, Missouri River Flood of 1993: Role of Woody Corridor Width in Levee Protection, *Journal of the American Water Resources Association (JAWRA)* 39(4):923-933, Paper No. 02129, August.

American River Flood Control District (ARFCD), 2012, Personal communications and field visits during January 2012.

Association of State Dam Safety Officials (ASDSO), 2002, A Technical Manual on the Effects of Tree and Woody Vegetation Root Penetration on the Safety of Earthen Dams, December.

Bawden, G., Bond, S., Howle, J., Chung, S., Berry, A., Kreylos, O., Kellogg, L., Cobos, D., Shriro M., 2012, Ultra-high Resolution 3D Imaging of Tree Root Systems and Mammal Burrow Complexes within Levees

Bayoumi, A., Meguid, M., 2011, Wildlife and Safety of Earthen Structures: A Review, *Journal of Failure Analysis and Prevention*, 11:295-319, DOI 10.1007/s

Benedict, R., 2008, Nevada Levee Failure, Newsletter Website, Institute for Crisis, Disaster and Risk Management, Volume 14 – Number 1, February.

Bligh, W. G., 1910, Dams, Barrages and Weirs on Porous Foundations, *Engineering News*, p. 708.

Cedergren, H., 1997, *Seepage, Drainage, and Flow Nets*, Third Edition, Wiley.

Chapuis, R., 2004, Predicting the Saturated Hydraulic Conductivity of Sand and Gravel Using Effective Diameter and Void Ratio. *Can Geotech J.* 41: 787-795.

Chung, S., Bawden, G., Keightley, K., Bond, S., Lichter, J., Berry, A., (in press), Tree Dimensional Quantitative Characterization of in-situ Tree Root Architecture using Ground-Based Tripod LiDAR Scanning, *New Phytologist*.

Clevenger, C., 1999, Mississippi Earthen Dams and the Beaver “Beavers and Earthen Dams Don’t Mix”, ASDSO/FEMA Specialty Workshop on Plant and Animal Penetrations of Earthfilled Dams. November 30-December 2, 1999.

Cobos-Roa, D., Shriro, M., Sitar, N., Bray, J.D., Bawden, G., Lichter, J., and Evans, R., 2012a, 3-D Stratigraphy and Root Geometry From Trench and Ground-Based LiDAR Mapping, American Society of Civil Engineers GeoCongress 2012, Oakland, CA, March.

Cobos-Roa, D., Shriro, M., Sitar, N. and Bray, J.D., 2014a, California Levee Vegetation Research Program, Influence of Tree Roots and Mammal Burrowing Activity on Levee Integrity: Volume 1: Literature Review, The California Department of Water Resources Contract No 4600008761 and Sacramento Area Flood Control Agency Contract No 984

Cobos-Roa, D., Shriro, M., Sitar, N. and Bray, J.D., 2014b, California Levee Vegetation Research Program, Influence of Tree Roots and Mammal Burrowing Activity on Levee Integrity: Volume 4: Field Evaluation of Burrowing Animal Impacts and Effectiveness of Remedial Measures, The California Department of Water Resources Contract No 4600008761 and Sacramento Area Flood Control Agency Contract No 984

Costa, R., 2012, Personal Communication during January 2012 California Levee Vegetation Research Program meeting.

D. Van Troostwijk, W., 1978, Muskrat Control in the Netherlands. In: Proceedings of the 8th Vertebrate Pest Conference, University of Nebraska Lincoln.

Daar, S., Klitz, W., Olkowski, W., 1984, The Role of Vegetation in an Integrated Pest Management Approach to Levee Management. California Riparian Systems: Ecology, Conservation and Productive Management, University of California Press, Berkeley, California.

Deltares, 1999, WATEX, computer program for estimation of pore pressures beneath impervious dykes, <http://www.deltares.nl/nl/software/1068756/watex>.

Dixon, J., 1922, Rodents and Reclamation in the Imperial Valley, Journal of Mammalogy, 3:136-146.

DWR (California Department of Water Resources), 2009, Internal Technical Memorandum, Assessment of Animal Burrow Hole Persistence on Project Levees, October.

FEMA, 2005, Technical Manual for Dam Owners, Impacts of Animals on Earthen Dams, FEMA Report 473, September.

Freeze, R., Cherry, J., 1979, Groundwater, Prentice-Hall Inc., Englewood Cliffs, N.J.

GEO-SLOPE INTERNATIONAL, 2008, Seepage Modeling with SEEP/W, Third Edition, March.

Gerke, H., Van Genuchten, M. Th., 1993, A Dual-Porosity Model for Simulating the Preferential Movement of Water and Solutes in Structured Porous Media, Water Resources Research, Vol. 29, No.2, pp 305-319, February.

Grey, D., Megahan, W., 1981, Forest Vegetation Removal and Slope Stability in the Idaho Batholith, USDA Research Paper INT-271, May.

Harder, L., Kroll, R., Buck, P., Inamine, M., Berry, A., 2012, Investigation of Tree Root Penetration into a Levee Soil-Bentonite Slurry Cutoff Wall – Part II, 2012 Levee Vegetation Symposium, Sacramento, CA.

Hatheway, A. W. (1982). "Trench, shaft and tunnel mapping". Association of Engineering Geologist Bulletin, v.19, p.173-180.

Hodák, J., Žatecký, S., Švarc, O., 2011, Failures on Small Dams due to Internal Erosion, powerpoint presentation, Czech Republic.

Kadlec, R., Priesb, J., Mustar, H., 2007, Muskrats (*Ondatra zibethicus*) in treatment wetlands. Ecol. Eng. 29, 143-153.

Khilar, K. C., Folger, H. S., Gray, D. H., 1985, Model for Piping-Plugging in Earthen Structures, Journal of Geotechnical Engineering, ASCE, 111(7), 833-846.

Kroll, R., 2012, Personal communication during January 2012 California Levee Vegetation Research Program meeting.

Lane, E. W., 1934, Security from Underseepage: Masonry Dams on Earth Foundations, Trans. ASCE, p. 1235-1272.

Harder, L., Vroman, N., Sills, G., Groves, C., and Kelley, J., Inspection of Levee Distress and Breaches During the Spring 2008 Midwest Flood, Association of Dam Safety Officials Conference.

MBK Engineers, 2009, Memorandum: Emergency Beaver Den Levee Repair, January 24-26, 2009. Report to Reclamation District 2041.

Ozkan, S., 2003, Analytical Study of Flood Induced Seepage Under River Levees, Doctoral dissertation, Louisiana State University, May.

Perri, J., Shewbridge, S. E., Cobos-Roa, D., Green, R. K., 2012, Steady State Seepage Pore Water Pressures Influence in the Slope Stability Analysis of Levees, American Society of Civil Engineers, Paper ID 569, GeoCongress 2012, Oakland, CA, March.

Peter, P., 1982, Canal and River Levees, Developments of Civil Engineering 29, Bratislava, Slovakia, Elsevier/North Holland Inc.

Phillips, M. W., 1972, Electrical Effects on Water Infiltration into Soils, Water Resources Research Catalog, 5,1.0056.

Richards, L. A., 1931, Capillary Conduction of Liquids Through Porous Mediums, Physics, 1, pp. 318-333.

Sacramento Area Flood Control Agency (SAFCA), 2010, 2009 Capital Outlay Funding Agreement, Quarter 10 Work Plan, July 1 2011 – September 30, 2011.

Seed R. B., Athanasopoulos-Zekkos, A., Cobos-Roa, D., Pestana, J., Inamine, M., 2012, U.S. Levee and Flood Protection Engineering in the Wake of Hurricane Katrina, State of the Art Paper, American Society of Civil Engineers, GeoCongress 2012, Oakland, CA, March.

Sellmeijer, J. B., 1989, On the Mechanism of Piping under Impervious Structures, PhD Thesis, Technical University, Delft.

Sellmeijer, J. B., 1991, A Mathematical Model for Piping, Applied Mathematical Modeling, Vol. 15(6), 646-651.

Sellmeijer, J. B., 2006, Numerical Computation of Seepage Erosion below Dams (piping).

Shields, F.D., and Gray, D., 1992, Effects of Woody Vegetation on Sandy Levee Integrity, Water Resources Bulletin, American Water Resources Association, Vol, 28, No. 5. October.

Shriro, M., Cobos Roa, D., Bray, J., Sitar, N., Lichter, J., Evans, R., Kroll, R., 2011, Study of Levee Seepage and Slope Stability in Relation to Roots, Association of Dam Safety Officials 2011 Conference, Washington D.C., September.

Shriro, M., 2014, Static and Seismic Performance of California Levees, Doctoral Dissertation, University of California, Berkeley.

Shriro, M., Cobos-Roa, D., Bray, J.D., and Sitar, N., 2014a, California Levee Vegetation Research Program, Influence of Tree Roots and Mammal Burrowing Activity on Levee Integrity: Volume 2: Field Test No. 1: Parallel Trench Wetting Front Test North Levee of the American River at Cal Expo, Sacramento, CA, The California Department of Water Resources Contract No 4600008761 and Sacramento Area Flood Control Agency Contract No 984

Shriro, M., Cobos-Roa, D., Bray, J.D., and Sitar, N., 2014a, California Levee Vegetation Research Program, Influence of Tree Roots and Mammal Burrowing Activity on Levee Integrity: Volume 2: Field Test No. 2: Crown Seepage Test, Northern Levee of Twitchell Island in Rio Vista, CA, The California Department of Water Resources Contract No 4600008761 and Sacramento Area Flood Control Agency Contract No 984

Sidle, R.C., 1992, A Theoretical Model of the Effects of Timber Harvesting on Slope Stability, *Water Resources Research*, 28(7): 1897-1910.

Singh, V.P., Ojha, C. S. P., Adrian, D. D., Ozkan, S., Sills, G., 2002, Role of Sand Boil Formation in Levee Failure.

Technical Advisory Committee on Flood Defences (TAW), 1998, Fundamentals on Water Defences, The Netherlands, published on <http://www.tawinfo.nl/asp/uk.asp?documentID=112>.

Technical Advisory Committee on Flood Defences, 1999, Technical Report on Sand Boils (Piping), The Netherlands, draft English version, August 2002.

Terzaghi, K. V., 1950, Mechanism of Landslides, in: *A History of Progress: Selected U.S. Papers in Geotechnical Engineering*, Volume 2. American Society of Civil Engineers, November.

Turnbull W.J., and Mansur C.I., 1961, Investigation of Underseepage-Mississippi River Levees. *Transactions, ASCE*, 126(1), pp. 1429-1485.

U.S. Army Corps of Engineers, 1956, Investigation of Underseepage and its Control, Lower Mississippi River Levees, TM 3-424.

U.S. Army Corps of Engineers (USACE), 2000, Design and Construction of Levees, Engineering Memorandum 1110-2-1923.

U.S. Army Corps of Engineers (USACE), 2003, Recommendations for Seepage Design Criteria, Evaluation and Design Practices, CESPCK Levee Task Force, July.

U.S. Army Corps of Engineers (USACE), 2005, Design Guidance for Levee Underseepage, Technical Letter 1110-2-569, May.

U.S. Army Corps of Engineers (USACE), 2008, Engineering Technical Letter 1110-2-571

U.S. Army Corps of Engineers (USACE), 2009, ETL 1110-2-571, Guidelines for Landscape Planting and Vegetation Management at Levees, Floodwalls, Embankments Dams, and Appurtenant Structures.

U.S. Army Corps of Engineers (USACE), 2011, Initial Research into the Effects of Woody Vegetation on Levees, Engineer Research and Development Center.

U.S. Army Corps of Engineers (USACE), 2011, International Levee Manual, Chapter 4, accessed via personal communications with Sacramento District.

U.S. Army Corps of Engineers (USACE), 2011a, Sandboil image, uploaded to http://commons.wikimedia.org/wiki/File:Sand_boil_discovered_in_Tallulah,_Louisiana.jpg by USACE on 16 May 2011

U.S. Army Corps of Engineers (USACE), Incident Report: Vegetation Impact to FRM Infrastructure. Series of Reports provided in 2011 via personal communications.

U. S. Department of the Interior Bureau of Reclamation. (1998). "Engineering Geology Field Manual". Second Edition.

URS, 2008, Truckee Canal Failure on 5 January 2008, Investigative Evaluation Report, Prepared for US Bureau of Reclamation, March.

URS, 2011, The Influence of Vegetation on Levee Past Performance – a Review of Historic Data Based on the Levee Evaluation Program Database, Report prepared for DWR.

URS, 2014, Urban Levee Evaluation Program Guidance Document, Rev10, Report prepared for DWR.

van Baars, S., 2009, The Causes and Mechanisms of Historical Dike Failures in the Netherlands.

Van Genuchten, M. Th., 1980, A closed-form equation for predicting the hydraulic conductivity of unsaturated soils. Soil Science Society of America Journal, 44:892-898.

Van Vuren, D., 2011, Habitat Associations of Burrowing Mammals along Levees in the Sacramento Valley, California, report to California Levee Vegetation Research Program, September.

Van Vuren, D., 2012, Personal communications as part of collaborations during the California Levee Vegetation Research Program.

Ventura County Watershed Protection District, 2006, Approved Integrated Pest Management Program, Rodent Control for Flood Control Facility Protection, Water and Environmental Resources Division, December.

Wejers, J. B., Sellmeijer, J. B., 1993, A New Model to Deal with Piping Mechanism, Filters in Geotechnical and Hydraulic Engineering, Balkema, Rotterdam, P. 349-355.

Ziemer, R., 1992, Effect of Logging on Subsurface Pipeflow and Erosion: Coastal Northern California, USA, Erosion, Debris Flows and Environment in Mountain Regions, Proceedings of the Chengdu Symposium, IAHS Publ. no. 209, July.